UNIVERSITY OF LIVERPOOL

In vivo analyses of Laminin N-terminus α31.

Thesis submitted in accordance with the requirements of the University of Liverpool for the degree of Doctor of Philosophy

By

Conor James Sugden

April 2022

Abstract

Laminins are essential components of all basement membranes where they regulate an extensive array of tissue functions. Alternative splicing from the laminin α3 gene produces a non-laminin but netrin like protein, Laminin N terminus α31 (LaNt α31). LaNt α31 is widely expressed in intact human tissue and is upregulated in epithelial cancers and during wound healing. In vitro functional studies have shown that LaNt α31 can influence numerous aspects of epithelial cell behaviour *via* modifying matrix organization, suggesting a new model of laminin auto-regulation. However, studies on LaNt α31 function in epithelial tissue have been limited to observational or 2D in vitro studies.

In this thesis, I describe the first ever in vivo model of LaNt α31 function. I generated and validated a transgenic mouse line, where the ubiquitin C promoter was used to drive inducible expression of LaNt α31. Prior to this, I established two new stable LaNt α31 overexpressing keratinocyte cell lines and used these in 3D organotypic models to extend the investigation of the consequences of LaNt α31 dysregulation in epithelia. Further, I determined LaNt α31 distribution in mouse using newly generated antibodies.

The results revealed that LaNt α31 dysregulation is detrimental to the epithelial layer integrity in 3D organotypic coculture models of skin and cornea. When expression was induced in vivo during development, LaNt α31 transgenic animals were not viable at birth, exhibiting localised regions of erythema. Histologically, the most striking defect was widespread evidence of extravascular bleeding across multiple tissues. Additionally, LaNt α31 transgene expressing animals exhibited kidney epithelial detachment, tubular dilation, disruption of the epidermal basal cell layer and of the hair follicle outer root sheath, and ~50% reduction of cell numbers in the liver, associated with depletion of hematopoietic erythrocytic foci.

The work detailed herein establishes that LaNt α31 has a potent ability to influence development and tissue morphogenesis in native tissue environment, while the methods used extend the toolbox for research into this exciting but relatively unstudied protein.

“God bless the band.”

— Liam Fray

Acknowledgements

It is no exaggeration to say that this PhD has provided me with life changing experiences and future opportunities that I could have never imagined. For this, I am eternally grateful to those who gave me the chance to do a PhD. Completing this PhD during a global pandemic presented unexpected challenges, and I'm deeply thankful for all those who helped me to reach the end.

First and foremost, thank you to my supervisors who made this project possible and gave me their expert guidance along the way. Thank you to Dr. Kevin Hamill. I will be eternally grateful for the opportunity that Kevin gave me to undertake this PhD project. For five years Kevin has pushed me to become a better researcher, has taught me so much along the way, and continues to do so every day. I hope I made you proud during this time. I would also like to express my deep gratitude to Prof. George Bou-Gharios, whose expertise in transgenics is unrivalled. Your pure scientific enthusiasm has been infectious, and you have provided me with great motivation during the tough times when things didn't seem to be going to plan. It has been a pleasure and a privilege to be work with both of you over the last few years.

I have been lucky to work with some brilliant colleagues during this PhD, and I thank them all. Thank you to Dr. Lee Troughton, who was a great mentor and a better friend. Seeing Lee walk the path before me in academia gave inspired me to believe that I could do the same. Also thank you to Mr. Liam Shaw, who provided so many laughs and made being in this place fun regardless of how experiments were going. I owe a great deal of thanks to Dr. Alexander Nyström, who supported and hosted my research during my time in Freiburg, Germany, and to Dr. Pauline Nauroy, who showed me the ropes with regards to 3D organotypic cocultures. I am thankful for the expertise of Dr. Ke Liu, who I would have been lost without at the beginning of this project. To Dr. Carl Sheridan for the encouragement throughout the years, and to Dr. Kazu Yamamoto, who always had the patience to answer my questions.

I am grateful for the friends I have made along the way during my time here. The list is long, but thanks to Michele for providing good vibes every single day, to Lorenzo, Adam, Euan, for the laughter, and to Mo, John, Asma, Thanos, to name but a few.

I feel grateful to those who mentored me before I even knew what a doctorate was, and before I knew it would be possible to become a Dr. myself! Specifically, to Dr. Kehinde Ross who gave me support during my undergraduate degree, and to Dr. Andrés Vacas Oleas, who acted as a mentor and friend at the University of Navarra. Without Andrés, I would not have pursued a PhD.

I am thankful to the funders; the Crossley Barnes Bequest fund, and the DAAD, who made this work possible, and I thank the Institute of Life Course and Medical Sciences and all the researchers there who have all helped me in some way.

Lastly, I would like to thank those outside the world of academia who have helped me along the way. Thank you to my parents, who have supported me in all of my choices. Thank you to Elena, who has given me so much support throughout my PhD, and thank you to Ollie and Ian, who kept me sane during this experience.

Table of Contents

CHAPTER 1: INTRODUCTION 1

CHAPTER 2: LITERATURE REVIEW 3

2.1 Basement membranes 3

2.2 Basement membrane assembly 3

2.2.1 Nidogen 3

2.2.2 Perlecan 4

2.2.3 Collagen IV 4

2.3 Laminins (LMs) 4

2.3.1 Laminin isoforms 4

2.3.2 Laminin globular (LG) domains 7

2.3.3 Laminin coiled-coil (LCC) domains 7

2.3.4 L4 domains 7

2.3.5 Laminin-type epidermal growth factor-like (LE) domains 8

2.3.6 Laminin N-terminal (LN) domains 8

2.3.7 LN domain structure 10

2.4 LM isoforms unable to form αβγ ternary nodes 11

2.5 LM receptors 12

2.5.1 Integrins 12

2.5.2 Signalling through LN domains and proteolytically cleaved fragments 13

2.5.3 Non-integrin LM receptors 14

2.6 Expression profiles 17

2.6.1 Development 17

2.6.2 Skin 18

2.6.3 Kidney 19

2.6.4 Lungs 20

2.6.5 Vessels 21

2.6.6 Stem cell niches 22

2.7 Breaching BMs 23

2.7.1 BM itself dictating breach points in normal biology 23

2.7.2 Cell dependent breaching (physical methods) 23

2.7.3 Enzymatic BM disrupting proteins 24

2.8 LN domain interactions in health and disease 24
2.8.1 LN domain mutations 25
2.8.2 Pierson syndrome 27
2.8.3 MDC1A 28
2.8.4 LAMB3 – Junctional epidermolysis bullosa (JEB) LN domain mutation 30
2.8.5 LAMA5 mutations 31
2.8.6 Mouse models of LN domains deletions/mutations 32
2.8.7 Other animals 33

2.9 Rescuing LN domain defects 33

2.10 Non-LM LN domain proteins 35
2.10.1 Netrins 35
2.10.2 Netrin 4 35
2.10.3 Netrin 4 overexpression 36

2.11 Laminin N-terminus α31 37
2.11.1 Comparisons of LaNt α31 and netrin 4 38

2.12 This thesis 39

2.12.1 Specific aims of this thesis 39

CHAPTER 3: METHODS 40

3.1 General Materials 40
3.1.1 Antibodies 40
3.1.2 Cell lines and culture conditions 41

3.2 General Methods 42
3.2.1 Cloning procedures 42
3.2.2 SDS-PAGE and western immunoblotting 42
3.2.3 Image acquisition 43
3.2.4 Image analysis 44
3.2.5 Ethics 44

3.3 Chapter 4 specific methods 45
3.3.1 Tissue processing 45
3.3.2 Immunohistochemistry 45

3.4. Chapter 5 specific methods 46
3.4.1 pLenti-LaNtα31-PAmCherry-P2A-Puro vector 46
3.4.2 Cell transduction 46

3.4.3 Photoactivation of PAmCherry 46
3.4.4 3D organotypic cocultures 47
3.4.5 Immunofluorescence microscopy 47
3.4.6 Single cell phenotypic assays 48
3.4.7 In vitro scratch assays 48
3.4.8 Organotypic coculture processing 48
3.4.9 Immunohistochemistry 49

3.5 LaNt α31 in vivo studies 50
3.5.1 Generation of pUbC-LoxP-LaNtα31-T2A-tdTomato 50
3.5.2 Cell transfections 50
3.5.3 Explant culture method 51
3.5.4 Ex-vivo scratch wound assays 51
3.5.5 Transgenic Line establishment 51
3.5.6 In Vivo Transgene Induction 52
3.5.7 DNA Extraction 53
3.5.8 PCR 53
3.5.9 Tissue processing 54
3.5.10 Hematoxylin and Eosin Staining 54
3.5.11 Immunohistochemistry 55
3.5.12 Transmission Electron Microscopy 55

CHAPTER 4: LANT A31 DISTRIBUTION IN MICE 56

4.1 Introduction 56
4.1.1 Aim 57
4.1.2 Objectives 57

4.2 Results 59
4.2.1 Antibody design and screening 59
4.2.2 Epithelium 64
4.2.3 Kidney 66
4.2.4 Lungs 67
4.2.5 Heart 68
4.2.6 Brain 69
4.2.7 Skin (newborn) 72
4.2.8 Blood vasculature 72

4.3. Discussion 74
4.3.1 Limitations 75
4.3.2 Next steps 76

4.3.1 Conclusion 77

CHAPTER 5: INVESTIGATING THE EFFECTS OF LANT A31 OVEREXPRESSION IN 3D ORGANOTYPIC CORNEAL AND SKIN EQUIVALENTS 78

5.1. Introduction 78

5.1.1. Aim 79

5.1.2. Objectives 79

5.1.3. Overexpression construct overview 80

5.2. Results 84

5.2.1. Lentiviral LaNt α31 overexpression construct validation 84

5.2.2. LaNt α31 overexpression leads to changes in NHK cell morphology and a reduction in migration rates 87

5.2.3. Validation of LaNt α31 overexpression in 3D organotypic cocultures. 91

5.2.4. LaNt α31 overexpression causes the formation of cyst-like structures in 7-day OCE cocultures 93

5.2.5. LaNt α31 overexpression causes the formation of gaps between basal keratinocytes in 7-day OSE cocultures. 93

5.2.6. LaNt α31 overexpression causes the formation of cyst-like structures in 4-week OSE and OCE. 95

5.2.7. LaNt α31 overexpression disrupts LM332 deposition at the stromal-epithelial junction. 96

5.3. Discussion 97

5.3.1. LaNt α31 dysregulation is detrimental to 3D OCE and OSE epithelial health 97

5.3.2. LaNt α31 modulates normal human skin keratinocyte morphology, behaviour, and ECM deposition. 98

5.3.3. Two new stable expressing epithelial lines established. 100

5.3.4. Caveats 101

5.3.5. Next steps 101

CHAPTER 6: LAMININ N-TERMINUS A31 EXPRESSION DURING DEVELOPMENT IS LETHAL AND CAUSES WIDESPREAD TISSUE-SPECIFIC DEFECTS IN A TRANSGENIC MOUSE MODEL. 104

6.1. Introduction 104

6.1.1. Aims 105

6.1.2. LaNt α31 transgene construct design and construct features 106

6.2 Results 110
6.2.1. Cloning steps for generating pUbC-LoxP-LaNtα31-T2A-tdTomato..... 110
6.2.2. Validation of genotyping primers 112
6.2.3. Inducible LaNt α31 construct generation and validation..... 112
6.2.4. Generation and validation of a LaNt α31 transgenic mouse line..... 116
6.2.5. mEFs isolated from UbCLaNtα31::R26CreERT2 embryos display reduced migration rates 121
6.2.6. UbCLaNt::R26CreERT2 expression in utero causes death and localised regions of erythema at birth. 121
6.2.7. LaNt α31 overexpression leads to epithelial detachment, tubular dilation and interstitial bleeding in the kidney and disruption of capillary BM integrity. 127
6.2.8. LaNt α31 overexpression disrupts epidermal basal cell layer organization. 130
6.2.9. Mice expressing the LaNt α31 transgene display structural differences in the lung and a reduction of hematopoietic colonies in the liver. 133

6.3. Discussion 136
6.3.1. Synopsis 136
6.3.2. LaNt α31-mediated LM network disruption as a cause of the transgenic mouse phenotype 136
6.3.3. Does LaNt α31 play a role in vascular homeostasis? 138
6.3.4. LaNt α31 acting in a non-disruptive manner 141
6.3.5. LaNt α31 may play a role in cell signalling 142
6.3.6. Growth factor sequestration 143
6.3.7. LaNt α31 as a regulator of stem cell niches 143
6.3.8. Conclusion 145

CHAPTER 7: FINAL SUMMARY 146

7.1 The role of LaNt α31 in 3 LN domain-containing networks 147

7.2 The role of LaNt α31 in 2 LN domain-containing networks (venules, veins) 149

7.3 The role of LaNt α31 in vessels with high levels of LM511 (arteries, arterioles) ... 151

7.4 LaNt α31 is a potential mediator of BM stiffness, composition, and architecture 152

7.5 Concluding remarks 154

APPENDICES 155

Appendix I: LaNtα31-PAmCherry1-P2A-Puro amino acid sequence and protein alignments 155

Appendix II: LaNtα31-T2A-tdTomato amino acid sequence 158

Appendix III: List of manuscripts and meeting abstracts 159

Peer reviewed papers 159

Preprint manuscripts 159

Published Abstracts 160

Accepted Abstracts 160

Appendix IV: Grants and Bursaries Awarded 162

Appendix V: Published manuscript relating to chapter 2 163

Appendix VI: Accepted manuscript relating to chapter 6 [Accpeted for publication in The FASEB Journal 05/04/2022] 173

Appendix VII: Cryopreservation records of LaNt α31 transgenic mouse lines. 192

REFERENCE LIST 194

List of figures

Figure 2.1. Schematic diagram of possible LM heterotrimes 6

Figure 2.2. LN domain orientations. 11

Figure 4.1. Screening of pre-immune sera and final bleed Rbt anti-MsLaNt α31 antibodies by western immunoblotting. 60

Figure 4.2. Rbt anti-MsLaNt a31 antibodies recognise a protein of the correct size only in samples from mice. 61

Figure 4.3. Peptide blocking using the specific epitope used to generate the anti-MsLaNt α31 antibodies prevents any anti-LaNt α31 immunoreactivity. 63

Figure 4.4. LaNt α31 is present in the basal epithelium and vasculature in tongue tissue. 65

Figure 4.5. LaNt α31 is present in the bowman's capsule parietal epithelium basement membrane, proximal tubes, and blood vasculature. 66

Figure 4.6. LaNt α31 is widely expressed throughout the lungs. 67

Figure 4.7. LaNt α31 immunoreactivity is observed around bronchioles, glands, and alveolar epithelium. 68

Figure 4.8. LaNt α31 is observed in multiple structures throughout the heart. 69

Figure 4.9. LaNt α31 is present in the brain. 70

Figure 4.10. LaNt α31 immunoreactivity is observed only in the vasculature in the brain. 71

Figure 4.11. LaNt α31 is present in large, but not small vessels. 73

Figure 5.1. Diagram of the LaNtα31-PAmCherry fusion protein. 80

Figure 5.2. Cloning steps for pLenti-CMV-LaNtα31-PAmCherry1-P2A-puro. 86

Figure 5.3. Lentiviral LaNt α31 overexpression construct validation. 87

Figure 5.4. LaNt α31 overexpression leads to changes in NHK cell morphology. 88

Figure 5.5. LaNt α31 causes a reduction in NHK migration rates. 89

Figure 5.6. LaNt α31 overexpression causes LM332 clustering. 90

Figure 5.7. Schematic of OSE and OCE culture set up. 91

Figure 5.8. Confirmation of LaNt α31 overexpression in OSE and OCE cultures. 92

Figure 5.9. H&E stained sections of 7-day OCE cocultures. 94

Figure 5.10. H&E stained sections of 7-day OSE cocultures. 94

Figure 5.11. H&E stained sections of 4-week OCE cocultures. 95

Figure 5.12. H&E stained sections of 4-week OSE cocultures. 95

Figure 5.13. LaNt α31 overexpression causes disorganised LM332 deposition in OCE cultures. 96

Figure 6.1. Cloning strategy for pUbC-LoxP-LaNtα31-T2A-tdTomato. 111

Figure 6.2. Genotyping primer validation. 112

Figure 6.3. UbC promoter drives the expression of LaNt α31 and tdTomato when cotransfected into cells expressing Cre recombinase in-vitro. 114

Figure 6.4. Timelapse of Cre recombinase-induced expression of LaNt α31-T2A-tdTomato. 115

Figure 6.5. Preparation of linearised pUbC-LoxP-LaNtα31-T2A-tdTomato DNA for pronuclear microinjection. 117

Figure 6.6. Validation of LaNt α31 transgene presence and expression in UbC-LaNtα31 F1 embryos. 119

Figure 6.7. Validation of LaNt α31 transgene presence and expression in UbC-LaNtα31 x R26CreERT2 mice. 120

Figure 6.8. LaNt α31 overexpressing mouse embryonic fibroblasts display reduced migration rates. 121

Figure 6.9. Genotyping of mice used in this study. 123

Figure 6.10. Transgenic mice overexpressing LaNtα31 are not viable at birth and display localised regions of erythema. 125

Figure 6.11. LaNt α31 overexpression leads to epithelial detachment, tubular dilation and interstitial bleeding in the kidney. 128

Figure 6.12. TEM of LaNt α31 transgenic mouse kidneys. 129

Figure 6.13. LaNt α31 overexpression disrupts epidermal-dermal cell organization. 130

Figure 6.14. Indirect immunofluorescence staining for of LaNt α31 transgenic mouse skin. 131

Figure 6.15. LaNt α31 overexpressing mice possess fewer, but larger, hemidesmosomes. 132

Figure 6.16. Mice expressing the LaNt α31 transgene display structural differences in the lung. 134

Figure 6.17. LaNt α31 transgenic mice display a reduction of hematopoietic colonies in the liver. 135

Figure 7.1. Proposed model of LaNt α31 interactions at normal levels and in excess in 3 LN domain containing LM networks. 148

Figure 7.2. Proposed model of LaNt α31 interactions at normal levels and in excess in 2 LN domain containing LM networks. 150

Figure 7.3. Proposed model of LaNt α31 interactions at normal levels and in excess in 2 LN domain containing LM networks. 152

List of tables

Table 2.1. Pathogenic LN domain mutations. 26

Table 6.1. Records of pronuclear microinjections. 118

Abbreviations

BM – Basement membrane

BPE – Bovine pituitary extract

cDNA – Complementary cDNA

CDS – Coding DNA sequence

cHS4 - HS4 chicken β-globin insulator

CMV – Cytomegalovirus

Col IV – Collagen IV

C-terminus - Carboxyl-terminus

DAPI - 4′,6-diamidino-2-phenylindole

DG – Dystroglycan

DMEM - Dulbecco's Modified Eagle Medium

E. coli - Escherichia coli

E1, E7, etc. – Embryonic day

ECM – Extracellular matrix

EDTA - Ethylenediaminetetraacetic acid

EGF - Epidermal growth factor

EGF - Epidermal growth factor

Floxed - **Fl**anked the *L**ox**P* sequences

GBM – Glomerular basement membrane

GFP – Green fluorescent protein

H&E - hematoxylin and eosin

HA - Human influenza hemagglutinin

hCG - Human chorionic gonadotropin

IF – Immunofluorescence

JEB – Junctional epidermolysis bullosa

k14 – Keratin 14

kDa - Kilodalton

kDa – Kilodaltons

KSFM – Keratinocyte serum free media

L4/LF - Laminin IV

LaNt – Laminin N-terminus

LCC – Laminin coiled-coil

LE - Laminin-type epidermal growth factor-like

LG – Laminin globular

LM– Laminin

LN – Laminin N-terminal

LoxP - locus of x-over, P1

LR – Laminin receptor

LTR - Long terminal repeats

mCherry – monomeric Cherry protein

MDC1A - Merosin-deficient congenital muscular dystrophy type 1A

MMP – matrix metalloproteinase

mRNA – Messenger RNA

Ms – Mouse

NGS – Normal goat serum

NMJ – Neuromuscular junction

OCE – Organotypic corneal equivalent

OCT - Optimal cutting temperature compound

OE – Overexpressing

OSE – Organotypic skin equivalent

OTC – Organotypic coculture

PAGE - Polyacrylamide gel electrophoresis

PAmCherry – Photoactivatable mCherry

PBS - Phosphate buffered saline

PBS-T - Phosphate buffered saline- tween 20

PCR – Polymerase chain reaction

PMSF - phenylmethysulfonyl fluoride

PMSG - Pregnant mare serum gonadotropin

polyA - Polyadenylation signal

R26 – Rosa26

Rbt – Rabbit

SD – Standard deviation

SDS - Sodium dodecyl sulfate

tdTomato – Tandem dimer tomato protein

TEM – transmission electron microscopy

TG – Transgenic

UbC – Ubiquitin C

WPRE - Woodchuck hepatitis virus posttranscriptional regulatory element

Chapter 1: Introduction

The work described within this thesis is focused on the relatively unknown protein Laminin N-terminus α3 (LaNt α31). Specifically, I present new data describing the distribution of LaNt α31 in mouse tissue (chapter 4), I detail the effect of LaNt α31 overexpression in 3D skin organotypic cocultures (chapter 5), and l present the first in vivo study of LaNt α31 overexpression in a newly developed mouse model (chapter 6).

The LaNt α31 protein is the newest member, both by evolution and by structure, of the laminin superfamily. This superfamily includes laminins, structural components of specialized regions of extracellular matrix known as basement membranes, and netrins whose major roles are considered to be axonal guidance but where at least one member can influence laminin organization. LaNt α31 differs from these two proteins families in important ways, but studies into laminins and netrins provides a framework to interpret LaNt α31-related work.

To establish the framework to discuss the new LaNt α31 work, Chapter 2 provides an overview of the core components of basement membranes before delving deeper into laminin biology, particularly focusing on what is known regarding the mechanisms behind network assembly. This includes discussion of the human genetic diseases associated with failure of laminin network assembly and description of the phenotype of animal models of these diseases. The relevant features of netrin biology are outlined, including transgenic animals and finally all the current knowledge of about LaNt α31

are described, particularly its distribution, association with pathology and results from in vitro functional studies and ex vivo manipulation experiments.

Chapter 2: Literature review

Part of this chapter was published (Appendix V):

Sugden CJ†, Shaw L†, and Hamill KJ (2021) LM Polymerization and Inherited Disease: Lessons From Genetics. Front. Genet. 12:707087. doi: 10.3389/fgene.2021.707087

2.1 Basement membranes

Basement membranes (BMs) are specialized extracellular matrix (ECM) structures with essential and remarkably diverse roles in most cell and tissue behaviours; including regulating differentiation, cell adhesion and migration [1,2]. BMs not only provide the mechanical attachment points that support sheets of cells to resist stresses but also influence signaling cascades via direct binding to cell surface receptors, through the sequestration and controlled release of growth factors, and by providing biomechanical cues, as reviewed in [3,4]. BMs are also dynamic structures that are remodelled in terms of composition and structure throughout life, with the most striking changes occuring during development [5,6]. At the core of every BM are two networks of structural proteins; type IV collagens and laminins (LMs)[7].

2.2 Basement membrane assembly

BMs are composed primarily of LMs, Col IV, nidogen and perlecan. The first step is LM deposition and polymerization[8,9]., which is followed by nidogen and perlecan binding, and next followed by col IV network assembly, resulting in the formation of a mature BM. Each component of the BM is described individually below[10-12].

2.2.1 Nidogen

Nidogen-1 and -2 are sulphated monomeric proteins ubiquitous to all BMs. Both isoforms contain an N-terminal globule linked to a C-terminal globule by a stalk consisting of cysteine-rich thyroglobulin homology repeat. Nidogens are generally viewed as linking molecules within the BM, with the ability to bind perlecan, collagen IV (Col IV), and the LE repeats of LM γ1 and γ3[13,14].

2.2.2 Perlecan

Perlecans are large proteins (~470 kDA) consistent of five domains (I-V) found in the ECM in multiple tissues; specifically smooth muscle, vascular endothelium, and most epithelium. Perlecan acts as a cross-linker for many BM components and cell surface molecules including binding the at least LN domain of LM α1 via perlecan domain IV[15-17].

2.2.3 Collagen IV

Col IV is the main type of collagen found across almost all BMs and the most abundant BM protein[10]. Six col IV (α1 – α6) chains have been identified, and different combinations of these self-assemble into triple-helical molecules which forms a net-like structure within the BM. Each collagen IV chain comprises of an N-terminal 7S domain, a middle-triple helical domain, and a C-terminal globular non-collagenous (NC1) domain. It is through the NC1 domains and triple-helical regions that col iv chains associate together, forming part of the final BM scaffold[18-22]. Col IV can associate into the BM in either directly via binding the LM globular regions, or indirectly via nidogens. The multiple ways in which col IV can interact with LMs, in conjunction with the multiple col IV chains, greatly contributes to the heterogeneity of possible BM compositions[10].

2.3 Laminins (LMs)

2.3.1 Laminin isoforms

Out of the constituent proteins of BMs, the LM family of glycoproteins is arguably the most important and the most diverse. They are the most abundant non-collagenous protein in the basement membrane[23]. LMs are composed of α-, β- and γ- subunits, which are encoded by 12 LM genes (LAMA1-5, LAMB1-3, and LAMC1-3). Adding further diversity, an additional isoform is generated via a second promoter in LAMA3, giving rise to a short LM α3a isoform, and a longer LM α3b isoform. Additional alternative splicing mechanisms give rise to further non-LM isoforms including **Laminin N-terminus α31 (LaNt α31)**, which is the focus of this thesis, and discussed in depth towards the end of this chapter. Also of relevance is the netrin family of

proteins, which are structurally and ancestrally related to LMs, and share common features with LaNt a31.

Each mammalian LM exists in a heterotrimeric α–β–γ form, of which there are 16 trimeric combinations[24] (Fig. 2.1). Each LM heterotrimer is named based on its' constituent chains i.e. the LM heterotrimer composed of LM α1, β1, and γ 1 is known as LM111. Observation of purified LM molecules by electron microscopy after rotary shadowing indicated that the three chains assemble to form an asymmetrical cross-shaped structure, with a long arm of around 75 nm in length, and three short arms of 10 nm – 60 nm[25-27]. Out of all possible combinations, LM111, 121, 211, 221, 213, 212, 222, 3a32, 3a11, 3a21, 3a33, 3b32, 411, 421, 423, 511, 521, 523[28] have been detected in basement membranes, but their expression is often tissue specific[29,30]. Although there are many conserved regions between LM isoforms, each LM chain has a different set of properties, and it in part because of this that BMs can exhibit such context and tissue specificity.

The specific properties of each LM chain arise from the complex make up of the LM chains (Fig. 2.1). Working from the C-terminus to the N-terminus, the archetypal LM chain comprises of LG domains, LCC domains, L4 domains, LE domains, and LN domains, all of which are described in detail below.

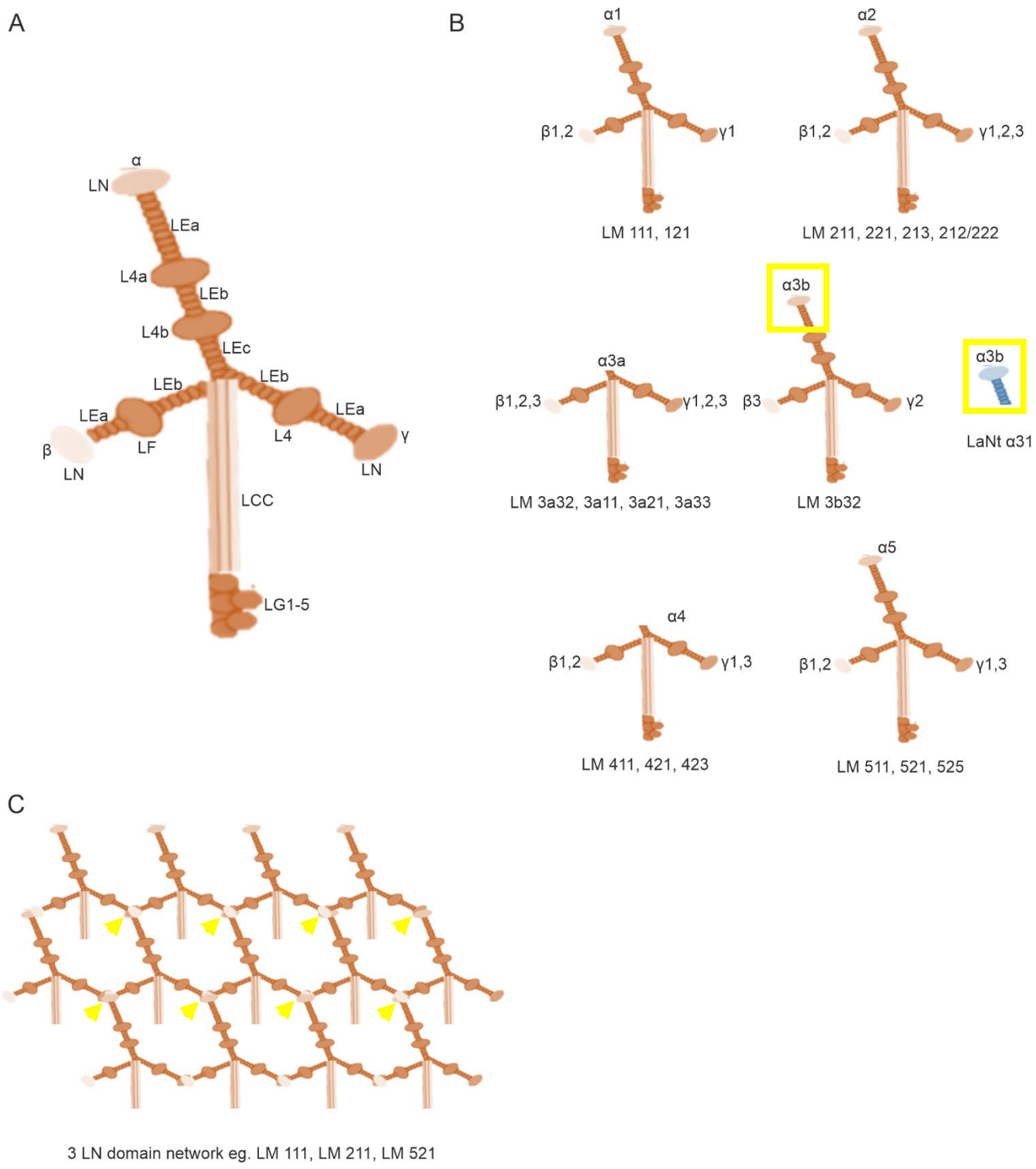

Figure 2.1. Schematic diagram of possible LM heterotrimers. A) Domain structure of the archetypal LM. B) Diagram of all described LM heterotrimers arranged by α chain. Yellow boxes highlight perfect homology between α3b and LaNt α31. C) Diagram of a 3 LN domain LM network. Abbreviations: LN, laminin N-terminal domain; LE, laminin epidermal growth factor-like repeats; L4, laminin 4 domain; LF, laminin four domain; and LG, laminin globular domain. Yellow arrowheads indicate αβγ ternary nodes. Adapted from Schéele, S., Nyström, A., Durbeej, M. et al. Laminin isoforms in development and disease. J Mol Med 85, 825–836 (2007). https://doi.org/10.1007/s00109-007-0182-5, figure 1[28]

2.3.2 Laminin globular (LG) domains

The LM globular domains (LG domains) are five (LG1-5) tandemly arranged globular domains located at the C-terminus of LM α chains, and are subunits responsible for the binding and interactions with cell surface receptors[31-34]. The LG domains are a hotspot for post-translational modifications, with N-glycosylation able to occur at one to three acceptor sites, and processing occurring between the LG3 and LG4 domains of the α2, α3, and α4 chains[33,34].

2.3.3 Laminin coiled-coil (LCC) domains

The LM coiled-coil domain (LCC) forms the basis of the LM 'long arm'[35] and is essential for LM trimerization[31,36]. This is facilitated through a left-handed coiled-coil between the α, β and γ chains[37]. LM heterotrimerisation is an intracellular process, whereby the β and γ chains form a disulphide linked dimer[36] which is retained in the cell cytoplasm until the incorporation of the α chain[38]. Secretion of the trimer is then mediated by the secretion signal of the α chain[38], allowing for deposition into the ECM[39]. It is worth noting that because the secretion signal on the α chain, it is possible for its secretion independent of the β and γ chains[38], which is particularly relevant when considering the non-LMs splice isoforms generated from the LAMA3 gene. In addition, β3 and γ2 chains have been found to be secreted independently in cancer situations[40]. Not all LM chains can trimerise with each other, suggesting the LCC domain contributes to the which LM chains can trimerise with each other. Indeed, less LM isoforms than are theoretically possible based on the number of chains have been identified[25,28].

2.3.4 L4 domains

The LM short arms contain domains which are important for LM network polymerization and have been implicated in cell receptor binding. Located within the LM short arms are the LM IV (L4/LF), the LM-type epidermal growth (EGF) factor-like (LE) domains, and the LM N-terminal (LN) domains[31]. L4 domains are found in the short arms of the α1, α2, α3b, and α5 chains separating stretches of LE repeats, and are also found in the BM

protein perlecan[41]. The functions of the L4 domains are not well understood, although the structure of the domains is similar to ephrin-binding domain of ephrin receptors, and MAM adhesion domains in various other eukaryotic cell-surface proteins, suggesting that the L4 domains could play a role in cell adhesion in the context of the LM trimer[41].

2.3.5 Laminin-type epidermal growth factor-like (LE) domains

Also residing in the short arms of α, β, and γ LM chains are tandem repeats of LE domains[42]. LE repeats are similarly found in LaNts, netrins[43], agrin, perlecan, usherin and in protocadherins. Though the binding capabilities of LE repeats remain elusive, LE repeat-induced EGFR signalling has been suggested from the proteolytically cleaved N-terminus of the LM γ2 chain[44,45], although whether this putative interaction is of biological has not been established. The exact number of LE repeats found in the LM chain short arms differs between chains, and these domains act as spacers between the various domains situated within the short arms[31].In addition to the structural role LE repeats play, they may also bind or signal in different contexts[31].

2.3.6 Laminin N-terminal (LN) domains

LN domains are globular domains of 252 to 264 amino acids, found at the amino terminus of the α1, α2, α3b, α5, β1, β2, β3, β4, γ1 and γ3 LM chains and in some other ECM proteins including LaNts and netrins, but not in LM α3a, α4 chains and netrin g2 . Within LN domains there is strict conservation of six cysteine residues, and 14% of all residues in LN domains are conserved. Once the domains are stratified into the α, β and γ LMs, this amino acid identity increases to 72% sequence between α1 and α2 and 77% between α3b and α5, 72% between β1 and β2 LN domains, and 64% between the γ1 and γ3 LN domains[46]. The lowest conservation within groups is between β3 and the β1 and β2 LN domains (38% and 42% respectively).

LM interactions have been studied over many years with important early work establishing the core “three-arm” model; LM polymerization can only occur where the LMs involved have LN domains on all three of their constituent chains [47]. This leads to the situation where LM3a32, the major

LM expressed in skin and LM411, a major blood vessel LM, cannot polymerize [48]. Moreover, the LN interactions must be heterotypic; in experiments with recombinant LM111 heterotrimers, deletion of any single LN domain or replacement of β1 LN or γ1 LN with α1 LN abolished polymerization[49].

The full process of assembly is divided into a temperature-dependent oligomerisation step and a calcium-dependent polymerization step, with calcium ions required to induce a conformational change in the γLN domains. In vitro binding analysis of LM short arm interactions in one study detected binary interactions with dissociation constants in the 0.01–1 μM (KD) range for the majority of α-α, α-β, α-γ and β-γ pairings [9]. However, the reported α5-α5, α5-β1 and α5-γ1 interactions have not been detected in subsequent studies, with only weak interactions being detected between the β1 and γ1 short arms (KD ≥5 μM) [9]. Consistent with the three-arm model, stable complexes were only observed in vitro when all three short arms (α5, β1 and γ1) were added together (KD ≥0.8 μM)[50] and have revealed that the ternary node assembly is a two-step process, comprised on an initial rapid but unstable interaction between β and γ LN domains that forms and unstable βγ pair that is only then stabilized through integration of the α LN chain in a reaction with slower on/off kinetics [50].

2.3.6.1 LaNt α31 organization

The *LAMA3LN1* transcript encodes a LaNt α31, a functional protein that differs in terms of domain organization compared to the LMs[51]. LaNt α31 is comprised of the LM α3 LN domain followed by a short stretch of LE domains and a unique C-terminal region with no conserved domain architecture. This protein is relatively unstudied. LaNt α31 is widely expressed in human tissue[52], influences cell behaviour[51,53,54], and is associated with breast cancer cell invasion[55] and re-epithelialization during wound healing[53], all of which are discussed below. The deep biological significance of this protein remains elusive, and this thesis aims to uncover the role of LaNt α31 in vivo.

2.3.7 LN domain structure

The crystal structures of LM α5LN, β1LN, γ1LN domains have been solved and these indicate that all LN domains share a similar overall structure. Of particular relevance to this thesis is the structure of the α5 LN domain, as this is highly homologous with the α3b LN domain in LaNt α31. In addition, numerous human diseases arise from mutations with the LM LN domain (Table 2.1), and many have been modelled in mice through making analogous LN domain mutations. Comparison between the phenotypes of these animal models and the LaNt α31 transgenics described in chapter 6 is useful when interpreting the outcomes of LaNt α31 overexpression.

Two regions of the LM α5 LN domain are conserved across vertebrates and invertebrates; termed the Patch 1 and Patch 2 motifs [50]. Patch 1 (“back face”) is not thought to be involved in LM polymerization, but may play a structural role in all LN domains [50,56]. The Patch 2 motif (“front face”) residues contain no potential glycosylation sites and are not conserved with β- or γ-chains, suggesting a role in LM polymerization. Consistent with this, mutant versions of residues within the patch 2 motif (L230A, E231K and E234K) all resulted in the inhibition of LM polymerization strongly supporting a role in the formation of the αβγ ternary node. The LN domain of LM α5 shares 77% homology with the LM α3b LN domain[46], which is the same LN domain found in LaNt α31[51].

The β and γ LN domains are based on the same overall structure as the alpha. However, key differences exist including the gamma chain including a calcium binding pocket and an additional loop on the beta chain. These differences in features are critical to the alpha/beta/gamma ternary node formation model. Recently the interactions to form this node were further resolved by negative staining electron microscopy[57] identifying a head to tail binding to form a triskelion i.e. each LN domain contacts two others at discrete sites within the LN fold[57] (Fig. 2.2). This triskelion arrangement becomes particularly important when comparing with netrin 4 as the crystal structure of netrin 4 revealed non-conservation of one of the binding pockets[58], the site where the alpha LN domain would normally interact. This critical difference means that although netrin 4 can interact with gamma

chains[58], the alpha chain cannot bind to complete the stable ring (discussed later in the chapter).

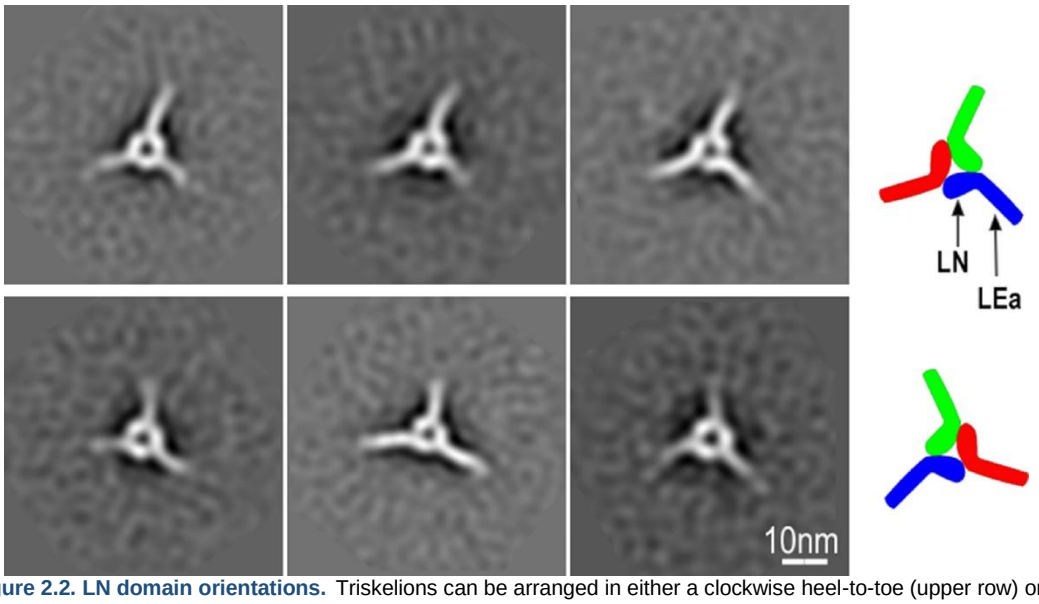

Figure 2.2. LN domain orientations. Triskelions can be arranged in either a clockwise heel-to-toe (upper row) or a counter-clockwise (lower row) orientation. This suggests that these structures are flat, lying either on one side or the other on the carbon support film. Figure taken from [57].

2.4 LM isoforms unable to form αβγ ternary nodes

Whereas the αβγ LN domain model sufficiently explains network formation of 'full-length' LMs (LM111, 211, 3b11, 511) which contain α, β and γ LN domains, this model suggests chains lacking one or more LN domains (LM3a11, 3a32, 3a21, 411, 421) either don't polymerise, polymerise through another mechanism, or that some tissues do not require a LM network. For example, LM α3a32 in epithelium lacks the α and γ LN domains, yet is a core part of the epithelial BM[59]. Likewise, LM411 is expressed almost ubiquitously throughout different vessel types, despite also lacking an α LN domain[60]. For example, LM α3a32 in epithelium lacks the α and γ LN domains, yet is a core part of the epithelial BM[59]. Likewise, LM411 is expressed almost ubiquitously throughout different vessel types, despite also lacking an α LN domain[60].

Considering that functional BMs exist without the need for three LN domains, one must assume polymerization, or at least functionality, is achieved

through the binding or other ECM components. In the case of LM3a32, it has been shown to associate with LM311[61], collagen VII[62], collagen XVII[63] and fibulin[64,65]. This array of ECM proteins could play a part in maintaining and stabilising the LM network, but the exact contributions are not clear. Additionally, LM321 and LM511 are all present in epithelial and may contribute to network formation[61].

Alternatively, if it is the case that αβγ ternary nodes are indispensable for LM network formation, LMs containing 'headless' chains could feasibly gain missing LN domains from proteolytically released LN domain-containing fragments or proteins such as LaNt α31. These proteins contain the relevant LN domains to fulfil the αβγ ternary nodes, yet do not contain the 'long arm' components and the associated domains. To consider the impact of the importance of LN-domains in different tissues, it is necessary to understand the different expression profiles of LM isoforms, and the composition of different BMs.

2.5 LM receptors

Out of all the BM components, LMs are the main proteins involved in cell-ECM adhesion. The binding capabilities of the different LM isoforms is of relevance when considering how LaNt α31-mediated changes to the LM network may affect receptor binding and downstream signalling cascades.

2.5.1 Integrins

Integrins play central roles as cell-LM adhesive devices. All integrins are composed of an α and a β subunit, with each subunit comprising a large extracellular domain, a single transmembrane domain and a cytoplasmic tail. Integrins function as transmembrane receptors to transduce bidirectional signals between extracellular adhesion molecules and intracellular cytoskeletal and signalling molecules, reviewed in[66,67]. The binding specificity of integrins is largely determined by the conformation adopted by the α and β subunits, though cellular context is also extremely important; the same cDNA transfected into two different cell lines can result in the cells acquiring different binding activities[68,69].

At least 24 kinds of integrin heterodimers have been identified[67], and out of these there are four main integrins are responsible for LM binding through the C-terminal LG domain of the LMs: α3β1, α6β1, α7β1 and α6β4 [70].α7β1 integrin has two isoforms, α7X1β1 integrin and α7X2β1 integrin, both of which have different LM binding properties[71]. Specifically, α7X1β1 integrin binds LM511 with higher affinities than LM111 and LM211, whereas α7X2β1 integrin binds more avidly to LM111 and LM211 than to LM511[66,72], illustrating the diversity of molecular binding partners of LMs, all which impacts cell behaviour.

The different integrins have different binding affinities for particular LMs. A3β1 and α6β4 integrins have a specificity for LM332 and LM511[73,74]. A6β1 integrin, on the other hand, has a much broader specificity, binding all LM isoforms but exhibiting a preference for LM111, LM332, LM511 and LM521[75,76]. α7X1β1 and α7X2β2 integrins do not bind to LM332. α7X1β1 integrin binds all LMs except LM332, with a preference for LM211, LM511 and LM521[71]. α7X2β2 integrin binds preferentially to LM111, LM211, and LM221[66]. A change in LM organization could in theory change the downstream signalling cascades and have important biological consequences.

2.5.2 Signalling through LN domains and proteolytically cleaved fragments

Although integrins bind primarily to the C-terminal of LMs, signalling through LN domain fragments and LN domain-containing proteins has been observed. Proteolytic processing of LMs has also been identified as releasing similar LN domain containing fragments from LM α1 [77], LM β1 [78], and LM α3b [79]. Some of the LN domain-containing netrin proteins and cryptic fragments have cell surface receptor binding capabilities and can act as signalling molecules. Specifically, the LM α1 LN domain binds to α1β1 and α2β1 integrins and to the heparan sulfate-containing domains of perlecan[77]. A LM β1 chain fragment generated by matrix metalloproteinase (MMP) 2 processing has been shown to downregulate MMP2 expression through interaction with α3β1 integrins[78], and a 190-kDa NH_2-terminal fragment generated by proteolytic cleavage of LM3b32 has been shown to promote adhesion, migration and proliferation through its interaction with integrin

α3β1[79]. Netrin 4 is another LN domain containing protein, discussed shortly, and a netrin 4/LM γ1 complex has been shown to signal through the integrin α6β1 receptor[80]. Direct integrin binding of LaNt α31 has not yet been conclusively proven[54], though these possibilities of LN domain signalling indeed suggest that LaNt α31 may behave in a similar manner.

The importance of integrin-mediated signalling is made clear in integrin-mutant transgenic mice. α6 integrin knockout (LM) mice exhibit a range of defects including defects in kidney and lung development, as well as skin blistering[81]. α7 integrin KO mice develop muscular dystrophy[82]. β1 integrin KO mice do not survive past embryonic day (E) 5.5[83], and β4 integrin KO mice also exhibit skin blistering, similar to their α subunit counterparts[84]. These severe phenotypes of integrin KO mice is not withstanding the fact that these examples are when only one single integrin subunit is knocked out. It is necessary to consider any non-physical effects caused by expression or cleavage of LN domain containing proteins, as this gives a further possible explanations for the phenotypes observed by LaNt α31 overexpression in 3D and in vivo (chapters 5 and 6 of this thesis).

2.5.3 Non-integrin LM receptors

Although integrins are the main and most well characterised LM receptors, other protein families exist and can also bind different LM subunits[85], which are described below.

2.5.3.1 Dystroglycans

Dystroglycan (DG) is an adhesion complex that links the cytoskeleton to the surrounding extracellular matrix in skeletal muscle and a wide variety of other tissues[34]. Dystroglycan synthesized as a single polypeptide, and then is cleaved autoproteolytically to yield a cell-surface α-subunit and a transmembrane β-subunit[86]. Following a series of complex posttranslational modifications, it is the α dystroglycan subunit responsible for LM binding[34]. α-DG binds tightly and in a calcium-dependent fashion to multiple extracellular proteins and proteoglycans, each of which harbours at least one, or, more frequently, tandem arrays of LM-globular (LG) domain. In the case of LMs, α dystroglycan binds LMs through their LG domains[34], so any situation where

BM of LM organization is changed or disrupted would have knock on effects for tissue function. Any abnormalities in the posttranslational processing of α dystroglycan result in in various congenital and limb-girdle muscular dystrophies[87]. Binding of dystroglycans to LN domains has thus far not been observed.

2.5.3.2 Syndecans

Syndecans are a type of transmembrane proteoglycans that have more recently attracted attention for their role in cell migration and adhesion[88]. The syndecan family is composed of four members, syndecan-1 and -2 (known as fibroglycan), syndecan-3 (N-syndecan) and syndecan-4 (also known as amphiglycan)[89-94]. Syndecans are composed of two domains: a 25 amino acid hydrophobic transmembrane domain and a 28-34 amino acid long cytoplasmic domain[94,95]. Syndecans bind several ECM components, including LMs, through their transmembrane domain to cell surface receptors such as integrins and EGF receptors[96,97].

Syndecans bind to multiple different regions on different LM chains and influence cell migration and attachment. Syndecan-1 and syndecan-4 bind overlapping but distinct sites of the LG4-5 domain of LM α3, and syndecan-4 also has the capacity to bind the LG4 domain of LM α1[98]. Syndecan-1, syndecan-2 and syndecan-4 are all able to bind the γ2 short arm of LM332[96,99,100]. Syndecans also interact with other LM receptors, with syndecan-4 able to interact with integrins α5β1, α2β1 and α6β4[101]. The functional implications of these types of interactions have been identified using LM α3 derived peptides, whereby clustering of syndecan-4 and β1 integrin promoted cell migration[102]. In vivo, syndecan-1 and syndecan-4 KO animals have impaired wound healing[103]. Similarly, defective wound repair is observed in mice overexpressing syndecan-1, suggesting a ‘threshold’ of acceptable levels of syndecan expression[104].

Syndecans themselves can also affect LM organization. In keratinocytes isolated from syndecan-1 mice, the LM332 deposition is dysregulated, demonstrating the importance of this receptor for correct LM organization[105]. Although direct interaction with netrins or LN domains has not been detected,

understanding the phenotypes caused by dysregulated expression of LM receptors allows for the understanding of the importance of correct BM organization, and furthermore help to interpret the data presented in the thesis when analysing phenotypes caused by LaNt α31 overexpression or dysregulation.

2.5.3.3 LM receptor

The ’67 kDa LM receptor’ (LR) is additional cell surface receptor with high affinity for LMs, and is an important molecule both in cell adhesion to the basement membrane and in signalling transduction[106]. The LR is derived from a 37 kDa protein precursor, though the way the LR is configured is not yet clear[106]. Potential routes of configuration that have been suggested are that the LR is formed from acylation followed by dimerization of the 37 kDa precursor by non-covalent bonds[107-109]. Although the name suggests specificity for LMs, the LR also acts as a receptor for viruses, such as sindbis virus and dengue virus, and is involved with internalization of the prion protein[106].

The LR receptor has also been implicated in LM related processes in cancer, including tumour cell attachment, cell migration, angiogenesis, tumour growth and metastasis[110-113]. Studies investigating LR / LM interactions are somewhat inconclusive but most data indicate interaction via the LCC region[42]. Interactions with netrins or LN domains have not been described.

2.5.3.4 Epidermal growth factor receptor (EGFR)

All LM chain short arms contain LE repeats, and although the functions of these remain elusive, LMs or LM-derived products have been shown to bind to EGF receptor in some situations. Of great interest is the LE repeat-containing fragment of LM γ2, which can be generated by MMP2 and MT1-MMP-mediated processing of LM332, can bind to EGFR and stimulate downstream signalling events (including EGFR and ERK1/2), MMP2 gene expression, and cell migration[45]. The upregulation of MMP induced by the LE domain containing fragment of LM γ2 suggests the existence of a positive feedback loop controlled by this mechanism, which may allow for tight regulation of MMP-mediated ECM degradation and remodelling. There are

no reports examining signalling from the LE repeats of the LM α3b chain or LaNt α31

2.6 Expression profiles

The greatest variation in BM make-up comes from the diversity of possible LM isoforms expressed in the BM. LM chain expression is spatially and temporally regulated, allowing the context specificity of different BMs. This leads to situations whereby different tissues have BMs composed of LMs with different numbers of LN domains; i.e. LM111 containing 3 LN domains, LM411 containing 2 LN domains, or LM3a32 containing a single LN domain. LM composition of BMs also changes throughout development, which presents an adapting and dynamic landscape.

2.6.1 Development

LMs first appeared in multicellular organisms about 500 million years ago when single cells started to aggregate and form multicellular organisms[114,115]. The expression of single LMβ and γ chains can be detected as early as the 2-4-cell embryo stage, highlighting the importance of LMs at the earliest stages of development. The earliest trimeric LMs expressed during mammalian embryogenesis are LM111 and LM511 and embryos lacking α1 or α5 chains die at an early developmental stage[116]. The LM α1 chain is primarily expressed in epithelial tissues during development, and expression deceases after birth. LM α5, on the other hand, has the most widespread distribution of all LM chains, with expression observed during development and in adults[28].

During embryogenesis, the LM α2 chain is expressed along developing muscles from E11[23]. The LM β2 chain is dispensable for embryogenesis as LM β1 substitutes for the absent chain[117,118]. In the embryo, it is upregulated during organ maturation in glomerular BMs[119], neuromuscular junctions (NMJ)[117], and smooth muscle cells in the aorta[28,118]. In the skin, LM332 expression can be detected as early as E10.5 in embryogenesis In the embryo, it is upregulated during organ maturation in glomerular BMs[119], neuromuscular junctions (NMJ)[117], and smooth muscle cells in the aorta[28,118].

In the skin, LM332 expression can be detected as early as E10.5 in embryogenesis[23,28].

Additionally, LM332 is expressed in most epithelial tissues, including the lung, intestine, stomach, and kidney[28,120]. Expression of the LM α4 chain begins at E7 of murine embryogenesis and expression peaks at E15–17[121], and expression of LM α4 is ubiquitous to BMs of the vasculature, combining with β1 and γ1[122]. At the later stages of development and following birth, LM α5 is also incorporated into vascular BMs, also combining with β1 and γ1[122]. The LM α4 chain is also found in the nerves, at the NMJ, in extraocular muscles, and adipocytes[123]. Clearly, the LM landscape is extremely dynamic during embryogenesis and changes rapidly. These changes become increasingly important when considering the investigations of LaNt α31 during development. The following tissues are of particular relevance to these studies.

2.6.2 Skin

The most abundant LMs in epithelial BMs, including the skin, are LM3a32 and LM511. LM3a32 is expressed abundantly at the dermal-epidermal junction (DEJ), whereas LM511 is expressed in the dermal vasculature and abundantly in the BM underlying the interfollicular epidermis [124,125], as well as the DEJ. Whereas LM α5 is incorporated into BMs before gastrulation, LM α3 as well as the β3 and γ2 chains are expressed at E10.5 during murine embryogenesis [126].[126]. LaNt α31 has also been shown to be present in human skin[51,52], and is further explored in mouse skin and epithelia in chapter 4 of this thesis.

Mice deficient in any of the three chains of LM332 die within 5 days of birth because of severe skin blistering[127,128]. The LM expression profiles observed in the skin are another example where the two isoforms have distinctly different properties. LM511 supports maintenance of the hair follicle stem cell niche. Follicular stem cells differentiate into hematopoietic, adipogenic, osteogenic, chondrogenic, myogenic, and neurogenic lineages[129,130], and epithelial stem cells residing in the bulge region of the hair follicle can differentiate into sebaceous gland, hair follicles, and epidermis after injury [131-

[133]. This is a very different role compared to the LM3a32 network, which acts as a supramolecular bridge between the basal keratinocytes of the epidermis and the underlying dermis[134].

LM3a32 also undergoes extensive proteolytic processing. LM3a32 is secreted as a 460 KDa protein, which is then processed to 440 KDa in low calcium conditions, and in high calcium conditions it is processed to 400 KDa [135]. These processing events result in the LM α3a chain shifting from 190/200 KDa to 160-170 KDa, and processing of the LM γ2 chain N-terminus resulting in a shift from 155 KDa to 105 KDa. The resulting, processed LM3a32 is considered to be 'mature'. The LM β3 chain of LM332 is does not undergo processing[136]. The multiplicity of processing events observed in the LM3a32 chain alone serves as a great example of how apparently subtle changes to the way that LMs are presented to cells impact many different cellular functions. This becomes relevant later on in chapters 5 and 6 when considering how the overexpression of LaNt α31 may change LM presentation.

2.6.3 Kidney

Another tissue where complex distribution patterns of LMs are seen is the kidney. Moreover, many LN domain defects have been established as manifesting in renal pathology. Nephrogenesis is a complex process during which the unique elements of the glomerular BM (GBM), mesangial matrix, tubular BM and blood vessels come together to eventually form a functioning kideny[137]. During nephrogenesis, the glomerular basement membrane initially contains LM111, is later replaced with LMs 511 and 521, but at maturity contains only LM521[138]. Studies of mice deficient in LM α5 and β2 chains have revealed that the LM α5 chain is essential for glomerulogenesis[139], whereas the LM β2 chain is important for the proper function of the glomerular filtration barrier, as the lack of LM β2 chain in mice results in a disorganized glomerular BM[140-143], and mutations to the β2 chain lead to a disorder named Pierson Syndome (discussed below). Outside of the glomeruli, the mesangium is rich in LM211 and LM411[137].

2.6.4 Lungs

LMs are essential for normal lung development, and LM isoforms expression changes throughout the lung development[144]. Studies of embryonic lung explants and organotypic co-cultures show that LM111 is important for epithelial branching morphogenesis[145], and that LM211 has a role in smooth muscle cell differentiation[144]. In vivo studies of LM α5-deficient mice indicate that this LM chain, found in LMs 511 and 521, is essential for normal lobar septation in early lung development, normal alveolisation, and distal epithelial cell differentiation and maturation in late lung development[146]. In epithelial BM of the developing lung, LM α1, α2, α3, and α5 chains are present but LM α1 is seen only in early stages while LM α2 expression decreases near the time of birth, and expression of LMs α3 and α5 remain constant[145,147].

In the adult lung, LM α5 is present in airway, alveolar, endothelial, and visceral pleura BM. Expression of LM α5 is evident beginning in early lung development and persists into adulthood[145]. The other abundant LM isoforms in the adult lungs are LM311, whereby LM α3 binds with either a β1 and γ1 chain (LM311), providing a 3-LN domain containing network[148], or LM3a32, a two LN-domain containing network[149]. In a normal lung, the LM α3 chain is distributed throughout the BM, and isolated alveolar epithelial cells isolated from lungs deposit LM311 in a fibrillar pattern[148,150].

Immunofluorescence staining of lung sections shows that normal distribution of LM α3 subunit is lost in patients suffering with idiopathic pulmonary fibrosis[151], and LM α3 subunit KO mice show worsened mortality, increased inflammation, and increased fibrosis after intratracheal administration of bleomycin[151]. Interestingly, the KO mice experienced no developmental abnormalities, and no detectable phenotype was observed compared to the control mice[151]. The reason for this is unclear, however this points to the LM α3 chain having a role in lung function and homeostasis rather than in development, as mice lacking the subunit still form lungs. Indeed, considering this, it is reasonable to suggest that any phenotype caused by LM-related mutations in the lung are likely due to disruption of the LM511 or LM111 networks during development.

2.6.5 Vessels

Vessels are another example of where LM expression changes after development, with multiple LM isoforms expressed each with different properties[60]. LM411, containing two LN-domains, is detectable throughout development and expression is maintained throughout adulthood. In contrast, for LM511, a 3-LN domain isoform, expression only begins in the vasculature at 3-4 weeks[122]. Expression also varies depending on the type of blood vessel (capillary, venule, postcapillary venule, vein or artery) and their maturation state[60,152,153]. In adults, LM α4 is the most ubiquitous component expressed as part as LM411 in the vessel wall, followed by wide expression of LM511. LM α2 expression is observed in some larger vessels, mainly contributed by the smooth muscle cells surrounding these structures. Additionally, the LM α3b chain has been detected in blood vessels, including capillaries, but the role it plays is not yet clear[154].

Although the postnatal incorporation of LM511 into vascular BMs has been observed, the functions of vascular LMs are still being uncovered. Leukocyte transmigration is observed at areas or low LM511 expression[155], and recent data has highlighted that LM511 stabilises cell junctions and barrier functions of the vessel BMs, severely restricting leukocyte transmigration[156].

Only LM α4, and not α5, is observed in normal lymphatic vessels[157]. In this environment, LM α4 actively supports the migration of leukocytes and promotes leukocyte extravasation[158-161], which is undoubtedly essential for a functioning lymphatic system. The LM α5 chain is only detected in the lymph vessels in ovarian carcinomas[162], where the presence of α5 chain LMs in the BM region of tumour lymphatic vessels suggests that these LMs could inhibit cell migration through the endothelium in these vessels. A stark contrast between LM411 and LM511 is the 2-LN domain network vs. the 3-LN domain network, whereby the αβγ ternary node in LM511 results in a more stable BM, preventing the transmigration of leukocytes. As LM511 appears to inhibit or block transmigration through the vessel BM, one could envisage a situation whereby disruption of LM511 could weaken vessels and allowing transmigration off cells into the surrounding tissues.[60]

Additionally, the LM α3b isoform is expressed throughout vasculature[154], though the role it plays there is not well understood. Published data from the Hamill Lab[52] and from chapter 4 of this thesis have revealed that LaNt α31 is also highly expressed in the vasculature, with the most recent data suggesting that LaNt α31 has higher expression in larger vessels. The role of LaNt α31 in vasculature is still being uncovered, although it's interactions with the 3-LN domain LM511 or 2-LN domain containing LM411 comes under the spotlight in this thesis.

2.6.6 Stem cell niches

LMs are key constituents of multiple stem cell niches. Indeed, LMs are commonly used in research as substrates to either cultures different types of stem cells or to differentiate cells[114]. To give an overview of the diverse functions of LMs in supporting stem cell maintenance and differentiation: LM111 primes inner cell mass pluripotent stem cells for differentiation[163], and is one of the most common substrates for growing pluripotent stem cells. LM121 supports neurite outgrowth [164]. Both LM211 and LM221 initiate embryonic stem cell differentiation to striated muscle fibres[165]. LM411 and LM421, together with LM521 drives differentiation of human embryonic stem cells into endothelial cells[166]. Both LM511 and 521 can alone support pluripotency of human embryonic stem cells[167], and LM521 also maintains pluripotency and promotes robust proliferation of stem cells[167]. Moreover, LM521 enables clonal expansion of pluripotent human embryonic stem cells[159,168]. LMs 411, 421, 511 and 521 can all individually support keratinocyte growth[169]. Finally, LM523 induces differentiation into photoreceptor progenitors[170].

The importance of LMs in stem cell maintenance is clear. Moreover, the correct LM network is required to maintain stemness, and a change to that network may cause differentiation defects and lead to deleterious consequences, something which could be caused by dysregulation of LMs or LM-related proteins such as LaNt α31.

2.7 Breaching BMs

The molecular ‘unpicking’ of LM networks becomes increasingly important in normal physiology when we consider how cells traverse basement membranes. For example, circulating immune cells are required to travel to the site in infection or injury which requires passing through one or multiple basement membranes. How this happens is not fully understood, although it is appreciated as a multi-level process involving regulation by the BM composition, physical dismantling, and enzymatic degradation[171].

2.7.1 BM itself dictating breach points in normal biology

When considering vascular BMs, containing predominantly LM411 and 511, it is clear that the LM isoforms within BMs dictate the extravasation possibilities through vessels. LM511 specifically contributes to endothelial tightness by stabilizing VE-cadherin at junctions and by downregulating expression of CD99L2, correlating with reduced neutrophil extravasation[156].[156]. Moreover, endothelial cells bind preferentially LM511 over 411, further inhibiting cell migration through the vessel wall[156].[156]. Specifically, results suggest that endothelial adhesion to LM511 via β1 and β3 integrins mediates RhoA-induced VE-cadherin localization to cell-cell borders, and while CD99L2 downregulation requires integrin β1, it is RhoA-independent[156]. Whilst vascular BMs are perhaps the most typical BMs where cellular transmigration is commonplace, there are many more instances in health and disease where BM breaching occurs, particularly during angiogenesis or in the progression of inflammatory diseases and cancer.

2.7.2 Cell dependent breaching (physical methods)

Whereas the tissue-specific composition of BM LMs can influence how easily a BM can be traversed, different cell types have different features which can allow them to cross the BM. Neural crest cells, leukocytes, and cancer cells can all cross the BM[172-174]. These cells use multiple of mechanisms to open BMs and/or degrade or rearrange existing proteins to create the portal to travel through.

Physical methods of BM breaching have been elegantly studied in vivo using C. elegans as a model organism. In BM breaching in C. elegans, anchor cells form invadopodia, which are invasive protrusions found at the matrix-opposed edge of the cell. This process is not fully understood, but elegant studies in C. elegans have helped to generate a model of basement membrane 'unzipping', where through physical and enzymatic methods cells can traverse the BM, with small amounts of reorganization and remodelling, but with overall minimal amounts of BM degradation[175].[175]. In cancer situations, cancer-associated fibroblasts (CAFs) facilitate the breaching of the BM in a MMP independent manner. CAFs pull, stretch, and soften the BM leading to the formation of gaps through which cancer cells can migrate[176].

2.7.3 Enzymatic BM disrupting proteins

Many of the mechanisms for breaching the BM overlap, and cells use a combination of physical and enzymatic, and non-enzymatic methods to breach the BM. For enzymatic degradation of the BM, MMPs are responsible for degrading the BM. A hallmark of cervical, oral, and breast cancers is upregulation of MMPs, which makes it easier for cancer cells to traverse the degraded BM[177-179]. MMP-mediated LM processing has been discussed previously, and it is clear the impact that MMP expression has on LM network modifications. A preprint study has shown that overexpression of LaNt α31 increases MMP activity, which in turn causes an increase in LM processing. This finding comes from 2D in vitro studies, so the effect on an intact 3D membrane is unclear, but there is one would be surprised if BM integrity and composition in vivo would remain unaffected in vivo[54].

2.8 LN domain interactions in health and disease

LN domain binding is not only interesting from a purely fundamental science perspective. There are many situations where mutations to the LN domain cause genetic diseases causing a great amount of suffering. To be able to cure these diseases in the future, the first step is understanding the effects of mutations on the LN domain, and the impacts these have on health. The LN

domain mutations discussed below cause a failure of LM network polymerization and are included to allow comparison of the phenotypes caused by these mutations to the phenotype of LaNt α31 dysregulation in vivo.

2.8.1 LN domain mutations

Thankfully, LN-domain related diseases are rare, although due the tissue-specific LM composition of basement membranes, several different syndromic disorders are observed depending on which LM isoform harbours the mutation (Table 2.1). Each affected LM results in a distinct set of syndromic disorders reflecting isoform-specific distribution and functions.

Table 2.1: Pathogenic LN domain mutations

Protein	Mutation	Effect	Phenotype	Refs
LMα1	Y265C	LN interaction	[mouse] Retinal vasculopathy	180
LMα2	C79R	LMpoly/ fold^{c}	[mouse] mild muscular dystrophy	181
	C86Y	fold^{p}	MDC1A	182
	Y138H	LMpoly^{p}	MDC1A	183
	W152G	fold^{p}	Limb-girdle–type dystrophy	184
	S157F	fold^{p}	MDC1A	185
	Q167P	LMpoly^{c}	Limb-girdle–type dystrophy	186
	S204F	fold^{p}	Mild muscular dystrophy, mild proximal weakness	187
	L243P	fold^{p}	Mild MDC1A	184
	S277L	fold^{p}	MDC1A	188
	G284R	LMpoly^{p}	limb-girdle–type dystrophy	184
LMα5	R286L	LMpoly^{c}	Focal segmental glomerulosclerosis, hearing loss, craniofacial dysmorphism, limb development	189
LMβ1	E215K	LMpoly^{c}	[fly] heart development defects	190
	V226E		[fly] heart development defects	190
	G286R		[fly] heart development defects	190
LMβ2	R246W	LMSecretion /	End-stage renal disease, nephrotic proteinuria, diffuse mesangial sclerosis,	191-194
	R246Q	Fold	focal and segmental glomerulosclerosis, microcoria, lens abnormalities, nystagmus hypotonia, cognitive defects, muscle delay	
	V79del	LMpoly^{p}	Retinal detachment, cataracts, progressive vision loss, diffuse mesangial sclerosis, end-stage renal disease	195
	S80R	LMpoly^{c}	Nephrotic proteinuria, atypical diffuse mesangial sclerosis, myopia, retinal detachment. [mouse S83R] Detrimental on Alport syndrome background	142,193
	H147R	LMfold^{p}	Nephrotic proteinuria, diffuse mesangial sclerosis, proliferative glomerulonephritis, hypertension, heart failure, microcoria, retinal detachment, lens abnormalities	196
	D167Y	LMSecretion ^{p}	End-stage renal disease, myopia, retinal detachment, severe visual impairment	197
	L139P	LMfold^{p}	Diffuse mesangial sclerosis, lens abnormalities, severe visual impairment, hypotonia, muscle delay, cognitive deficits	193
	S179F	LMfold^{p}	End-stage renal disease, focal and segmented glomerulosclerosis, retinal detachment, severe visual impairments	198
LMβ3	E210K	Splicing^{c} + fold^{p}	Skin fragility, nail dystrophy, alopecia	199

2.8.2 Pierson syndrome

Pierson syndrome was first described in 1963[200] when two siblings presented with congenital nephrotic syndrome and peculiar eye abnormalities. Such was the severity and rapid onset of these symptoms, that neither sister survived the first 2-weeks of life. Pierson syndrome was later discovered to result from mutations in the LAMB2 gene, which encodes LM β2, and which is highly expressed in the glomerular basement membrane, multiple structures in the eye including the lens, retina and cornea, and neuromuscular synapses [117,201-203]. The two defining symptoms of Pierson Syndrome are congenital nephrotic syndrome that rapidly progresses to end-stage renal failure, and microcoria, however not all patients present with both issues, and many patients develop additional complications of motor delay, speech difficulties, intellectual disability, and seizures[204]. In humans, the histopatholgical findings manifest as mesangial sclerosis accompanied by crescent formation[205], although these histopathologic characteristics are tough to reconcile with mouse models where there are no major changes to the glomeruli[119,206].

Indeed, the spectrum of related phenotypes arising from mutations in the LAMB2 gene is vast, with at least 50 discrete mutations from 40 families identified. The severe forms of the disease are associated with KO mutations. However, the majority of pathogenic missense and indel mutations cluster in or near the LN domain and result in milder forms of the disease, with many patients surviving into adolescence and early adulthood (Table 2.1).

One of the earliest of LM β2 LN domain mutations characterized was R246W, which is characterized by severe end-stage renal disease and microcoria and was independently observed in five unrelated families with nonsense mutations on the second allele[207]. The high conservation of this arginine has led to suggestions that mutations hamper LM polymerization and in vitro studies revealed that although this mutant was able to polymerize, they did so substantially less effectively than the wild-type protein[192]. However, mutations to R246 also lead to reduced abundance of LM in BMs, likely due to protein processing being disturbed[193]. A second

mutation in the same residue, R246Q, resulted in severe glomerular abnormalities and impaired the secretion of LM[141]. Together these data paint a picture that this arginine has a key role in protein folding. A second well-studied missense mutation, S80R, affects the highly conserved βa-βb and is known to prevent LN-LN domain interactions and induce loss of polymerization in vitro [9,56,141,193]. The importance of this region was further highlighted by identification of a separate case with a V79del mutation [195]. Patients with these mutations present with milder cases of Pierson Syndrome, presenting with atypical diffuse mesangial sclerosis, retinal detachment and myopia[195].

Other mutations found within the β2LN domain include H147R, L139P, D167Y[197], and S179F with variable phenotypes (Table 2.1). H147R was tested in vitro and yielded similar effect to R246Q in terms of a partial reduction in polymerization ability. The D167, H147 residues lie adjacent to core residues R246 and W172 that are involved in LN interaction, suggesting partial destabilization of these residues, rather than full disruption may account for the milder phenotypes. L139P and D167Y mutations predicted to affect the fold of the LN domain are within close proximity to each other, as well as R246, suggesting this region of the LN domain is particularly sensitive to changes. L139P, which is expected to cause major LN domain misfolding due to interference in the hydrophobic core, is associated with a particularly severe phenotype; all three patients with this mutation did not survive beyond the first year of life[197192194].

2.8.3 MDC1A

As the LM α4 chain lacks an LN domain, it is unable to polymerize and the result is a weakened BM. LM α4 and LM α2 also differ in their receptor binding interaction repertoire and affinities, for example, LM α2 can bind integrin α7β1 whereas LM α4 cannot, and LM α4 has weaker affinity for α-dystroglycan [66]. Comparison between missense mutations and KO mutations provides a means to differentiate between polymerization and receptor-mediated effects although this is complicated by not every affected tissue expressing LM411. Recent work (described below) has begun to exploit the presence of LM α4 in MDC1A patients to rescue the phenotype.

In LM α2 KO conditions MDC1A presents with disabilities of the proximal and distal limb muscles, with patients unable to walk more than a few steps unaided [208,209]. Weakness in facial muscles result in patients having weaker sucking and swallowing capabilities, which may require a feeding tube, and cases with intellectual disability and epilepsy have been have also been reported [208,210,211]. Life-threatening problems arise in MDC1A from failure of the respiratory muscles, which may require the assistance of mechanical ventilation [211].

Many mutations have been reported throughout LAMA2's 65 exons in MDC1A and are catalogued in the Leiden Open Variation Database-powered LAMA2 gene variant database (https://www.lovd.nl/LAMA2) Of particular interest here are the point mutations affecting the LN domain, which again contains a cluster of pathogenic missenses or in frame deletions[181,182]. For example, a point mutation in the highly conserved CxxC motif, C79R, led to the onset of a milder form of MDC1A, which showed no mortality in mice but did affect the myelination of Schwann cells in the spinal roots and the stability of the skeletal muscles[181]. This amyelination and dystrophy were not attributed to a change in abundance or mislocalization of LM α2, with normal protein levels and indirect immmunofluorescence revealing no change in distribution compared to the WT mice[181]. Despite this, in vitro assays confirmed a dramatic effect on LM polymerization, although this may be due to disruption of the domain fold rather than loss of a residue involved in LN-ternary node formation[181].

Other pathogenic missense variants include Q167P, Y138H, G284R on the surface of α2 LN domain and C86Y, W152G, S157F, S277L, S204F, L243P in the interior [212]. The S204F mutation lies at one extreme of the phenotypic spectrum, whereby the patient was misdiagnosed with a peripheral neuropathy. The S204F mutation causes a mild proximal weakness, and muscle biopsy revealed subtly depleted LM α2 expression, diffusely upregulated LM α5 expression, and depletion of LM α2 in intramuscular nerves [187]. To the other extreme, Q167P maps to the face of the LN near the residues involved in polymerization and causes a 60% drop in in vitro polymerization capability, and this leads to more severe ambulatory muscular

dystrophy [207]. More severe still, G284R causes proximal weakness, with a loss of functional gait with age, accompanied by frequent falls, and epilepsy. This is predicted to be caused by defective LM network polymerization, though this is yet to be confirmed[184].

2.8.4 LAMB3 – Junctional epidermolysis bullosa (JEB) LN domain mutation

LM β3 is highly expressed in most epithelial tissues where it forms a heterotrimer with LM α3a or α3b and with LM γ2 [213,214]. The resulting heterotrimers have either one or two LN domains and are unable to form independent polymers in vitro [47,215]. One would therefore assume that LN domain mutations would be tolerated for this LM chain. However, patients with mild junctional epidermolysis bullosa (JEB) were identified where the pathogenic mutation caused E210K in combination with a nonsense or frame shift mutation on the other allele, and a phenotype of trauma-induced blisters, nail dystrophy and alopecia [199,216,217]. For comparison, homozygous KO of LM β3 (or LM α3 or LM γ2) leads to much more extensive skin blistering complications and early lethality [127,128,218,219].

Interpretation of the E210K mutation is complicated by the affected base-pair being at the splice junction of exon 7. The equivalent change in a knock-in mouse model of JEB led to skipping of the out-of-frame exon 7, generation of a premature termination codon and no detectable LM β3 in the mice skin. However, in humans, miss-splicing has been reported for some, but not all patients, and this miss-splicing can be rescued by second site mutations leading to revertant mosaicism [220]. Separate analysis has also suggested that numerous alternative splice products are produced, including some full-length transcripts. Modelling of the E210K mutation against the LM β3 crystal structure indicates the change affects a residue on the surface of the LN domain that is unlikely to be required for LM polymerization, but which is also not predicted to affect protein folding or secretion [221]. The most commonly occurring in-frame deletion, is predicted to remove several of the central β-strands and would disrupt the fold. Overall, therefore, the evidence for these patients does not point toward a LM polymerization effect but does suggest a role for the LM β3 LN domain in protein function.

Further evidence indicating the importance of the LM β3 LN domain was obtained in experiments where skin equivalents were generated from keratinocytes expressing either full-length LM β3 or LM β3 with the LN domain deleted and the resulting cultures then grafted onto immunodeficient mice [222]. Analysis revealed that the LN deleted versions displayed subepidermal blistering and erosions, and prominent granulation tissue. These phenotypic outcomes were not associated with reduced LM332 immunoreactivity at the dermal-epidermal junction but with poor quality hemidesmosome adhesion complexes. Consistent with these data, the LM β3 LN domain has been shown to directly influence stable adhesion complex formation [223]. Together these data indicate that LN domains matter to tissue function, but that function may not be entirely dependent on their role in mediating LM-LM interactions. This consideration is important to keep in mind when interpreting the data in chapter 6 of this thesis.

2.8.5 LAMA5 mutations

Of particular relevance to this thesis, a mutation (R286L) within the PLENGE sequence of the LM α5 LN domain, necessary for LM network polymerization, was identified in humans giving rise to a syndromic developmental disorder characterised by defects in kidney, craniofacial, and limb development, and a range of other craniofacial defects[189]. The sequence of the affected residue, and those residues up and downstream of the site are highly conserved in the LM α1, α2, and α5 subunits, allowing authors to study the impact of this mutation using established protocols for assessing LM network polymerization. Following identification of this mutation in a child, authors generated recombinant proteins of LM α1 harbouring the analogous mutation and carried out Schwann cell assays and solution-based polymerization assays, identifying that the equivalent mutation in the LM α1 LN domain (R263L) does not allow for polymerization[189]. Transgenic mice harbouring the analgous mutation (R291L) were generated using CRISPR-Cas9,and displayed a phenotype mirroring that seen in humans, discussed below.

2.8.6 Mouse models of LN domains deletions/mutations

LN domain mutations in humans are rare as they are often incompatible with life. Transgenic mouse models of LN domain mutations and deletions have provided and continue to provide an incredible opportunity to gain a deeper understanding of LN domain functionality in vivo. Mice contain orthologs of all LM genes found in humans, including splice isoforms such as LaNt α31, with the mirroring isoforms performing functionally identical roles. Many of the phenotypes caused from mutations in LMs in humans are recapitulated in mice, which is described in detail in the following paragraphs.

Mice with LM β2 LN domain mutations or deletion of the LM β2 LN domain exhibit renal defects, and, although viable at birth, become progressively weaker and die between postnatal day 15 and 30[117,119,224-227]. The mouse LAMB2 S83R in mice (analogous to the human S80R mutation) has been shown to inhibit LM polymerization on Schwann cells in vitro[142]. In humans, this mutation manifested as late onset proteinuria and mild diffuse mesangial sclerosis and tubular atrophy. Transgenic mice were generated expressing the LM β2 S83R mutation under the control of a mouse nephrin promoter on a $Lamb2^{-/-}$ background, limiting LM β2 S83R expression to podocytes[142].

Surprisingly, mice homozygous for the S83R mutation alone did not exhibit any phenotype. The authors hypothesised that the murine model lacked contextual factors required to elicit the pathogenicity of the LAMB2 S83R mutation and may act as a modifier allele in mice. To test this, they crossed the LAMB3 S83R mice with an existing mouse model of Alport syndrome, harbouring the $Col4a3^{-/-}$ mutation. On the $Col4a3^{-/-}$ background, even heterozygous $Lamb2^{+/-}$ mice showed a significant reduction in survival compared with $Lamb2^{+/+}$; $Col4a3^{-/-}$ littermates, displaying glomerulosclerosis, crescents, and tubular protein casts in the kidney, indicating a dominant pathogenic effect of the LAMB2-S83R protein[142], highlighting the complex interplay of BM components, and how different phenotypes can manifest in transgenic mouse models[142].

Additionally, LM α1 Y265C[180] and LM α2 C76R[181] LN domain mutations have been described in mice. Both of these mutations prevent LM polymerization.

The LM α1 Y265C mutation led to retinal vasculopathy in mice, whereas the LM α2 C79R caused a mild muscular dystrophy[180,181]. These mutations have not been described in humans but again connect LM networks dysfunction with specific phenotypic outcomes dependent on which LM is affected.

Transgenic mice harbouring the Lama5 R291L to mimic the human LAMA5 patient described above have also been generated using CRISPR-Cas9. These animals displayed defects in foetal development and growth, as well as gross developmental defects including syndactyly[189]. Whereas the Lama5 KO mouse phenotype extends to development of exencephaly, defective hair follicle and tooth morphogenesis, renal agenesis and significant defects in placental vascularisation[228], all of these features are absent or considerably reduced in Lama5 R291L mice[189]. This further illustrates how mutations affecting polymerization can have severe consequences that differ from total LM KOs. The phenotypes observed in the Lama5 R29L mice share similarities to what is observed in the LaNt α31 transgenic mice described in chapter 6, and point towards a failure of network polymerization caused by LaNt α31 overexpression.

2.8.7 Other animals

Non-mammalian animal models provide a further tool to investigate LM polymerization. Random mutagenesis screens in Drosophila have led to identification of three LN domain mutations in LM β1 that lead to heart developmental defects, E215K, V226E, and G286R[190]. Of these, E215K was tested in in vitro assays and reduced polymerization[207]. LaNt α31 has not been identified in drosophila, but generating transgenic LaNt α31 expressing drosophila lines could represent a useful model system to gain mechanistic insight in to LaNt α31 biology.

2.9 Rescuing LN domain defects

The standard toolbox of gene and protein therapy approaches are available to treat LN domain disorders. However, the large size of the LM genes coupled to the requirement of producing, purifying and delivering sufficient quantities of recombinant therapy-grade heterotrimeric LMs presents some

additional challenges. Despite these challenges, some work, such as adding LM521 to blood stream, shows promising results in terms of rescuing some aspects of Pierson syndrome[229]. Another alternative for some LM disorders, is to upregulate expression of a compensatory LMs, such as LM α1 in LM α2-deficient individuals. Indeed, some encouraging progress has been made in this area using guide RNA to target the LM α1 promoter with an inactive Cas9 coupled to VP160 transcription activation domain which led to increased muscle expression of LM111 [230].

A particularly innovative solution that exploits the knowledge gained through studying LM polymerization and which counteracts to some of the inherent LM size problems is use of smaller protein chimeras to act as linkers [231-233]. Two such “Frankenstein” proteins have been created, one which fuses a functional LN domain with the LM binding region of nidogen, and second that is either a miniature form of the protein agrin (mini-agrin) containing only the LM-binding and α-dystroglycan binding regions or fusion between LM-binding domains of agrin and dystroglycan domain of perlecan. In MDC1A, LM411 is upregulated but cannot compensate for LM211 dysfunction. Here the nidogen/LN domain chimeric protein can bind to the γ1 chain of LM411 via the nidogen region and then effectively provides the missing αLN domain needed to convert LM411 into a polymerization competent protein [232].

The mini-agrin chimera can be used in concert with the nidogen chimera to compensate for LM α4 relative inability to binding α-dystroglycan [234,235]. In conditions where the patient harbours missense LN mutations, only the nidogen fusion would be required, whereas for KO both the LN/nidogen and mini-agrin would be necessary. Very promising results have been observed with these chimeras in mouse models paving the way for development into human therapies. Moreover, by switching the LN domain in the fusion from an αLN to βLN, it is likely to also be effective for other Pierson syndrome patients. It is through understanding of LN domain interactions that these therapies are possible. The therapies described all work of the principle of allowing LM network polymerization. Though our understanding of the role of LaNt α31 is still developing, one wonders if LaNt α31 may one day turn out to be a suitable protein to modify LM network polymerization, discussed below.

2.10 Non-LM LN domain proteins

While the importance of LMs is clear, additional members of the LM superfamily exist. These LM related proteins are shorter proteins than the full-length LM chains and contain the LM LN domain, and importantly do not contain LCC or LG domains, and are not required to form part of a heterotrimer. These include LaNt α31, netrin 4 and proteolytically released cryptic LN domain containing fragments. LaNt α31 shares many structural similarities with the netrin family of proteins. By understanding the biological function and protein structures of the netrin family, perhaps light can be shed on the functions and *raison d'être* of LaNt α31.

2.10.1 Netrins

The netrins are a family of proteins that are structurally and ancestrally related to LMs [236,237]. Netrins are most highly expressed in subsections of the brain and nervous system during development although netrin 1 can also be found in spinal cord neurons, oligodendrocytes and in the ovaries, and netrin 4/β in kidney, ovary, and heart. Epithelial expression has also been identified in the epithelia of the pancreas, reviewed by [238]. Each netrin consists of a LN domain and short stretch of LE repeats followed by C-terminal regions that are unique to the netrins [239,240], a general protein organization similar to LaNt α31.

Netrins were traditionally viewed only as axon guidance cues, directing neurons via binding to their cell surface receptors deleted in colorectal cancer (DCC), neogenin, and UNC5 family members via their C-terminus[43,241,242] . This is no longer the picture. Netrins have since been shown to be involved in cell migration and tissue remodelling processes through binding to integrins[243] and interacting with LMs[244]. For example, netrin 1 can regulate epithelial cell adhesion and migration via the netrin 1 C-terminal binding to α6β4integrins and α3β1 integrins[242].

2.10.2 Netrin 4

Of particular relevance to this thesis is Netrin 4, which can interact with LM networks through its N-terminal domain. Netrin 4 lacks the ability to incorporate fully into an αβγ ternary node, instead only possessing the ability

to bind the γ LN domain, not the α LN domain[58].[58]. This results in a situation where netrin 4 can disrupt pre-existing BMs, but cannot strengthen ternary nodes lacking an α LN domain. Netrin 4i is most similar to β-type LN domains but importantly only the γLN domain binding pocket is conserved. The effect is a potent and dose dependent disruption of LM networks [58,244,245]. The physiological implications of this ability are only beginning to be appreciated; however, recent work has demonstrated that netrin 4 expression levels are a key determinant of basement membrane stiffness which has knock-on effects to cell behavior and particularly tumour metastasis [58,245].

Netrin 4, which contains a beta LN domain, has been shown to dismantle LM networks due to having a higher affinity LN domain than the native beta LM LN domain. Not only this, but netrin 4 lacks one of the binding faces of the LM beta LN domain, which results in netrin 4 having the capacity to disrupt LN ternary nodes, without possessing the binding domains required to stabilise the nodes[58]. Molecular unpicking of the LM network by netrin 4 leads to a softened BM, which in cancer situations leads to a less favourable microenvironment for tumour development and metastasis[246]. The effect of this basement membrane softening outside of a cancer situation is not yet known, but it is possible that unpicking the LM network could provide an easier avenue of BM traversion for cells. It is also possible that LaNt α31 has a similar effect on basement membranes.

2.10.3 Netrin 4 overexpression

Netrin 4 overexpression induces growth of lymphatic vessels and blood vessels in the skin of transgenic mice[247], and increases tumour metastasis through a several (assumed) mechanisms, whereby increased blood supply to the tumour, and an alteration in properties of the surrounding ECM microenvironment provide more favourable conditions for tumour metastasis[247]. In in vitro and in vivo assays netrin 4 has been demonstrated to increase lymphatic permeability by activating small GTPases and Src family kinases/FAK, and down-regulating tight junction proteins[247].

When adding netrin 4 protein exogenously, the effects on the ECM are even more clear. Addition of netrin 4 disrupts pre-existing LM networks through a 'de-coupling' of LM ternary nodes[58]. This network disruption leads to an overall change in stiffness of BMs, contributing to metastasis-favouring conditions[246].[246]. Moreover, addition of netrin 4 affects angiogenesis through ECM reorganization, and induces neurite outgrowth[248]. Taken together, much of these recently discovered roles for netrin 4 highlights the importance of LN domain containing, non-LM proteins, and shines the spotlight on how these network mediators can important molecules in ECM homeostasis.

2.11 Laminin N-terminus α31

In recent years, understanding of the impact of LaNt α31 on cellular behavior has increased tremendously. Through observational experiments in human and porcine tissue, knockdown and overexpression of LaNt α31 in vitro in different cell types, and in 3D cell invasion models, it appears that LaNt α31 is dynamically regulated and it is clear that dysregulation of LaNt α31 influences cell migration and can alter ECM organisaton.

LaNt α31 is expressed in the basal layer of epithelia in the skin [51], cornea [53] and digestive tract, the ECM around terminal duct lobular units of the breast and alveolar air sacs in the lung, and is widely expressed by endothelial cells [249]. Increased expression is associated with breast ductal carcinoma and in vitro adenoviral overexpression leads to a change in the mode of breast cancer cell invasion through LM-rich matrices, whereby LaNt α31 overexpressing MDA-MB-231 cells favour individual cellular-invasaion into matrigel, as opposed to multicellular streaming[250].

LaNt α31 is also transiently upregulated during re-epithelialization ex vivo burn wounds and in stem cell activation assays [53]. Specifically, during active alkali burn wound repair, LaNt a31 displayed increased expression in limbal regions of an ex-vivo porcine eye and loss of basal restriction within the cornea. Distribution returned to predominately basal cell restricted once the wounded epithelium matured, suggesting a role in wound repair[53].

In epidermal keratinocytes, siRNA-mediated knockdown of LaNt α31 impairs cell attachment in vitro over 30 minutes, and causes a reduction in 2D

scratch wound closure over 15 h[51]. In corneal keratinocytes, overexpression experiments revealed that modulating LaNt α31 levels leads to reduced migration rates and modifying cell-to-matrix adhesion [51,53,251]. Consistent with a role in matrix assembly, increased expression LaNt α31 causes striking changes to LM332, including formation tight clusters beneath cells rather than diffuse arcs. Enhanced recruitment of Col XVII and bullous pemphigoid antigen 1e to β4 integrin was observed, indicating early maturation of hemidesmosomes, and changes to focal adhesion distribution were also identified by indirect immunofluorescence microscopy[54]. In further analysis of the LaNt α31 overexpression phenotype in corneal keratinocytes, LaNt α31 overexpressing cells exhibited increased proteolytic processing of LM α3 by MMPs[251]. Inhibiton of MMP activity rescued the LM phenotypes, suggesting LaNt a31 dysregulation has further downstream consequences to cell physiology and matrix biology.

2.11.1 Comparisons of LaNt α31 and netrin 4

Whereas netrin 4 can only disrupt ternary nodes[58], LaNt α31 is a perfect α LN domain[51], and therefore has the potential to have two opposing roles; the LaNt α31 LN domain could stabilize at βγ ternary node, strengthening LM networks containing only 2 LN domains, or conversely the LaNt α31 LN domain could compete with α chain LMs and disrupt existing or developing basement membranes, preventing full network polymerization.

This disruption effect may be the case in BMs containing αβγ ternary nodes, such as LM521 in the kidney or patches of 511 in vessels. For example, if LaNt α31 can disrupt LM511, this would lead to a situation in vessels where any increase of LaNt α31 would weaken the areas of LM511 in vessels where cell transmigration across vessels is reduced. Weakening the LM511 network, and changing the matrix architecture in this way, could cause the vessels to become ‘leaky’, allowing an excess of cells to cross the vessel membrane. This is explored in chapter 6.

LaNt α31 expression is interesting as it is produced by a process of intron retention and alternative polyadenylation. If LaNt α31 could be implicated in a signalling pathway causing some sort of feedback loop, the combination of

this, combined with intron retention and alternative polyadenylation, would provide an extraordinarily precise mechanism to regulate levels of LaNt α31. All studies thus far have investigated LaNt α31 in either in vitro or ex vivo models, but the understanding of the biological importance of LaNt α31 in vivo is still in its infancy, and it is this question that this thesis will explore.

2.12 This thesis

The importance of LN domains in health and disease is clear. It is only through our understanding of the fundamental biology of LN domains that scientists have finally been able to engineer life changing solutions for those suffering from diseases caused by LN domain mutations. The first step to being able to improve human lives is first uncovering the secrets of our biology that have thus far eluded us. This thesis sets out to uncover more about the LaNt α31 protein. To do this, I have used newly generated antibodies to uncover more about the distribution of LaNt α31 in mice, I have generated new stable cell lines expressing LaNtα31and used these in 3D organotypic cocultures, and finally I have for the first time used transgenic mice to investigate the role of LaNt α31 in vivo.

2.12.1 Specific aims of this thesis

- Assess the distribution of LaNt α31 in mice (Chapter 4).
- To evaluate the effect of LaNt α31 overexpression on development of skin and corneal 3D equivalent models (Chapter 5).
- Investigate the effects of LaNt α31 dysregulation during mouse development (Chapter 6).

Chapter 3: Methods

3.1 General Materials

3.1.1 Antibodies

Rabbit polyclonal antibodies were raised against a synthetic peptide corresponding to mouse LaNt α31 residues 465-480; CLNSDSSMFSLSPRML (Eurogentec, Liege, Belgium) conjugated to Keyhole Limpet Hemocyanin (KLH). Antibodies were screened by ELISA against the unconjugated peptide then by western immunoblotting against total protein extracts from mouse keratinocytes. Screened antibodies were then affinity-purified using the unconjugated peptide. The purified antibody obtained was used for immunofluorescence (IF) at 1:200. For specificity testing, antigen depletion was performed by pre-incubating the anti-mouse LaNt α31 antibodies with the antigenic peptide (1 μM in 15 mM Na2CO3 35 mM NaHCO3 pH 9.6) overnight at 4°C. Rabbit monoclonal antibodies against the influenza hemagglutinin epitope (HA) (C29F4, Cell Signalling Technology, Danvers, MA) were used for western immunoblotting at 67 ng ml^{-1}. Rabbit monoclonal antibodies raised against type XVII collagen (clone EPR18614, ab184996) were used at 10 μg mL^{-1}. Rabbit polyclonal antibodies raised against LM332 (J18)[252] were used at 1:200 for IF (generous gifts from Jonathan Jones, Washington State University, WA). Rabbit polyclonal antibodies against laminin 111 (ab11575, Abcam) were used at 3.5 ug mL^{-1}. Mouse monoclonal antibodies against FLAG were used at at 5 μg ml^{-1} (Sigma Aldrich). Goat polyclonal antibodies against DDDDK (equivalent to Flag sequence, ab1257, Abcam, Cambridge, UK), rabbit polyclonal antibodies against 6X-His (ab137839, Abcam), and rabbit polyclonal antibodies against lamin A/C (4C11, Cell Signalling Technology) were used at 1 μg ml^{-1} for western immunoblotting. Mouse monoclonal antibodies against LaNt α31 were used at 0.225 μg ml^{-1} for western immunoblotting. Antibodies against laminin α4-subunit (clone 377b) and laminin α5-subunit (clone 504) were kindly provided by Dr. L. Sorokin (Institute of Physiological Chemistry and Pathobiochemistry; Münster University)[253]. Alexa fluor 647 conjugated goat anti-rabbit IgG recombinant secondary antibodies were obtained from Thermo Fisher Scientific

(Waltham, MA, United States) and used at 2 µg ml^{-1} for indirect immunofluorescence microscopy.

3.1.2 Cell lines and culture conditions

Telomerase-immortalised human corneal epithelial cells (hTCEpi) cells[254] were cultured in Keratinocyte Serum-Free Medium (KSFM, ThermoFisher) supplemented with 5 ng mL^{-1} EFG, 0.05 mg mL^{-1} bovine pituitary extract (BPE) and 0.15 mM $CaCl_2$ (final concentration) (all ThermoFisher). Immortalised Normal Human Keratinocytes (NHK) were a kind gift from Alexander Nyström (Albert Ludwig University of Freiburg, Germany) and were cultured in keratinocyte SFM (Gibco, Grand Island, NY, USA) with 50 µg mL^{-1} of Bovine Pituitary Extract (BPE, Gibco, USA) and 5 ng mL^{-1} of EGF (Gibco, USA). Normal Human fibroblasts (NHF) were a kind gift from Alexander Nyström (Albert Ludwig University of Freiburg, Germany), and cultivated in DMEM (Gibco, USA) with 10% Fetal Bovine Serum (FBS, Gibco, USA), 1% Antibiotic-Antimycotic (Invitrogen, Waltham, MS, USA), 4 mM of L-glutamine (Gibco, USA), and 1 mM of sodium pyruvate (Gibco, USA). Cells were cultivated in a humidified incubator at 37˚C and 5 % CO_2.KERA-308 murine epidermal keratinocyte cells[255], were purchased from CLS (Cell Lines Service GmbH, Eppelheim, Germany) and maintained in high glucose (4.5 g L-1) Dulbecco's Modified Eagle Medium (DMEM, Sigma Aldrich) supplemented with 10% foetal calf serum (LabTech, East Sussex, UK) and 2 mM L-glutamine (Sigma Aldrich). HEK293A (ATCC, Manassas, USA) cells were maintained in high glucose (4.5 g L-1) Dulbecco's Modified Eagle Medium (DMEM, Sigma Aldrich) supplemented with 10% foetal calf serum (LabTech, East Sussex, UK) and 2 mM L-glutamine (Sigma Aldrich).

3.2 General Methods

3.2.1 Cloning procedures

Restriction digests were set up with 1 µg of plasmid DNA or 100 ng of gBlock DNA, 20 U of each enzyme and CutSmart buffer (50 mM Potassium Acetate, 20 mM Tris-acetate, 10 mM magnesium acetate, 100 µg ml-1 BSA (New England Biolabs) and incubated at 37°C for 1 h. Enzymatic activity was inactivated by 20 min incubation at 65°C. PCR or cloning products were separated using 1% (w/v) agarose gels (Thermo Fisher Scientific) dissolved in 1 x TAE electrophoresis buffer (40 mM Tris pH 7.6, 20 mM acetic acid, 1 mM EDTA) containing ethidium bromide, and ran at 120V for 40 minutes. A 1Kb molecular weight marker (New England Biolabs) was used. Gels were stained with peq green (Thermo Fisher) and visualised using a UV transilluminator ChemiDoc MP System (BioRad, Hercules, CA). DNA bands were excised from the gel and purified using GenElute™ Gel Extraction Kit, following manufacturer's protocol (Sigma Aldrich, St. Louis, Missouri, United States). Purified inserts were ligated into vectors at 3:1 molar ratios, either using Instant Sticky-end Ligase Master Mix (New England Biolabs) following manufacturers protocol, or using 400 U of T4 DNA ligase and 1X reaction buffer (50 mM Tris-HCl, 10 mM MgCl2 1 mM ATP, 10 mM DTT, New England Biolabs) at 16°C overnight, followed by enzymatic inactivation at 65°C for 10 min. Ligated DNA was heat-shock transformed into One-Shot TOP10 chemically competent E. coli cells (Thermo Fisher Scientific) following manufacturer's protocol, then plated onto LB plates containing the appropriate antibiotic (100 µg ml-1 ampicillin, 50 µg ml-1 kanamycin or 25 µg ml-1 chloramphenicol, Sigma Aldrich). Plasmid DNA was extracted from bacteria using GenElute™ Plasmid Miniprep Kit (Sigma Aldrich), following the manufacturer's protocol. Plasmids were sequenced by DNASeq (University of Dundee, Dundee, UK).

3.2.2 SDS-PAGE and western immunoblotting

Cells were homogenized by scraping into 90 µL Urea/SDS buffer: 10 mM Tris-HCl pH 6.8, 6.7 M urea, 1% w/v SDS, 10% v/v glycerol and 7.4 µM bromophenol blue, containing 50 µM phenylmethysulfonyl fluoride (PMSF)

and 50 µM N-methylmaleimide (all Sigma Aldrich). For conditioned media samples, media was either collected and mixed with urea/SDS buffer at a 1:1 ratio, or protein was precipitated out of the conditioned media using 100% (w/v) trichloroacetic acid (Sigma), before being resuspended in urea/SDS buffer. Lysates were sonicated and 10% v/v β-mercaptoethanol (Sigma Aldrich) added. Proteins were separated by sodium dodecyl sulfate-polyacrylamide gel electrophoresis (SDS-PAGE) using 10% polyacrylamide gels; 1.5 M Tris, 0.4% w/v SDS, 10% acrylamide/ bis-acrylamide (all Sigma Aldrich), electrophoresis buffer; 25 mM tris-HCl, 190 mM glycine, 0.1% w/v SDS, pH 8.5 (all Sigma Aldrich). Electrophoresis was performed at room temperature at 40mA until the samples had passed through the stacking gel, and then 80mA through the resolving gel. Proteins were transferred to a nitrocellulose membrane using the TurboBlot™ system (BioRad) for 7 mins (1.3A, 25V) and blocked at room temperature in Odyssey® TBS-Blocking Buffer (Li-Cor BioSciences, Lincoln, NE, United States) for 1h. The membranes were probed overnight at 4°C diluted in blocking buffer, washed 3 x 5 min in PBS with 0.1% Tween (both Sigma Aldrich) and probed for 1 h at room temperature in the dark with IRDye® conjugated secondary antibodies against goat IgG (800CW) and rabbit IgG (680CW), raised in goat or donkey (LiCor BioSciences), diluted in Odyssey® TBS-Blocking Buffer at 0.05 µg ml^{-1}. Membranes were then washed for 3 x 5 min in PBS with 0.1% Tween, rinsed with ddH2O and imaged using the Odyssey® CLX 9120 infrared imaging system (LiCor BioSciences). Image Studio Light v.5.2 was used to process scanned membranes.

3.2.3 Image acquisition

H&E images were acquired using a Zeiss Axio Scan Z1 equipped with an Axiocam colour CCD camera using ZEN Blue software (all from Zeiss, Oberkochen, Germany). Live cell images were acquired using a Nikon Eclipse Ti-E microscope (Nikon, Tokyo, Japan). Immunofluorescence images of tissues were acquired using a Zeiss LSM 800 confocal microscope (Zeiss).

3.2.4 Image analysis

Images were processed using either Zen 2.6 (blue edition) (Zeiss) or ImageJ (National Institutes of Health, Bethesda, MD, United States)[256]. Immunofluorescence images were manually thresholded, and particles analyzed. Stardist plugin was used for segmentation of nuclei from H&E images. Images were thresholded manually to remove areas containing no tissue in the images in quantification of livers. To quantify expression at the dermal-epidermal junction, a 4 mm x 6 mm selection was drawn around the dermal-epidermal junction and mean grey value measured using ImageJ per individual measurement.

3.2.5 Ethics

All procedures were licensed by the UK Home Office under the Animal (Specific Procedures) Act 1986, project license numbers (PPL) 70/9047 and 70/7288. Mice were housed and maintained within the University of Liverpool Biological Services Unit in specific pathogen-free conditions in accordance with UK Home Office guidelines. Food and water were available ad libitum.

Written informed consent was obtained before the use of healthy control and patient skin according to the Declaration of Helsinki and the study using cells approved by the Ethics Committee of Freiburg University, approval number (425/14).

3.3 Chapter 4 specific methods

3.3.1 Tissue processing

Mice were culled by cervical dislocation, dissected, and organs fixed in 4% paraformaldehyde (Merck) overnight at 4°C. Samples were cryoprotected in 30% sucrose/PBS solutions then in 30% sucrose/PBS:O.C.T (1:1) solutions (Tissue-Tek, Sakura Finetek Europe, Alphen aan den Rijn, The Netherlands), each overnight at 4°C. Samples were then embedded in OCT compound and transferred on to dry ice. Embedded samples were sectioned at 8 µm using a Leica CM1850 cryostat (Leica, Wokingham, UK).

3.3.2 Immunohistochemistry

Slides were incubated in ice-cold acetone for 10 min, transferred into PBS for 10 min, then blocked in PBS containing 10% normal goat serum (NGS) at room temperature for 1 h. Next, samples were probed with the primary antibodies diluted in PBS-Tween (0.05%) with 5% NGS at 4°C overnight. Samples were then washed for 3 x 5 min in PBS-Tween (0.05%), before being probed with secondary antibodies diluted in PBS-Tween (0.05%) with 5% NGS at room temperature for 1 h. Samples were washed for 3 x 5 min in PBS-Tween (0.05%) and mounted with VECTASHIELD® Antifade Mounting Medium with DAPI (VECTASHIELD®, Burlingame, CA).

3.3.3. Mice

C57Bl6CBAF1 females (Charles River Laboratories) between 12 and 16 weeks were used for all tissue stainings in chapter 4 unless otherwise stated as ‘newborn’, whereby the mice were terminated at P0. Food and water were available ad libitum.

3.4. Chapter 5 specific methods

3.4.1 pLenti-LaNtα31-PAmCherry-P2A-Puro vector

A gBlock was synthesised (Integrated DNA Technologies, Coralville, IA) containing EcoRI enzyme site, T7 promoter binding site [257], Kozak consensus sequence[258], Igκ secretion signal (METDTLLLWVLLLWVPGSTGD), LaNt α31-encoding cDNA (amino acids 38-488), Flag (DYKDDDDK), HA (YPYDVPDYA) tag sequences, full PAmCherry-encoding cDNA, with the stop signal removed (amino acids 1-235), and NheI. The gBlock DNA was inserted into pLenti-P2A-Puro (OriGene Technologies GmbH, Herford, Germany) using EcoRI and BamHI, producing pLenti-LaNtα31-PAmCherry-P2A-Puro.

3.4.2 Cell transduction

Lentiviral particles were produced using pLenti-LaNtα31-PAmCherry-P2A-Puro by OriGene Technologies (GmbH, Herford, Germany). For transductions, 3 x 10^4 cells were seeded in a 12 well plate. The following day, cells were transduced with LaNtα31-PAmCherry-P2A-Puro lentiviral particles using a multiplicity of infection of 10, alongside polybrene at a concentration of 8 µg mL^{-1}. The following day, media was replenished. For puromycin selection of transduced cells, cells were trypsinised and seeded into a 35mm dish 48h after transduction. Cells were grown in KSFM (supplemented for either hTCEpi or NHK) containing 0.25 µg mL^{-1} puromycin. Puromycin-containing media was replenished every 14 days, and cells were maintained in their standard media thereafter.

3.4.3 Photoactivation of PAmCherry

Activation of the PAmCherry fluorphore was performed on an ANDOR dragonfly microscope (Andor Technology Ltd, Belfast, Ireland). Cells were exposed to a 405 nm laser for 4000 ms prior to imaging.

3.4.4 3D organotypic cocultures

2 mg mL^{-1} of rat tail collagen (Corning, Corning, NY, USA) was diluted in 0.1% of acetic acid. 250 µl of Hank's Balanced Salt solution (HBSS, Gibco, USA), 2 ml of rat tail collagen, and 250 µl of FBS containing 1 million fibroblasts were mixed in condition and neutralized with 1M NaOH. 2.5 ml of the mixture was inserted into a cell culture insert. After solidification a sterile glass ring was placed on the gel, and the gel was incubated with DMEM at 37°C overnight. 1 million of hTCEPi's or NHK's were added into the glass ring placed on the gel. The cells were cultured for either 1 or 3 weeks with co-culture-medium containing 500 ml of DMEM, 500 ml of Ham's F12, 5% of FBS, 100 U of penicillin, 100 mg ml^{-1} of streptomycin, 5 mg ml^{-1} of insulin, 0.1 mM of Adenine, 0.4 mg ml^{-1} of hydrocortisone, 1 ng ml^{-1} of EGF, and 50 mg ml^{-1} of L-ascorbic acid.

3.4.5 Immunofluorescence microscopy

Cells or ECM deposits were fixed in ice cold methanol for 15 min, or in 3.7% formaldehyde (Sigma-Aldrich) for 10 min followed by 10 min in 0.2 % Triton-X (Sigma-Aldrich) in PBS to permeabilise where necessary. Samples were blocked for 40 mins at RT in 10% normal goat serum (Jackson Labs) diluted in PBS. Primary antibodies were diluted in PBS with 10% normal goat serum (Jackson Labs) and incubated at 4 °C overnight; coverslips were then washed 3x for 5 min with PBS containing 0.05 % tween-20 (PBS-T, Sigma-Aldrich) before probing for 1 h at room temperature with Alexa Fluor 594nm or 647nm/ Cy5 conjugated secondary antibodies diluted in PBS. Coverslips were washed 3x for 5 min with PBS-T, counterstained with DAPI (ThermoFisher Scientific) for 10 min, rinsed thoroughly with PBS and mounted with Vectashield (Vector Laboratories, Burlingame, California, USA). Images were obtained using a Zeiss LSM800 confocal microscope (Zeiss, Cambridge, UK). For staining the cytoskeleton, Rhodamine-Phalloidin (ThermoFisher Scientific) was used in place of a secondary antibody, otherwise following the same protocol.

3.4.6 Single cell phenotypic assays

For cell morphology analyzes cells were seeded at 1 x 10^4 cells/well onto uncoated 12-well plates (Greiner-Bio One) and cultured for either 2h or 6h prior to fixation.

For laminin deposition analysis, cells were seeded at 1 x 10^4 cells/well on to no. #1 round 456 16 mm glass coverslips (Pyramid innovations Ltd, Polegate, UK) inside uncoated 12-well plates (Greiner-Bio One) and cultured for either 2h or 6h, after which cellular material was removed with 0.18 % NH_4OH for 5 min followed by extensive PBS washes, prior to fixation.

3.4.7 In vitro scratch assays

For scratch assays, cells were seeded at 3 x 10^5 cells/well onto uncoated 12-well plates (Greiner-Bio One). The following morning, a scratch was introduced using a sterile 200µl pipette tip, and the cell debris was washed away, and a brightfield image was taken of the cells every on a Nikon TiE epifluorescence microscope with a 10X objective at 0, 6 and 16 h (Nikon, Tokyo, Japan). Gap closure was measured as a percentage relative to starting area using the freehand tool in Image J (NIH, Bethesda, Massachusetts, USA).

3.4.8 Organotypic coculture processing

For frozen sections, OTC cultures were placed in 50% sucrose:PBS at 4 °C for 2h, followed by 2M sucrose at 4 °C for 2h, before being placed in OTC compound. Samples were embedded in OCT compound and transferred on dry ice. Embedded samples were sectioned at 8 µm using a Leica CM1850 cryostat (Leica, Wokingham, UK).

For paraffin sections, Tissues were fixed in 10% neutral buffered formalin (Leica,) for 24 h, then processed through graded ethanol and xylene before being embedded in paraffin wax. 5 µm sections were cut using a rotary microtome RM2235 (Leica), adhered to microscope slides, then dried overnight at 37°C. Sections were dewaxed and rehydrated with xylene

followed by a series of decreasing ethanol concentrations; specifically immersion in xylene for 5 minutes, followed by immersion in 100%, 95%, and 75% ethanol for 2 x 3 minutes each, and in tap water for 5 minutes.

3.4.9 Immunohistochemistry

Sections were dewaxed and rehydrated with xylene followed by a series of decreasing ethanol concentrations (described in the paragraph above). Sections were then stained in Harris hematoxylin solution (Leica) for 5 min, H2O for 1 min, acid alcohol (Leica) for 5 s, H2O for 5 min, aqueous eosin (Leica) for 3 min, H2O for 15 s, followed by dehydration through graded ethanol and xylene. Slides were coverslipped with DPX mounting media (Sigma Aldrich).

3.4.10 Tricholroacetic acid precipitation of proteins

100% (w/v) TCA (Merck) was added to the protein samples to bring the TCA to a final concentration to 20%. Samples were incubated for 1h on ice. Next, samples were centrifuged at ~13,000rpm in a microcentrifuge for 10 min. Protein pellets were washed 3X with a solution of ice cold 0.01 M HCl / 90% acetone, and pellets were allowed to air dry. Pellets were resuspended directly in 50µl lysis buffer.

3.5 LaNt α31 in vivo studies

3.5.1 Generation of pUbC-LoxP-LaNtα31-T2A-tdTomato

A gBlock was synthesised (Integrated DNA Technologies, Coralville, IA) containing NdeI and NdeI restriction enzyme sites, T7 promoter binding site[257], Kozak consensus sequence[258], Igκ secretion signal (METDTLLLWVLLLWVPGSTGD)[259], LaNt α31-encoding cDNA (amino acids 38-488)[51], Flag (DYKDDDDK)[260] and HA (YPYDVPDYA)[261] tag sequences, T2A sequence (EGRGSLLTCGDVEENPGP)[262], and BamHI. The gBlock DNA was inserted into pCSCMV:tdTomato (a gift from Gerhart Ryffel, Addgene plasmid #30530 ; http://n2t.net/addgene:30530; RRID:Addgene_30530) using NdeI and BamHI (New England Biolabs, Ipswich, MA), to produce pCS-LaNtα31-T2A-tdTomato. LaNtα31-T2A-tdTomato was then removed from this backbone using NheI and EcoRI, and inserted into a vector containing the Ubiquitin C (UbC) promoter and a floxed stop cassette, all flanked by cHS4 insulator elements, producing pUbC-LoxP-LaNtα31-T2A-tdTomato.

3.5.2 Cell transfections

1 x 10^6 KERA-308 or 4 x 105 HEK293A cells were seeded in 6-well plates (Greiner-BioOne, Kremsmünster, Austria) 24 h prior to transfection. For KERA-308 cells, 2 µg of hK14-LaNtα31-T2A-mCherry or LaNt-α31-pSec-Tag and 2 µl Lipofectamine 2000 (Thermo Fisher Scientific) were used. For HEK293A cells, either 1 µg pCAG-Cre:GFP and 2 µl Lipofectamine 2000, 2 µg of pUbC-LoxP-LaNtα31-T2A-tdTomato and 5 µl Lipofectamine 2000, or 2 µg of pUbC-LoxP-LaNtα31-T2A-tdTomato, 1 µg of pCAG-Cre:GFP and 7 µl Lipofectamine 2000 (Thermo Fisher Scientific), were mixed with 2 ml of Gibco™ Opti-MEM™ Reduced Serum Medium (Thermo Fisher Scientific) and incubated for 10 min at room temperature. The DNA-lipofectamine complex was added to the wells, and the media was replaced with DMEM high glucose after 6 h.

3.5.3 Explant culture method

Hair was removed from mouse skin tissue using Veet hair removal cream (Reckitt Benckiser, Slough, UK) and the skin washed in Dulbecco's Phosphate Buffered Saline (DPBS) containing 200 U ml^{-1} penicillin, 200 U ml^{-1} streptomycin, and 5 U ml^{-1} amphotericin B1 (all Sigma Aldrich). The skin was then dissected into 2-3 mm^2 pieces using a surgical scalpel and 3 or 4 pieces placed per well of a 6-well dish (Greiner Bio-One, Kremsmünster, Austria) with the dermis in contact with the dish. 300 µl of DMEM supplemented with 20% FCS, 2 mM L-glutamine, 200 µg ml^{-1} penicillin, 200 µg ml^{-1} streptomycin, and 5 µg ml^{-1} fungizone (all Sigma Aldrich) was added to the wells. After 24 h, each well was topped up with 1 ml of media, and the media was replenished every 48 h thereafter.

3.5.4 Ex-vivo scratch wound assays

For ex-vivo scratch assays, dermal fibroblasts were obtained from transgenic mice, and cells were seeded at 3 x 10^5 cells/well onto uncoated 12-well plates (Greiner-Bio One). The following morning, a scratch was introduced using a sterile 200µl pipette tip, the cell debris was washed away with PBS, and a brightfield image was taken of the cells every on a Nikon TiE epifluorescence microscope with a 10X objective at 0 and 16 h (Nikon, Tokyo, Japan). Gap closure was measured as a percentage relative to starting area using the freehand tool in Image J (NIH, Bethesda, Massachusetts, USA).

3.5.5 Transgenic Line establishment

Generation of transgenic mice were carried out based on the protocol described in[263]. C57Bl6CBAF1 females (Charles River Laboratories, Margate, Kent, UK) between 6-8 weeks were superovulated by intraperitoneal (IP) injections of 5 IU pregnant mare's serum gonadotrophin (PMSG; in 100µl H2O), followed 46 h later by 5 IU of human chorionic gonadotropin (hCG, Sigma Aldrich). Treated females were mated with C57Bl6CBAF1 males overnight. Mated females were identified from the

presence of copulation plugs, anaesthetised, and oviducts removed and dissected in M2 media (Millipore, Watford, UK). Day-1 oocytes (C57BL/6Jx CBA F1) were transferred into clean media by mouth pipetting. Cumulus cells were removed by hyaluronidase (300 µg ml^{-1}, Merck, Darmstadt, Germany) treatment in M2 media with gentle shaking until detached from the egg surface. Oocytes were then rinsed and transferred to M16 media (Millipore, Speciality Media, EmbryoMax) ready for injection.

DNA was diluted to a final concentration of 2 ng $µl^{-1}$ in embryo water (Sigma Aldrich) and filter-purified using Durapore-PVDF 0.22 µM centrifuge filters (Merck). Injection pipettes were used to pierce the outer layers of the oocyte and to inject DNA. DNA was injected into the pronuclei of the oocyte. Undamaged eggs were transferred to clean M16 media and incubated at 37°C until transferred into pseudopregnant CD1 females on the same day. Meanwhile, pseudopregnant females were obtained by mating vasectomised CD1 males overnight. Copulation plugs were checked and females were used 1 day post-coitum. Females were anaesthetised by inhalation of isoflurane (Sigma Aldrich). 30 injected oocytes were transferred to plugged pseudopregnant female oviducts through the infundibulum.

In generating the pUbC-LoxP-LaNtα31-T2A-tdTomato line, 460 mouse zygotes were injected over four sessions. 87% of these zygotes survived and were transferred into 11 recipient CD1 mothers. From these mothers, 42 pups were born. Of the 10 F0 mice that gave a positive genotype result, four passed on the transgene to the F1 generation. Mice that did not pass on the transgene to the F1 generation were culled, the four F0 mice were mated to expand colonies for cryopreservation, and one line was continued for investigation.

R26CreERT2 (Jax Lab 008463),[264] mice were purchased from The Jackson Laboratory (Bar Harbor, Maine, United States).

3.5.6 In Vivo Transgene Induction

Tamoxifen (Sigma Aldrich) was dissolved in corn oil (Sigma Aldrich) and administered via IP at a concentrations of 25 mg kg^{-1} or 75 mg kg^{-1}.

Progesterone (Sigma Aldrich) was dissolved in corn oil (Sigma Aldrich) and was co-administered alongside tamoxifen at a dose of exactly half of the corresponding tamoxifen dose (12.5 mg kg^{-1} or 25 mg kg^{-1}).

3.5.7 DNA Extraction

Four weeks after birth, ear notches were collected from mouse pups and digested in 100 µl lysis buffer (50 mM Tris-HCl pH 8.0, 0.1 M NaCl, 1% SDS, 20 mM EDTA) and 10 µl of proteinase K (10 mg ml-1, all Sigma Aldrich) overnight at 55°C. The following day, samples were cooled, spun at 13,000 rpm for 3 min and the supernatant transferred to clean 1.5 ml tubes (Eppendorf, Hamburg, Germany). An equal volume of isopropanol (Sigma Aldrich) was added, gently inverted and span at 13,000 rpm, and supernatant discarded. Pellets were washed with 500 µl of 70% EtOH (Sigma Aldrich), then air-dried for 10 min, and resuspended in 50 µl ddH20.

3.5.8 PCR

50 ng of genomic DNA was mixed with 12.5 µl of REDtaq ReadyMix PCR Reaction Mix (20 mM Tris-HCl pH 8.3, 100 mM KCl, 3 mM MgCl2, 0.002% gelatin, 0.4 mM dNTP mix, 0.06 unit/ml of Taq DNA Polymerase, Sigma Aldrich) and 0.5 µM of each primer; ddH20 was added to make the reaction mixture up to 25 µl. Primer pairs for genotyping were as follows: LaNt α31 to tdTomato Forward 5’ –ATCTATGCTGGTGGAGGGGT – 3’, Reverse 5’ – TCTTTGATGACCTCCTCGCC – 3’; Cre Forward 5’ – GCATTACCGGTCGATGCAACGAGTGATGAG – 3’, Reverse 5’ – GAGTGAACGAACCTGGTCGAAATCAGTGCG – 3’; Recombination Forward 5’ – TCCGCTAAATTCTGGCCGTT – 3’, Reverse 5’ – GTGCTTTCCTGGGGTCTTCA – 3’(all from Integrated DNA Technologies). Cycle conditions were as follows: Genotyping – 1 cycle of 95°C for 5 min, 35 cycles of 95°C for 15 s; 56°C for 30 s; 72°C for 40 s, followed by a final cycle of 72°C for 5 min. For checking recombination: 1 cycle of 95°C for 5 min, 35 cycles of 95°C for 15 s; 60°C for 30 s; 72°C for 90 s, followed by a final cycle

of 72°C for 7 min. PCR products were separated by gel electrophoresis and imaged using a BioRad Gel Doc XR+ System.

3.5.9 Tissue processing

For cryosections, P0 pups were culled by cervical dislocation, and fixed in 4% paraformaldehyde (Merck) overnight at 4°C. Samples were cryoprotected in 30% sucrose/PBS solutions then in 30% sucrose/PBS:O.C.T (1:1) solutions (Tissue-Tek, Sakura Finetek Europe, Alphen aan den Rijn, The Netherlands), each overnight at 4°C. Samples were embedded in OCT compound and transferred on dry ice. Embedded samples were sectioned at 8 µm using a Leica CM1850 cryostat (Leica, Wokingham, UK). For paraffin sections, Tissues were fixed in 10% neutral buffered formalin (Leica) for 24 h, then processed through graded ethanol and xylene before being embedded in paraffin wax. 5 µm sections were cut using a rotary microtome RM2235 (Leica), adhered to microscope slides, then dried overnight at 37°C. Sections were dewaxed and rehydrated with xylene followed by a series of decreasing ethanol concentrations; specifically immersion in xylene for 5 minutes, followed by immersion in 100%, 95%, and 75% ethanol for 2 x 3 minutes each, and in tap water for 5 minutes. Antigen retrieval was performed by microwaving sections in preheated 0.01 M citrate buffer pH 6 (Sigma Aldrich) for 5 min.

3.5.10 Hematoxylin and Eosin Staining

Sections were dewaxed and rehydrated with xylene followed by a series of decreasing ethanol concentrations (described in paragraph above). Sections were then stained in Harris hematoxylin solution (Leica) for 5 min, H2O for 1 min, acid alcohol (Leica) for 5 s, H2O for 5 min, aqueous eosin (Leica) for 3 min, H2O for 15 s, followed by dehydration through graded ethanol and xylene. Slides were coverslipped with DPX mounting media (Sigma Aldrich).

3.5.11 Immunohistochemistry

Slides were incubated in ice-cold acetone for 10 min, then transferred into PBS for 10 min blocking, then blocked in PBS containing 10% normal goat serum (NGS) at room temperature for 1 h. Next, samples were probed with the primary antibodies diluted in PBS-Tween (0.05%) with 5% NGS at 4°C overnight. Samples were then washed for 3 x 5 min in PBS-Tween (0.05%), before being probed with secondary antibodies diluted in PBS-Tween (0.05%) with 5% NGS at room temperature for 1 h. Samples were washed for 3 x 5 min in PBS-Tween (0.05%). Slides were mounted with VECTASHIELD® Antifade Mounting Medium with DAPI (VECTASHIELD®, Burlingame, CA).

3.5.12 Transmission Electron Microscopy

Kidneys and skin were dissected from the p0 mice and placed immediately into 4% (w/v) paraformaldehyde, 2.5% (w/v) glutaraldehyde in cacodylate pH7.4 for 30 min at room temperature. Kidneys were then dissected into 3mm3 pieces and placed into fresh fixative and rotated overnight at room temperature. Samples were washed 4 x 5 min with 0.1M cacodylate buffer, before staining with reduced osmium (final concentration 1% (w/v) OsO_4, 1.5% (w/v) potassium ferrocyanide, 0.1 M cacodylate buffer) in a Pelco Biowave®Pro (Ted Pella Inc., Redding, CA). Following this, samples were washed 5 x 5 min in ddH_2O, and incubated overnight in aqueous 1% uranyl acetate at 4°C. After further ddh2O washes Samples were dehydrated through increasing concentrations of acetone (30%, 50%, 70%, 90% for 15 min each then 3 x 100%) Samples were infiltrated in 1:1 acetone TAAB 812 medium resin for 2 d followed by 4 x 100% resin for 1 h each, before final embedding and curing at 60°C for 48 h. Tissue was sectioned at 70-75nm on a ultramicrotome (Lieca) and the viewed in a FEI 120Kv Tecnai Spirtit BioTwin TEM (FEI Company, Hillsboro, OR), fitted with a Gatan RIO16 digital camera (Gatan, Pleaseanton, CA).

Chapter 4: LaNt α31 distribution in mice

4.1 Introduction

This chapter focuses LaNt α31 distribution in mice using newly produced rabbit polyclonal antibodies to the mouse from of LaNt α31.

Previous studies have focused on the human version of LaNt α31, initially at the mRNA (LAMA3LN1) and then protein level. LAMA3LN1 expression was identified in a wide array of tissues including the heart, brain, placenta, lung, pancreas, spleen, thymus, prostate, testis, ovaries, small intestine, and in leukocytes[51].

At the protein level, LaNt α31[51,53,54] was identified in the basal layers of the skin and corneal epithelia with localised enrichment in limbal epithelial sub-populations, and in stromal structures including blood vessels. Upregulation of the protein was observed during ex vivo corneal wound repair and in stem cell activation assays [51,53,54]. A more recent study, published during the work in this thesis, expanded these analyzes to reveal more widespread distribution including epithelial, vascular and stromal cells throughout most tissues, and neurons in the central nervous system[52]. This distribution was wider than that of LM α3, despite LaNt a31 and LM α3 sharing the same promoter. These human studies have been incredibly important on shedding the localization of LaNt α31 in normal biology.

No study thus far has investigated the distribution of LaNt α31 in mice. One may predict a similar distribution pattern to that seen in humans, and one may also draw inspiration from previous studies of the distribution of the LM α3 chain in mice. In situ hybridization revealed that the LM α3a and LM α3b chains are present in nasal epithelia, and in the basement membrane of the upper gastrointestinal tract [265]. The Lama3a transcript was preferentially expressed in the basement membrane of skin, and in the developing neurons of the trigeminal ganglion, where LAMA3B transcripts are also found [265]. The Lama3b transcript was preferentially expressed in salivary glands and developing teeth where Lama3a transcripts were also found. Lama3b mRNA was exclusively detected in the bronchi and alveoli of developing lung, the whisker pads, stomach and intestinal crypts, and in the central

nervous system. In the developing brain, Lama3b transcripts were observed in the neuroectoderm and expression in the thalamus, Rathke's pouch, and the periventricular subependymal germinal layer, and further studies confirmed that the LM α3 chain was expressed preferentially in epithelial basement membranes[121].

Gaining an insight into the distribution of LaNt α31 in mice becomes relevant for transgenic and future KO studies in mice. Knowing the localization of LaNt α31 in mice provides a guide into where one might expect the most severe phenotypes. When the LaNt α31 distribution is viewed in context of the tissue-specific laminin isoforms expressed in BMs, one can start to hypothesise how an α-LN domain containing protein may factor into the tissue biology. Whereas most in vitro data thus far has been in keratinocytes or cancer cell lines, the function LaNt α31 has may be different in non-epithelial or non-cancerous tissues. Considering the context-specific functions of laminins, it would follow that LaNt α31 also has tissue specific effects. Uncovering the localization of LaNt α31 in the mouse is the first step to being able to postulate context specific roles of LaNt α31.

Investigating the localization of LaNt α31 in a different species, using a distinct antibodies preparation, recognising a different epitope, allows one to triangulate data on LaNt α31 distribution and increase confidence of any conclusions made, while also providing potential to determine distribution in a wider selection of normal tissue and developmental states and for use in disease and genetic model tissue.

4.1.1 Aim

Validate a new rabbit anti-mouse LaNt α31 antibody and determine LaNt α31 distribution in mouse tissue.

4.1.2 Objectives

i) Validate a new anti-mouse LaNt α31 antibody

ii) Investigate where LaNt α31 is expressed in mouse tissue

4.2 Results

4.2.1 Antibody design and screening

Rabbit polyclonal antibodies were raised against a synthetic peptide corresponding to mouse LaNt α31 residues 465-480; CLNSDSSMFSLSPRML conjugated to KLH. These amino acids are derived from intronic sequence relative to the full length laminin protein, and are therefore unique to the LaNt α31 protein. Local alignment using BLAST[266], of the synthetic peptide vs all other mouse LM chains did not provide any hits to suspect cross reactivity with other chains based on sequence. Indeed, the sequence used to generate the synthetic peptide is not conversed in any other LM. These specific residues are not conserved in human LaNt α31. Antibodies were screened by ELISA against the unconjugated peptide by Eurogentec, then by western immunoblotting against total protein extracts from mouse keratinocytes (Fig. 4.1). Only final bleed antibodies produced positive bands via western immunoblotting, which were not observed when using the pre-immune sera. The rabbit 1336 antibodies were used in all subsequent experiments in this chapter (Fig. 4.1, second and third lanes). Screened antibodies were affinity-purified using the unconjugated peptide prior to use in downstream applications.

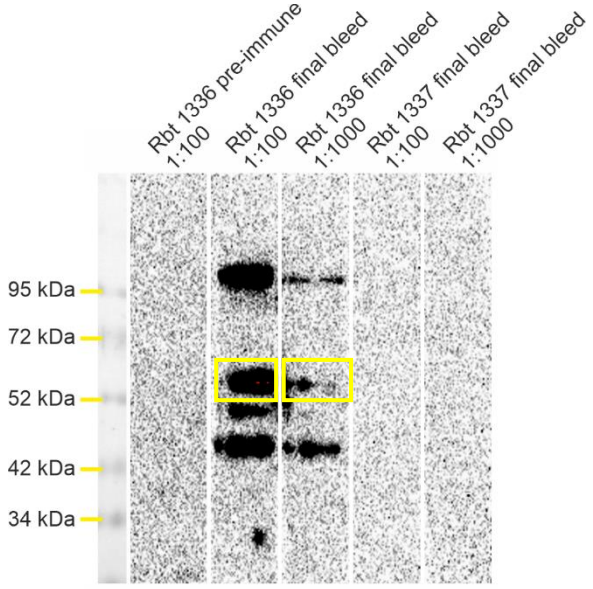

Figure 4.1. Screening of pre-immune sera and final bleed Rbt anti-MsLaNt α31 antibodies by western immunoblotting. Western immunoblotting using pre-immuni sera and final bleed sera Rbt anti-MsLaNt α31 antibodies at various concentrations probing primary mouse keratinocytes whole cell extract. Yellow box inidicates a band at the predicted size (~64 kDa).

4.2.2 The Rbt anti-MsLaNt α31 antibody recognises a protein of the predicted size by western immunoblotting

Western immunoblotting using the Rabbit anti-MsLaNt α31 antibodies yielded a ~64 kDa band in lysates from whole mouse eE18.5 embryo. This size corresponds with the predicted molecular weight. No bands were detected in lysates from human HaCaT cells that are known to express human LaNt α31 (Fig. 4.2).

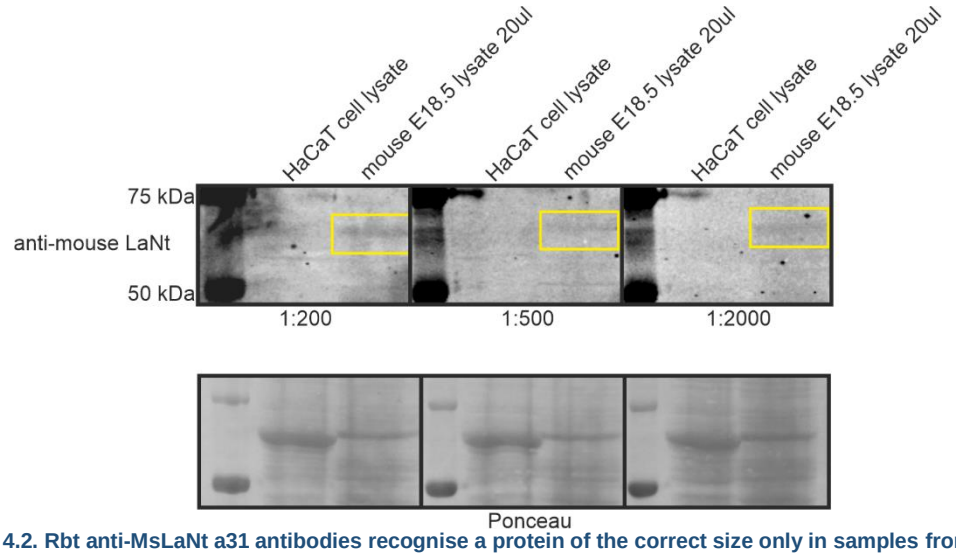

Figure 4.2. Rbt anti-MsLaNt a31 antibodies recognise a protein of the correct size only in samples from mice. Western immunoblotting using Rbt anti-MsLaNt α31 antibodies at the indicaticated concentrations probing against either HaCaT cell lysates or E18.5 whole mouse lysates. Yellow box inidicates a band at the predicted size (~64 kDa).

4.2.3 Peptide depletion of the Rbt anti-MsLaNt α31 antibody prevents anti-LaNt α31 immunoreactivity.

To ensure that Rbt anti-MsLaNt α31 antibodies specifically recognised the original LaNt α31 antigen used for immunization during antibody generation, a peptide blocking experiment was carried out using the original antigen (CLNSDSSMFSLSPRML peptide). Specifically, Rbt anti-msLaNt α31 antibodies were incubated with the peptide overnight at 4°C prior to probing tissues. These antibodies were then used to probed OCT sections of mouse tongue tissue, as this tissue contains structures where strong LaNt α31 positivity is expected (vessels), and other structures where LaNt α31 reactivity is not expected (muscle). Rbt anti-MsLaNt α31 antibodies clearly recognised vessles, and this vessel signal was not detected in IgG only processed tissue (Fig. 4.3 top and middle rows). Tissues probed with the peptide-blocked Rbt anti-MsLaNt α31 antibodies did not yield any positive signal around vessels in mouse tongue tissue (Fig. 4.3). Indeed, the only signal obtained from the blocked sample closely matched that of the IgG control.

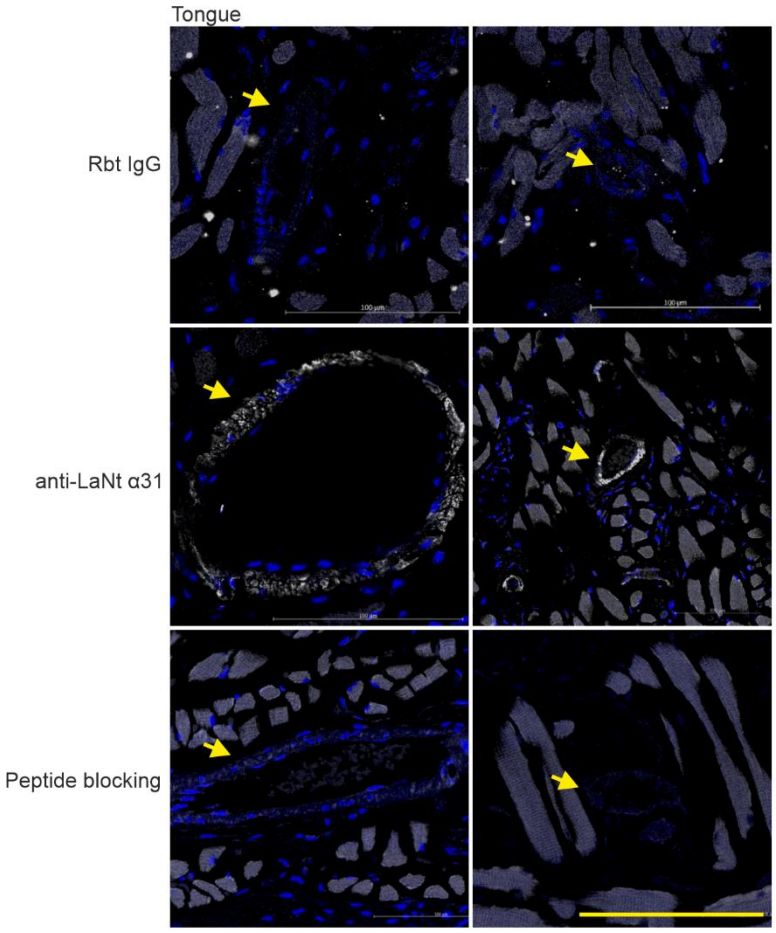

Figure 4.3. Peptide blocking using the peptide used to generate the anti-MsLaNt α31 antibodies prevents any anti-LaNt α31 immunoreactivity. Wild-type mouse tongue OCT sections (10 µm) processed for immunohistochemistry using Rbt IgG (top), Rbt anti-MsLaNt α31 antibodies (middle) or peptide-blocked Rbt anti-MsLaNtα31 antibodies (bottom). Yellow arrows indicate vessels. Scale bar = 100µm.

4.2.2 Epithelium

After confirming that the Rbt anti-MsLaNt α31 antibodies lost immunoreactivity following peptide blocking, I next processed sections of whole mouse tongue to determine LaNt α31 distribution. Rbt anti-MsLaNt α31 immunoreactivity was observed throughout basal layer of the epithelium, with areas of localised enrichment (Fig. 4.4A). No immunoreactivity was observed in the underlying stroma, with the exception of some vessels which displayed strong immunoreactivity against the anti-LaNt α31 antibodies (Fig. 4.4B,C). No LaNt α31 positivity was observed in the muscle tissue within the tongue (Fig. 4.4B). Next, I processed adult mouse tongue tissue in OCT for cryosectioning. In humans, the LaNt α31 protein has been shown to be present in the BM of skin and enriched in basal epithelial cells of the corneal limbus[53], while in situ hybridization demonstrated that the mRNA (LAMA3LN1) is enriched in the basal layer of the epidermis and hair follicles[51]. More recent data confirmed LaNt α31 protein expression in the basal layer of the epidermis with localised enrichment in a sub-population of cells[52]. LaNt α31 follows a similar distribution in mouse epithelium, displaying staning of the basal epithelium, as well as areas of localised enrichment (Fig. 4.4A). No staining was observed in the underlying stroma, with the exception of specific vessels which displayed strong immunoreactivity against the anti-LaNt α31 antibodies (Fig. 4.4B,C). No LaNt α31 positivity was observed in the muscle tissue within the tongue (Fig. 4.4B).

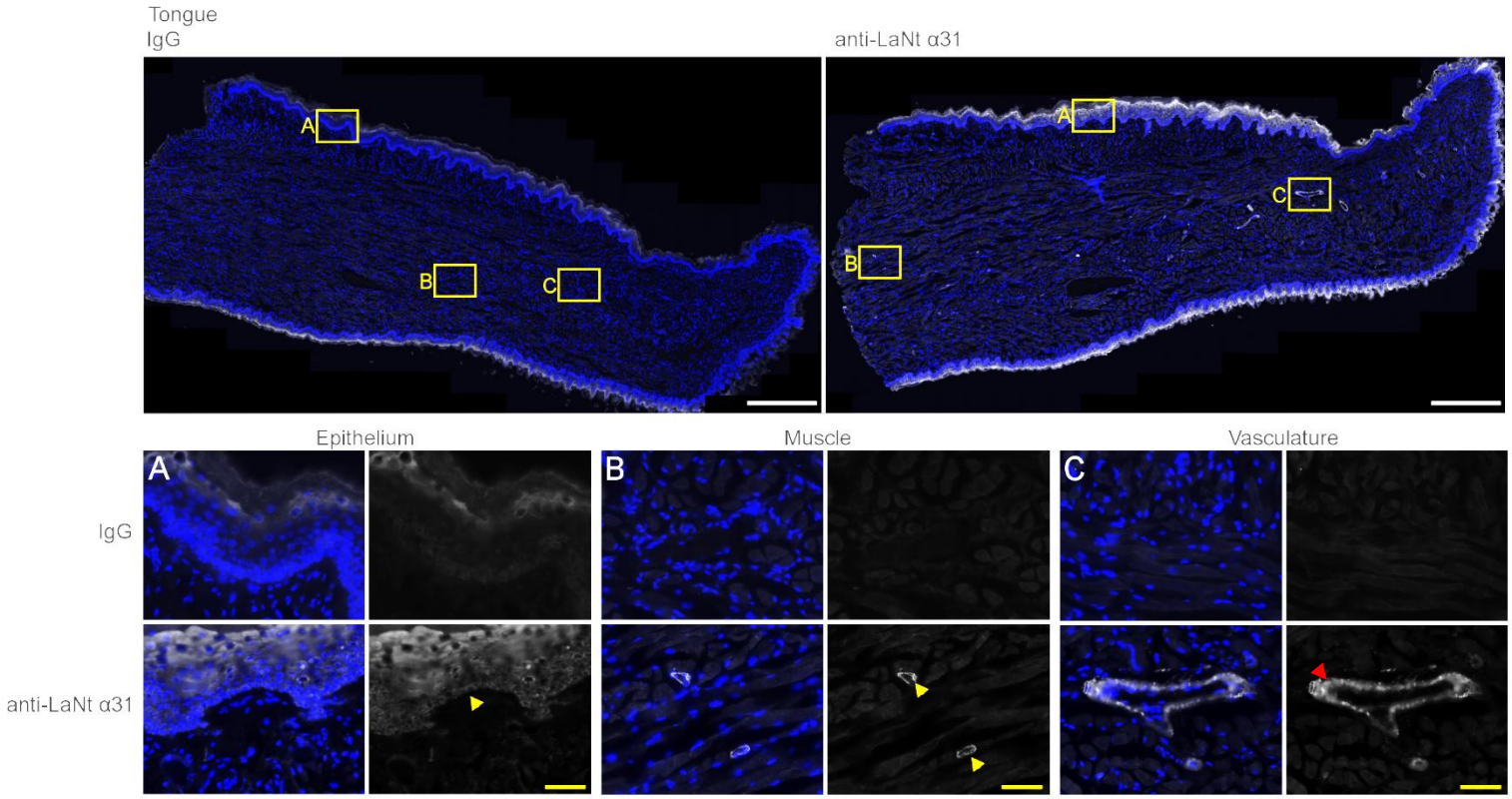

Figure 4.4. LaNt α31 is present in the basal epithelium and vasculature in tongue tissue. Wild-type mouse tongue OCT sections processed for immunohistochemistry with Rbt IgG antibodies (left) or Rbt anti-MsLaNtα31 antibodies (right). Scale bar = 500 μm. Yellow boxes indicate areas of increased magnification (bottom panel). Scale bar = 50 μm. Red arrows represent location of basement membranes.

4.2.3 Kidney

Next, I continued to investigate tissues where LaNt α31 expression has been confirmed in humans. In the mouse kidney. LaNt α31 immunoreactivity was observed in the Bowman's capsule parietal epithelium basement membrane (Fig. 4.5). Immunoreactivity was also observed in collecting ducts, with varied staining intensity between ducts. Weak immunoreactivity was observed in proximal and distal tubules (Fig. 4.5). No anti-LaNt α31 immunoreactivity was observed in the kidney cortex (Fig. 4.5). Dtrong signal was again obtained throughout the kidney vasculature (Fig. 4.5)

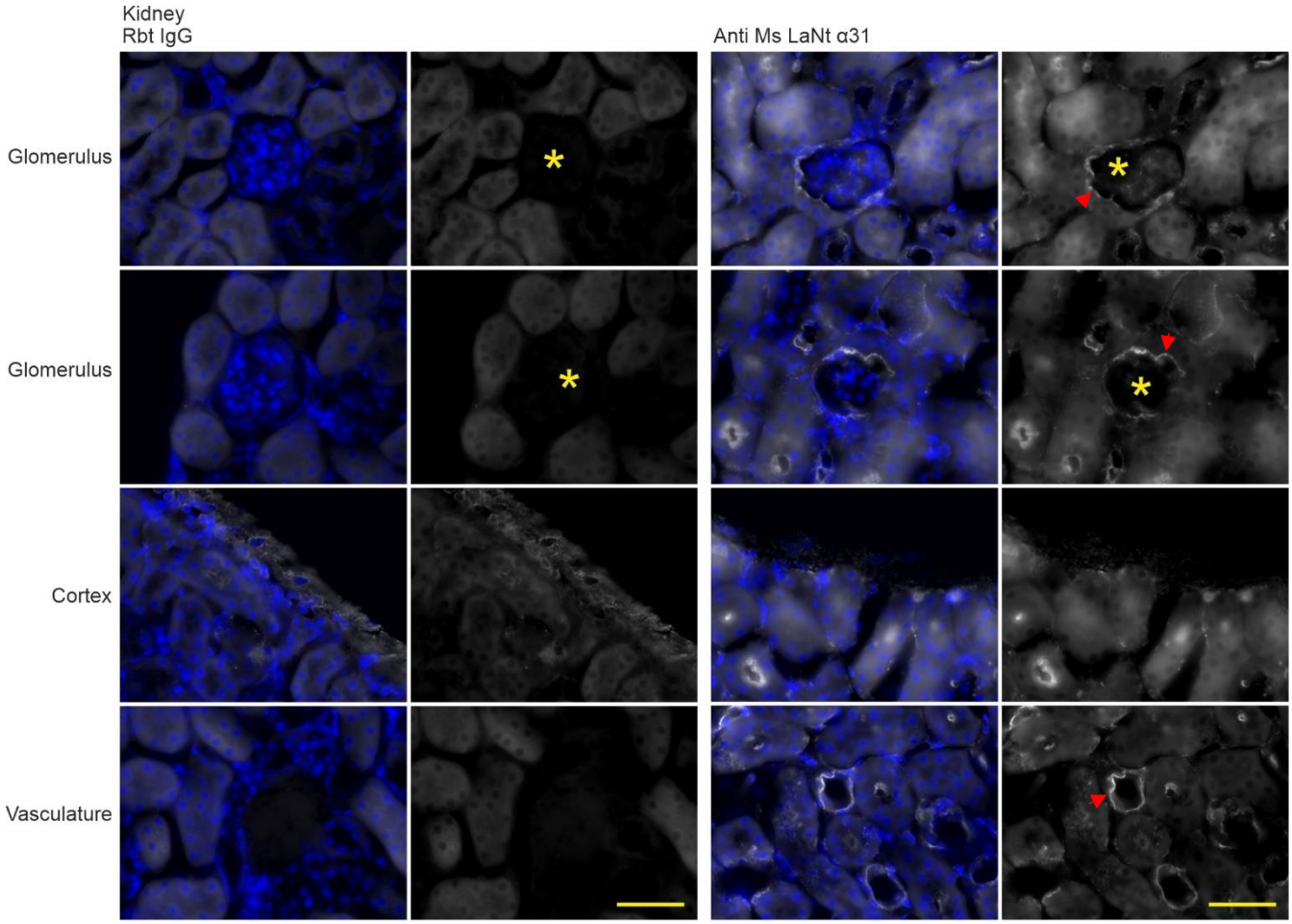

Figure 4.5. LaNt α31 is present in the bowman's capsule parietal epithelium basement membrane, proximal tubes, and vasculature. Wild-type mouse kidney OCT sections (10 µm) processed for immunohistochemistry with Rbt IgG antibodies (left) or Rbt anti-MsLaNtα31 antibodies (right). Yellow asterisks indicate glomeruli. Scale bar = 50 µm. Red arrows represent location of basement membranes.

4.2.4 Lungs

Strong anti-LaNt α31 immunoreactivity was observed throughout the lungs (Fig. 4.6). Specifically, cells within the simple cuboidal epithelium surrounding bronchioles, and the tissue area beneath the epithelium exhibited strong LaNt α31 immunoreactivity (Fig. 4.7, left), as well the surrounding elastic fibres (Fig. 4.7, left) and glands (Fig. 4.7, middle). Anti-LaNt α31 signal was observed throughout the alveolar epithelium, with enrichment is sub-populations of alveolar cells (Fig. 4.7, right).

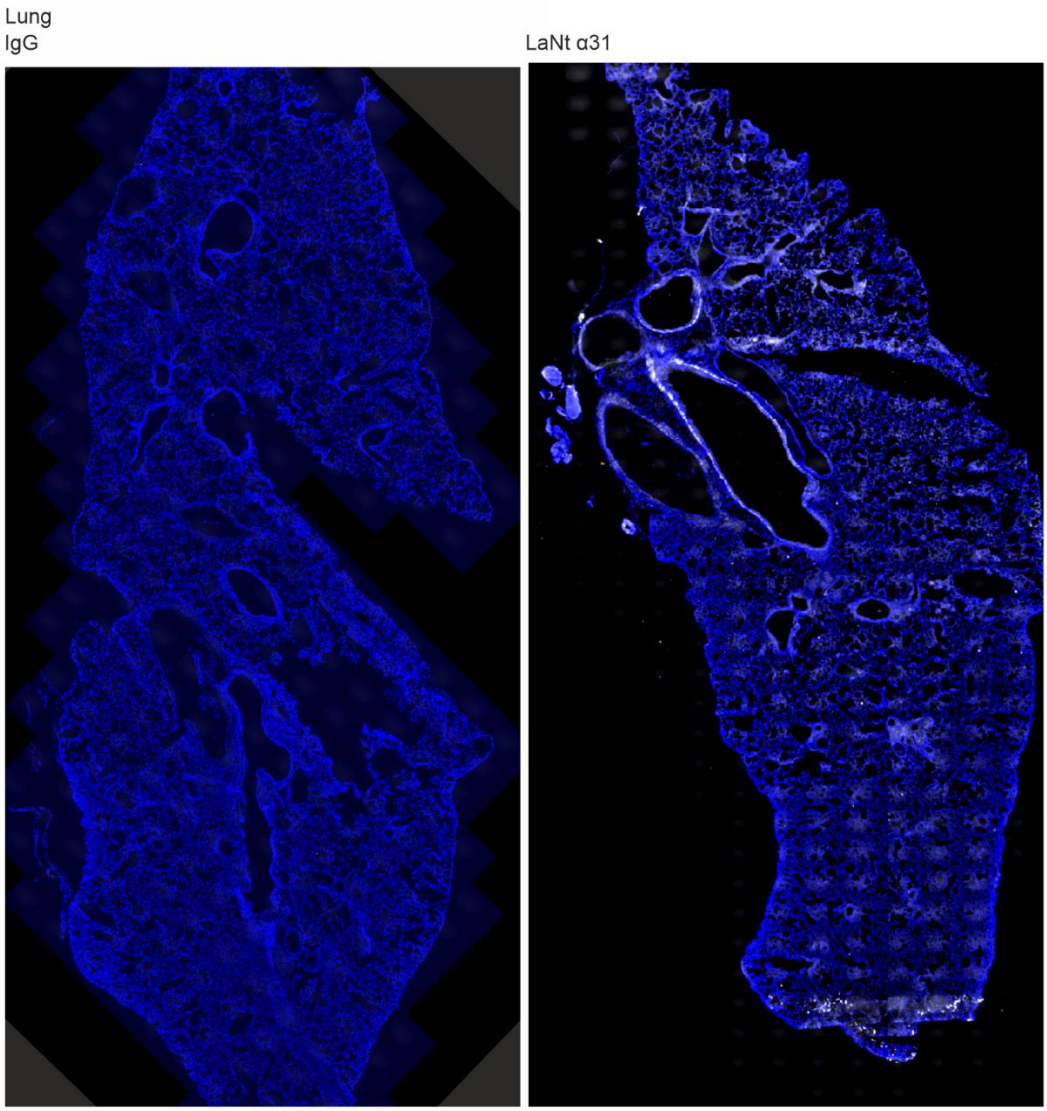

Figure 4.6. LaNt α31 is widely expressed throughout the lungs. Wild-type mouse lung OCT sections (10 µm) processed for immunohistochemistry with Rbt IgG antibodies (left) or Rbt anti-MsLaNtα31 antibodies (right).

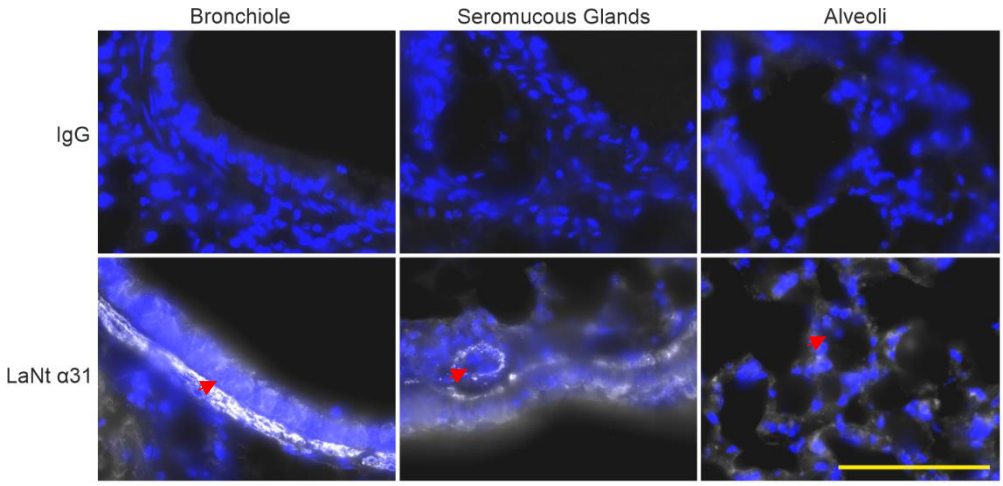

Figure 4.7. LaNt α31 immunoreactivity is observed around bronchioles, glands, and alveolar epithelium. Wild-type mouse whole lung OCT sections (10 µm) processed for immunohistochemistry with Rbt IgG antibodies (top) or Rbt anti-MsLaNtα31 antibodies (left). Scale bar = 100 µm. Red arrows represent location of basement membranes.

4.2.5 Heart

The heart was not previously investigated in humans. I wanted to assess LaNt α31 presence in heart tissue, as presence within the blood vasculature is a common feature in all tissues investigated. Interestingly, anti-LaNt α31 immunoreactivity was observed throughout cardiac muscle, which was not seen in other types of muscle (Fig. 4.8A). As expected, strong LaNt α31 immunoreactivity was observed in vasculature within the heart, and cellular positivity was observed in epicardiac tissue (Fig. 4.8B,C).

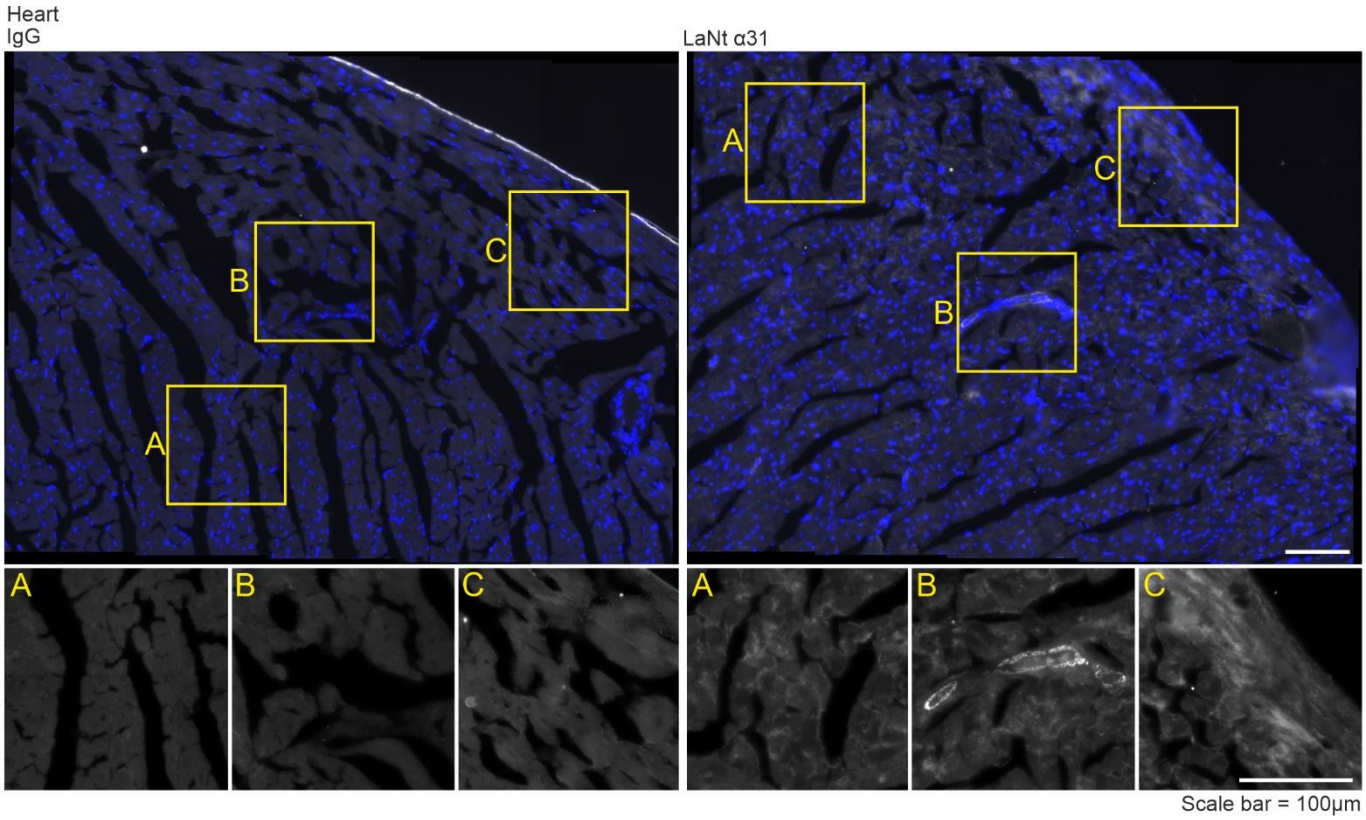

Figure 4.8. LaNt α31 is observed in multiple structures throughout the heart. Wild-type mouse heart OCT sections (10 μm) processed for immunohistochemistry with Rbt IgG antibodies (left) or Rbt anti-MsLaNtα31 antibodies (right). Yellow boxes indicate areas of increased magnification (smaller boxes, bottom row). Scale bar = 100 μm.

4.2.6 Brain

An advantage of using mouse tissue is that I was able to look at expression across the entirety of the brain. The only areas positive for LaNt α31 were the large vessels within the brain (Fig. 4.9, 4.10). Anti-LaNt α31 immunoreactivity was observed in any area where large vessels were present within the brain, and was not restricted to vessels within a particular sub region of the brain (Fig. 4.10A,B,D,F).

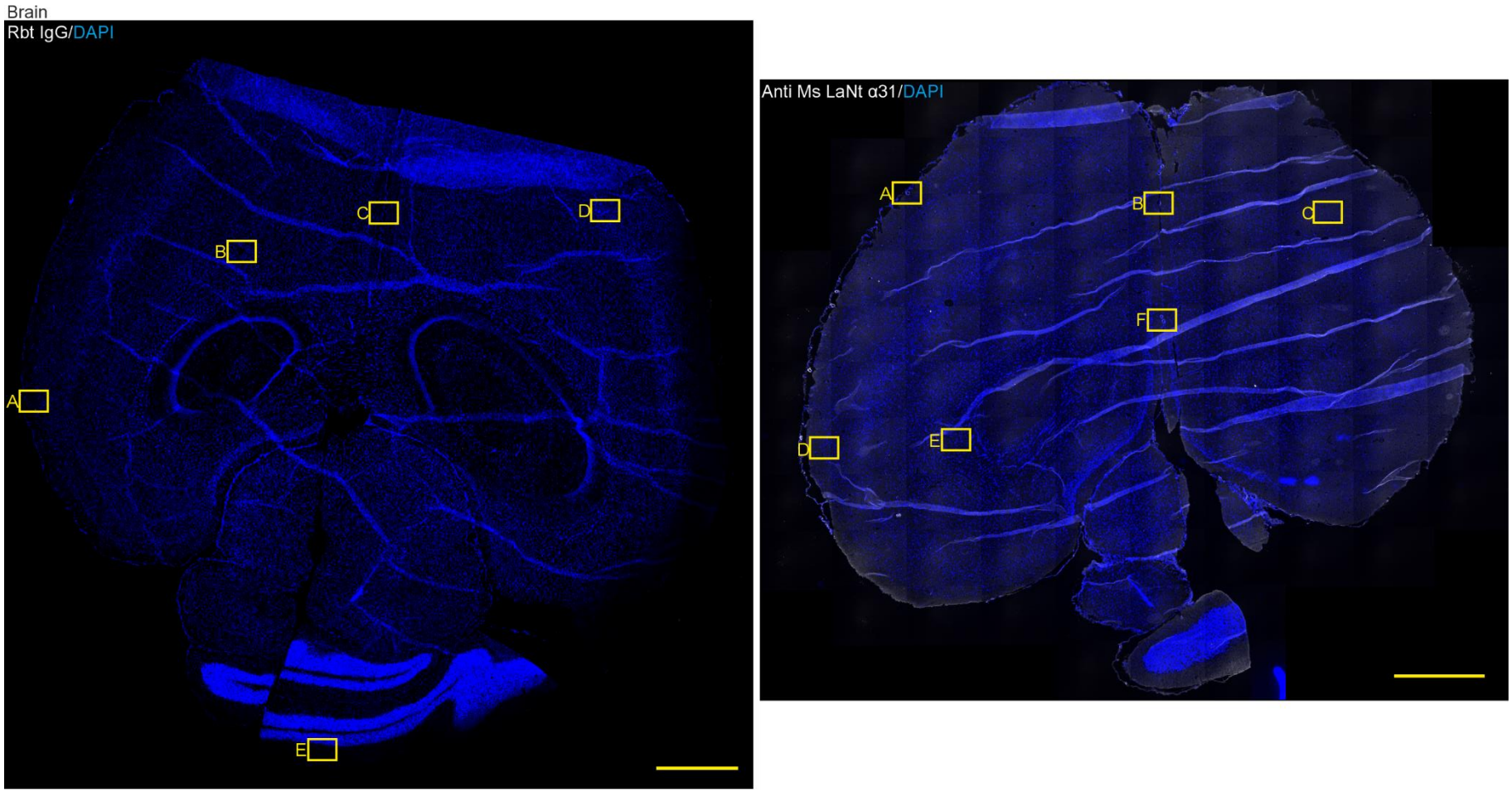

Figure 4.9. LaNt α31 is present in the brain. Wild-type mouse whole brain OCT sections (10 µm) processed for immunohistochemistry with Rbt IgG antibodies (left) or Rbt anti-MsLaNtα31 antibodies (right). Yellow boxes indicate areas of increased magnification (following figure). Scale bar = 500 µm.

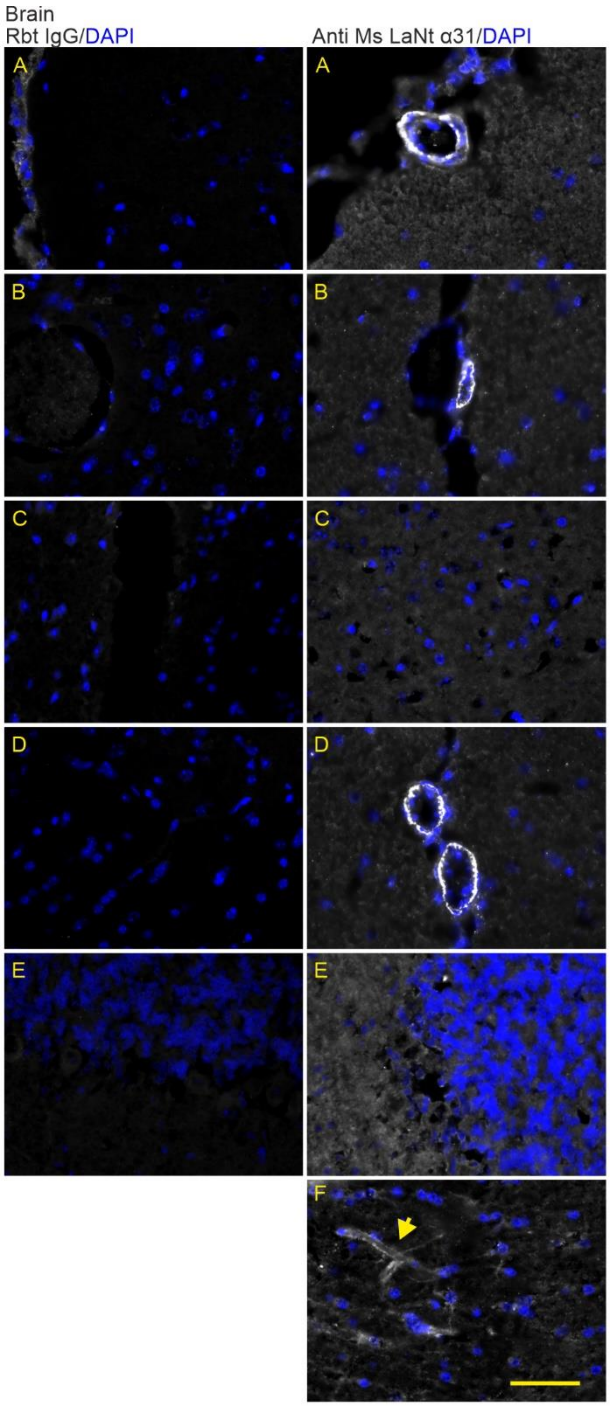

Figure 4.10. LaNt α31 immunoreactivity is observed only in the vasculature in the brain. Wild-type mouse brain OCT sections (10 µm) processed for immunohistochemistry with Rbt IgG antibodies (left) or Rbt anti-MsLaNtα31 antibodies (right). Yellow arrow indicates vessels running longitudinally. Scale bar = 50 µm.

4.2.7 Skin (newborn)

Next, I next assessed if LaNt α31 was present in the skin of newborn mice, as all human studies in skin and cornea had come from adults. LaNt α31 has been shown to be present in the BM of adult skin and enriched in corneal epithelial cells, while in situ hybridization demonstrated that the mRNA is enriched in the basal layer of the epidermis and hair follicles. Consistent with the findings in adult human tissues, LaNt α31 immunoreactivity was observed throughout the epidermis and hair follicle, with enrichment observed in the outer root sheath (Fig. 4.11, bottom).

4.2.8 Blood vasculature

As LaNt α31 antibodies had consistently recognised the vasculature in multiple tissue types, I next compared the distribution of LaNt α31 to a known vessel marker, CD31[267], by processing serial sections of newborn mouse skin. Whereas CD31 immunoreactivity was observed in all vessels, as expected, strong anti-LaNt α31 immunoreactivity was observed only in larger vessels (Fig. 4.11) and in individual pericyte cells surrounding and embedded in the vessel wall. Further investigation is required to find out specifically which types of vessels LaNt α31 is present. In comparison with CD31 immunoreactivity highlighted that LaNt α31 was either not present, or was expressed at a much lower lever, in smaller vessels (Fig. 4.11).

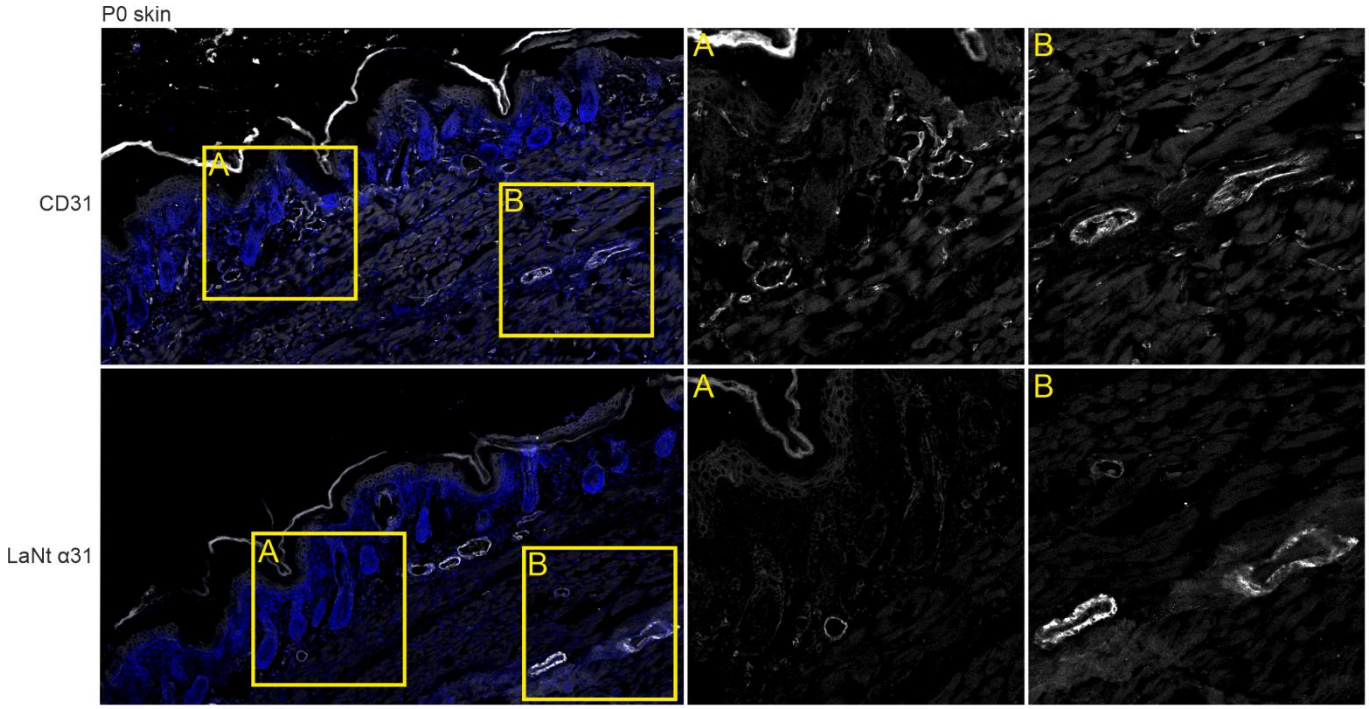

Figure 4.11. LaNt α31 is present in large, but not small vessels. Wild-type mouse lung OCT sections (10 µm) processed for immunohistochemistry with Rbt anti-CD31 antibodies (top row) or Rbt anti-MsLaNtα31 antibodies (bottom row). Yellow boxes indicate areas on increased magnification (middle and right columns).

4.3. Discussion

The results presented in this chapter show that LaNt α31 has widespread distribution in mice, and the Rbt anti-MsLaNt α31 antibodies used in this chapter represent a new tool for further investigation of the role LaNt α31 plays in mice. From the selection of tissues investigated, it is clear that LaNt α31 distribution in the mouse closely mimics that of humans. These findings have highlighted the strong vasculature expression of LaNt α31, and further illustrated the localization of LaNt α31 to structures within the kidney. The ability to image the entire mouse lung has made it clear to see the how LaNt α31 is located across most features of the lung. Along with the recent publication investigating LaNt α31 distribution across human tissues[52], it is clear that LaNt α31 is expressed more widely than initially thought, and is expressed in tissues where LM α3 expression is not observed.

One surprising result in this chapter comes from the comparison of LaNt α31 distribution compared to that of the pan-vascular marker CD31[268,269]. Indeed, LaNt α31 appears to be present only in larger vessels, with no positivity observed in microvessels within the skin. At this point it is difficult to predict why this is the case. Laminin 411 is a major component of all vessels[270], though laminin 511 is only found in patch-like distributions in large vessels[28,121,122,125,153,271,272]. LaNt α31 being in the same locations as vessels where laminin 511 may be expressed is interesting, as 511 contains 3 LN domains[31,48], and LaNt α31 would be placed in a situation where it may disrupt the 511 ternary nodes at high concentrations[9]. The effect of this as yet unknown, although this may have the potential to reduce the integrity of basement membranes, or the vessel as a whole, in locations where 511 is expressed.

Future directions related to the localization of LaNt α31 must co-stain tissues with different laminin components to see how these tie together. LM α3b has been shown to be present in blood vessel BMs[154]. The role of this protein in vessels is not well understood, but it is interesting in the fact the LaNt α31 is produced from the same promoter[51]. The LM α3b isoform is down-regulated in malignant skin cancers[154]. Comparisons of LM α3b and LaNt α31 in malignant cancers may reveal an interesting interplay between the two

proteins; ie. Is the down regulation of LM α3b a result of a change in splicing, in which case would one see an upregulation of LaNt α31? It is known that LaNt α31 is upregulated in invasive ductal breast cancer and changes the mode of tumour invasion, and perhaps the potential BM-disrupting capabilities of LaNt α31 would contribute to the cancer phenotype[55].

One point that must be appreciated is that there appears to be some tissues where LaNt α31 is present where laminin α3 is not known to be produced. This is the case for the kidney, where LaNt α31 immunoreactivity is observed in the glomerular basement membrane. The presence of LaNt α31 would suggest a unique function in the kidneys, and removes a LaNt α31-laminin α3 connection, as laminin α3 is absent from glomeruli, tubules, and vasculature of the renal cortex[121]. As far as the mature GBM is concerned, the major LM in the glomerular BM is LM 521. However, during the processes of GBM formation and maturation that occur during glomerulogenesis, there are developmental transitions in laminin trimer deposition, briefly summarized as LM-111 to LM-511 to LM-521[121,273-275]. All of the laminin chains within these heterotrimers contain an LN domain, and are therefore capable of polymerising into a LM network, and presence of LaNt α31 provides an additional α LN domain which could potentially compete for α chain interactions. The importance of this in normal biology is not yet known, although consequences of LaNt α31 dysregulation in the kidney are investigated in chapter 6.

4.3.1 Limitations

No single tool is perfect, and each tool comes with their own set of limitations. To validate an antibody, it must be shown to be specific and reproducible[276]. With regards to the newly generated Rbt anti-MsLaNt α31 antibody, it benefits from being able to triangulate the data with that obtained from existing tools, primarily the anti-human LaNt α31 antibodies[52]. One expected to see a similar distribution profile to that seen in humans, and the data in this chapter show that indeed that is the case. IgG controls were included for all tissues, which did not produce positive immunoreactivity. Moreover, peptide-blocking experiments prevented any immunoreactivity from the Rbt anti-MsLaNt α31 antibodies. In this chapter, OCT frozen

sections were used throughout, as the anti-MsLaNt α31 is not compatible with paraffin sections. This is not uncommon, particularly with antibodies against ECM proteins, potentially because of the harsh processing, which can be more damaging to the exposed ECM proteins. This presents an added difficulty with sample generation, handling, and storage. Nonetheless, the use of OCT sections does not undermine the validation of the anti-MsLaNt α31 antibodies.

All of these methods of validation allow one to be confident in the specificity of the LaNt α31 antibody. Additionally, the stringent screening procedures followed when producing the antibodies are described in the chapter 2. If one wanted to further validate this new antibody, a pull-down assay could be performed followed by mass spectrometry, to be sure of which proteins the antibody binds to. Additionally, this protein should be further tested in reducing vs non-reducing conditions, as posttranslational modifications may affect the interpretation of the results. Nonetheless, the with the validation shown in this chapter, and the triangulation with LaNt α31 distribution in humans, one can be confident that the findings in this chapter are real and robust.

4.3.2 Next steps

In the same vein, the localization of LaNt α31 in mice reflects what is seen in human strengthens the existing data that LaNt α31 has a widespread distribution particularly in the vasculature and epithelial basement membranes. Comparison to vascular marker CD31 has revealed LaNt α31 is present in larger, but not small vessels. The significance of this is yet to be appreciated, though future studies should co-stain tissue sections with anti-MsLaNt α31 antibodies and other anti-laminin antibodies, as well as other vascular markers to truly determine the type of vessel in which LaNt α31 is present. Moreover, future studies should address LaNt α31 distribution during development, and to see how, if at all, the expression of LaNt α31 changes from the embryo to the adult. Doing so will shed light on how basement membranes are regulated and deepen fundamental understanding of mammalian biology.

Considering LaNt α31 is produced by intron retention and alternative polyadenylation from the LAMA3 gene, a change in LaNt α31 expression from embryo to adult would suggest a tightly regulated and unappreciated mechanism of basement membrane regulation by LaNt α31. With the data generated here, together with the human LaNt α31 distribution study[52], there are new target tissue types to investigate with regards to the role LaNt α31 plays in the context of the composition of the surrounding ECM.

4.3.1 Conclusion

LaNt α31 has widespread protein distribution in mice, and based on its distribution, potentially plays a role in vascular homeostasis, as well as epithelial basement membranes. The new antibodies validated in this chapter adds to the growing toolbox of methods to enhance understanding of LaNt α31 and, in turn, basement membrane biology.

Chapter 5: Investigating the effects of LaNt α31 overexpression in 3D organotypic corneal and skin equivalents

The work presented in this chapter was in part supported by a research scholarship awarded by The German Academic Exchange Service (DAAD) and took place at Universität Freiburg, Germany.

5.1. Introduction

The published studies [51-53,55] and preprints [54] on LaNt α31, have examined LaNt α31 function in epithelial keratinocytes, have described its distribution in human adult tissues and describe changes in breast cancer. [51-53,55] and preprints [54] on LaNt α31, have examined LaNt α31 function in epithelial keratinocytes, have described its distribution in human adult tissues and describe changes in breast cancer. Functional studies including knockdown and overexpression experiments in vitro point toward a role for LaNt α31 in skin and corneal keratinocyte adhesion and migration [51,53], and in modifying ECM deposition and organization [51]. In ex vivo models of wound repair and stem cell activation, observational studies indicated LaNt α31 was upregulated during the re-epithelialization process then redistributed to the basal epithelium as the wounds healed[53].

Although the prior work all point toward LaNt α31 being a potentially important functional protein, at the start of this PhD, all the manipulative studies had been performed only in 2D cell culture. The effect of LaNt α31 had not yet moved into more physiologically complete 3D tissue-equivalent models.

This chapter describes the establishment and validation of two newly generated LaNt α31 stable overexpressing cell lines, and then the use of those lines to study the effect of LaNt α31 overexpression upon 3D organotypic cocultures.

5.1.1. Aim

To evaluate the effect of LaNt α31 overexpression on development of skin and corneal 3D equivalent models.

5.1.2. Objectives

i) Assess the phenotype caused by stable LaNt α31 overexpression in 2D culture

ii) Investigate the effects of long-term LaNt α31 overexpression using 3D organotypic coculture models of epithelial tissues

5.1.3. Overexpression construct overview

Previous functional studies investigations have used transient adenoviral overexpression to study LaNt α31 function[53-55]. To investigate LaNt α31 in long-term 3D organotypic coculture models, it was necessary to generate new tools to allow stable expression.

I designed a lentiviral construct for constant LaNt α31 overexpression. The construct contained a CMV promoter driving expression of the human LaNt α31 cDNA with its native secretion signal replaced by mouse immunoglobulin κ leader sequence, and Flag and HA epitope tags and photoactivatable mCherry fused to the C-terminus. Following the LaNt α31-PAmCherry fusion protein was a P2A element and puromycin resistance gene, The entire construct was flanked by HIV-1 long terminal repeats (LTR), allowing for integration into the target cell line genomes[277] (Fig. 5.1).

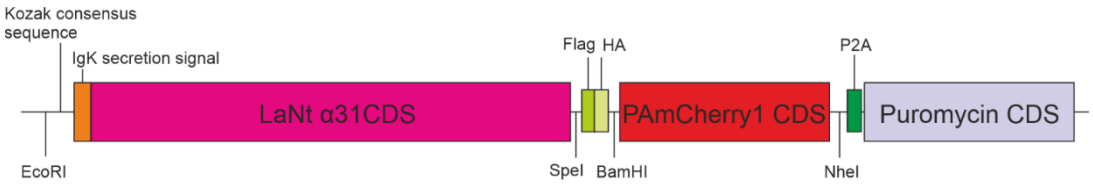

Figure 5.1. Diagram of the LaNtα31-PAmCherry fusion protein. Diagram of the expressed gene once integrated into the cell genome. LaNt α31-PAmCherry1 is expressed as a fusion protein, whilst puromycin is cleaved due the 'self-cleaving' mechanism of the P2A element.

5.1.3.1. Human cytomegalovirus (CMV) promoter

The CMV promoter has been successfully used before to drive expression in primary keratinocytes and in keratinocyte cell lines (HaCaT and hTCEpi) [53,54,278], making it an attractive choice to drive lentiviral-mediated gene expression in skin 3D cultures. The CMV promoter is a commonly used constitutive promoter for strong mammalian expression [279]. Although the CMV promoter generally provides robust gene expression across tissues, it is susceptible to silencing in some cell types such as neurons[280]. Despite this, many lentiviral constructs use the CMV promoter to drive gene expression, in part due to its small size and strength [279,281]. The CMV promoter has been successfully used before to drive expression in primary keratinocytes and in keratinocyte cell lines (HaCaT and hTCEpi) [53,54,278],

making it an attractive choice to drive lentiviral-mediated gene expression in skin OTC cultures.

5.1.3.2. Murine Immonoglobulin (Ig) kappa (κ) chain secretory leader sequence (IgK leader sequence)

I primarily wanted to study the effects of LaNt α31 as an extracellular matrix molecule. Therefore, I chose to design in features to a) increase the proportion of LaNt α31 in the ECM, and b) reduce potential for cellular effects associated with any build-up of intracellular LaNt α31. Protein secretion is strongly mediated by the N-terminal signal peptide[282]. Therefore to enhance LaNt α31 secretion, I replaced the native secretion signal with a strong secretion signal from the murine immunoglobulin kappa (IgK)[282].

5.1.3.3. LaNt α31

The human LaNt α31 coding DNA sequence was synthesised with some additional changes. A T7 promoter binding site was added 5' to the IgK sequence. 'SignalP - 6.0' in silico software was used to predict the LaNt α31 secretion signal. This was replaced with the IgK sequence, and the rest of the LAMA3LN1 CDS was included.

To allow cloning, specific restriction sites BamHI and ScaI within the LaNt α31 sequences were destroyed by making single nucleotide changes at wobble bases. NdeI, EcoRI, HpaI, EcoRV and NheI sites were added 5' to the LaNt α31 transcript and BamHI, SpeI and KpnI sites were added 3' to the LaNt α31 sequence. These edits did not cause any change of the LaNt α31 amino acid sequence but were designed to maximise flexibility for using this construct going forward.

5.1.3.4. HA and Flag tags

HA and Flag epitope tags were appended in frame to the C-terminus of the LaNt α31 transcript to increase detection and purification options. The HA tag is derived from the human influenza hemagglutinin (HA) molecule corresponding to amino acids 98-106, and the Flag-tag was the first epitope tag designed for fusion proteins, with amino acid sequence DYKDDDK [260,261]. Both epitope tags have been studied extensively, with a wide variety of well-characterised commercial antibodies available[260,261].

5.1.3.5. PAmCherry fluorophore

Genetically encoded photoactivatable proteins make up a small category of fluorescent proteins[283], and have now become an established tool for super-resolution microscopy techniques[284]. PAmCherry1 is a 26.8 kDa photoactivatable red fluorescent protein derived from *Discosoma* sp.[285]. The PAmCherry fluorophore is initially dark until it is activated by 405nm wavelength light, thereafter it exhibits an excitation maximum of 564nm and an emission maximum of 595 nm[285]. The photoactivatable property of PAmCherry makes the protein suitable for superesolution microscopy techniques such as photoactivated localization microscopy (PALM)[286], fluorescence photoactivated localization microscopy (FPALM)[287] and stochastic reconstruction microscopy (STORM)[288]. This was tag included as a directly-fused protein tag 3' of the LaNt α31, to provides the option for studying the spatial distribution and dynamics of LaNt α31. Genetically encoded photoactivatable proteins make up a small category of fluorescent proteins[283], and have now become an established tool for super-resolution microscopy techniques[284].

5.1.3.6. 2A element

Porcine teschovirus-1 2A peptides, (sequence ATNFSLLKQAGDVEENPGP) are part of a family of 18-22 amino acid 2A oligopeptides that mediate cleavage of polypeptides during translation in eukaryotic cells, allowing for the expression of multiple non-fusion proteins from the same promoter[289,290]. Multiple 2A peptides are commonly used [291], derived from different virus, although all share a highly conserved sequence at the C-terminus of the peptide GDVEXNPGP, which is essential for the 'self-cleaving' mechanism in these peptides. Essentially where the ribosome does not form a peptide bond between the Gly and Pro at the C-terminus of the peptide [292,293]. The inclusion of this element allowed for the co-expression of the LaNt α31-PAmCherry fusion protein *and* a puromycin resistance cassette as two separate proteins.

5.1.3.7. Puromycin resistance cassette

Puromycin is an antibiotic which is toxic to eukaryotic cells and leads to rapid death of non-resistant cells. The inclusion of a puromycin resistance

cassette, encoded by the gene puromycin N-acetyl-transferase, allowed for selection by puromycin for rapid identification of cells that had taken up and expressed the transgene.

5.1.4.8. Woodchuck Hepatitis Virus Posttranscriptional Regulatory Element (WPRE)

The woodchuck hepatitis virus post-transcriptional regulatory element (WPRE) increases expression from viral vectors, particularly when placed downstream of the transgene, proximally to the polyadenylation signal[294]. To achieve maximal expression of the transgene following incorporation into the host cell genome, I included the WPRE element 3' of the LaNt α31-PAmCherry and puromycin sequences.

5.2. Results

5.2.1. Lentiviral LaNt α31 overexpression construct validation

A gBlock containing a Kozak sequence, the *LAMA3LN1* coding sequence, Flag and HA tags, and the PAmCherry coding DNA sequence was synthesized and inserted into the pLenti-P2A-puromycin (Fig. 5.2).

Two cell lines were used for these studies; hTCEpi, a hTERT immortalised limbal-derived corneal epithelial cell line that was used in functional adenoviral studies[54] and which has previously been used by others in 3D culture studies[254], and human papillomavirus16 E6/E7 immortalized normal human keratinocytes (NHKs), which have been used extensively in skin equivalent models[295] , and have been shown by proteomic analysis to display high phenotypic stability, keep cell linage–specific characteristics, and show only minor changes compared with primary keratinocytes[295,296].

hTCEpi and NHK cells were transduced with the CMV-LaNtα31--PAmCherry-P2A-puromycin lentiviral particles, and antibiotic selected to obtain a pool of hTCEpi or NHK cells expressing the LaNtα31-PAmCherry-P2A-puromycin gene. Expression and functionality of the LaNtα31-PAmCherry-P2A-puromycin gene was confirmed by western immunoblotting, indirect immunofluorescence, and live cell imaging before and after photoactivation of PAmCherry (Fig. 5.3).

Western blotting using monoclonal anti-HA antibodies confirmed expression of the predicted ~81 kDa band from cell lysates from transduced and selected cells and conditioned media, also confirming cleaving of the puromycin resistance gene by the P2A element (Fig. 5.3A,B). One additional smaller band (~70 kDa) was observed in cell lysate samples (Fig. 5.3B). Transduced cells were prepared for indirect immunofluorescence microscopy and processed with monoclonal anti-HA antibodies (Fig. 5.3C). Anti-HA immunoreactivity was observed only in cells transduced with the LaNtα31-PAmCherry-P2A-puromycin transgene. The intensity of anti-HA immunoreactivity varied greatly from cell to cell within the population. PAmCherry signal was observed in samples transduced with LaNtα31-PAmCherry-P2A-puromycin lentiviral particles following activation with 405

nm wavelength light, signal strength was heterogenous among cells, mirroring the heterogeneity seen in the samples processed for indirect immunofluorescence (Fig. 5.3D). No difference was observed in the growth of WT vs LaNt OE cells, though this was not formally tested. A proliferation assay should be done in the future to confirm.

Taken together, these results demonstrate the transduction with CMV-LaNtα31-LaNtα31-PAmCherry-P2A-puromycin lentiviral particles generates cells that express the LaNt α31-PAmCherry fusion protein.

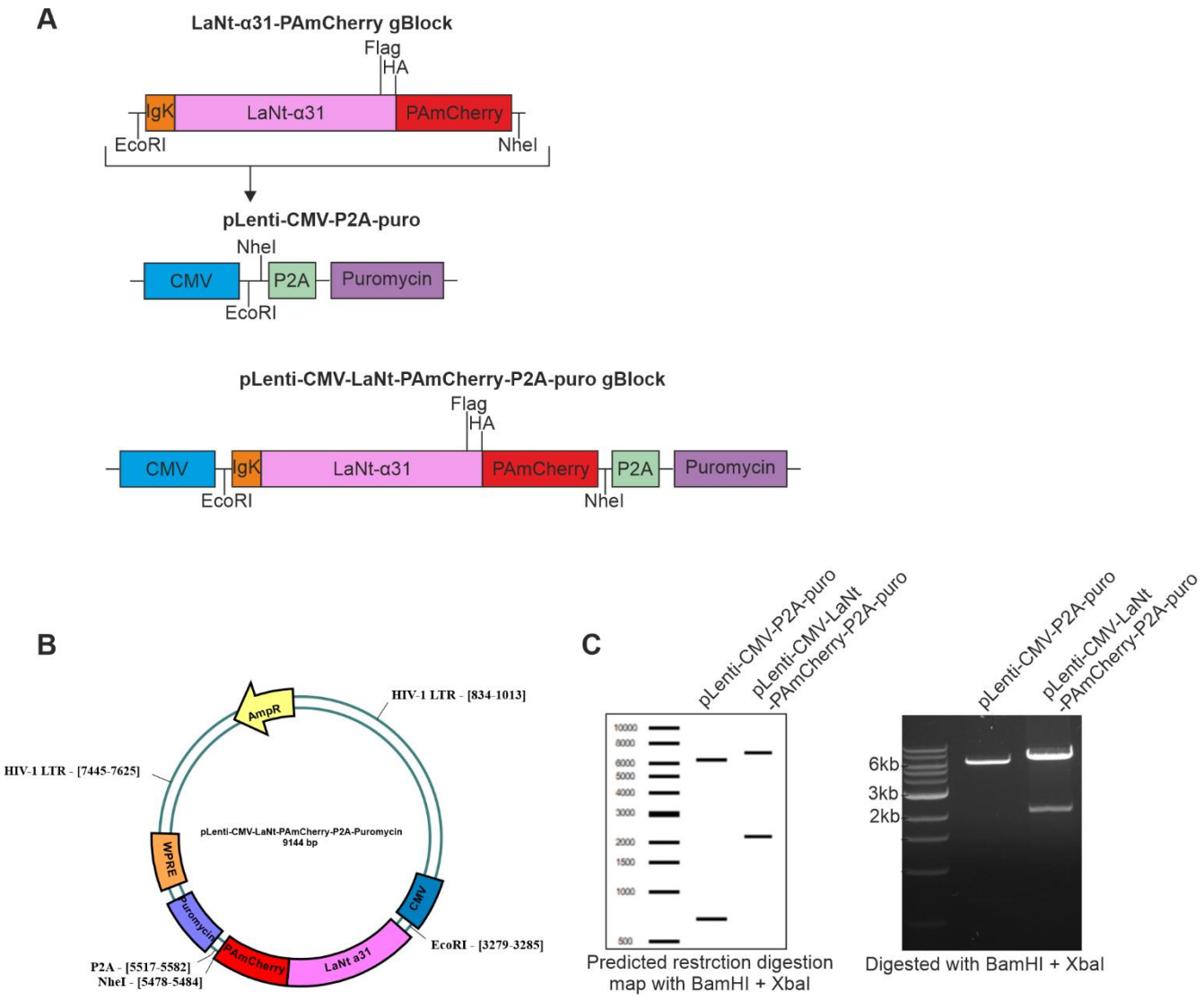

Figure 5.2. Cloning steps for pLenti-CMV-LaNtα31-PAmCherry1-P2A-puro. A) A gBlock was synthesised containing the IgK sequence, LaNt α31 CDS, Flag and HA tags, and the PAmCherry1 CDS was inserted into pLenti-CMV-P2A-puro between EcoRI and NheI cloning sites, producing pLenti-CMV-LaNt-PAmcherry-P2A-puro. B) Vector map showing relevant features of pLenti-CMV-LaNt-PAmcherry-P2A-puro. C) Diagnostic restriction enzyme digests confirmed correct size of pLenti-CMV-LaNt-PAmcherry-P2A-puro and correct orientation of the insert.

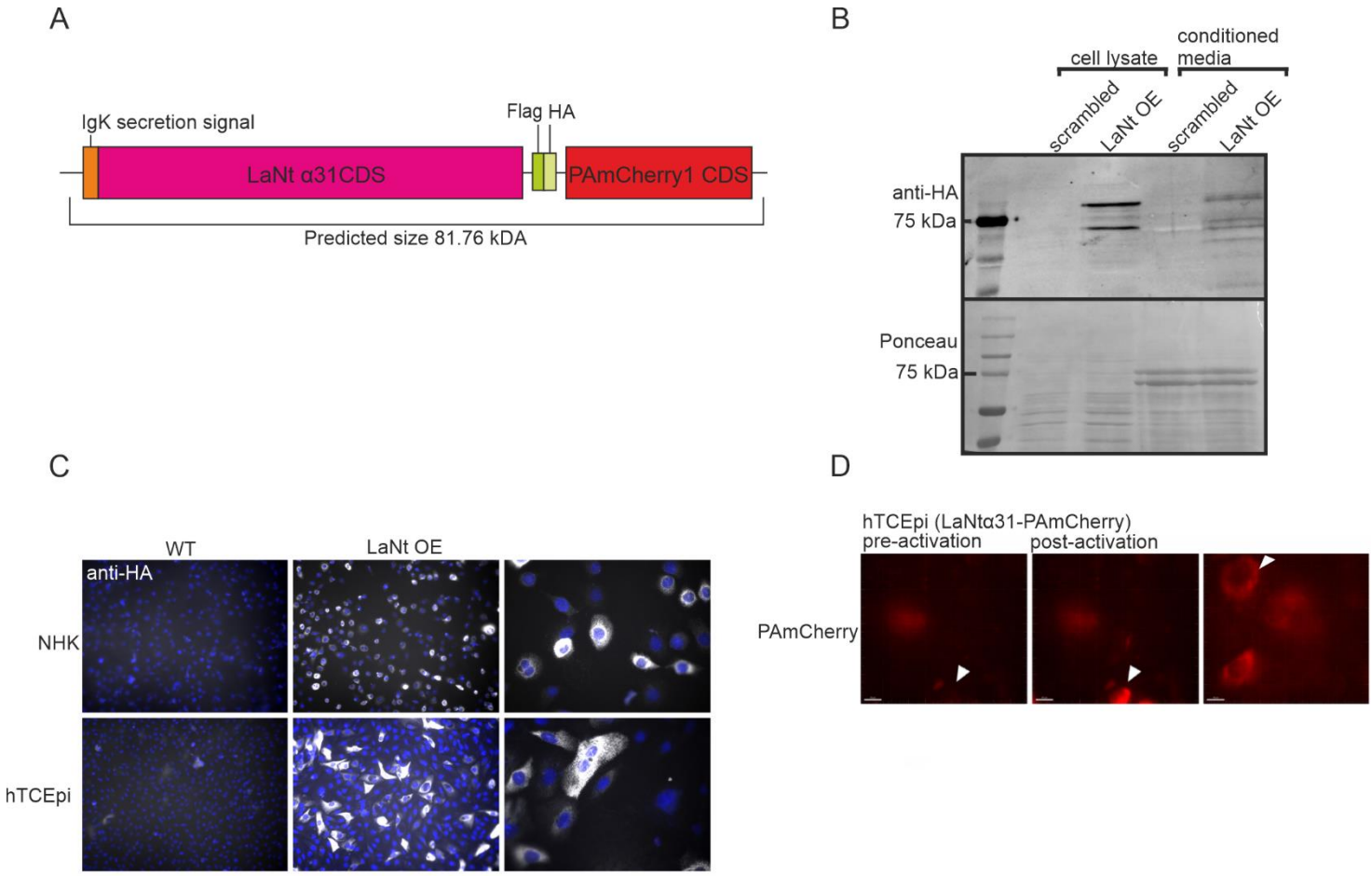

Figure 5.3. Lentiviral LaNt α31 overexpression construct validation. A) Diagram of the predicted size of the LaNtα31-PAmCherry fusion protein. B) Western blot of lysates and conditioned media from lenti-GFP or LaNt OE NHKs processed with anti-HA antibodies. Molecular weight ladder is shown in the left lane. C) NHK (top) and hTCEpi (bottom) cells processed for indirect immunofluorescence microscopy using anti-HA antibodies. D) Fluorescence microscopy of LaNt OE hTCEpi cells pre-activation (left box) and post-activation with 405 nm light (middle and right boxes). White arrowhead indicates the same cell in all images.

5.2.2. LaNt α31 overexpression leads to changes in NHK cell morphology and a reduction in migration rates

LaNt α31 overexpression causes changes in cell morphology and cell migration in primary limbal-derived corneal epithelial cells[53] and in hTCEpi's[54]. The newly generated lentiviral overexpressing NHK cells allowed the opportunity to triangulate these findings in a new cell line while simultaneously confirming that the new lentiviral construct produced a functional protein. I analyzed the shape and migration of cells overexpressing the LaNtα31-PAmCherry gene (Fig. 5.4). In NHKs, LaNt OE

cells were compared against NHKs transduced with a GFP-encoding lentivirus, to control for any variables related to the transduction and antibiotic selection process, as well as any phenotype caused by the overexpression of fluorescent proteins.

There was no statistically significant change in 2D cell area compared to GFP controls at 2h or at 6h after seeding (mean ± SD size μm^2 2h GFP = 130 ± 57 N=158, LaNt α31 OE = 140 ± 73 N=158, p = 0.09, 6h GFP = 283 N=94 ± 141, LaNt α31 OE = 292 ± 149 N=73, p = 0.71) (Fig. 5.4C). However, LaNt α31 OE cells were less round at 2h compared to GFP controls (mean ± SD cell roundness GFP = 0.81 ± 0.13 N=158, LaNt α31 OE = 0.72 ± 0.18 N=158, p = <0.001). This difference was not present once the cells had been allowed to spread for 6h (mean ± SD cell roundness GFP = 0.73 ± 0.13 N=95, LaNt α31 OE = 0.75 ± 0.13 N=73, p = 0.22)(Fig. 5.4D).

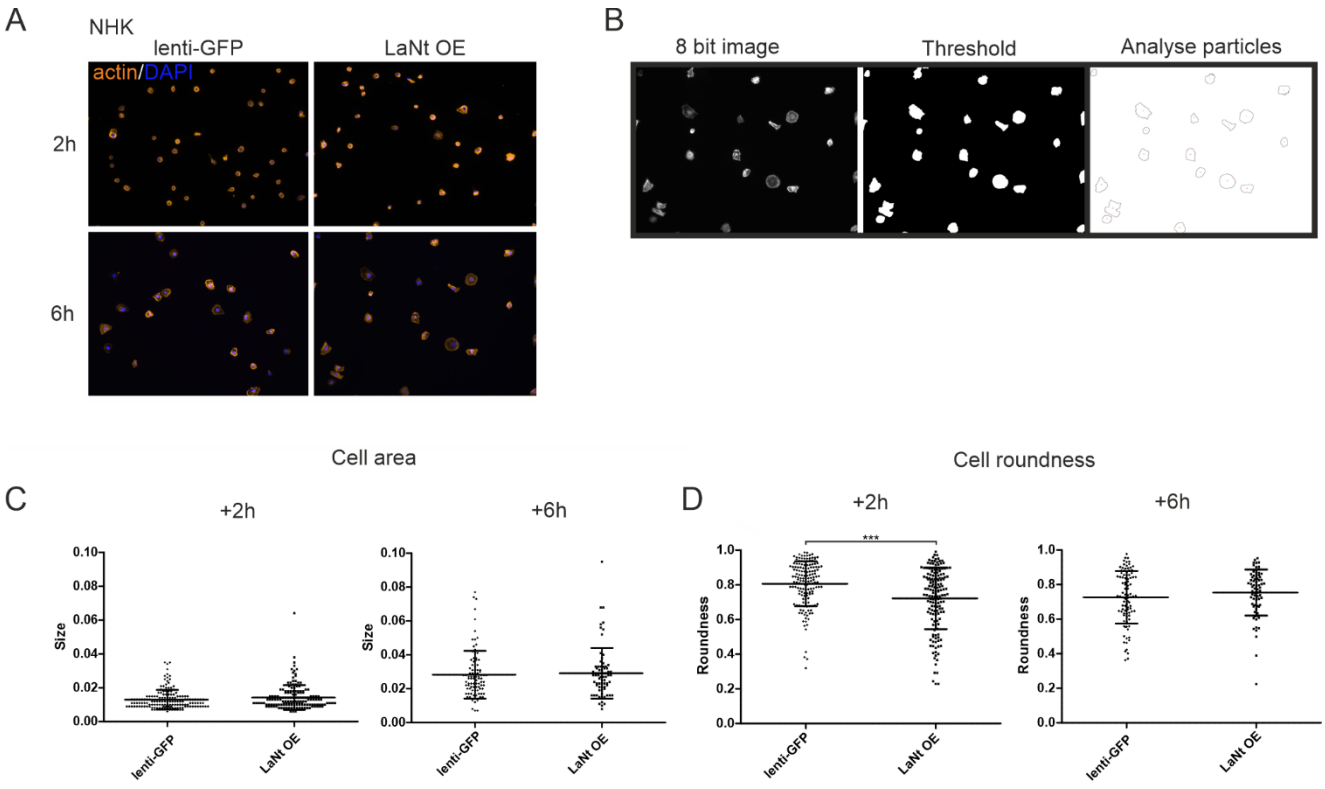

Figure 5.4. LaNt α31 overexpression leads to changes in NHK cell morphology. A) Representative images of NHK cells processed for indirect immunofluorescence microscopy using phalloidin and DAPI at 2h (top row) and 6h (bottom row) after seeding, cell area and roundness plotted in (C) and (D). B) Representative image analysis method of determining cell area and cell roundness. C and D) Cell area (C) and cell roundness (D) was measured in lenti-GFP or LaNt OE NHKs 2h (left) or 6h (right) after seeding. N= at least 99 individual cells across 3 separate experiments. *** in (D) denotes p< 0.001 between lenti-GFP and LaNt OE, determined by a two-tailed t test.

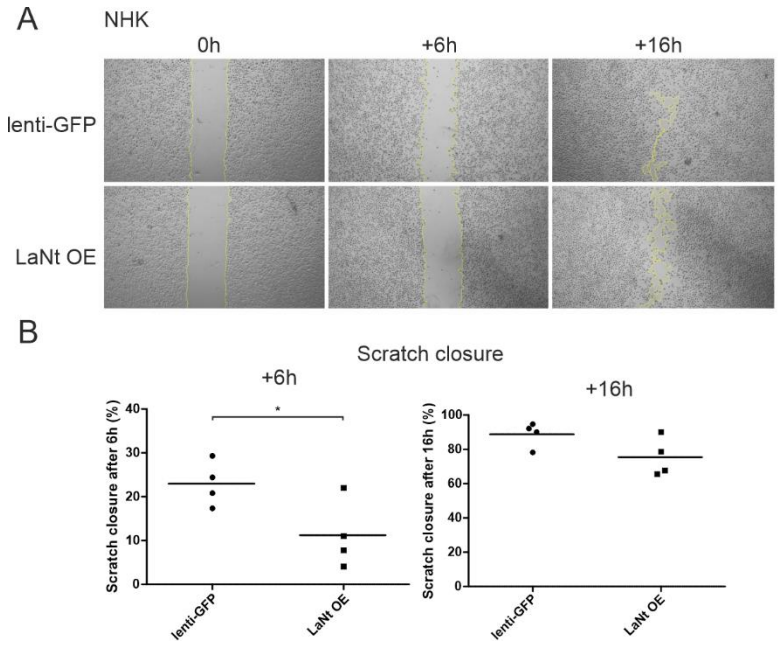

Figure 5.5. LaNt α31 causes a reduction in NHK migration rates. A) lenti-GFP or LaNt OE NHK cells were plated overnight at confluence and a scratch wound introduced 16 h later. A) Representative images from immediately after scratching (0 h, left panels) and at 6 h (middle panels) and 16 h (right panels) of recovery. Yellow lines indicate wound margins. B) Gap area closure measured at 6 h (left) and 16 h (right) after wounding plotted as percentage of the initial wound area with each point representing an independent experiment with either 2-3 technical repeats per experiment. * denotes $p<0.05$ compared with controls determined by a two-tailed t test.

2D scratch assays revealed a 48% reduction in scratch wound closure in LaNt α31 stable cell lines as measured 6h after scratch compared to the GFP control cells (mean ± SD scratch closure % GFP = 23 ± 5, LaNt α31 OE = 11 ± 8 N=4, p = 0.045), and a 16% reduction at 16h (GFP = 89 ± 7 N=4, LaNt α31 OE = 75 ± 11 N=4, p = 0.095)(Fig. 5.5A,B).

In hTCEPi cells, adenoviral LaNt α31 overexpression causes a clustering of LM332 when deposited[54]. Indirect immunofluorescence microscopy was used to determine if a similar phenotype was observed in NHKs overexpressing LaNt α31. Whereas GFP-expressing NHKs deposited LM332 in broad arcs and contiguous lines, NHKs cells overexpressing LaNt α31 deposited LM332 into tight, small clusters (Fig. 5.6).

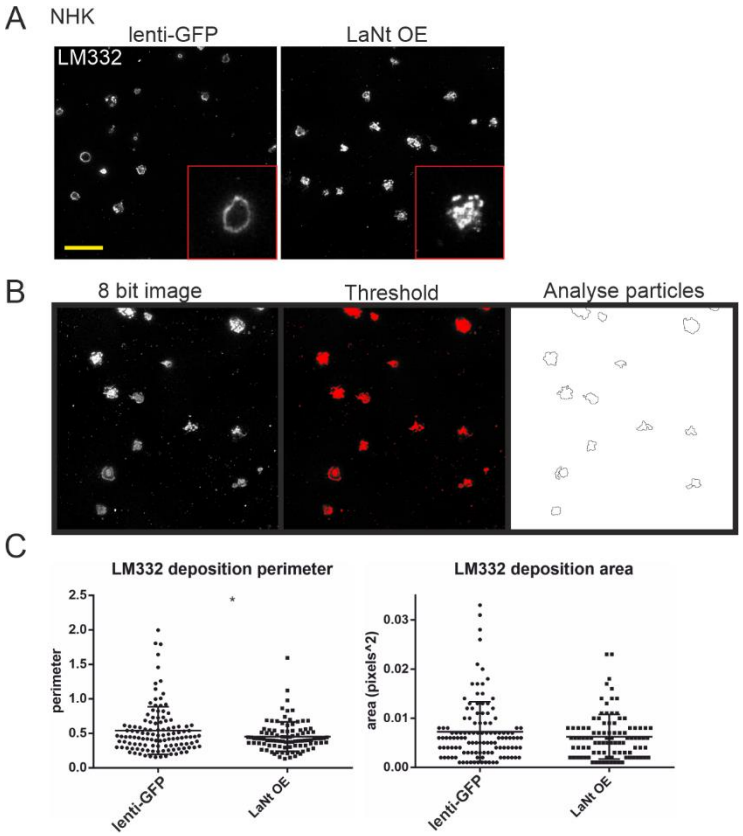

Figure 5.6. LaNt α31 overexpression causes LM332 clustering. A) lenti-GFP or LaNt OE NHK cells were plated at low density on uncoated glass coverslips then processed for immunofluorescence microscopy with antibodies against LM α3 after 6 h. Insets represent areas of higher magnification. Scale bar = 50 μm. B) Representative image analysis method of determining LM332 deposition perimeter and area. C) LM332 deposition perimeter (left) and area (right) was measured in lenti-GFP and LaNt OE NHKs. N= at least 80 individual cells across 3 separate experiments. * denotes $p<0.05$ compared with controls determined by a two-tailed t test.

5.2.3. Validation of LaNt α31 overexpression in 3D organotypic cocultures.

I next used the newly generated stable cell lines to establish 3D organotypic cocultures[297]. These consisted of a ‘dermis’ composed of primary normal human fibroblasts (NHFs) from three different donors with I next used the newly generated stable cell lines to establish 3D organotypic cocultures[297]. These consisted of a ‘dermis’ composed of primary normal human fibroblasts (NHFs) from a different donor per coculture embedded in a collagen gel, and an epithelium composed of either the lentiviral transduced hTCEpi or the NHK cell lines (Fig. 5.7). The co-cultures were raised to the air/surface interface then cultured for 7 days to generate organotypic skin equivalents (OSE) or corneal equivalents (OCE). These were then embedded in paraffin or OTC medium for histological and immunofluorescence analysis.

Expression of the LaNt α31 transgene was again confirmed by anti-FLAG and anti-HA immunoreactivity, with fluorescence observed only in the epithelial layers of the OCE (Fig. 5.8A) or OSE (Fig. 5.8B) from cultures generated using the stably expressing cell lines.

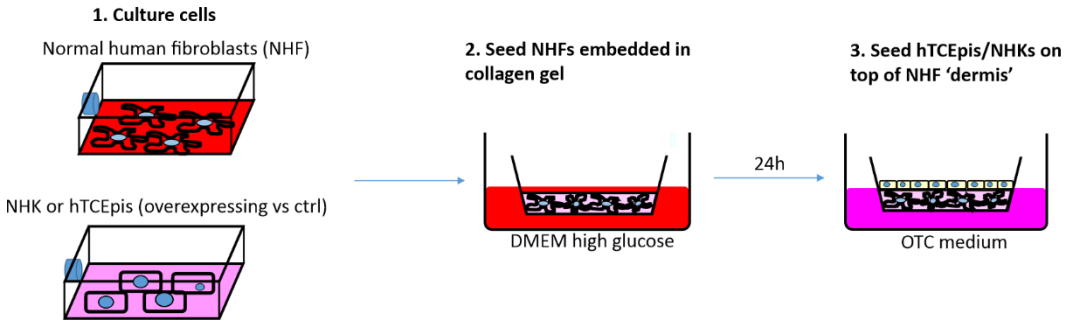

Figure 5.7. Schematic of OSE and OCE culture set up. NHKs or hTCEpis were cultured in normal conditions. Next, normal human fibroblasts were embedded in a collagen gel and placed into cell inserts in DMEM high glucose culture media. Finally, NHKs or hTCEpis were seeded on top of the normal human fibroblasts after 24 h.

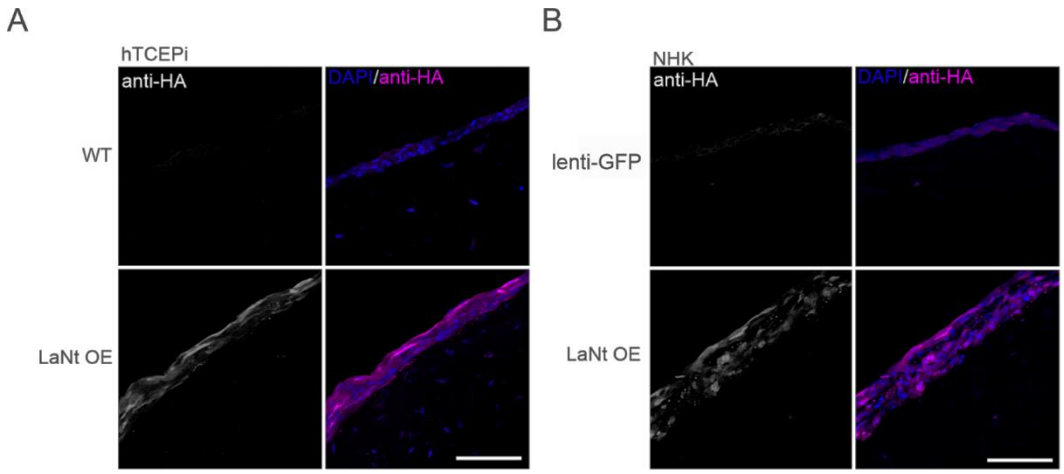

Figure 5.8. Confirmation of LaNt α31 overexpression in OSE and OCE cultures. hTCEpi organotypic corneal equivalents (OCE) or NHK organotypic skin equivalents (OSE) were embedded in OCT medium after 7 days and processed for immunohistochemistry. OCE (A) and OSE (B) sections (8 µm) were probed with anti-HA antibodies and costained with DAPI in the merged image. Scale bars 100µm.

5.2.4. LaNt α31 overexpression causes the formation of cyst-like structures in 7-day OCE cocultures.

Paraffin sections of the OCE cultures were stained with haematoxylin and eosin. Large cyst-like structures were observed in the epithelium of LaNt α31 overexpressing cultures in the hTCEpi OCEs, (Fig. 5.9, yellow arrows). These were not restricted to a particular position within the epidermal structure. LaNt α31 overexpressing hTCEpi cells also appeared to be larger than the WT counterparts in the outer layers of the epithelium structure (Fig 5.9). No difference was observed between different NHF donors.

5.2.5. LaNt α31 overexpression causes the formation of gaps between basal keratinocytes in 7-day OSE cocultures.

Similar differences were observed between the GFP and LaNt α31 overexpressing epithelium in NHK OSEs as for the OCEs; however, generally, the changes were more subtle (Fig. 5.10). In LaNt α31 OSEs, gaps formed between basal keratinocytes, which were generally not present in the GFP OSE (Fig. 5.10, yellow arrows).

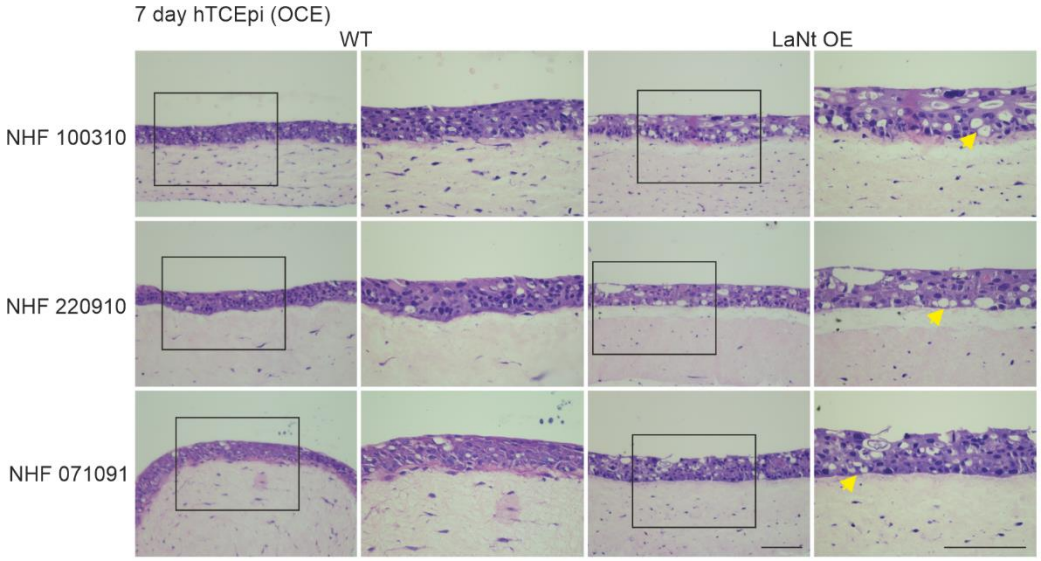

Figure 5.9. H&E stained sections of 7-day OCE cocultures. H&E staining of FFPE sections (5 µm) of WT (left two columns) and LaNt OE (right two columns) 7 day OCE cocultures. Black squares indicate areas of increased magnification. Each row shows OCEs with normal human fibroblasts from different donors. Yellow arrows indicate cyst-like structures. Scale bar = 200 µm.

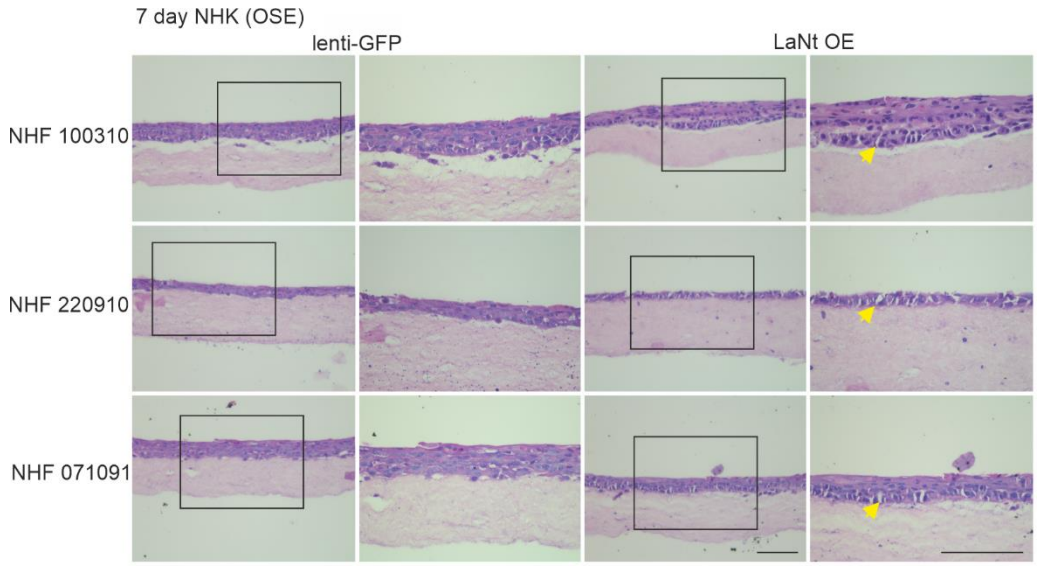

Figure 5.10. H&E stained sections of 7-day OSE cocultures. H&E staining of FFPE sections (5 µm) of WT (left two columns) and LaNt OE (right two columns) 7 day OSE cocultures. Black squares indicate areas of increased magnification. Each row shows OSEs with normal human fibroblasts from different donors. Yellow arrows indicate cyst-like structures Scale bar = 200 µm.

5.2.6. LaNt α31 overexpression causes the formation of cyst-like structures in 4-week OSE and OCE.

To assess how the observed phenotype progressed, whether the disorganization became more severe or was recovered, OCE's and OSE's were cultured for 4 weeks. At this timepoint, for both OCE's and OSE's, epithelial disorganization was observed in the control and LaNt OE conditions, making it difficult to draw robust conclusions. However, the most "disorganised" samples were in LaNt OE OCE's, with cyst-like features and cell enlargement being a prominent feature.

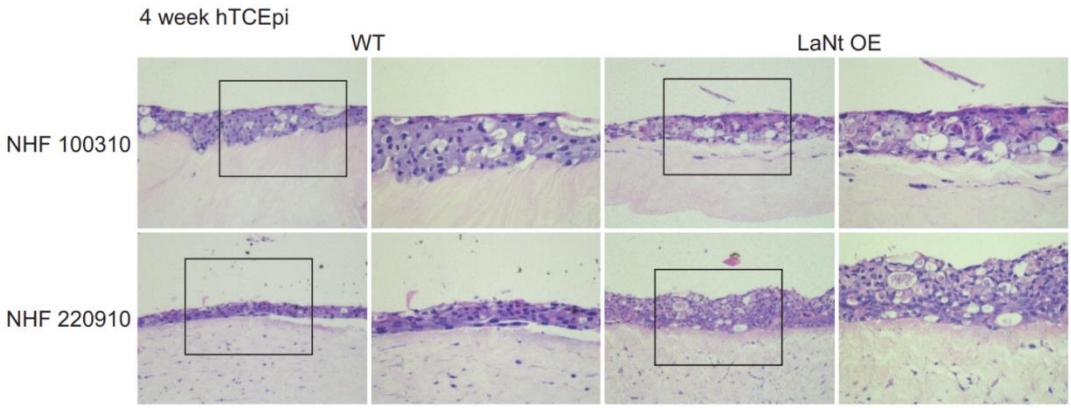

Figure 5.11. H&E stained sections of 4-week OCE cocultures. H&E staining of FFPE sections (5 µm) of WT (left two columns) and LaNt OE (right two columns) 4-week OCE cocultures. Black squares indicate areas of increased magnification. Each row shows OCEs with normal human fibroblasts from different donors. Scale bar = 200 µm.

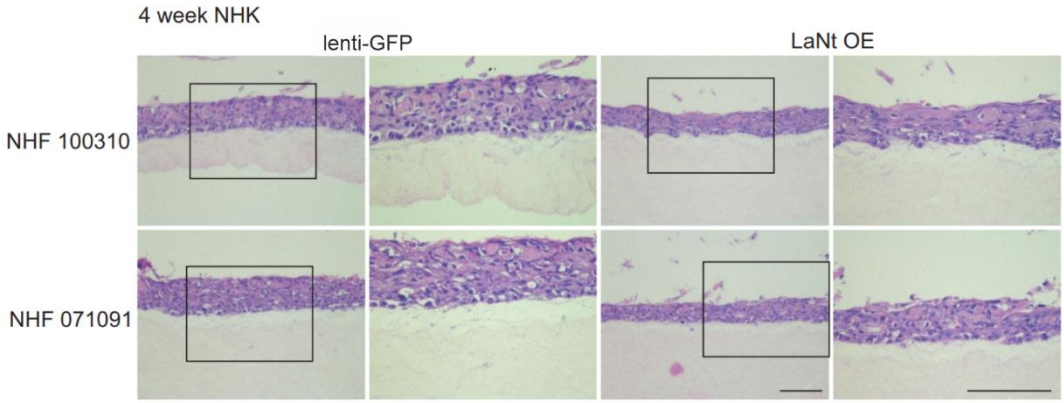

Figure 5.12. H&E stained sections of 4-week OSE cocultures. H&E staining of FFPE sections (5 µm) of WT (left two columns) and LaNt OE (right two columns) 4-week OSE cocultures. Black squares indicate areas of increased magnification. Each row shows OSEs with normal human fibroblasts from different donors. Scale bar = 200 µm.

5.2.7. LaNt α31 overexpression disrupts LM332 deposition at the stromal-epithelial junction.

Cryosections from 7-day OCE cocultures were processed using anti-LM332 antibodies (Fig. 5.13). This revealed a difference in LM332 distribution along the stromal-epithelial junction, with a loss of contiguity in the LaNt overexpressing samples (Fig. 5.13, arrows). LM332 deposition at the stromal-epithelial junction was also thicker, with immunoreactivity observed penetrating into the epithelial cell layer, compared to in WT samples where LM332 deposition was limited to the basal aspect of the bottom layer of keratinocytes.

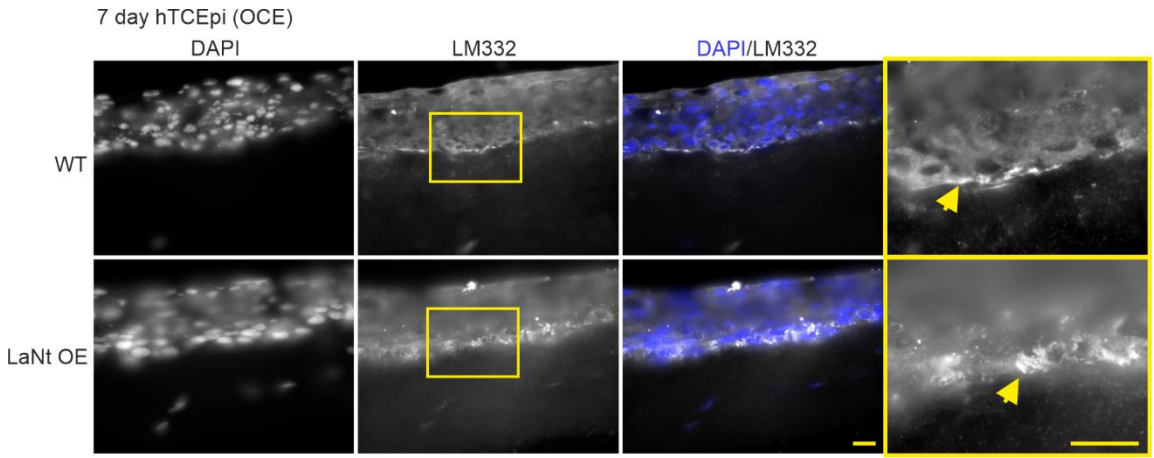

Figure 5.13. LaNt α31 overexpression causes disorganised LM332 deposition in OCE cultures. hTCEpi organotypic corneal equivalents (OCE) were embedded in OCT medium after 7 days and processed for immunohistochemistry. WT (top row) or LaNt OE (bottom row) OCE sections (8 µm) were probed with anti-LM332 antibodies and DAPI. Yellow boxes indicate areas of increased magnification. Yellow arrows indicate LM332 positivity at the stromal-epithelial junction. Scale bar = 50 µm.

5.3. Discussion

The findings presented here demonstrate stable overpexpression of LaNt α31 influences cell morphology, migration rates and LM deposition in vitro in corneal keratinocytes and in normal human skin keratinocytes and that LaNt α31 dysregulation is detrimental to the epithelial layer integrity in 3D organotypic coculture models of skin and cornea. These findings further support that LaNt α31 can regulate cell behaviour in vitro and provide a first suggestions of what this might mean for tissue function.

5.3.1. LaNt α31 dysregulation is detrimental to 3D OCE and OSE epithelial health

The main advantage of generating and validating stable expressing skin and corneal cell lines was to be able to observe the effect of LaNt α31 in long term 3D studies. Based on prior 2D results suggesting stronger cell adhesion, one would have predicted more mature OSE and OCE cultures, particularly in the 7-day cocultures. However, the findings here cast doubts upon this hypothesis. Indeed, the histological observation indicate that epithelial LaNt α31 overexpression was detrimental to the integrity of 3D OSE and OCE cultures. Moreover, LM332 localization is disrupted at the stromal-epithelial junction of LaNt α31 OSE cocultures. The reason for both of these outcomes may be two-fold. Indeed, a disruption to the BM in LaNt α31 OE cultures points towards a direct, physical interaction preventing LM from being deposited in the correct manner; instead of forming a single, contiguous network, which would be clear from immunostaining, there is a dysregulated, broken network. To assess what the reasons for this, next steps would include electron microscopy to assess BM ultrastructure and integrity, as well as comparing hemidesmosome structure.

Why would LaNt α31 disrupt the epidermal-dermal BM? The answer may lie in the specificities in the LM332 isoforms. In hTCEpis and NHKs, the predominant isoform is LM3a32, along with smaller amounts of LM511, 311, 521, and 111 [202,214,298-302]. Although not enough is known yet about LM polymerization in these tissues to draw definite conclusions, there are data to indicate a covalent interaction between LM311 and LM321 with LM332. It is through these LM332 interactions that a LM network can form in epithelia[61]. If

this method of network formation is the correct, and allows for ternary nodes to form and a full LM network to be established, LaNt α31 may compete for αLN interactions, once again bringing us back to the network disruption hypothesis.

5.3.1.1. Does LaNt α31 overexpression cause differentiation defects?

The phenotype observed in LaNt α31 OSE and OCE cultures resemble keratinocyte differentiation defects. The reason for this is yet to be dissected, although any direct disruption to the LM network would affect integrin-mediated cell signalling. Moreover, LaNt α31 may possess direct signalling capabilities through integrin binding.

It has been previously reported that the cleaved N-terminal of LM α3b binds to α3β1 integrin, and inhibiting this interaction blocks the ability of the LM α3b LN domain to influence cell migration and adhesion[79]. Not only would this direct binding to integrin α3β1 directly influence signalling, it may also prevent LM3a32 binding to the receptor, which in turn could increase LM3a32 binding to α6β4 integrin. Although data suggests this leads to earlier hemidesmosome maturation[54], it is difficult to predict the phenotype this would cause in a 3D skin equivalent model where excess LaNt α31 is present. Moreover, LM N-terminal domain-mediated signalling has been observed with LM β1. Specifically, LM β1 N-terminus was shown to bind α3β1 integrin on embryonic stem cells, where it induced MMP9 and E-cadherin expression, key proteins associated with epithelial-mesenchymal transition[78]. If LaNt α31 acted in a similar way and could bind integrins or other receptors, this could cause differentiation defects.

5.3.2. LaNt α31 modulates normal human skin keratinocyte morphology, behaviour, and ECM deposition.

One of the additional benefits of the new lentiviral expression system is that it allowed validation and triangulation of results from previous studies. I also expanded the epithelial cell types investigated into immortalised normal human skin keratinocytes (NHKs) derived from a healthy patient. The lentiviral overexpression is a different system; integrating into the genome,

and with some small difference in the expressed protein; inclusion of the IgK secretion signal and a PAmCherry C-terminal tag. However, the phenotype caused by stable LaNt α31 overexpression in NHKs and hTCEPis was extremely similar to the phenotype using adenoviral overexpression although the differences in cell shape, migration, and LM deposition were generally less pronounced in the new stable LaNt α31 cells. This is not surprising, as although lentivirus can result in strong expression at high MOIs, adenovirus typically results in the highest expression due to very high copy number.

Previous data indicate that LaNt α31 driven phenotypes occur predominantly at early timepoints of cell attachment and subsequently LM deposition[54], an effect that is mirrored in stable LaNt α31 overexpression in NHKs. Why this is the case is unclear, though it is possible that the addition of an extra LM α3 LN domain aids the rapid maturation of the LM network, allowing for strong attachments to the cell substrate, which is why cells overexpressing LaNt α31 migrate less rapidly and have a more clustered LM deposition pattern early on.

As LaNt α31 is produced by alternative splicing from LM genes, these new data support that control of LaNt α31 to LM ratio adds a layer of self-regulation of LM function. Combined with LaNt α31 protein being enriched in numerous adult tissues[52], also shown in chapter 4 of this thesis, the results here continue to support that LaNt α31 may be part of a LM autoregulatory mechanism that could have widespread implications particularly for wound repair and other situations where BM remodelling is required, such as tissue morphogenesis and development.

Combined with LaNt α31 protein being enriched in numerous adult tissues[52], also shown in chapter 4 of this thesis, the results here continue to support that LaNt α31 may be part of a LM autoregulatory mechanism that could have widespread implications particularly for wound repair and other situations where BM remodelling is required, such as tissue morphogenesis and development. For example, could LaNt α31 be important for the early stages of BM network formation, creating a more favourable

microenvironment for cells to initially attach and migrate before remodelling and completing a mature BM? These are open questions.

5.3.3. Two new stable expressing epithelial lines established.

The tools generated in this study will be useful for the community and researchers. These include the two new stable LaNt α31 overexpressing cell lines. These have important advantages over the current systems used for LaNt α31 overexpression. Firstly, stable overexpression removes any variables caused from the cellular stress during and shortly after adenoviral transduction of plasmids. Secondly, using stable expressing lines now allows for long-term studies to be conducted Using transient systems, transgene expression generally peaks around 48h-72h, and then begins to drop off [303], though the protein half-life is likely longer than this. Whilst these systems are very useful, stable expressing lines allow the research to be sure that the transgene expression remains constant.

A specific further advantage of a stable cell line is that using these cell lines can mimic pathological situations where LaNt α31 is chronically upregulated. Unpublished findings have highlighted that LaNt α31 is upregulated in squamous cell carcinomas[298], so modelling this in vitro or in 3D models requires stable overexpression to observe the impact of long-term overexpression on cell behaviours. Unpublished findings have highlighted that LaNt α31 is upregulated in squamous cell carcinomas[298], so modelling this in vitro or in 3D models requires stable overexpression to observe the impact of long-term overexpression on cell behaviours. Although the normal keratinocytes used here do not model the full SCC profile, the lentiviral tools have now been validated and further cell lines can be generated using the same constructs.

The LaNt α31 transgene expressed has a C-terminal PAmCherry tag, and this will allow researchers to ask questions about LaNt α31 localization, especially in regard to laminin 332, which was not previously possible with existing constructs or technologies. The design of the construct also includes additional restriction enzyme sites for maximum utility, whereby any of the

components (LaNt α31, HA and Flag tags, PAmCherry) can be switched out with simple cloning procedures.

5.3.4. Caveats

The lentiviral overexpression construct uses a CMV promoter to express the LaNt α31 gene, which generally provides much higher levels of expression than is seen in normal biology. This leads to the question of i) are cells negatively affected by the high levels of protein production of this gene and ii) are the ECM phenotypes observed down to the large amounts of LaNt α31, which may not be observed in normal biology. Option i) can be reasonably ruled out, as a control lentivirus expressing GFP was used to account for lentiviral overexpression defects. On top of this, the LaNt α31 OE cells were a heterogenous population, so each cell would have a different integration point of the lentivirus in the genome, meaning any negative effects caused by the random integration of the lentivirus would be diluted. The question of high expression from the CMV promoter is harder to address. For future experiments, different lentiviral constructs containing different promoters could be used, such as CAG, Ubiquitin C, or Keratin 14, to titrate levels of expression. Alternatively, purified recombinant LaNt α31 protein could be used and added exogenously, which would also help to differentiate between phenotypes caused by extracellular vs intracellular LaNt α31 expression, although this may not be unsuitable for long-term coculture experiments depending on the half-life of the protein.

5.3.5. Next steps

This keratinocyte-fibroblast model allows for the investigation of keratinocyte-specific expression, and has revealed the profound phenotype caused by dysregulated LaNt α31 levels but the mechanism behind the severe disruption seen in LaNt α31 overexpressing OCE's and OSE's is yet to be ascertained. To maximise the data obtained from these corneal and skin equivalent models, further analysis of BM proteins should be performed, including LM α5, further LM332, Col IV and Col XVII staining, accompanied

by ultrastructural examination of the BM by transmission electron microscopy (TEM)[304]. The difference in cell morphology may point towards a keratinocyte defect, in which case OCE's and OSE's should be examined for differentiation markers, such as different keratins as markers such as involucrin, loricrin, transglutaminase, filaggrin, and caspase 14[305-308]. Additionally, analysis of the keratinocyte cell junctions using markers such a ZO-1 and occludin will also shed light on any differentiation defects[309] as well as making it possible to automate cell morphology analysis on ImageJ or similar programs. Furthermore, the newly established stable cell lines in this chapter had not been cloned out. By doing so in future, one can investigate LaNt α31 overexpression in a dose-dependent manner, whereby LaNt α31 overexpression can be quantified, and multiple cell lines can be established ranging from baseline to high levels of overexpression.

Despite the benefits of these OSE and OCE models, the system is still extremely simplistic when compared to LaNt α31 expression in vivo. Indeed, the epithelium is much more than just keratinocytes and fibroblasts, and is a complex composition of ECM proteins, which develops and grows throughout embryogenesis. Recent data on LaNt α31 localization in humans[52] and mice (Chapter 4) reveal that LaNt α31 is much more widespread than initially thought. LaNt α31 is expressed throughout the blood vasculature, terminal ducts, kidney, pancreas, liver, spleen, reproductive organs and in neurons. To begin to understand the biological significance of LaNt a31 in vivo, I next generated an inducible LaNt α31 transgenic mouse model, as discussed in the next chapter.

5.3.7 Conclusion

The stable-LaNt α31 overexpressing OSEs and OCEs represent the beginnings of a robust model to investigate LaNt α31 in epithelial tissues. From the data presented in this chapter, it is clear that LaNt α31 dysregulation is detrimental to tissue structure of OSEs and OCEs, further demonstrating the importance maintaining normal levels of this protein. These models will further serve researchers in the future, and will perhaps begin to allow researchers to understand the role of LaNt α31 in normal

epithelial homeostasis, as well as providing a platform to investigate the dynamic redistribution of LaNt α31 in wound healing[310].

Chapter 6: Laminin N-terminus α31 expression during development is lethal and causes widespread tissue-specific defects in a transgenic mouse model.

The work presented in this chapter has been published:

Sugden, CJ, Iorio, V, Troughton, LD, et al. Laminin N-terminus α31 expression during development is lethal and causes widespread tissue-specific defects in a transgenic mouse model. *FASEB J*. 2022; 36:e22318. doi:10.1096/fj.202002588RRR

6.1. Introduction

In this chapter, I investigate the expression of LaNt α31 for the first time in vivo, generating and validating a transgenic mouse model to determine the role of LaNt α31 in mammalian development.

Basement membranes in vivo are multilayered, tightly regulated, and fined tuned biological structures, of which we are still developing our understanding. The complexities of BMs can not be truly recreated in vivo. Whilst studies have shown that LaNt α31 can modulate cell behavior, it is impossible to know the impact, or function, LaNt α31 plays in normal biology without studying this protein in vivo, in particular the role it plays in matrixes that are actively being remodeled. Previously, it was attempted to generate transgenic mice constitutively overexpressing LaNt α31 under the driven by the keratin 14 promoter, for epitheial-specific expression, although researchers were unable to generate ay offspring expressing the LaNt α31 transgene[311]. It should be noted, however, that litter sizes obtained from F0 mice were unusually small, and although not possible to confirm, it is likey that constitutive overexpression of LaNt α31 is not compatible with life. To overcome this concern, a new inducible LaNt α31 overexpressing transgenic

mouse model was developed. This chapter describes these in vivo studies of LaNt α31[311].

6.1.1. Aims

- Generation and validation of an inducible LaNt alpha 31 overexpressing mouse model.
- Investigate the effects of LaNt α31 overexpression across development.

6.1.2. LaNt α31 transgene construct design and construct features

To investigate LaNt α31 in vivo, I designed an inducible overexpression construct with features to enable temporally controlled overexpression of LaNt α31 while co-expressing a non-directly tagged fluorescent reporter. The expression constructs in chapter 5 and this chapter differ greatly in their features. Indeed, the only sequence they share is the IgK-LaNtα31 sequence and HA and Flag tags. The features of the construct desgined for in vivo use are described below:

6.1.2.1. Human ubiquitin C promoter (UBC)

To achieve transgene expression across all cell types, I included the human ubiquitin C promoter to drive overexpression of the LaNt α31 transgene. Ubiquitin proteins have been found in all eukaryotic cell types[312], therefore require promoter activity across all tissues. The human ubiquitin C promoter has been shown to direct high ubiquitous expression of transgenes in mice[313], is less prone to silencing than other commonly used promoters such as CMV and the chicken beta-actin promoter[314-316].

In this study, the choice of using the UBC promoter to drive transgene expression was based on the broad expression across many tissues. Combining the use of a ubiquitous promoter in a cre-lox system with other regulatory elements driving cre recombinase was essential in allowing spatial and temporal control over LaNt α31 overexpression.

6.1.2.2 Floxed stop cassette

The Cre-LoxP system is a commonly used method to create inducible expression constructs[317]. Cre recombinase (Cre) is a tyrosine site-specific recombinases, which recognises specific DNA fragment sequences termed ‘locus of x-over, P1’ (*LoxP*) sites. Cre mediates the site-specific deletion of sequences flanked by the *LoxP* sites. Here, for the purpose of inducible gene expression, a cassette containing a series of polyA sites were **fl**anked the *L**ox**P*** sequences (‘floxed’), and this floxed stop cassette inserted immediately following the promoter of an expression construct. This means that even when the promoter is active, transcription will cease when it reaches the stop cassette. However, when Cre recognises the *LoxP* sites

and removes the floxed stop cassette, the rest of the transgene can be transcribed. Put simply, this means mice would not overexpress LaNt α31 until exposed to Cre recombinase.

As administering Cre enzyme is a logistical challenge in vivo, systems have been developed for the expression of Cre recombinase, described below. Briefly, the use of mice expressing a modified version of the Cre enzyme are bred with mice harbouring floxed stop cassettes, whereby expression can then be induced using tamoxifen[264], providing either temporal or spatial control. The R26Cre-ERT mouse line used in this study express Cre recombinase (Cre) fused to a mutant estrogen ligand-binding domain (ERT2) that requires the presence of tamoxifen for activity[264,318]. In the presence of tamoxifen, the ERT-bound Cre recombinase translocates to the nucleus, where it can excise DNA that is flanked by LoxP sites[318].

6.1.2.3. LaNt α31 sequence

I primarily wanted to study the effects of LaNt α31 expression has as an extracellular matrix molecule, so replaced the native LaNt α31 secretion signal with the mouse IgK secretion signal, described in chapter 5.

6.1.2.4. tdTomato fluorophore

In this expression construct, the tdTomato sequenced was cloned downstream of the T2A element, allowing visualization of cells where the construct is active, without directly tagging LaNt α31.To improve the LaNt α31 construct for in vivo use, I included the tdTomato fluorophore as a reporter. tdTomato is a constitutively 54.2 kDa fluorescent orange fluorescent protein derived from Discosoma *sp.*., with an excitation maximum at 554 nm wavelength, and an emission maximum at 581 nm[319]. The tdTomato gene consists of two copies which are fused of the extremely bright mTomato, which when translated forms an intramolecular dimer, so is considered monomeric[319]. tdTomato is the brightest commercially available orange-red fluorescent protein[319], a with a rapid maturation time ($t_{0.5}$ = 1 hr), and has the same photostabiltiy as the commonly used mCherry[319]. These properties make tdTomato and extremely useful reporter for use in transgenic animal studies, and has been used to great effect for live-imaging studies in mice

[320]. In this expression construct, the tdTomato sequenced was cloned downstream of the T2A element, allowing visualization of cells where the construct is active, without directly tagging LaNt α31.

6.1.2.5. Simian virus 40 late polyadenylation (SV40 polyA) signal

sPolyadenylation signals (polyA) are sequences that are terminate transcription when recognised by RNA polymerases. These then facilitate the addition of the poly(A) 3' tail, and initiate the process of releasing newly synthesised RNA from the transcription machinery[321]. The addition of the polyA tail is extremely important for the stability of the transgene mRNA, as well as nuclear export and degradation[321], so including a polyA sequence in expression constructs in favourable for transgene expression. The SV40 polyadenylation signal as used as it contains additional helper sequences compared to other commonly used polyA signals (such as hGH and BGH), making it more efficient at terminating transcription[322,323].

6.1.2.6. HS4 chicken β-globin (cHS4) insulator

Generating transgenic animals using pronuclear microinjection of the transgene DNA leads to random integration of the transgene. Because of the random integration into the host genome, transgenes introduced by pronuclear microinjection are susceptible to transcriptional silencing and positional effects depending on the chromosomal DNA sequences at their integration site[324].[324]. To combat this, insulator sequences were included in the transgene construct, flanking the entire transgene, to negate any undesirable effects arising from the random integration of the transgene. The cHS4 insulator possesses both enhancer- and barrier-blocking effects[324], and has been used successfully to enhance transgene expression. The inclusion of these cHS4 elements would provide a better chance of transgene expression, regardless of where the transgene DNA landed in the mouse genome[324,325].

Altogether, the design of this construct allows for temporal and tissue specific control of LaNt α31 overexpression in mice, establishing a tool to investigate the roles LaNt α31 plays in vivo for the first time.

6.2 Results

6.2.1. Cloning steps for generating pUbC-LoxP-LaNtα31-T2A-tdTomato

To investigate the consequences of LaNt α31 overexpression in vivo, an inducible system for conditional LaNt α31 transgene expression was generated (Fig. 6.1). Cloning methods for generating the intermediate and final LaNt α31 constructs are describe full in chapter 3. All intermediate constructs were validated by restriction digest, and final constructs were sequenced to confirmed the predicted sequence was correct (Fig. 6.1A-F).

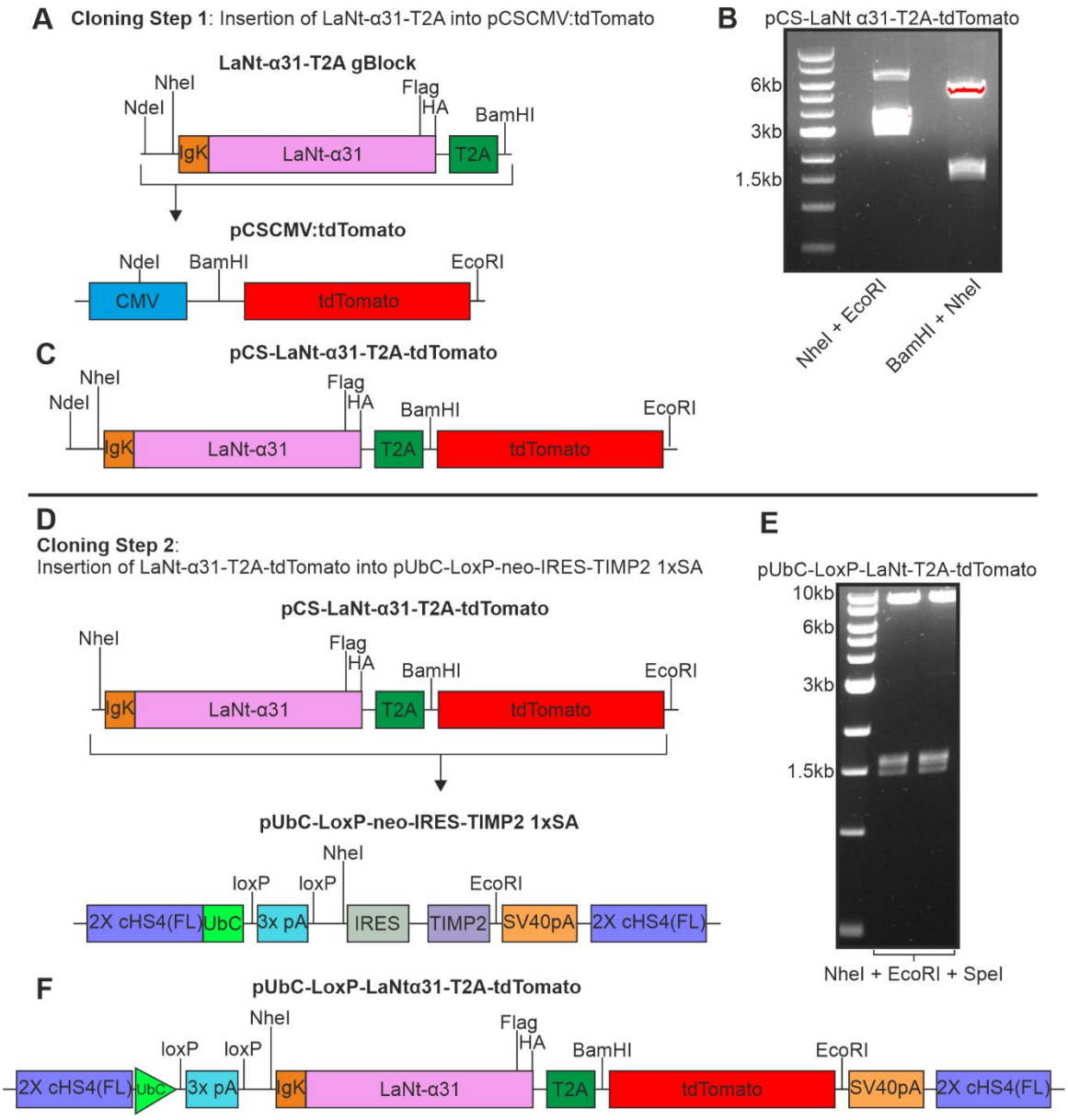

Figure 6.1. Cloning strategy for pUbC-LoxP-LaNtα31-T2A-tdTomato. A) LaNt-α31-T2A, including IgK, 5' UTR, HA and Flag tag, was inserted into pCSCMV:tdTomato vector using NdeI and BamHI, to give pCS-LaNt-α31-T2A-tdTomato. B) Diagnostic restriction enzyme digest to verify pCS-LaNt-α31-T2A-tdTomato ligation products ran on a 1% agarose gel, using NheI + EcoRI, and BamHI + EcoRI. C) LaNtα31-T2AtdTomato sequence, including IgK, 5' UTR, HA and Flag tag, was excised from pCS-LaNtα31-T2A-tdTomato using NheI and EcoRI and inserted in place of IRES-TIMP2 into pUbC-LoxP-neo-IRES-TIMP2 1xSA, producing pUbC-LoxP-LaNtα31-T2A-tdTomato. D) Diagnosticmrestriction enzyme digest to verify pUbC-LoxP-LaNtα31-T2A-tdTomato ligation products ran on a 1% agarose gel, using NheI + EcoRI + SpeI.

6.2.2. Validation of genotyping primers

Two primer pairs were designed for genotyping by PCR for the presence of the LaNt α31 transgene or the tdTomato reporter (Fig. 6.2A). Primer specificity was checked using NCBI Blast, and optimal primer conditions were determined by gradient PCRs. Both primer pairs generated products from the LaNt α31 construct and nothing from wild-type mouse genomic DNA (Fig. 6.2B).

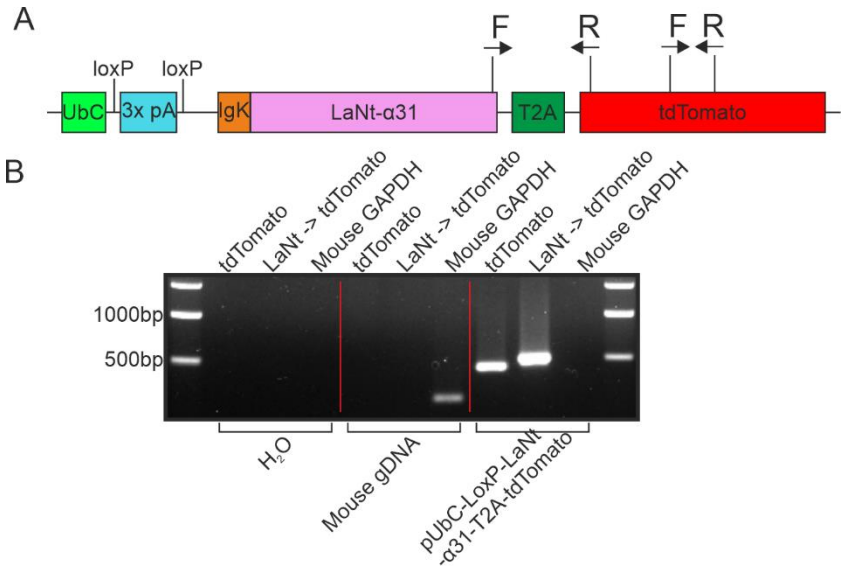

Figure 6.2. Genotyping primer validation. A) Primers were designed from LaNt -> tdTomato. Mouse GAPDH primers were also designed to use as a positive control. B) a PCR was performed using these primers on mouse DNA, and the pUbC-LoxP-LaNt-α31-T2A-tdTomato and ran on a 1% agarose gel.

6.2.3. Inducible LaNt α31 construct generation and validation

To confirm the construct expressed only following exposure to Cre recombinase, the pUbC-LoxP-LaNtα31-T2A-tdTomato was co-transfected alongside pCAG-Cre:GFP, encoding GFP-tagged Cre recombinase[326], into HEK293A cells. tdTomato signal was observed only in cells transfected with both plasmids (Fig. 6.3A). To confirm the construct expressed only following exposure to Cre recombinase, the pUbC-LoxP-LaNtα31-T2A-tdTomato was co-transfected alongside pCAG-Cre:GFP, encoding GFP-tagged Cre recombinase[326], into HEK293A cells. tdTomato signal was observed only in cells transfected with both plasmids (Fig. 6.3A).

PCR using primers flanking the STOP cassette further confirmed that the cassette was removed only in cells transfected with both plasmids (Fig. 6.3B,C).

Western blotting using polyclonal anti-Flag antibodies yielded a ~57 kDa band in the co-transfected cell lysates, (Fig. 6.3D), the predicted size of the LaNt α31 construct after cleavage of the T2A element and release of the tdTomato tag. To further validate Cre-induced expression of the LaNt α31 construct, fluorescence of co-transfected cells was observed over 28h. Cre-GFP expression was observed as soon as 6h following transfection, followed by expression of the LaNtα31-T2A-tdTomato transgene 12h post-transfection (Fig. 6.4), these data further confirmed that the LaNt α31 transgene expression was dependent on Cre-induction.

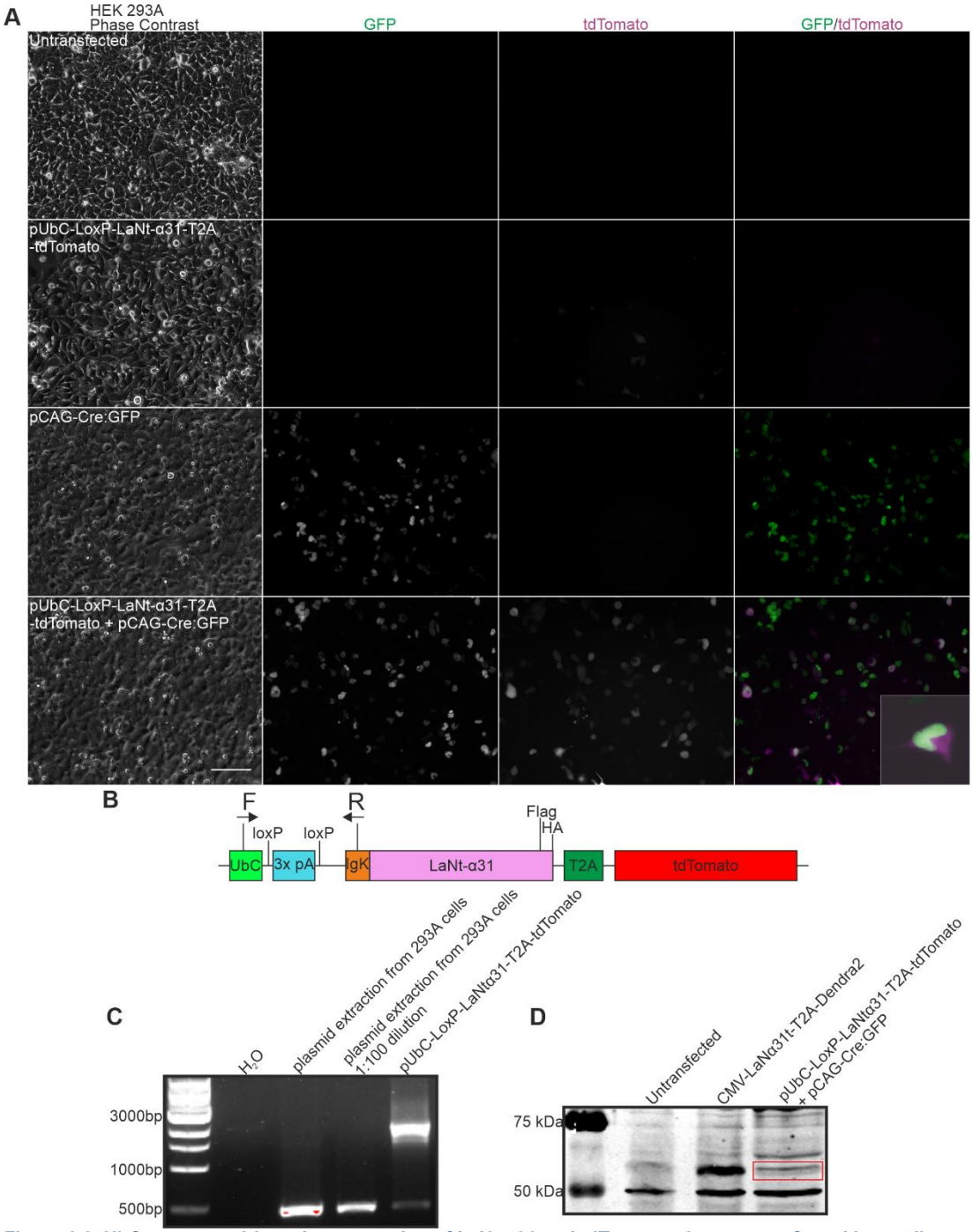

Figure 6.3. UbC promoter drives the expression of LaNt α31 and tdTomato when cotransfected into cells expressing Cre recombinase in-vitro. A) HEK 293A cells were either untransfected or transfected with pUbC-LoxP-LaNt-α31-T2A-tdTomato, pCAG-Cre:GFP, or pUbC-LoxP-LaNt-α31-T2A-tdTomato and pCAG-Cre:GFP and imaged on a Nikon TIe microscope 48h after transfection. DNA and protein was then extracted from HEK293 cells transfected with various plasmids. B) primers were designed flanking the floxed stop cassette to check for DNA recombination after being exposed to cre recombinase. C) A PCR was performed using these primers on DNA extracted from HEK293A cells co-transfected with pUbC-LoxP-LaNt-α31-T2A-tdTomato and pCAG-Cre:GFP. PCR products were ran on a 1% agarose gel and stained with EtBr. D) A western blot was performed using lysates from HEK293 cells either untransfected or transfected with CMV-LaNt-α31-T2A-Dendra2, or pUbC-LoxP-LaNt-α31-T2A-tdTomato and pCAG-Cre:GFP and samples were probed with an anti-flag polyclonal primary antibody and a donkey anti-goat fluorescent secondary antibody.

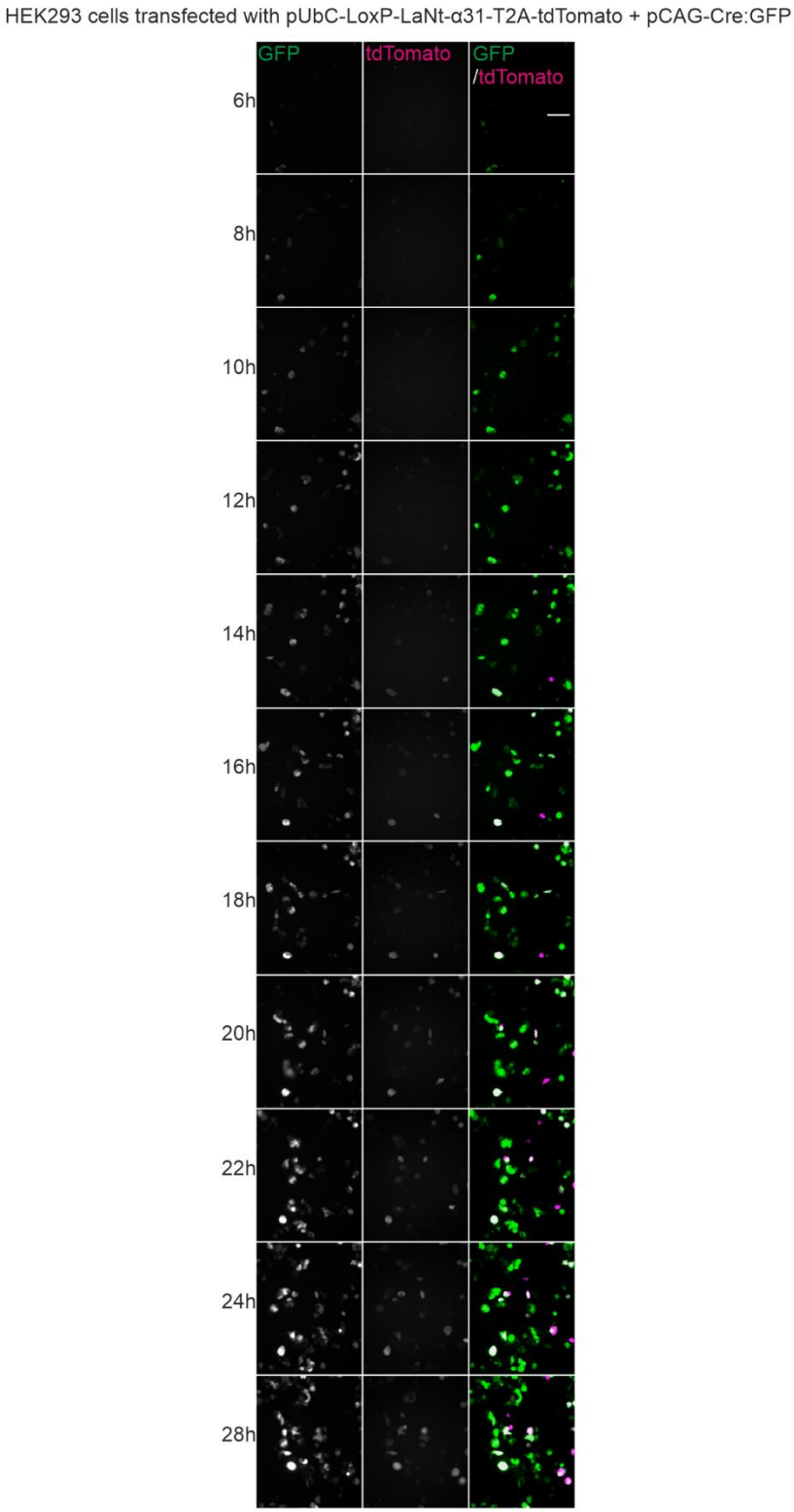

Figure 6.4. Timelapse of Cre recombinased-induced expression of LaNt α31-T2A-tdTomato. HEK 293A cells were transfected with pUbC-LoxP-LaNt-α31-T2A-tdTomato and pCAG-Cre:GFP and imaged at 2 hour intervals between 6 and 28 hours after transfection. Cells exhibit green fluorescence first, followed by red fluoresence. Scale bar = 100 μM

6.2.4. Generation and validation of a LaNt α31 transgenic mouse line.

To prepare the pUbC-LoxP-LaNtα31-T2A-tdTomato for microinjection, plasmid DNA was linearised with AseI and SacI enzymes to remove the plasmid backbone, and digestion products visualized on a 1% agarose gel to confirm size and DNA quality (Fig. 6.5A,B). The linearised transgene was then isolated, column purified, and eluted in ultrapure embryo water. Purified linearsed DNA was then ran against a λ-DNA/HindIII ladder for quantification (Fig. 6.5C). Three separate preparations of purified linear DNA were produced, and four rounds of embryonic microinjections were performed. (Table 6.1). Three UbC-LaNtα31 transgenic mouse lines were generated (line 3.1, line 7.5, and line 9.3) Transgenic line 3.1 was selected for further breeding, based on expression levels determined by western blotting. All lines were cryopreserved using simple vitrification of mouse embryos (appendix VII).

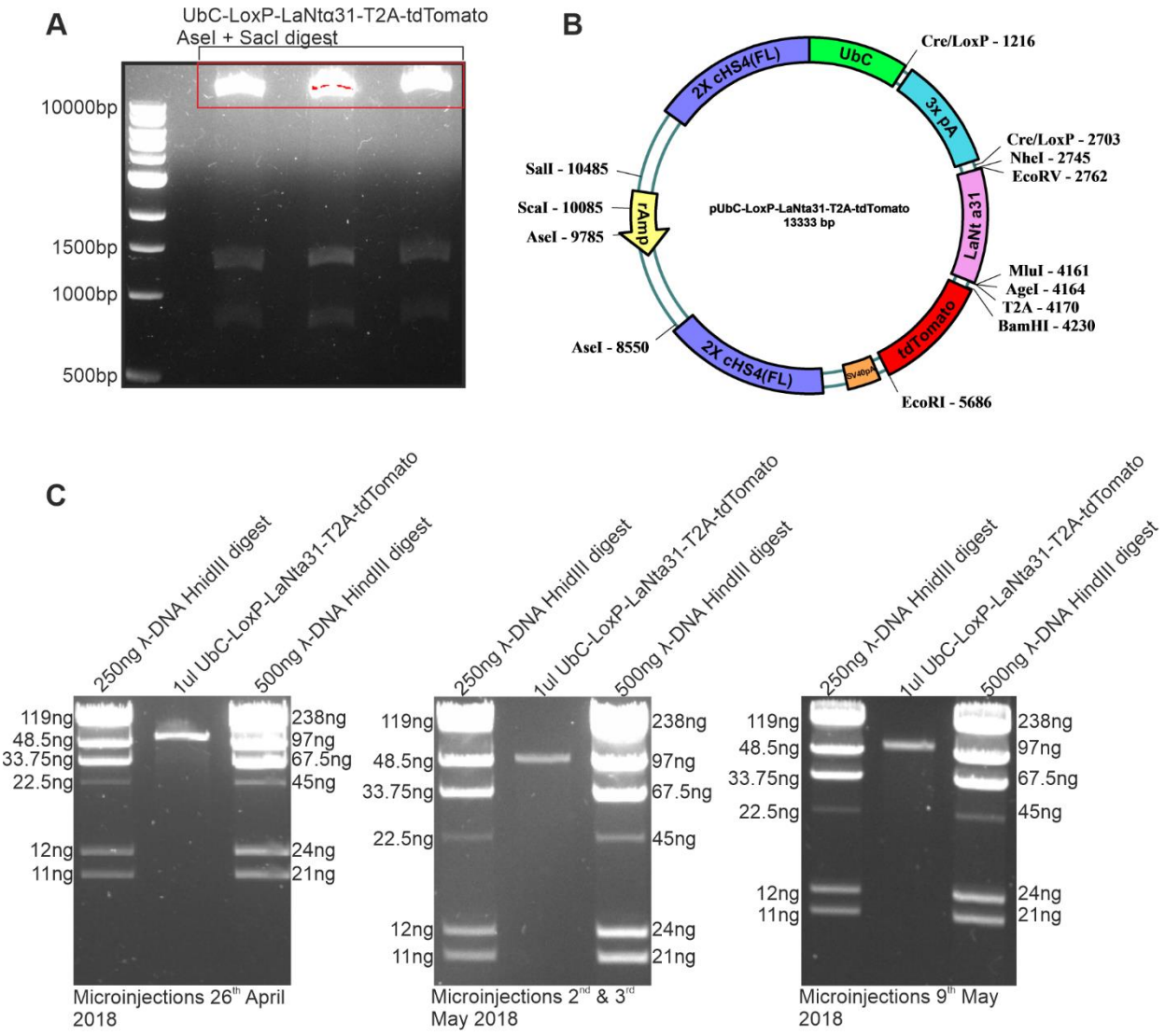

Figure 6.5. Preparation of linearised pUbC-LoxP-LaNtα31-T2A-tdTomato DNA for pronuclear microinjection. A) pUbC-LoxP-LaNt-α31-T2A-tdTomato was digested to linearise the DNA and remove the backbone. Digestion products were ran on a 1% agarose gel and stained with EtBr. The linearised construct band (red box) was then gel purified. B) Representative diagram of restriction enzyme site locations C) Purified linearised pUbC-LoxP-LaNt-α31-T2A-tdTomato DNA was then ran on a 1% agarose gel against dilutions of a λ-DNA digest and stained with EtBr, to quantify prior to injection.

Table 6.1. Records of pronuclear microinjections

Date	No. embryos isolated	No. embryos injected	No. embryos survived	Survival (%)
26.04.18	150	140	120	86
02.05.18	110	100	90	90
03.05.18	140	130	110	85
09.05.18	100	90	80	89

To confirm transgene expression, F0 mice were mated with WT (C57BL/6J) mice and embryos were collected at E11.5. mEFs were then isolated from the embryos. Presence of the UbC-LoxP-LaNtα31-T2A-tdTomato transgene (hereafter UbCLaNt) was confirmed by PCR (Fig. 6.6A). mEFs were transduced with an adenovirus encoding codon-optimised Cre recombinase (ad-CMV-iCre). Analysis by immunoblotting with anti-HA-antibodies (Fig. 6.6B) revealed a ~57 KDa band and fluorescence microscopy confirmed tdTomato expression only in the samples containing both the UbC-LaNt transgene and the ad-CMV-iCre (Fig. 6.6C).

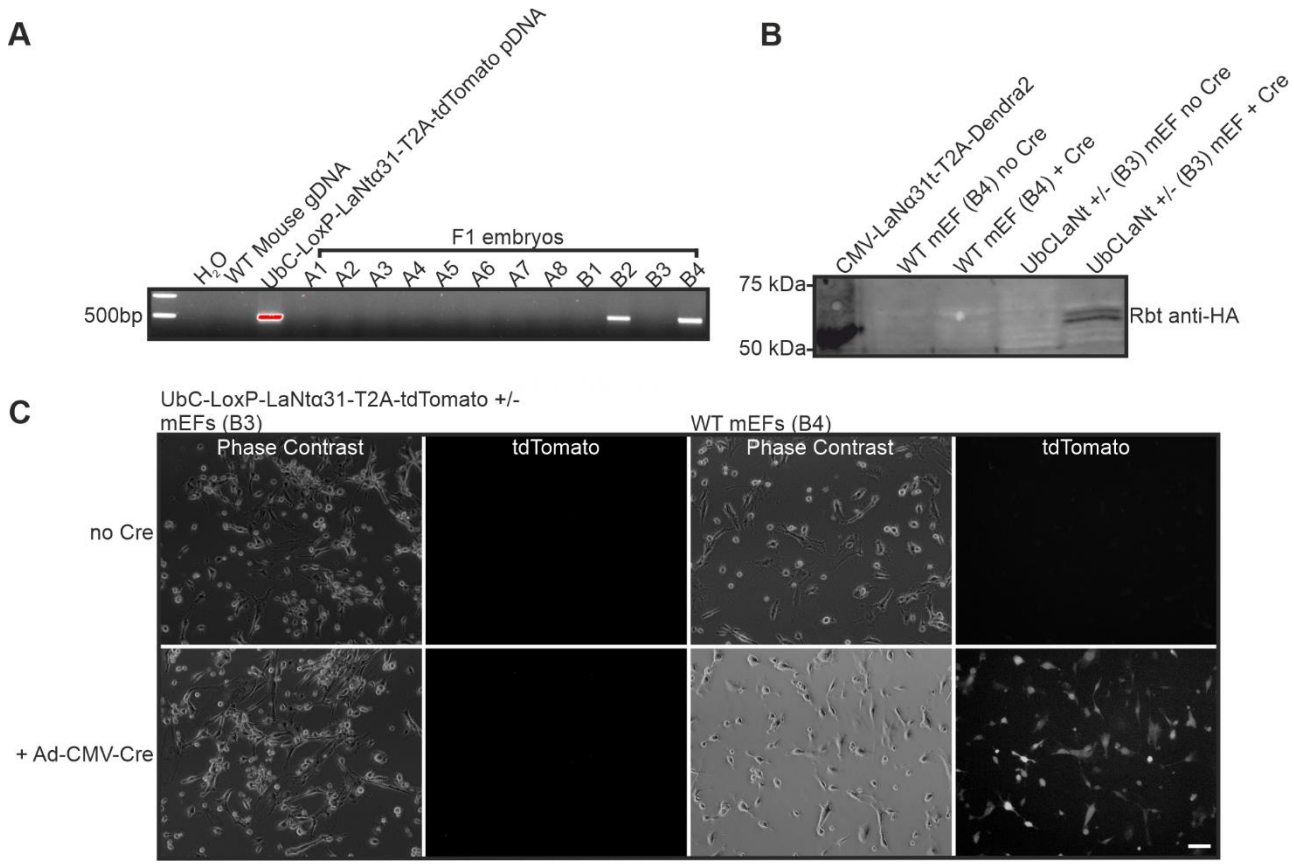

Figure 6.6. Validation of LaNt α31 transgene presence and expression in UbC-LaNtα31 F1 embryos. A) PCR amplicons produced using primers amplifying the UbC-LoxP-LaNt-α31-T2AtdTomato transgene from gDNA of F1 UbC-LoxP-LaNt-α31-T2A-tdTomato embryos . B) Western blot of protein lysates from explanted F1 mouse embryonic fibroblasts processed with anti-HA antibodies. C) Fluorescence microscopy images of explanted cells from UbCLoxP-LaNt-α31-T2A-tdTomato F1 mice. Scale bar = 100 µm.

Male UbCLaNt mice were generated by pronuclear microinjection into oocytes and mated with females from the tamoxifen-inducible ubiquitous Cre line R26CreERT2[264]. Transgene expression was induced by gavage of tamoxifen at E13.5, and embryos collected at E19.5. PCR from tail snipsMale UbCLaNt mice were generated by pronuclear microinjection into oocytes and mated with females from the tamoxifen-inducible ubiquitous Cre line R26CreERT2[264]. Transgene expression was induced by gavage of tamoxifen at E13.5, and embryos collected at E19.5. PCR confirmed that Cre/LoxP mediated recombination only occurred in the embryos with both the UbCLaNt and the R26CreERT2 transgenes (Fig. 6.7A). Explants were generated from the skin of these embryos, and only the explants grown from double transgenic embryos exhibited tdTomato expression by fluorescence microscopy (Fig. 6.7B) and HA-tagged LaNt α31 expression by western

immunoblotting (Fig. 6.7C). Together, these data confirmed the generation of tamoxifen-inducible LaNt α31 mouse line, without detectable leakiness (UbCLaNt::R26CreERT2).

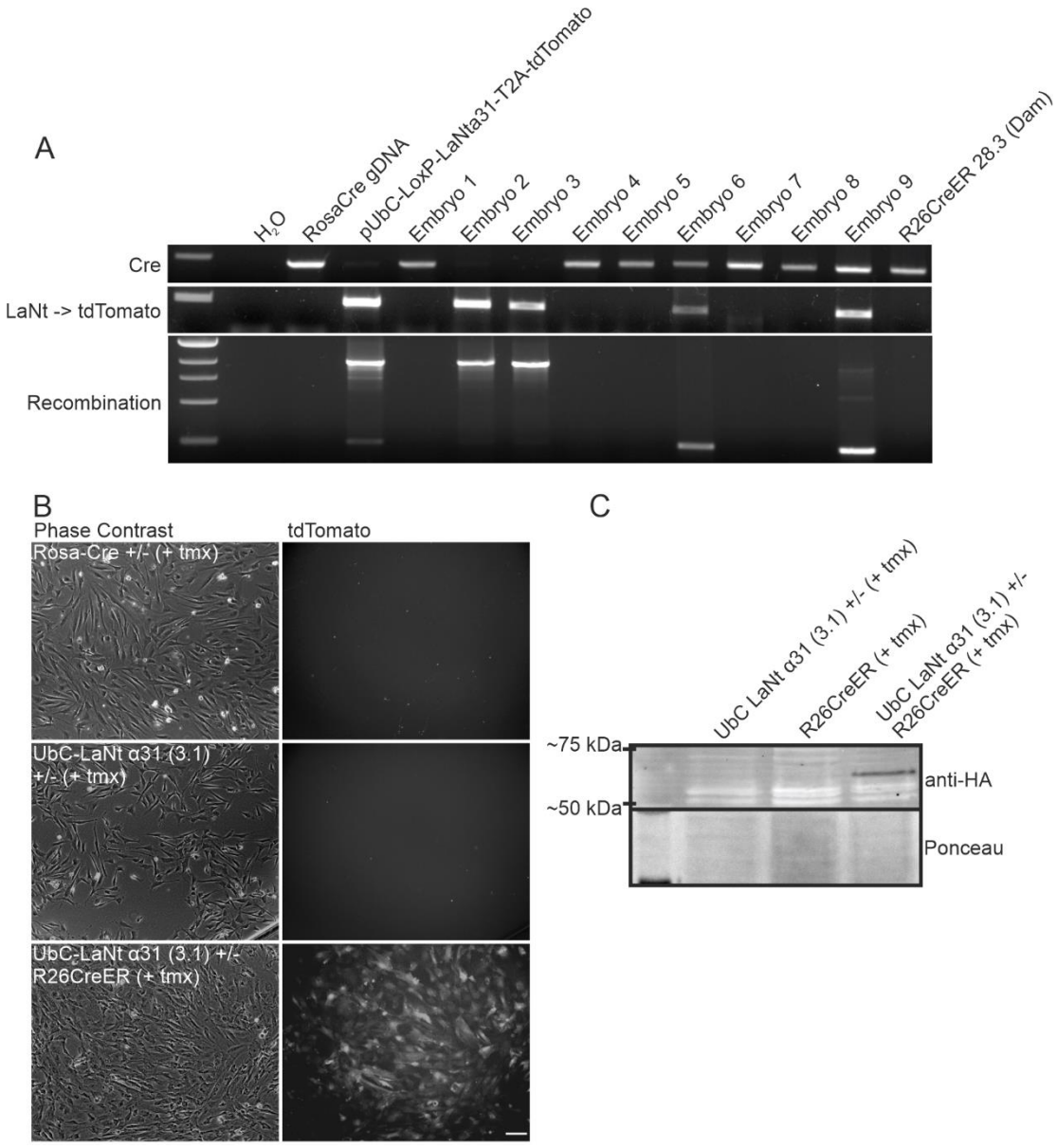

Figure 6.7. Validation of LaNt α31 transgene presence and expression in UbC-LaNtα31 x R26CreERT2 mice.

PCR products on DNA extracted from transgenic mouse from UbCLaNtα31 x R26CreERT2 mating embryos using Cre primers, LaNt α31 primers, and primers flanking the stop cassette. B) Phase contrast and fluorescence microscopy images of explanted cells from UbCLaNtα31::R26CreERT2 embryos. Scale bar = 100 µm. C) Western blot of lysates from UbCLaNtα31::R26CreERT2 embryo explants processed with anti-HA antibodies.

6.2.5. mEFs isolated from UbCLaNtα31::R26CreERT2 embryos display reduced migration rates

Scratch wound closure assays were performed using the mouse embryonic fibroblasts isolated from UbCLaNtα31::R26CreERT2 embryos, These experiments revealed that the LaNt α31 expressing cells displayed a ~22% less scratch wound closure at 16h compared to non-expressing mEFs. (mean ± SD scratch closure % non-expressing = 73 ± 6 LaNt α31 OE = 52 ± 6, N=6, p=0.0002)(Fig 3E, F).

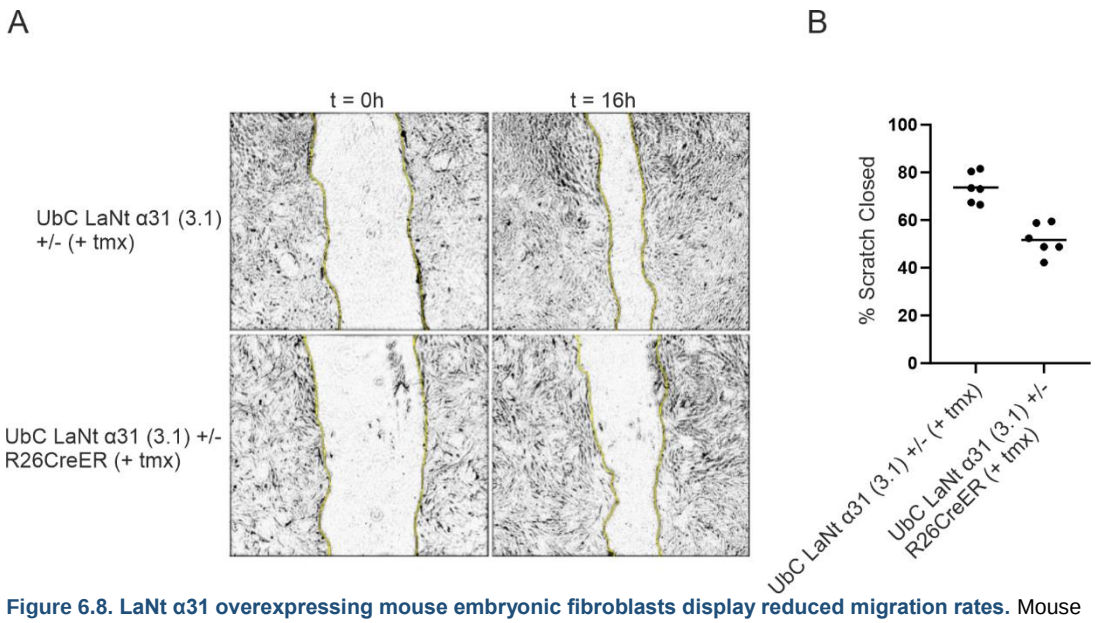

Figure 6.8. LaNt α31 overexpressing mouse embryonic fibroblasts display reduced migration rates. Mouse embryonic fibroblasts from either LaNt α31 overexpression mice or littermate controls were plated overnight at confluence and a scratch wound introduced 16 h later. A) Representative images from immediately after scratching (0 h, left panels) and at 16 h (right panels) of recovery. Yellow lines indicate wound margins. B) Gap area closure measured at 16 after wounding plotted as percentage of the initial wound area with each point representing one technical repeat.

6.2.6. UbCLaNt::R26CreERT2 expression in utero causes death and localised regions of erythema at birth.

To determine the impact of LaNt α31 during development, tamoxifen was administered to pregnant UbCLaNt::R26CreERT2 mice at E15.5 via gavage and pregnancies allowed to continue to term. Across three litters from three different mothers, two from six pups, three from five pups, and one from five pups respectively were intact but not viable at birth, while the remaining littermates were healthy. Endpoint PCR genotyping using primers amplifying

the LaNt α31 transgene and Cre recombinase transgene confirmed mice possessed both transgenes (Fig. 6.9).

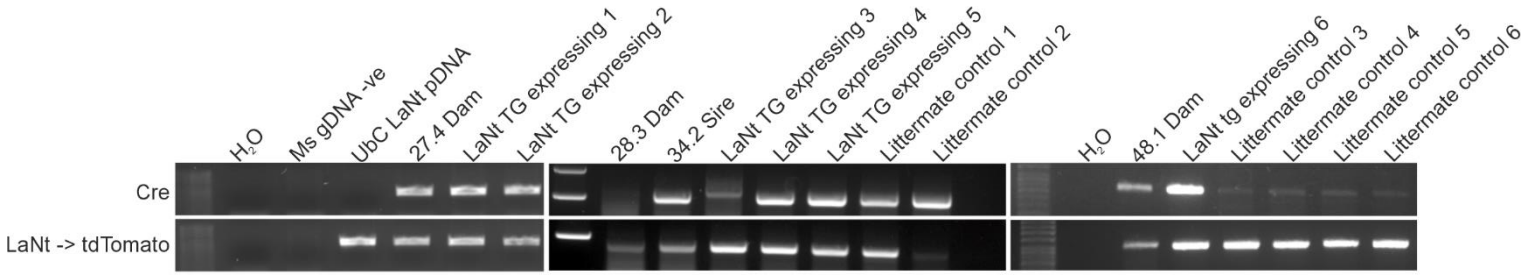

Figure 6.9. Genotyping of mice used in this study. A) PCR amplicons produced using primers amplifying either the Cre recombinase gene or UbC-LoxP-LaNt-α31-T2A-tdTomato transgene on gDNA extracted from transgenic mouse embryos from the mating of UbCLaNtα31 x R26CreERT2 mice.

The non-viable pups displayed localised regions of erythema with varying severity between the mice but were otherwise fully developed and the same size as littermates (Fig. 6.10A).

To confirm that the lack of viability was associated with transgene expression, OCT-embedded skin sections of UbCLaNt::R26CreERT2 were imaged using confocal microscopy, revealing tdTomato fluorescence only in the non-viable animals (Fig. 6.10B) and skin explants were established and tdTomato fluorescence in explants from non-viable pups was confirmed by microscopy (Fig. 6.10C).

Western immunoblot analysis of total protein extracts from the explanted cells and from whole embryo lysates also confirmed transgene expression in non-viable pups, with expression levels differing between the mice (Fig. 6.10D). Together these data confirmed that only non-viable mice expressed the LaNt α31 transgene.

Hereafter, UbCLaNt::R26CreERT2 animals are therefore labelled as either as “LaNt α31 TG-expressing” or, for non-expressing animals, as “littermate controls”.

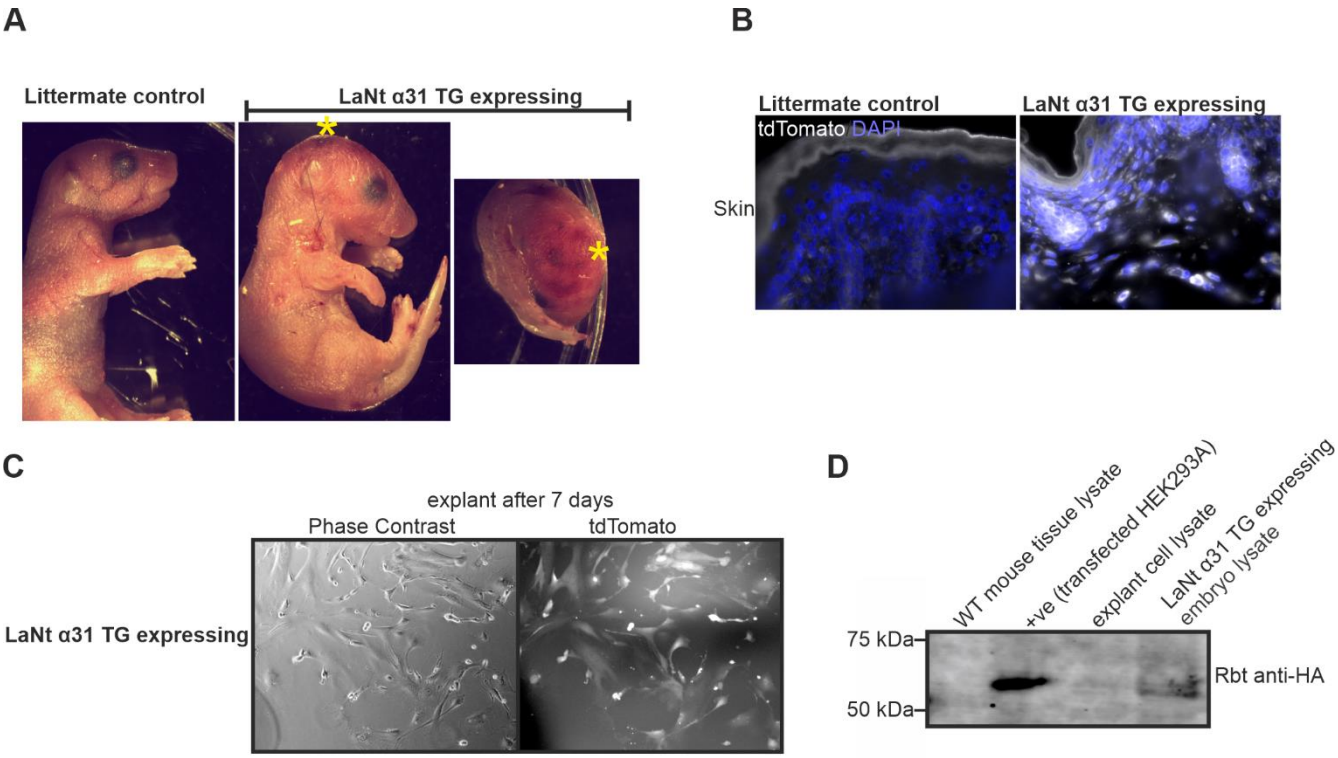

Figure 6.10. - Transgenic mice overexpressing LaNtα31 are not viable at birth and display localised regions of erythema. A) Representative images of UbCLaNtα31::R26CreERT2 embryos. Animals subsequently confirmed as expressing the LaNt α31 transgene are labelled as LaNt α31 TG expressing. Yellow asterisk indicates regions of visible erythema. B) Representative fluorescence microscopy of UbCLaNtα31::R26CreERT2 OCT sections exhibiting tdTomato fluorescence. Scale bar = 100 µm. C) Fluorescence microscopy images of explanted cells from LaNt α31 TG expressing mice. D) Western blot of tissue lysates from WT, UbCLaNtα31::R26CreERT2 embryos or explanted cells processed with anti-HA antibodies. HEK293A cells cotransfected with the LaNt α31 transgene expression construct and Cre-GFP expression construct are included as a positive control.

To identify LaNt α31 effects at the tissue level, the pups were formalin-fixed and paraffin-embedded then processed for H&E staining and immunohistochemistry. All organs were present in the mice and appeared intact at the macroscopic level. A consistent feature in every transgenic animal was extensive evidence of bleeding within tissues. Indeed, although there was mouse-to-mouse variability in extent of this bleeding, every major organ in all animals were affected to some extent.

I focused our attention on kidney, skin and lung as examples of tissues where the BMs have with distinct differences in LM composition and where LaNt α31 could, elicit context-specific effects. Specifically, the predominant LMs in the kidney contain three LN domains, and mutations affecting LM polymerization lead to Pierson syndrome [141,192,193,327,328], whereas the major LM in the skin contains one LN domain, LM332, and loss of function leads to skin fragility, reviewed in [134], and granulation tissue disorders[329,330]. In the lung, LM311, a two LN domain LM, is enriched[147,150], and absence of LMα3 is associated with pulmonary fibrosis[151].

6.2.7. LaNt α31 overexpression leads to epithelial detachment, tubular dilation and interstitial bleeding in the kidney and disruption of capillary BM integrity.

Dissected kidneys from the transgene-expressing animals were markedly darker than non-expressing animals (Fig. 6.11A). Histological examination confirmed that this difference reflected differences in the vessels of the kidney, with extensive bleeding into the interstitial and subtubular surroundings (Fig. 6.11B, yellow arrows). Detachment of the lining epithelia in collecting ducts and uteric bud segments was also apparent (Fig. 6.11B, black arrows).

Indirect IF processing of tissue using pan-LMantibodies revealed LM localization to be largely unchanged (Fig. 6.11C). However, ultrastructural examination by transmission electron microscopy not only identified that the majority of extravascular red blood cells present in the tissue were outside of capillary structures (Fig. 6.12A), but also that the BMs of capillaries appeared disrupted in the LaNt α31 TG expressing animals (Fig. 6.12B).

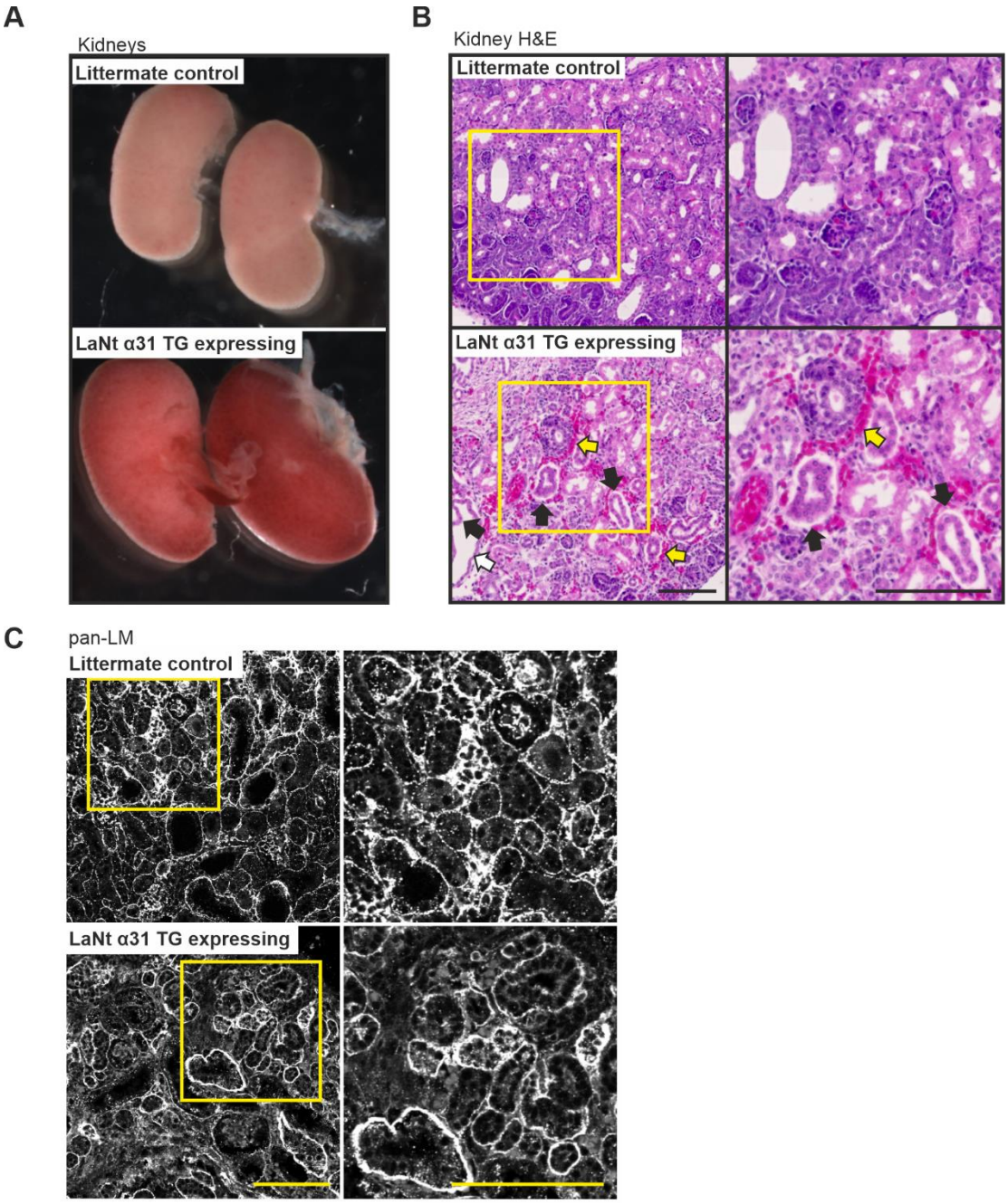

Figure 6.11. LaNt α31 overexpression leads to epithelial detachment, tubular dilation and interstitial bleeding in the kidney. A) Representative images of whole kidneys of newborn UbCLaNtα31::R26CreERT2 mouse kidneys from non-expressing littermate controls (top) or LaNt α31 TG expressing animals (bottom). B) Representative images of H&E stained FFPE sections (5 µm) of newborn littermate controls of LaNt α31 TG expressing mouse kidneys. Right column shows areas of increased magnification. Black arrows point to areas of epithelial detachment. White arrows point to tubular dilation. Yellow arrows point to areas of interstitial bleeding. C) FFPE sections (5 µm) from littermate controls or LaNt α31 TG expressing animals processed for immunohistochemistry with pan-laminin polyclonal antibodies. Right column shows areas of increased magnification. Scale bars = 100 µm.

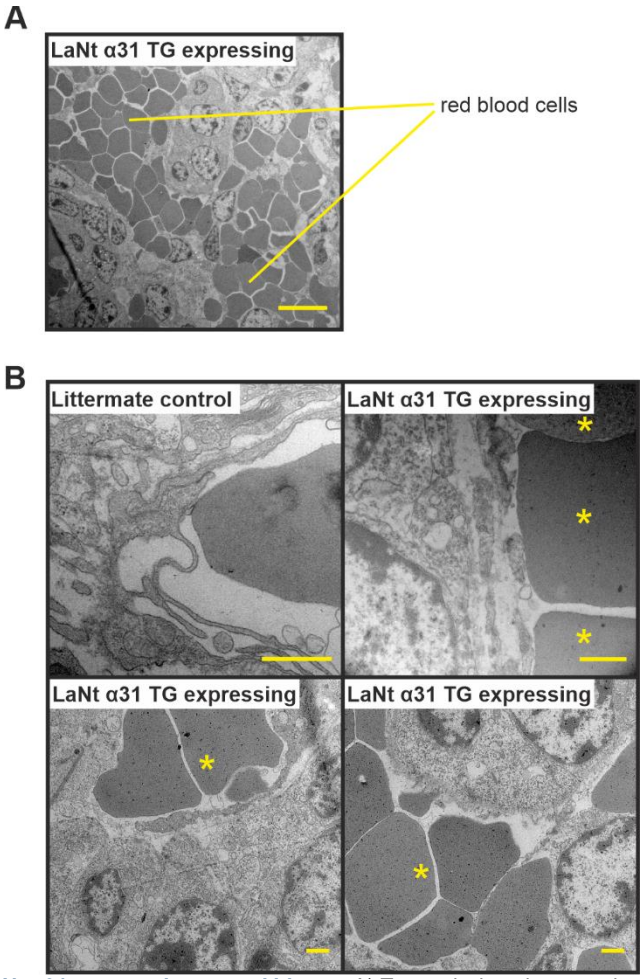

Figure 6.12. TEM of LaNt α31 transgenic mouse kidneys. A) Transmission electron micrographs of LaNt α31 TG expressing kidney, extensive red blood cell infiltration is labelled. Scale bar = 10 µm. B) Transmission electron micrographs of littermate controls and LaNt α31 TG expressing capillary structures. Asterisks indicate red blood cells. Scale bars 1 µm.

6.2.8. LaNt α31 overexpression disrupts epidermal basal cell layer organization.

Histological examination of the dorsal skin of the LaNt α31 TG expressing mice revealed localised disruption of the epidermal basal cell layer, with a loss of the tight cuboidal structure of the stratum basale (Fig. 6.13A). Basal layer disruption was also observed in the outer root sheath of the hair follicles (Fig. 6.13A). There was no evidence of blistering at the dermal-epidermal junction. However, extravascular erythrocytes were observed through the skin (Fig. 6.13A, yellow chevron).

Indirect IF processing revealed that the localization of LM α5, LM332, and type IV collagen was unchanged in LaNt α31 TG expressing animals, though increased immunoreactivity of LM α5 was observed (Fig. 6.14A,B). This increase in immunoreactivity was also observed in samples processed with a pan-LMantibody (Fig. 6.14B). The immunoreactivity of LM α4 appeared unchanged in vessels; however, LM α4 was also detected at the dermal-epidermal junction in LaNt α31 TG expressing animals (Fig. 6.14A).

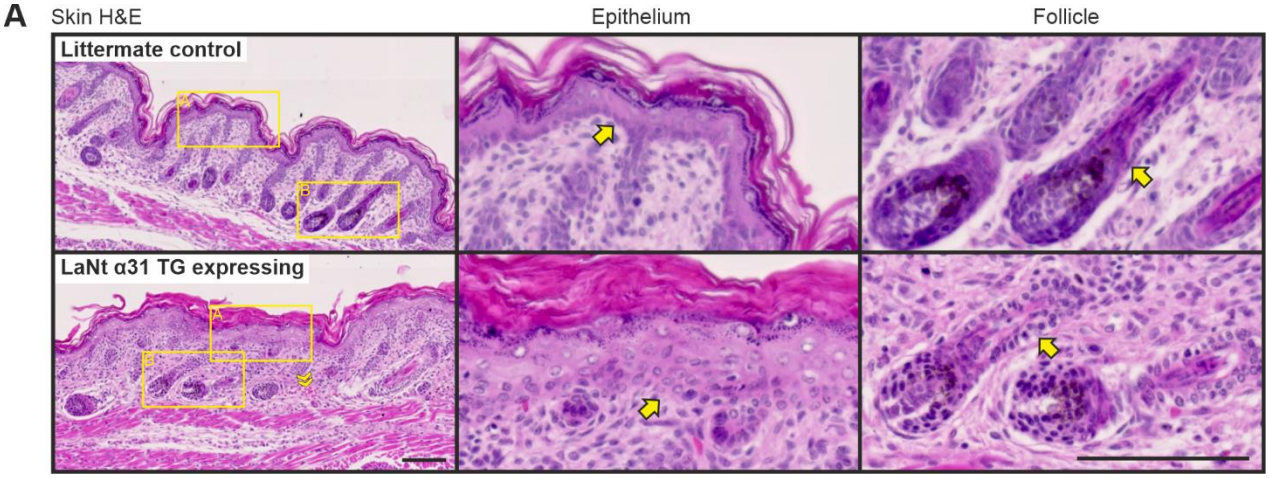

Figure 6.13. LaNt α31 overexpression disrupts epidermal-dermal cell organization. A) H&E staining of FFPE sections (5 µm) of newborn UbCLaNtα31::R26CreERT2 transgenic mice dorsal skin. Upper panel non-expressing littermate controls, lower panels LaNt α31TG expressing animals. Yellow chevrons indicate areas of extravascular erythrocytes. Middle and right columns show increased magnification of the epithelium or hair follicles respectively. Yellow arrows indicate basal layer of epithelial cells. Scale bar = 100 µm.

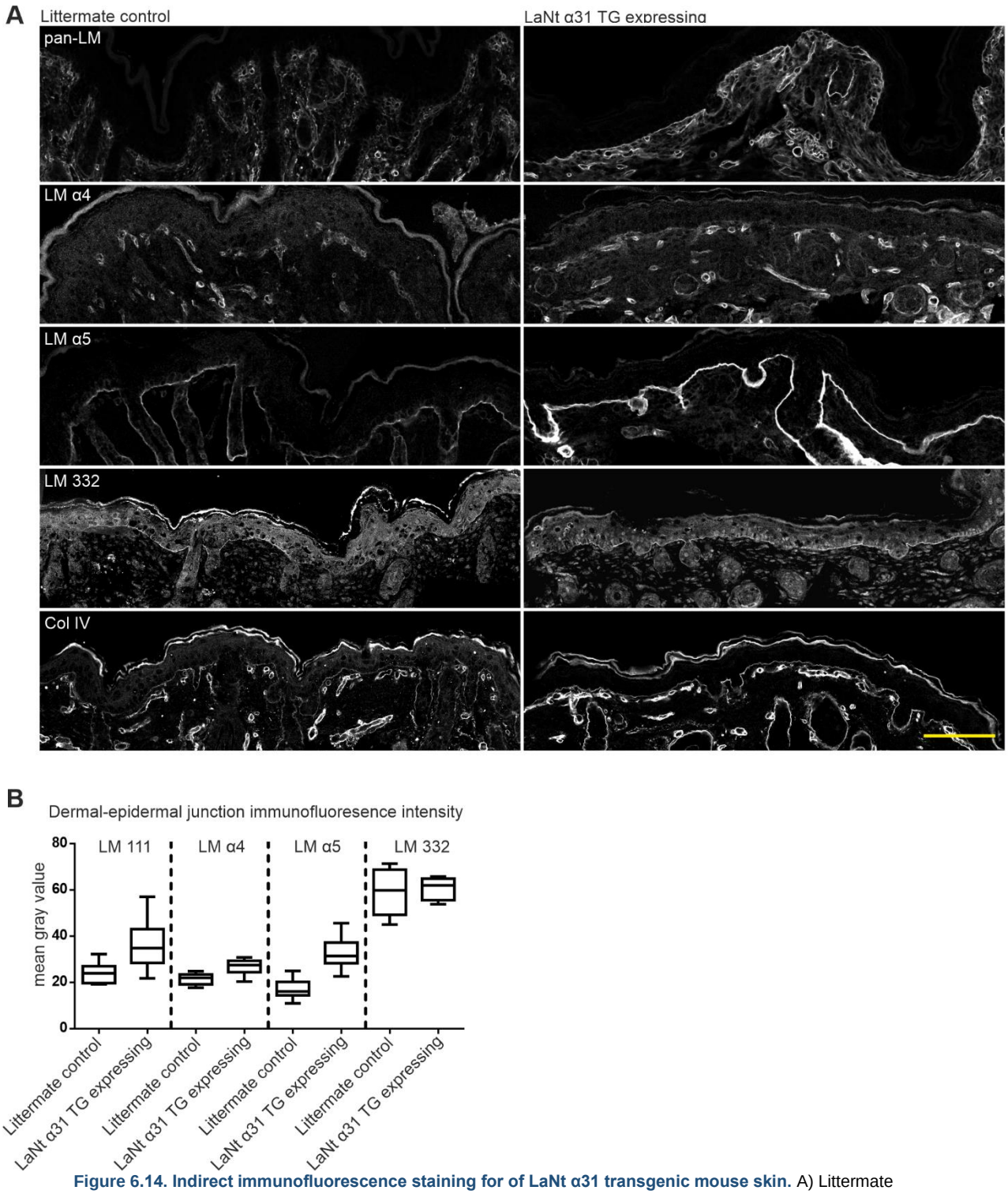

Figure 6.14. Indirect immunofluorescence staining for of LaNt α31 transgenic mouse skin. A) Littermate controls (left) or LaNt α31 TG expressing OCT sections (10 µm) processed for immunohistochemistry with anti-laminin 111 (pan-LM), anti-laminin α4 (LM α4), 910 anti-laminin α5 (LM α5), anti-laminin 332 (LM332) and anti-Type IV collagen (Col IV). Scale bar = 50 µm. B) Mean gray intensity of immunofluorescence intensity of different anti-laminin antibodies at the dermal-epidermal junction. Each box and whisker plot represents at least ten individual measurements.

Ultrastructural analyzes of the dermal-epidermal junction revealed no major disruption to the BM but some subtle differences. Specifically, in the LaNt α31 TG specimens, hemidesmosomes were larger (Fig. 6.15A, chevrons, Fig. 6.15B, littermate median 0.11 95%CI 0.09-0.12 µm, LaNt α31 TG median 0.26 95%CI 0.24-0.28 µm, p<0.001 Mann-Whitney test).

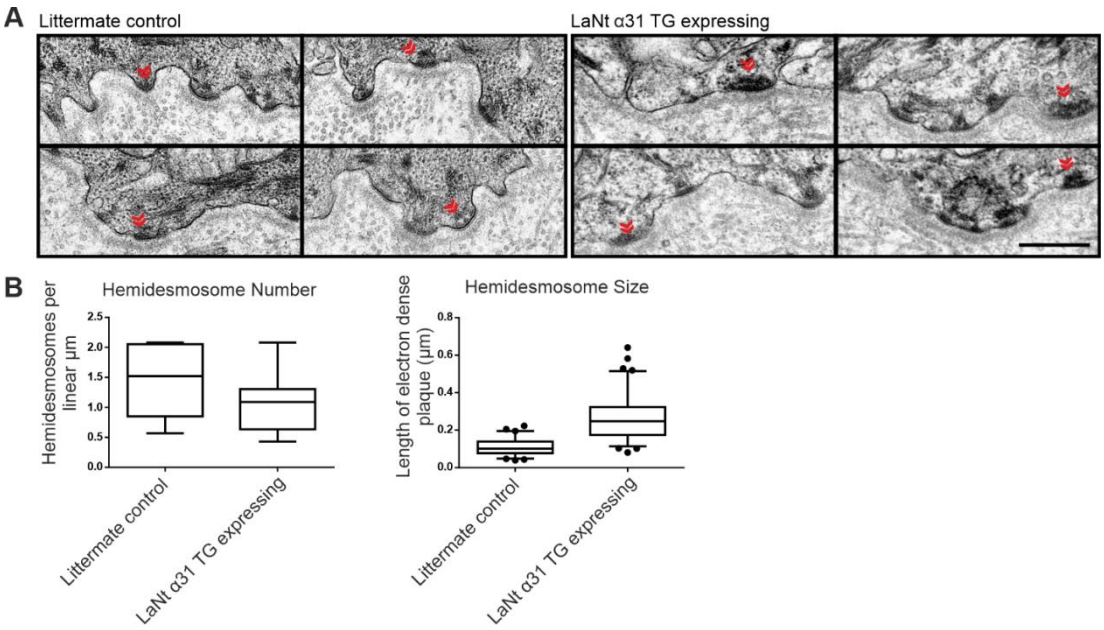

Figure 6.15. LaNt α31 overexpressing mice possess fewer, but larger, hemidesmosomes. Transmission electron micrographs of littermate control or LaNt α31 TG expressing skin sections imaged at the dermal-epidermal junctions. Chevrons indicate hemidesmosomes. Scale bar = 0.5 µm. B) Box and whisker graphs of quantification of hemidesmosome number per µm of basement membrane (n=12 and 17 images), and of size of the hemidesmome measured as the length of the electron dense plaque at the cell membrane (n=67 and 81 hemidesmosomes). Boxes represent 25th -75th percentile with line at median, whiskers 5th and 95th percentile. Dots represent outliers.

6.2.9. Mice expressing the LaNt α31 transgene display structural differences in the lung and a reduction of hematopoietic colonies in the liver.

Erythrocytes were present throughout the lung tissue (Fig. 6.16) and liver tissue of transgene expressing animals (Fig. 6.17A). Structural differences were also apparent in the lungs, although it should be noted that the lungs of P0 mice were not inflated prior to fixation and are not ideal for direct comparison. Mice expressing LaNt α31 displayed fewer, and less densely packed alveolar epithelial cells (Fig. 6.16).

The livers of mice expressing the LaNt α31 transgene exhibited a reduction in hematopoietic foci (Fig. 6.17A, B, yellow arrows). This reduction corresponded to a >33% reduction of total cell number (mean ± SD nuclei/mm^2 littermate controls = 11.0 ± 0.52, LaNt α31 expressing = 5.8 ± 0.50, p = < 0.0001 determined by unpaired t test; Fig. 6.17C, D). The bile ducts, sinusoid endothelium and hepatocyte morphology were histologically unchanged.

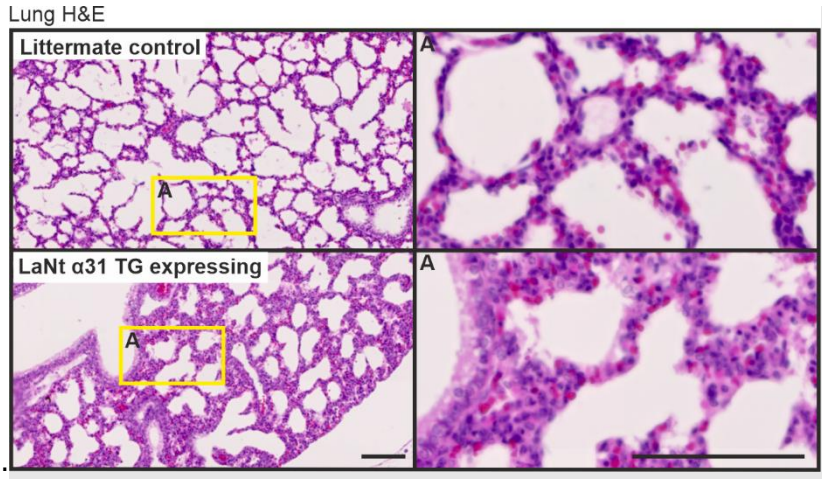

Figure 6.16. Mice expressing the LaNt α31 transgene display structural differences in the lung. H&E staining of FFPE sections (5 µm) of newborn UbCLaNtα31::R26CreERT2 transgenic mice lungs. Yellow boxes indicate areas of increased magnification of the alveolar epithelium.

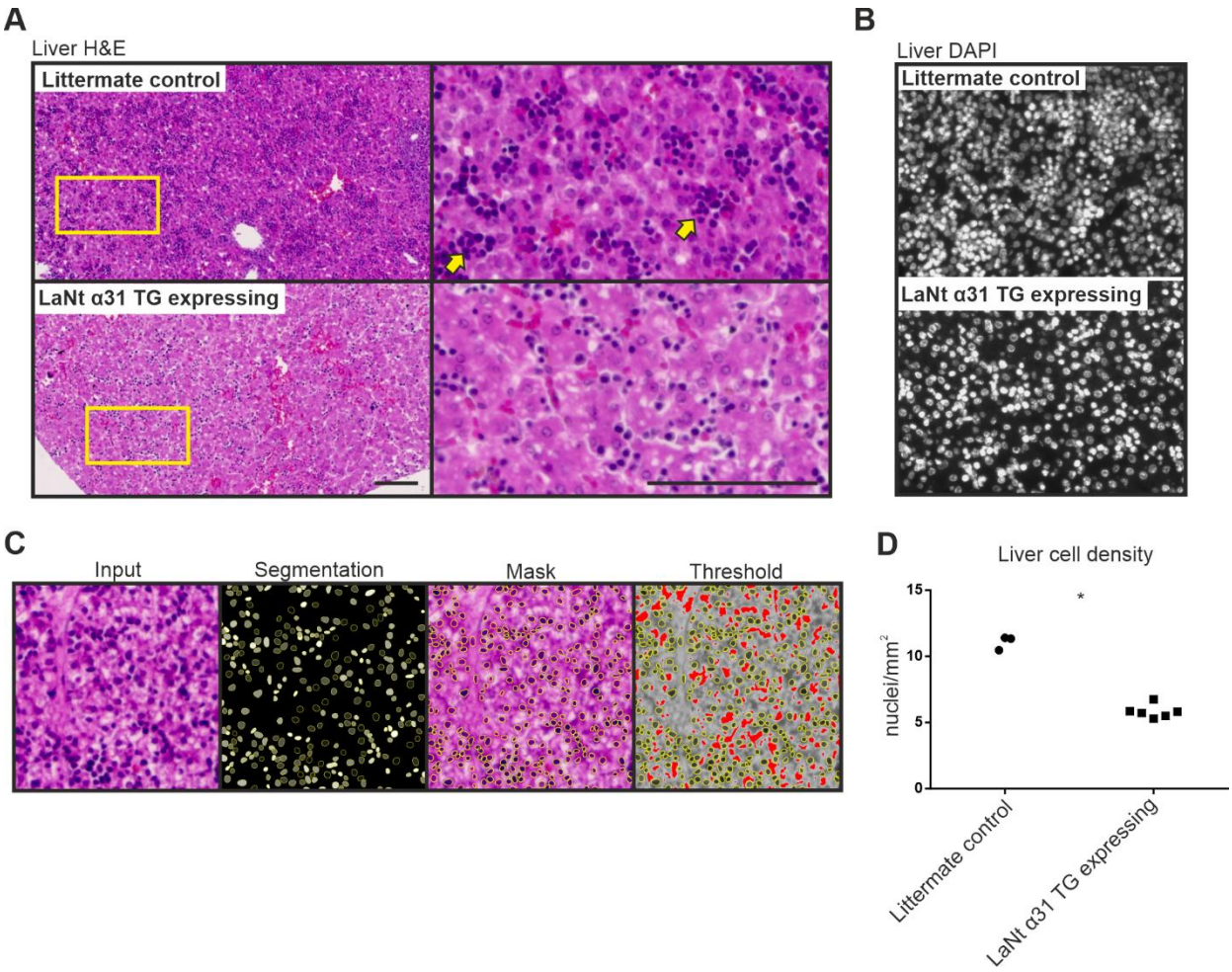

Figure 6.17. LaNt α31 transgenic mice display a reduction of hematopoietic colonies in the liver. A) H&E staining of FFPE sections (5 µm) of newborn UbCLaNtα31::R26CreERT2 transgenic mouse liver. Upper panel non-expressing littermate controls, lower panels LaNt α31 TG expressing animals. Right columns show increased magnification. Yellow arrowheads highlight areas of increased cell density. Scale bars = 100 µm. B) DAPI staining of littermate controls or LaNt α31 TG expressing mouse livers. C) Representative image analysis method of determining nuclei count. D) Quantification of nuclei. Each point represents the mean of the quantification of nuclei/mm^2 from 2 separate microscope slides at different sectioning depths per mouse.

6.3. Discussion

6.3.1. Synopsis

This study has demonstrated that LaNt α31 overexpression ubiquitously during development is lethal, causing widespread blood exudate throughout most tissues as well as changes to the tubules of the kidney and the basal layer of the epidermis, depletion of hematopoietic colonies in the liver, and evidence of BM disruption at the dermal-epidermal junction. These findings substantiate the prior in vitro and ex vivo work that have implicated LaNt α31 in the regulation of cell adhesion, migration, and LM deposition[51,53,251]. The findings described in this chapter provide the first in vivo evidence that this little-studied *LAMA3*-derived splice isoform and newest member of the laminin superfamily has biological importance in BM and tissue formation during development and provide a valuable platform for onward investigation.

6.3.2. LaNt α31-mediated LM network disruption as a cause of the transgenic mouse phenotype

There are several plausible overlapping reasons that can explain the phenotype. As LM network assembly requires binding of an α, β and γ LN domain[9,47,50,56,331], the presence of an α LN domain within LaNt α31 could influence LM-LM interactions and therefore BM assembly or integrity. Indeed, LaNt α31, contains a perfect match to the LM α3b LN domain and biochemical assays have shown that the LM α3b LN domain is the most potent of the LM LN domains at disrupting LM111 polymerization in vitro[46]. Consistent with network disruption, much of the LaNt α31 TG phenotype resemble those from mice where LM networks cannot form due to LN domain mutations[9,47,50,56,331].

Specifically, here I propose a mechanism whereby overexpression of the LaNt α31 protein is disrupting BMs through inhibition of network formation by competing for αLN domain interactions. In comparison with other LN-domain specific mutant lines, the LaNt α31 TG expressing animals BM-associated defects are somewhat similar although the overall effect is more severe and affects more tissues than each individual LN mutant line as anticipated by

the more widespread expression of the transgene driven by UBC and R26 promoter activities.

No LaNt α31 KO mouse lines exist to date. Indeed, due to the complex splice regulation of the LAMA3 gene, it is not currently possible to knock out LaNt α31 without causing a total LMα3b KO. Work is ongoing to uncover the elements regulating LAMA3 gene splicing, which may allow a LaNt α31 KO line to be generated in future. Despite this, many of the phenotypic features of LaNt α31 overexpressing mice mirror what is observed in other LM mutant mice.

The LaNt α31-overexpressing transgenic animals die at birth and exhibit a range of BM-related defects across multiple tissues. When comparing this to studies using non-polymerising LM α5[189] it is plausible that the isoform specificity of the LM α5 LN mutant mice, whilst having a similar cause behind the phenotypes (inability for LM network to polymerise), prevents these mice from exhibiting the same catastrophic phenotypes seen in the LaNt α31 transgenic mice. That is to say, the global expression of LaNt α31 means that the LaNt α31 LN domain, homologous to the LM α3B LN domain, means that there is the potential to compete with any α LN domain, or disrupt any network work the LaNt α31 LN domain has a binding affinity to the relevant β and γ LN domains.

Transgenic mice harbouring the analgous mutation (R291L) were generated using CRISPR-Cas9, and LM α5 LN domain mutants were born at term with some animals surviving for weeks or months after birth[189]. The LM α5 LN domain mutant mice exhibited defective lung development and vascular abnormalities in the kidneys[332], which are similar to the defects observed in the LaNt α31 transgenic mice. Although the severity of the LM α5 mutant mice phenotype was varied, a number of transgenic animals died peri- or neonatally[189]. Out of seven homozygous mice, five were found dead at or shortly after birth, one mouse died at P15, and the other survived until four months of age. Both surviving mice were smaller than their littermates. Mice that had died at or around birth had empty stomachs, indicating that they had not fed[189].

LaNt α31 transgenic mice share kidney defects observed in LM α5 LN domain mutant mice. LM521 is a major component of the glomerular BM, and a lack of polymerization here, as well as in other BMs, would likely defects in glomerular BM integrity and renal function. Indeed, TEM examination of the glomerular BM of E18.5 LM α5 transgenic mouse kidneys revealed intermittent areas of BM disorganization[189]. Due to the severity of the phenotype, further studies of renal phenotype in aged mice was not possible. The kidney defects here resemble those seen in LaNt α31 overexpressing mice, alluding to a similar mechanism behind the phenotype.

The defects observed in the glomeruli of the LM α5 LN domain mutant mice were largely vascular, which becomes particularly interesting when we begin to compare the phenotype with the LaNt α31 overexpressing mice. Although both the LaNt α31 transgenic mice and the LM α5 LN domain mutant mice exhibit somewhat similar defects, particularly when assessing kidney BMs by TEM, the phenotypes are not directly comparable.

Similarities between LaNt α31 transgenic mice and LM α5 LN domain mutant mice point towards a network disrupting role for LaNt α31. For example, in LM521 containing networks in LM α5 LN domain mutant mice, network disruption occurs because of the inability of the αLN domain to facilitate polymerization. Similarly, overexpression of LaNt α31 in LM521 containing networks would allow the LaNt α LN domain to compete for αLN interactions with the native LM α5 LN domain. Though through different mechanisms, it is easy to imagine how this could result in similar organizational changes and therefore similar phenotypic changes, discussed further in the next chapter. This represents two different causes behind a disruption of LM511 or 521 networks.

6.3.3. Does LaNt α31 play a role in vascular homeostasis?

LaNt α31 OE mice may exhibit phenotypes on any LM network containing compatible β and γ LN domains, such as the case with LM411. LM411 is expressed throughout all haem and lymphatic vessels, and is the main vascular LM throughout development and vasculogenesis, and one might

have anticipated that the LaNt α31 LN domain could compensate for the "missing" α LN domain in the vasculature and stabilise the weak, transient βγ LN dimers made by the LM β1 and γ1 LN domains[47,50,56]. However, the observed phenotype of blood exudate throughout the mouse tissues and capillary BM disruption evident by TEM suggests instead indicates that the LaNt α31 has a disruptive rather than stabilising role. Additionally, previous studies have shown that the LM γ2 LN domain can increase vascular permeability and is implicated in aberrant vascular functions in cancer tissues[333], so a vascular leakage defect caused by LN-domain containing proteins are not unprecedented.

6.3.3.1. LaNt α31 could disrupt vascular LM511 networks

One possible explanation for this indeed relates back to the complex composition of BM LMs in the vasculature. In lymph and early blood vessels, LM411 is the main BM component, but as vessels mature LM511 is produced and becomes part of the vascular BM. Whereas LM411 is a 'two-headed' LM, containing only a β1 and γ1 LN domain, LM511 is able to polymerise as it can form the αβγ ternary node. Previous elegant studies has shown that endothelial LM α5 contributes to junctional tightness, inhibiting T-lymphocyte migration into the brain and inhibits general leukocyte transmigration both directly and indirectly[156,334].

Overexpression of LaNt α31 indeed provides a scenario whereby the areas of LM511 networks in the vasculature are disrupted due to competition with the LaNt α31 LN domain, leading to a weakened basement membrane in areas where LM511 would normally be inhibiting cell migration through the vessel walls, providing a simple yet incomplete explanation of why vascular leakage is observed in LaNt α31 transgenic animals. This explanation however only addresses the physical mechanisms through which LaNt α31 may act in a disruptive manner.

LMs have been implicated in cell signalling in a great number of situations, ranging from development to disease situations, largely mediated through integrin binding. LM511 affects endothelial barrier function by stabilizing VE-cadherin at junctions and downregulating expression of CD99L2, correlating

with reduced neutrophil extravasation[156]. Binding of endothelial cells to laminin 511, but not laminin 411 or non-endothelial laminin 111, enhanced transendothelial cell electrical resistance (TEER) and inhibited neutrophil transmigration[156]. Data suggest that endothelial adhesion to laminin 511 via β1 and β3 integrins mediates RhoA-induced VE-cadherin localization to cell-cell borders, and while CD99L2 downregulation requires integrin β1, it is RhoA-independent[156].

Though it appears that disruption of the LM511 network would have both direct and indirect consequences for cell migration through vessels, it becomes more difficult to envisage the effects of LaNt α31 binding would casue in LM411 networks. LM α4 lacks an LN domain, so the LM411 heterotrimer posses only β and γ LN domains. LaNt α31 possesses the domains to bind to β1 and γ1 LN domains. Indeed, current models of LMternary node formation state that first LMs assemble into a β-γ dimer in a rapid interaction and is then stabilised by the α LN domain, forming the ternary node. Based on this, LaNt α31 would in theory provide the necessary α LN domain to form a stable complex.

LaNt α31 transgenic mice share some phenotypic resemblance to Lama4 null mice[335]. Absence of LM α4 weakens the capillary BM, and consequently ruptures the microvascular walls causing haemorrhages as demonstrated by bleeding throughout embryonic development[335]. Specifically, in Lama4 null mice, haemmorhages could be observed in E11.5 mice, but were most apparent in newborn mice, possibly aggravated by the physical stress of parturition, and authors of the study observed that haemorrhages were concentrated in the soft tissues of the head and lower back; tissues which are subject to heavy mechanical stress during delivery[335]. Though mortality in the first 2 days after birth in Lama4 null mice was only slightly elevated, the haemorrhaging described is similar to what is observed in LaNt α31 transgenic mice.

The less severe phenotype observed in Lama4 null mice compared to LaNt α31 transgenic mice may be explained by finding that these mice expressed normal LM α5, and mice lacking LM α4, show a compensatory even

distribution of laminin 511 in all endothelial cell basement membranes. It remains to be seen why in both these scenarios (Lama4 null vs LaNt α31 OE) transgenic mice are born with varying degrees of visible haemorrhaging. Despite this, disruption of the normal LM411 network could be a cause of the haemorrhaging phenotype, which illustrates that vascular BM interactions and homeostasis are even more complex than is currently thought.

6.3.3.2. Does LaNt α31 fine-tune vascular BMs?

For what reason would LaNt α31 have evolved in the context of vascular regulation? Indeed, an alternative splice isoform generated through a complex process of intron retention and alternative polyadenylation would provide a mechanism for the fine-tuning of BMs, especially if small amounts of LaNt α31 could cause profound effects on the surrounding contextual microenvironment. In this study the UbC promoter was used to replicate more physiological levels of overexpression, rather than a strong promoter such as CMV or CAG. Even with this, a deleterious phenotype is observed, illustrating how potent LaNt α31 can act upon the vasculature. Considering LaNt α31 is expressed in normal vasculature, it is situated in a position to play a role in vessels. Increased levels of LaNt α31 may provide a mechanism where vasculature can be temporarily weakened or disrupted to allow for extravasation of immune cells in times of inflammation or infection, without major changes in gene expression.

6.3.4. LaNt α31 acting in a non-disruptive manner

Within the model of LaNt α31 inhibiting LM network assembly, there remains the question of how LaNt α31 influences tissues where there the expressed LMs do not contain an α LN domain, and therefore are not able to polymerise[9]. For example, The LM composition present within vessel BMs during development and lymph vessels is rich in the non-polymerising LM411 [122,157,270]. Here it should be noted that transgenic mice expressing the potent LM network disrupting protein netrin 4 under the control of the K14 promoter were born smaller, redder, and with increased lymphatic permeability[247]. Whereas netrin 4 can only disrupt, as it lacks one of the necessary LN

domain binding regions, LaNt α31 contains a perfect LN domain, endowing it with the ability to either compete for LN-LN interactions, or indeed stabilise LM networks in situations where the LM isoforms do not possess αβγ LN domains. Out of the 12 LM chains, LMs α3A, α4, and γ2 do not possess LN domains. This leads to LMs 3A32 lacking an α and γ LN domain, and LM411 lacking just an α LN domain. In these situations LaNt α31 may replace the 'missing' α LN domain and help to stabilise networks.

6.3.5. LaNt α31 may play a role in cell signalling

It is also possible that the LaNt α31 transgene effects represent a signalling rather than structural role. Integrin-mediated signalling from LaNt α31-like proteolytically released LN-domain containing fragments from LM α3b, α1, and β1 chains have been reported[77-79] and some aspects of the UbCLaNt::R26CreERT2 phenotype are consistent with LaNt α31 acting in this way. For example one of the most striking phenotypes observed in the LaNt α31 transgenic mice was depletion of hematopoietic colonies in the liver, an essential stem cell niche during development[336-338].

Integrins α6 and β1 are highly expressed in hematopoietic stem cells, and are central to the process of migration both in and out of the fetal liver[339-341]. A netrin 4/laminin γ1 complex has been shown to signal through the integrin α6β1 receptor to ERK1/2 and regulate neural stem cell proliferation and migration[80]. LaNt α31 is also enriched in human and porcine limbal stem cell niche of adult corneas, with expression further upregulated upon ex vivo stem cell activation and wound repair[53]. While these combined data suggest that direct signalling effects are possible with LaNt α31 binding to cell surface receptors, indirect effects are also probable. The biological activity of the LaNt α31 C-terminus is currently unknown.

6.3.5.1. LaNt α31 C-terminus signalling

We do not at this moment know of the signalling capabilities of the C-terminus of LaNt α31. If indeed LaNt α31 forms a ternary node complex with LM411, the question remains whether or not the exposed C-terminus of Lant α31 plays a role in signalling which could add further Though speculative,

any binding of LaNt α31 to existing LMnetworks would not only modify the network and the subsequent biological activity, the C-terminus of LaNt α31 would also be present and may bind to as of yet unidentified receptors, further modifying cell or tissue behaviour.

6.3.6. Growth factor sequestration

Altering ECM structural organization changes cell signalling through various avenues such as through changing the presentation of ligands or by directly cleaving aspects of the ECM or bound growth factors allowing them to affect tissues outside of the ECM[342-344]. The ECM may sequester many different growth factors such as epidermal growth factor (EGF), fibroblast growth factor (FGF) and other signalling molecules (such as WNTs, transforming growth factor-β (TGFβ) and amphiregulin). ECM degradation or reorganization may also begin a feedback loop whereby components released through ECM cleavage also regulate ECM architecture and influence cell behaviour. Moreover, cells are constantly rebuilding and remodelling the ECM through synthesis, degradation, reassembly and chemical modification[345]. These processes are complex and need to be tightly regulated to maintain tissue homeostasis, particular during development and in response to injury and inflammation[346].

6.3.7. LaNt α31 as a regulator of stem cell niches

Indeed, LM networks are critical for maintaining progenitor cell “stemness” [167,347-349]. Dissecting the direct versus indirect roles of LaNt α31 in intact tissue contexts is now a priority and the new transgenic line provides a valuable resource to facilitate those onward investigations. As alluded to above, LaNt α31 transgenic animals display a reduction in hematpoietic stem cell colonies in the liver. Whether this is due to vascular leakage or signalling defects is currently unknown, though both provide plausible explanations. The main LMreceptor are the integrins. Any changes in integrins may lead to a cascade of signalling and mechanical defects within cells and tissues, the effects of which would be amplified during development.

During development the liver acts as the main reservoir for hemaopoietic stem cells, before the cells migrate into the bone marrow in late development and after birth. The consequences of defective integrin signalling in relation to fetal hematopoietic stem cells are obvious. The β1 integrin subunit in fetal hematopoietc stem cells is involved in colonization of the fetal liver, spleen, and bone marrow. Migration, but not the differentiation, of hematopoietic stem cells into these tissues is impaired in animals lacking the β1 integrin subunit[340]. Integrin β1 is expressed as a dimer with integrin α6 in the liver and is highly expressed, and this integrin has been shown to be the one of the main receptor for LMs 411, 511, and 521[350]. A LaNt α31-induced change in organization of these LMs may indeed have knock-on effects for integrin-mediated signalling and in turn have consequences for the migration of hematopoietic stem cells.

Outside of the liver, LMs play an essential role in maintaining almost every stem-cell niche in both development and during normal homeostasis. Recombinant LMs are commonly used as a differentiation substrate in 2D and 3D cell cultures, and simply the LM isoform used can determine the fate of multipotent or pluripotent stem cells. On top of this, LMs are often used to maintain the stemness of cells in culture. In animals, of course the role of LMs is far more complex, though it is easy to see that a disruption of LM networks caused by overexpression of LaNt α31 may lead to negative consequences.

So far, we cannot determine which effects seen in LaNt α31 transgenic mice are caused by physical, signalling, or a combination of both possibilities. Even in the skin of LaNt α31 transgenic mice, the difference observed in the skin and keratinocytes may be related to differentiation defects. It is now a focus points of future work to determine the specific binding partners of LaNt α31, and to biochemically determine the effects of LaNt α31 on polymerization. Partnering this, it ascertaining the signalling capabilities of the LaNt α31 protein will be of paramount importance for our understanding of the significance of LaNt α31 in wider BM and ECM biology.

6.3.8. Conclusion

Moving forward, the role of LaNt α31 can now be determined in a tissue and context specific manner. Considering the widespread expression of LaNt α31[52], and the dramatic effects observed in this study, it is now important to determine effects in adult animals in normal conditions and following intervention and under lineage specific control. These studies should also include tissues where no overt LaNt α31-induced phenotype was observed. For example, although we did not observe muscle effects in these animals, LM network integrity is critical to muscle function, with the effects of LMα2 LN domain mutations or deletions developing muscular dystrophy and peripheral neuropathy with time[351-353]; therefore, longer-term studies may reveal further phenotypes once tissues are placed under stress.

Inherited disorders driven by variants to α LN domain have robustly established that LN domains are important for tissue function[142,181,193,212,332]. However, the findings here add a new layer to this regulation. LaNt α31 is a naturally occurring protein generated from a laminin-encoding gene via alternative splicing. The findings here now show that LaNt α31 is functional within a biological context. This is important as it raises the possibility of active regulation of LaNt α31 production via control of the splicing event as a mechanism to influence BM assembly/disassembly or matrix-signalling by titrating LaNt α31 levels[51]. Alternative splicing rates often change in normal situations during development and tissue remodelling, or in response to damage such as in wound repair, and are frequently dysregulated in pathological situations including frequently in cancer[354-356]. Considered in this way, the finding the LaNt α31 is biologically active in vivo has exciting and far-reaching implications for our understanding of BM biology.

Chapter 7: Final summary

The findings described in this thesis all point towards LaNt α31 being an potent disruptor of normal tissue homeostasis and mammalian development when overexpressed. Indeed, the dramatic phenotype observed in OSE and OCE models in chapter 5, and the phenotype of the transgenic mice in chapter 6, underline the biological significance of LaNt α31. The work presented in this thesis should serve as a springboard for future studies rather than an endpoint, and although this research represents a significant contribution to the field of ECM biology, it is clear there are many questions that remain unanswered.

The phenotypes seen in different tissues of the LaNt α31 overexpressing mice all point towards a disruption of LM network integrity. It is unknown at this stage the precise molecular mechanism behind this, but here I present the following models of LaNt α31-mediated BM membrane disruption.

7.1 The role of LaNt α31 in 3 LN domain-containing networks

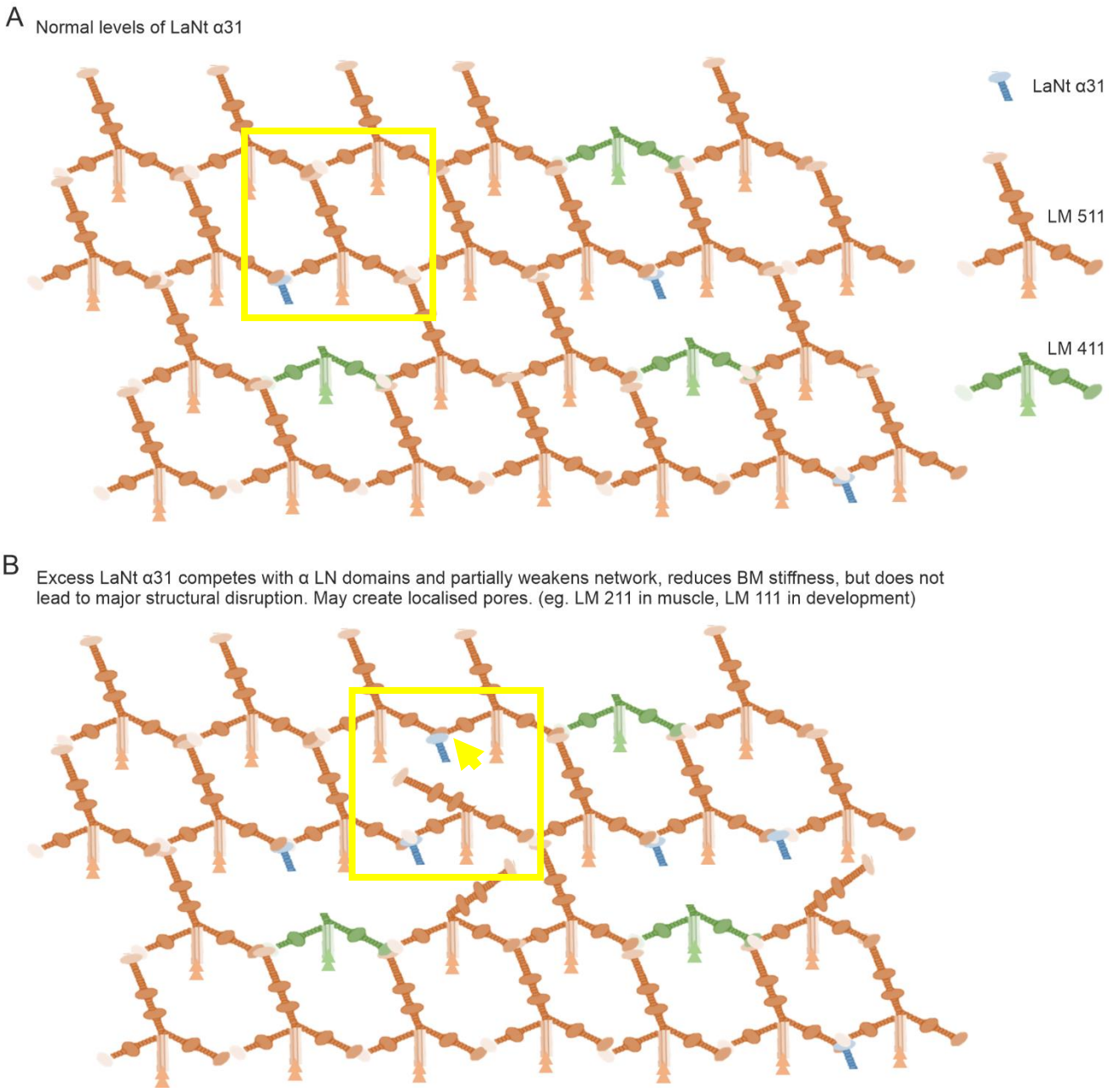

Figure 7.1. Proposed model of LaNt α31 interactions at normal levels and in excess in 3 LN domain containing LM networks. A) Normal levels of LaNt α31 contributes to normal BM homeostasis. B) Excess levels of LaNt α31 competes for with α LN domains and partially weakens LM network. Yellow boxes highlight comparable areas between A) and B). Yellow arrowhead points to a ternary node where LaNt α31 is preventing normal LM binding.

LaNt α31 is likely to play different roles in different tissue BMs depending on the LM composition. It is rarely the case that any single BM contains entirely one single isoform, and it is this interplay of different LM isoforms that

contributes to the complexity of BMs. If we consider a 3 LN domain network, such as LM211 in muscle or LM111 during development, it is possible that at normal levels, LaNt α31 is a part of the network and is required to modulate the stiffness of the BM (Fig. 7.1A). In situations where LaNt α31 is overexpressed, however, the increased concentration of LaNt α31 may compete for α LN domain interactions, reducing BM stiffness and creating larger, localised pores[245]. Despite this, network polymerization would still be possible, and one would not observed major structural disruption (Fig. 7.1B). Because LM polymerization would still be possible to an extent, this is perhaps why although LaNt α31 mice were not viable at birth, they continued to develop after transgene induction.

7.2 The role of LaNt α31 in 2 LN domain-containing networks (venules, veins)

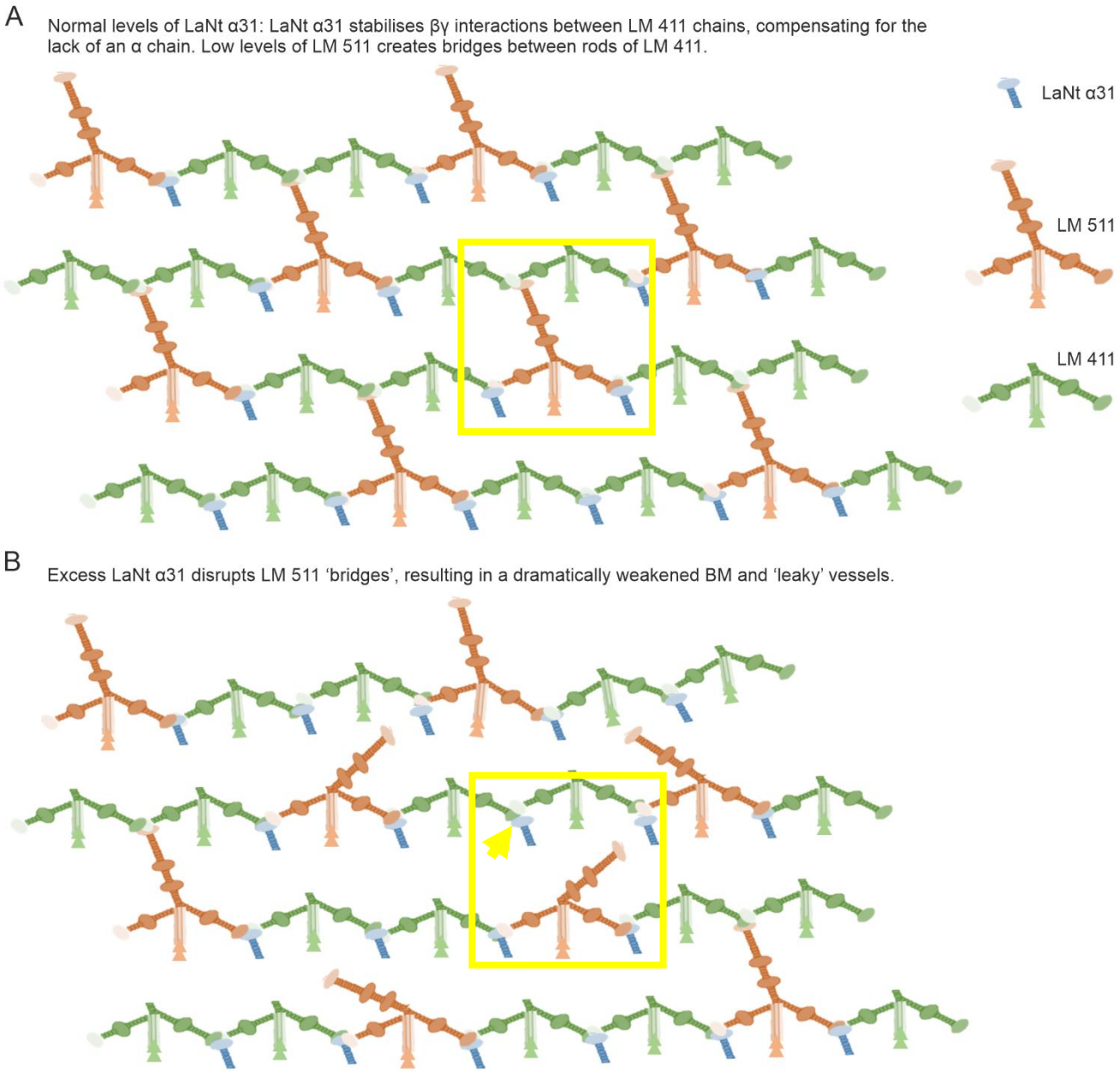

Figure 7.2. Proposed model of LaNt α31 interactions at normal levels and in excess in 2 LN domain containing LM networks. A) Normal levels of LaNt α31 stabiles βγ interactions in LM411 networks. B) Excess levels of LaNt α31 disrupts LM511 bridges, destabilising the BM and compromising vessel structure. Yellow boxes highlight comparable areas between A) and B). Yellow arrowhead points to a ternary node where LaNt α31 is preventing normal LM binding.

One of the prominent phenotypic features of LaNt α31 transgenic mice was the presence of blood exudate throughout multiple tissues. All vessels contain LM411, and LM511 is present but greatly enriched in arteries and arterioles. Previous data130 and chapter 4 of this thesis have also

highlighted that LaNt α31 is present throughout many vessels, indicating that it is likely to play a role in these structures. I suggest that at normal levels, LaNt α31 stabilises LM411 βγ interactions, compensating for the lack of an α LN domain. Here, small amounts of LM511 creates bridges between the LM411 polymers, allowing for normal tissue function (Fig. 7.1A). When LaNt α31 is overexpressed in these tissues, the excess LaNt α31 competes for the α LN domain interaction provided by LM α5, and destroys or prevents the LM511 ‘bridges’ from linking LM411 polymers, resulting in a dramatically weakened BM. It is because of this disruption ‘leaky’ vessels are observed in the LaNt α31 transgenic mice. If this is the case, LaNt α31 would appear to be an important modulator of vascular BMs, a role hitherto unexplored.

7.3 The role of LaNt α31 in vessels with high levels of LM511 (arteries, arterioles)

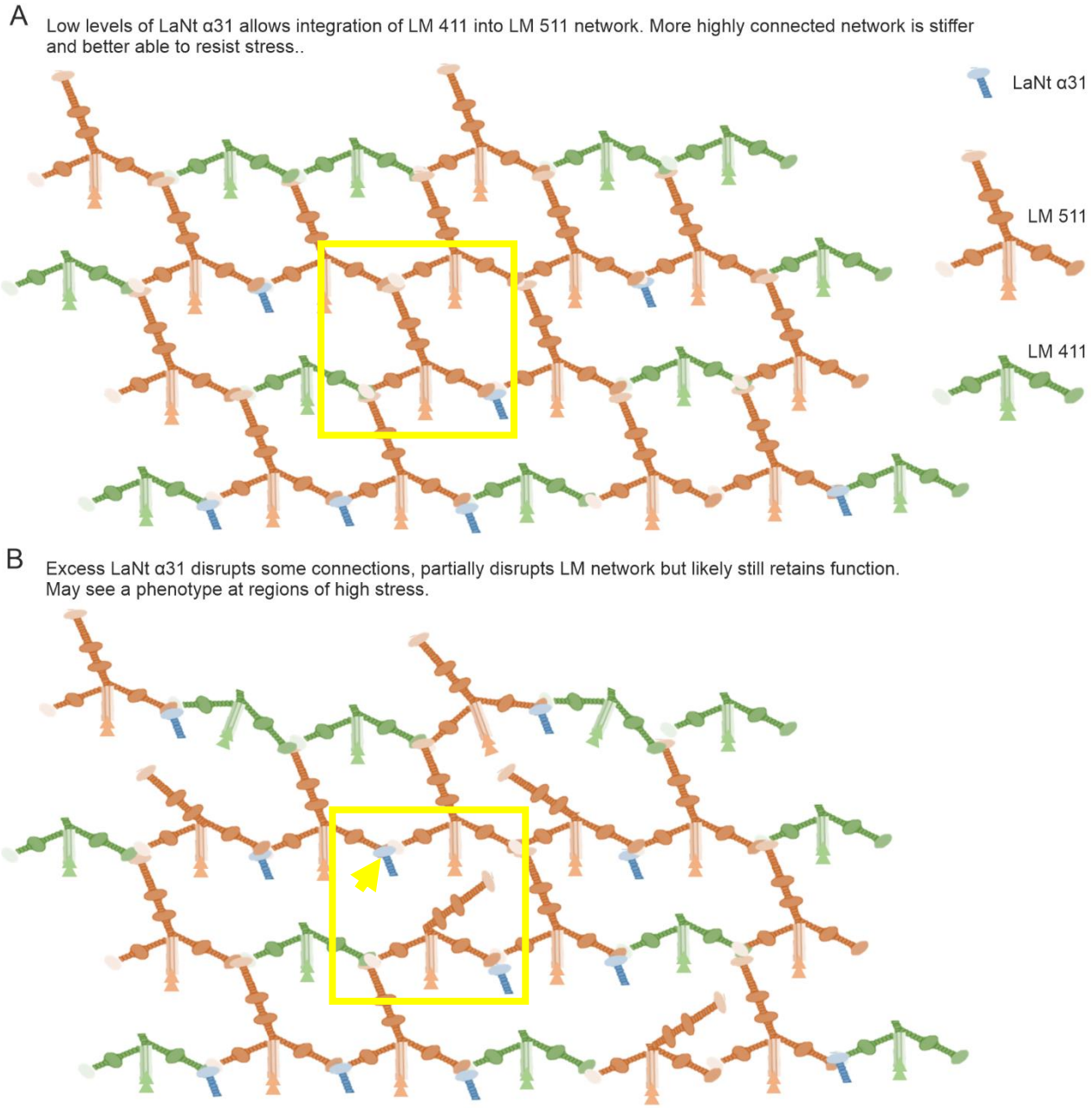

Figure 7.3. Proposed model of LaNt α31 interactions at normal levels and in excess in 2 LN domain containing LMnetworks. A) Normal levels of LaNt α31 allows integration of LM411 into networks of LM511. B) Excess levels of LaNt α31 partially disrupts LMnetwork but the LMremains functional. Yellow boxes highlight comparable areas between A) and B). Yellow arrowhead points to a ternary node where LaNt α31 is preventing normal LM binding.

LM511 is also a component of some vessel, particularly in arteries or arterioles. How the LM411 and LM511 isoforms integrate within these networks is not yet fully understood, but here I propose a mechanism whereby LaNt α31, at normal levels, allows the integration of LM411 into

LM511 networks. On one hand, LaNt α31 may stabilise βγ interactions of LM411 and LM511. On the other hand, LaNt α31 may compete for LN domain interactions of the LM511 α chain, temporarily weakening the network, and enabling integrations of LM411 into the network. With LaNt α31, LM511, and LM411 all present, this provides a situation where a highly interconnected network can form, which would hypothetically be stiffer than a LM411 network alone and would be better able to resist stress (Fig. 7.3A). When LaNt α31 is overexpressed in this situation, some disruptions of the network may occur, but the combined LM511 and LM411 composition of the network would likely still allow the network to retain its function, though a phenotype may be seen at regions of high stress (Fig. 7.3B).

7.4 LaNt α31 is a potential mediator of BM stiffness, composition, and architecture

The 3 models outlined above illustrate the role LaNt α31 may play in different networks. The work in this thesis investigated the role of LaNt α31 during development, but the models described may be extended to other situations. If LaNt α31 can weaken networks, this could in turn affect the stiffness of BM. It has long been known that changes in ECM stiffness regulate the hallmarks of cancer[357], and it has been shown recently that specifically BM stiffness determines metastases formation[246].

LaNt α31 is upregulated in invasive ductal breast cancer and changes the mode of tumour invasion[55], and the models above may help to explain some of the mechanisms behind this. LaNt α31 is upregulated in invasive ductal breast cancer and changes the mode of tumour invasion[55], and the models above may help to explain some of the mechanisms behind this. On top of changing BM stiffness, by competing for α LN domain interactions, LaNt α31 may also change the architecture of BMs, introducing different pore sizes and allowing different LM isoforms to integrate with one another. The consequences of pore size and LM integration is hard to predict at this stage, though it would likely affect receptor binding and cell extravasation through networks, to name but two.

7.5 Concluding remarks

Importantly, this thesis has shown not only that LaNt α31 is widespread in it's distribution, but that the protein is biologically relevant in vivo, and normal homeostasis is required for healthy tissue function and structure in vivo and in 3D organotypic models.

Future research should now focus on the biochemical mechanisms behind LaNt α31 mediated disruption, and indeed how this influences BM stiffness and architecture. Furthermore, it is abundantly clear that LaNt α31 is present within the vasculature. The role of LaNt α31 in vascular homeostasis and angiogenesis should be uncovered, as doing so will greatly increase our understanding of fundamental mammalian biology.

The importance of the LaNt α31 protein cannot be understated, as dysregulation of LaNt α31 during development is lethal and causes widespread tissue-specific defects, with a more severe phenotype than was expected. When one considers that LaNt α31 is produced through a tightly regulated process of intron retention and alternative polyadenylation[51,298], one can only marvel at the elegance and complexity of how this splice isoform may be a part of an elegant auto-regulatory mechanism that controls the properties of LM networks. A protein that has such influence of BM homeostasis, by extension, is a protein that is of major importance to mammalian biology.

Appendices

Appendix I: LaNtα31-PAmCherry1-P2A-Puro amino acid sequence and protein alignments

LaNtα31-PAmCherry1-P2A-Puro

METDTLLLWVLLLWVPGSTGDDPGAAAGLSLHPTYFNLAEAARIWATATCGERGPG
EGRPQPELYCKLVGGPTAPGSGHTIQGQFCDYCNSEDPRKAHPVTNAIDGSERWWQ
SPPLSSGTQYNRVNLTLDLGQLFHVAYILIKFANSPRPDLWVLERSVDFGSTYSPW
QYFAHSKVDCLKEFGREANMAVTRDDDVLCVTEYSRIVPLENGEVVVSLINGRPGA
KNFTFSHTLREFTKATNIRLRFLRTNTLLGHLISKAQRDPTVTRRYYYSIKDISIG
GQCVCNGHAEVCNINNPEKLFRCECQHHTCGETCDRCCTGYNQRRWRPAAWEQSHE
CEACNCHGHASNCYYDPDVERQQASLNTQGIYAGGGVCINCQHNTAGVNCEQCAKG
YYRPYGVPVDAPDGCIRKFHFKLVYLSLCVLPQRSHQANFGSVNNFLHALSLQSIS
CARYVTSVTYTVSLNFGFIACKWKTSDYKDDDDKYPYDVPDYAGSMVSKGEEDNMA
IIKEFMRFKVHMEGSVNGHVFEIEGEGEGRPYEGTQTAKLKVTKGGPLPFTWDILS
PQFMYGSNAYVKHPADIPDYFKLSFPEGFKWERVMKFEDGGVVTVTQDSSLQDGEF
IYKVKLRGTNFPSDGPVMQKKTMGWEALSERMYPEDGALKGEVKPRVKLKDGGHYD
AEVKTTYKAKKPVQLPGAYNVNRKLDITSHNEDYTIVEQYERAEGRHSTGGMDELY
KASGPTRTRPLVWVGSGATNFSLLKQAGDVEENPGPMTEYKPTVRLATRDDVPRAV
RTLAAAFADYPATRHTVDPDRHIERVTELQELFLTRVGLDIGKVWVADDGAAVAVW
TTPESVEAGAVFAEIGPRMAELSGSRLAAQQQMEGLLAPHRPKEPAWFLATVGVSP
DHQGKGLGSAVVLPGVEAAERAGVPAFLETSAPRNLPFYERLGFTVTADVEVPEGP
RTWCMTRKPGA*

Protein alignments for pLenti-LaNtα31-PAmCherry1-P2a-Puro

LaNt α31 sequence

pLenti-LaNtα31-PAmCherry1-P2A-puro sequence LaNtα31 sequencing alignment with original IgK-LaNtα31 design

```
Seq_1  1     METDTLLLWVLLLWVPGSTGDDPGAAAGLSLHPTYFNLAEAARIWATATCGERGPGEGRP  60
             ||||||||||||||||||||||||||||||||||||||||||||||||||||||||||||
Seq_2  1     METDTLLLWVLLLWVPGSTGDDPGAAAGLSLHPTYFNLAEAARIWATATCGERGPGEGRP  60

Seq_1  61    QPELYCKLVGGPTAPGSGHTIQGQFCDYCNSEDPRKAHPVTNAIDGSERWWQSPPLSSGT  120
             ||||||||||||||||||||||||||||||||||||||||||||||||||||||||||||
Seq_2  61    QPELYCKLVGGPTAPGSGHTIQGQFCDYCNSEDPRKAHPVTNAIDGSERWWQSPPLSSGT  120

Seq_1  121   QYNRVNLTLDLGQLFHVAYILIKFANSPRPDLWVLERSVDFGSTYSPWQYFAHSKVDCLK  180
             ||||||||||||||||||||||||||||||||||||||||||||||||||||||||||||
Seq_2  121   QYNRVNLTLDLGQLFHVAYILIKFANSPRPDLWVLERSVDFGSTYSPWQYFAHSKVDCLK  180

Seq_1  181   EFGREANMAVTRDDDVLCVTEYSRIVPLENGEVVVSLINGRPGAKNFTFSHTLREFTKAT  240
             ||||||||||||||||||||||||||||||||||||||||||||||||||||||||||||
Seq_2  181   EFGREANMAVTRDDDVLCVTEYSRIVPLENGEVVVSLINGRPGAKNFTFSHTLREFTKAT  240

Seq_1  241   NIRLRFLRTNTLLGHLISKAQRDPTVTRRYYYSIKDISIGGQCVCNGHAEVCNINNPEKL  300
             ||||||||||||||||||||||||||||||||||||||||||||||||||||||||||||
Seq_2  241   NIRLRFLRTNTLLGHLISKAQRDPTVTRRYYYSIKDISIGGQCVCNGHAEVCNINNPEKL  300

Seq_1  301   FRCECQHHTCGETCDRCCTGYNQRRWRPAAWEQSHECEACNCHGHASNCYYDPDVERQQA  360
             ||||||||||||||||||||||||||||||||||||||||||||||||||||||||||||
Seq_2  301   FRCECQHHTCGETCDRCCTGYNQRRWRPAAWEQSHECEACNCHGHASNCYYDPDVERQQA  360

Seq_1  361   SLNTQGIYAGGGVCINCQHNTAGVNCEQCAKGYYRPYGVPVDAPDGCIRKFHFKLVYLSL  420
             ||||||||||||||||||||||||||||||||||||||||||||||||||||||||||||
Seq_2  361   SLNTQGIYAGGGVCINCQHNTAGVNCEQCAKGYYRPYGVPVDAPDGCIRKFHFKLVYLSL  420

Seq_1  421   CVLPQRSHQANFGSVNNFLHALSLQSISCARYVTSVTYTVSLNFGFIACKWKTSDYKDDD  480
             ||||||||||||||||||||||||||||||||||||||||||||||||||||||||||||
Seq_2  421   CVLPQRSHQANFGSVNNFLHALSLQSISCARYVTSVTYTVSLNFGFIACKWKTSDYKDDD  480

Seq_1  481   DKYPYDVPDYA  491
             ||||||||||| 
Seq_2  481   DKYPYDVPDYA  491
```

PAmCherry1 sequence

pLenti-LaNtα31-PAmCherry1-P2A-puro sequence alignment to PAmCherry1 (Uniprot)

```
Similarity : 236/236 (100.00 %)

Seq_1  1     MVSKGEEDNMAIIKEFMRFKVHMEGSVNGHVFEIEGEGEGRPYEGTQTAKLKVTKGGPLP  60
             ||||||||||||||||||||||||||||||||||||||||||||||||||||||||||||||
Seq_2  1     MVSKGEEDNMAIIKEFMRFKVHMEGSVNGHVFEIEGEGEGRPYEGTQTAKLKVTKGGPLP  60


Seq_1  61    FTWDILSPQFMYGSNAYVKHPADIPDYFKLSFPEGFKWERVMKFEDGGVVTVTQDSSLQD  120
             ||||||||||||||||||||||||||||||||||||||||||||||||||||||||||||||
Seq_2  61    FTWDILSPQFMYGSNAYVKHPADIPDYFKLSFPEGFKWERVMKFEDGGVVTVTQDSSLQD  120


Seq_1  121   GEFIYKVKLRGTNFPSDGPVMQKKTMGWEALSERMYPEDGALKGEVKPRVKLKDGGHYDA  180
             ||||||||||||||||||||||||||||||||||||||||||||||||||||||||||||||
Seq_2  121   GEFIYKVKLRGTNFPSDGPVMQKKTMGWEALSERMYPEDGALKGEVKPRVKLKDGGHYDA  180


Seq_1  181   EVKTTYKAKKPVQLPGAYNVNRKLDITSHNEDYTIVEQYERAEGRHSTGGMDELYK  236
             ||||||||||||||||||||||||||||||||||||||||||||||||||||||||
Seq_2  181   EVKTTYKAKKPVQLPGAYNVNRKLDITSHNEDYTIVEQYERAEGRHSTGGMDELYK  236
```

Appendix II: LaNtα31-T2A-tdTomato amino acid sequence

METDTLLLWVLLLWVPGSTGDDPGAAAGLSLHPTYFNLAEAARIWATATCGERGPG
EGRPQPELYCKLVGGPTAPGSGHTIQGQFCDYCNSEDPRKAHPVTNAIDGSERWWQ
SPPLSSGTQYNRVNLTLDLGQLFHVAYILIKFANSPRPDLWVLERSVDFGSTYSPW
QYFAHSKVDCLKEFGREANMAVTRDDDVLCVTEYSRIVPLENGEVVVSLINGRPGA
KNFTFSHTLREFTKATNIRLRFLRTNTLLGHLISKAQRDPTVTRRYYYSIKDISIG
GQCVCNGHAEVCNINNPEKLFRCECQHHTCGETCDRCCTGYNQRRWRPAAWEQSHE
CEACNCHGHASNCYYDPDVERQQASLNTQGIYAGGGVCINCQHNTAGVNCEQCAKG
YYRPYGVPVDAPDGCIRKFHFKLVYLSLCVLPQRSHQANFGSVNNFLHALSLQSIS
CARYVTSVTYTVSLNFGFIACKWKTSDYKDDDDKYPYDVPDYATGTREGRGSLLTC
GDVEENPGPGTINWDPATMVSKGEEVIKEFMRFKVRMEGSMNGHEFEIEGEGEGRP
YEGTQTAKLKVTKGGPLPFAWDILSPQFMYGSKAYVKHPADIPDYKKLSFPEGFKW
ERVMNFEDGGLVTVTQDSSLQDGTLIYKVKMRGTNFPPDGPVMQKKTMGWEASTER
LYPRDGVLKGEIHQALKLKDGGHYLVEFKTIYMAKKPVQLPGYYYVDTKLDITSHN
EDYTIVEQYERSEGRHHLFLGHGTGSTGSGSSGTASSEDNNMAVIKEFMRFKVRME
GSMNGHEFEIEGEGEGRPYEGTQTAKLKVTKGGPLPFAWDILSPQFMYGSKAYVKH
PADIPDYKKLSFPEGFKWERVMNFEDGGLVTVTQDSSLQDGTLIYKVKMRGTNFPP
DGPVMQKKTMGWEASTERLYPRDGVLKGEIHQALKLKDGGRYLVEFKTIYMAKKPV
QLPGYYYVDTKLDITSHNEDYTIVEQYERSEGRHHLFLYGMDELYK*

Appendix III: List of manuscripts and meeting abstracts

Peer reviewed papers

Sugden, CJ, Iorio, V, Troughton, LD, et al. Laminin N-terminus α31 expression during development is lethal and causes widespread tissue-specific defects in a transgenic mouse model. *FASEB J*. 2022; 36:e22318. doi:10.1096/fj.202002588RRR

Sugden, C. J.†, Shaw, L.†, and Hamill, K. J. (2021). Laminin Polymerization and Inherited Disease: Lessons From Genetics. Front. Genet. 12:707087. doi: 10.3389/fgene.2021.707087

Troughton LD, Reuten R, **Sugden CJ**, Hamill KJ (2020) Laminin N-terminus α31 protein distribution in adult human tissues. PLoS ONE 15(12): e0239889. https://doi.org/10.1371/journal.pone.0239889

Preprint manuscripts

Lee D. Troughton, Valentina Iorio, Liam Shaw, **Conor J. Sugden**, Kazuhiro Yamamoto, Kevin J. Hamill (2020). Laminin N-terminus α31 regulates keratinocyte adhesion and migration through modifying the organization and proteolytic processing of laminin 332. doi: https://doi.org/10.1101/617597 [Preprint]

Published Abstracts

Sugden, C. J., Troughton, L. D., Liu, K., Bou-Gharious, G., & Hamill, K. J. (2020). Development and validation of an inducible LaNt alpha 31 overexpressing mouse model. International Journal of Experimental Pathology Vol. 101 (pp. A5-A5). **[Abstract]**

Sugden, C. J., Troughton, L. D., Liu, K., Bou-Gharious, G., & Hamill, K. J. (2019). Development and validation of an inducible LaNt alpha 31 overexpressing mouse model. International Journal of Experimental Pathology Vol. 100 (pp. A36-A37). **[Abstract]**

Accepted Abstracts

September 2021

BSMB Autumn Meeting 'Extracellular Matrix in Rare Diseases' Online; Laminin N-terminus α31 expression during development is lethal and causes widespread tissue-specific defects in a transgenic mouse model. **CJ Sugden**, V Iorio, LD Troughton, K Liu, G Bou-Gharios, KJ Hamill. (Poster)

May 2020

Matrix Biology Europe 2020, Florence, Italy; Transgenic overexpression of the laminin α3 LN domain is lethal and disrupts the epidermal basement membrane. **CJ Sugden**, LD Troughton, K Liu, G Bou-Gharios, KJ Hamill. (Poster) [Abstract accepted, conference postponed due to Covid-19]

September 2019

BSMB Autumn Meeting 'Cell Adhesion Networks in Health and Disease', Norwich; Development and validation of an inducible LaNt α31 transgenic mouse line. **CJ Sugden**, LD Troughton, K Liu, G Bou-Gharios, KJ Hamill. ***Poster Prize Winner**

April 2019

BSMB Spring Meeting 'Stroma, Niche and Repair', Liverpool; Development and validation of an inducible LaNt α31 transgenic mouse line. **CJ Sugden**, LD Troughton, K Liu, G Bou-Gharios, KJ Hamill. (Poster)

February 2019

Faculty of Health and Life Sciences Poster Day, Liverpool; Development and validation of an inducible LaNt α31 transgenic mouse line. **CJ Sugden**, LD Troughton, K Liu, G Bou-Gharios, KJ Hamill. ***Poster Prize Runner Up**

March 2017

The Assembly, Dynamics and Organization of Filaments and Cellular Responses Workshop, Durham University; Intron Retention and Alternative Polyadenylation in LAMA3. **Conor J. Sugden**, Lee D. Troughton, Kevin J. Hamill. (Poster)

Appendix IV: Grants and Bursaries Awarded

German Academic Exchange Service (DAAD) Short Term Research Grant: Scholarship to fund a 3-month placement in the Nyström Lab, Department of Dermatology, Medical Centre, University of Freiburg, Germany.

British Society for Matrix Biology travel bursary: £500 towards Matrix Biology Europe, Florence, Italy, 2020 (Postponed due to Covid-19)

Appendix V: Published manuscript relating to chapter 2

frontiers in Genetics

MINI REVIEW
published: 12 August 2021
doi: 10.3389/fgene.2021.707087

Laminin Polymerization and Inherited Disease: Lessons From Genetics

*Liam Shaw†, Conor J. Sugden† and Kevin J. Hamill**

Institute of Life Course and Medical Sciences, University of Liverpool, Liverpool, United Kingdom

The laminins (LM) are a family of basement membranes glycoproteins with essential structural roles in supporting epithelia, endothelia, nerves and muscle adhesion, and signaling roles in regulating cell migration, proliferation, stem cell maintenance and differentiation. Laminins are obligate heterotrimers comprised of α, β and γ chains that assemble intracellularly. However, extracellularly these heterotrimers then assemble into higher-order networks *via* interaction between their laminin N-terminal (LN) domains. *In vitro* protein studies have identified assembly kinetics and the structural motifs involved in binding of adjacent LN domains. The physiological importance of these interactions has been identified through the study of pathogenic point mutations in LN domains that lead to syndromic disorders presenting with phenotypes dependent on which laminin gene is mutated. Genotype-phenotype comparison between knockout and LN domain missense mutations of the same laminin allows inferences to be drawn about the roles of laminin network assembly in terms of tissue function. In this review, we will discuss these comparisons in terms of laminin disorders, and the therapeutic options that understanding these processes have allowed. We will also discuss recent findings of non-laminin mediators of laminin network assembly and their implications in terms of basement membrane structure and function.

Keywords: laminin, netrin, Pierson syndrome, MDC1A, basement membrane, junctional epidermolysis bullosa

OPEN ACCESS

Edited by:
Tom Van Agtmael, University of Glasgow, United Kingdom

Reviewed by:
Patricia Rousselle, Centre National de la Recherche Scientifique (CNRS), France
Nicolina Cristina Sorrentino, Telethon Institute of Genetics and Medicine (TIGEM), Italy

****Correspondence:***
Kevin J. Hamill
khamill@liverpool.ac.uk

†These authors have contributed equally to this work and share first authorship

Specialty section:
This article was submitted to Genetics of Common and Rare Diseases, a section of the journal Frontiers in Genetics

Received: *08 May 2021*
Accepted: *13 July 2021*
Published: *12 August 2021*

Citation:
Shaw L, Sugden CJ and Hamill KJ (2021) Laminin Polymerization and Inherited Disease: Lessons From Genetics. Front. Genet. 12:707087. doi: 10.3389/fgene.2021.707087

INTRODUCTION

Basement membranes (BMs) are flexible 40–120 nm sheets that separates cells from underlying connective tissue and regulate important cell behaviors such as cell polarity and migration, metabolism, and in inducing differentiation (Paulsson, 1992). Most BMs consist of two layers; an electron-lucent layer, lamina lucida comprised predominantly of laminins (LMs) and nidogens, and an electron dense layer, lamina densa of type IV collagen (col IV) and perlecan (Paulsson, 1992). BMs assemble through a multistep process, with the LM network assembling first (Kalb and Engel, 1991; Smyth et al., 1998; Li et al., 2002, 2005; McKee et al., 2007, 2009) *via* anchoring of the LMs cell surface receptors (Kalb and Engel, 1991; Smyth et al., 1998; Li et al., 2002, 2005; McKee et al., 2007, 2009). Anchorage increases local LM concentration, allows polymerization and recruitment of other components to the LM scaffold.

THE LAMININS

Laminins are an obligatory feature of every BM. Each LM is an αβγ heterotrimer comprised of one of five α chains (encoded by LAMA1-5), one of four α chains (LAMB1-4) and one of three γ (LAMC1-3) chains (Aumailley et al., 2005; Domogatskaya et al., 2012; Aumailley, 2013). Use of alternative promoters in LAMA3 gives rise to either the short LMα3A or the longer LMα3B form, which are functionally and structurally distinct (Ryan et al., 1994; Ferrigno et al., 1997). Restrictions in heterotrimerization potential means that only 16 αβγchain combinations are possible (Paulsson et al., 1985; Engel et al., 1991; Nissinen et al., 1991; Utani et al., 1994). These are differentially expressed and play context specific roles. For example, α1β1γ1 (LM111) is essential for embryonic development and knockout of any of those genes is not compatible with life, whereas α3Aβ3γ2 (LM332) is highly expressed in mature epithelial tissues and loss of function leads to epidermal fragility.

The LM family has arisen by gene duplication and rearrangement, and common structural motifs are shared between members (**Figure 1A**). Archetypal LM chains consists of a laminin N-terminal domain (LN domain) followed by rod-like stretches of epidermal growth factor-like repeats (LE domains) interspersed with globular domains (L4 or LF domains) and followed by a coiled coil domain (LCC domain) through which αβγ heterotrimers form (Paulsson et al., 1985; Engel et al., 1991; Nissinen et al., 1991; Zimmerman and Blanco, 2007). In α chains, the LCC domain is followed by five LM globular domains (LG1-5), which harbor the highest affinity cell surface receptor sites (Timpl et al., 2000). While this architecture holds true for most LMs, not all chains contain all domains. Importantly, the α3A, α4, and γ2 chains contain shorter amino terminal arms lacking LN domain (Aumailley et al., 2005; Hamill et al., 2009).

LN Domains

Laminin N-terminal domain are 252–264 amino acid globular domains found not only in LMs but also other ECM proteins including netrins. 14% of all residues in LN domains are conserved with strict conservation of six key cysteines. There is 72% homology between LMα1 and LMα2, 77% between LMα3B and LMα5, 72% between LMβ1 and LMβ2, and 64% between LMγ1 and LMγ3 LN domains. Lowest conservation is between LMβ3 and the β1 and β2 LN domains (38 and 42%, respectively) (Garbe et al., 2002).

Laminins interactions have been studied over many years with important early work establishing a "three-arm" model; polymerization only occurs when all the constituent chains contain LN domains (Yurchenco and Cheng, 1994; Hohenester and Yurchenco, 2013). Moreover, interactions must be heterotypic, involving an α, β and γ LN domain (McKee et al., 2007). The assembly process is divided into a temperature-dependent oligomerization step and a calcium-dependent polymerization step. *In vitro* analyses have further shown that the αβγ ternary node assembly involves rapid but unstable formation of βγ pairs that are then stabilized through integration of an αLN domain (Hussain et al., 2011; **Figure 1B**). In line with the three-arm model, LMs that lack one or more LN domain cannot polymerize independently (Hohenester and Yurchenco, 2013). These include LM332 and LM411, which are abundantly expressed in many epithelial and endothelial BMs. For these LMs, alternative methods of interaction with other LM isoforms may be required for BM assembly. For LM332, incorporation into skin BM can be partly explained by an interaction between LM332's β3LN domain with the LE domain of α3 in LM311. These LM dimers could then self-associate into higher order networks (Champliaud et al., 1996; Rousselle and Beck, 2013). Non-network forming LM BM incorporation likely also depends on compensatory interactions with other BM/ECM components, such as the β3LN domain binding of the NC1 domain of type VII collagen, nidogen binding to the γ1 LE repeats (Chen et al., 1997; Rousselle et al., 1997; Rousselle and Beck, 2013).

The crystal structures of α5, β1, γ1 LN domains have been solved, and these combined with conservation of residues between chains allows inferences as to which regions are involved in domain folding and those involved αβγ ternary node formation (**Figure 1C**). The crystals revealed a similar overall structure of an antiparallel β sandwich with 8 β sheets forming a jelly roll motif held in conformation by cysteines C200 and C220 (**Figure 1D**; Hussain et al., 2011; Carafoli et al., 2012). In the α5LN domain, two conserved motifs Patch 1 and Patch 2 are of particular relevance (Hussain et al., 2011). Patch 1 within the conserved β1-β2-β7-β4-β5 "back face," consists of E178, P189, R265, and R267. These residues are blocked by a glycan attached to N148 (Hussain et al., 2011), suggesting that Patch 1 plays a structural, non-polymerizing role (Carafoli et al., 2012). Patch 2 is located across the β6-β3-β8 "front face," residues W132 and N168, and the β5-β6 loop, residues P229, L230, and E231. Patch 2 is not glycosylated nor conserved with β- or γ-chains but is important for polymerization as mutation of PLENGE residues in the β5-β6 loop all result in inhibition of polymerization (Hussain et al., 2011; Carafoli et al., 2012). The β-sandwiches of β1LN and γ1LN domains have similar structure with the main differences in peripheral regions (Carafoli et al., 2012). β1LN contains two particular regions of functional importance: the βa-βb hairpin and the β7-α4 loop. The βa-βb hairpin sits at the top of the domain with S80 a key residue for β-γLN interactions (Purvis and Hohenester, 2012). One notable difference in γ1LN domain is a calcium binding site located within a short α-helix and flanked by highly conserved D106 and T114 (Carafoli et al., 2012). Testing inferences about residue function is a laborious task but elegant *in vitro* analysis using LN domain- fusion proteins have been performed and improve interpretation of clinical findings, discussed in context below (McKee et al., 2018).

Laminin N-terminal domains, in addition to polymerization, are implicated in cell adhesion, neurite outgrowth, perlecan, heparin and heparan sulfate binding (Nielsen and Yamada, 2001; Nomizu et al., 2001; Garbe et al., 2002; Kunneken et al., 2004). The LN domain of LMα1, α2, and α5 can interact with integrins α1β1, α2β1, and α3β1, and presumed between LMα3b and integrin α3β1 based on antibody inhibition (Pfaff et al., 1994; Colognato et al., 1997; Ettner et al., 1998; Kariya et al., 2004; Hozumi et al., 2012). These interactions are lower affinity than

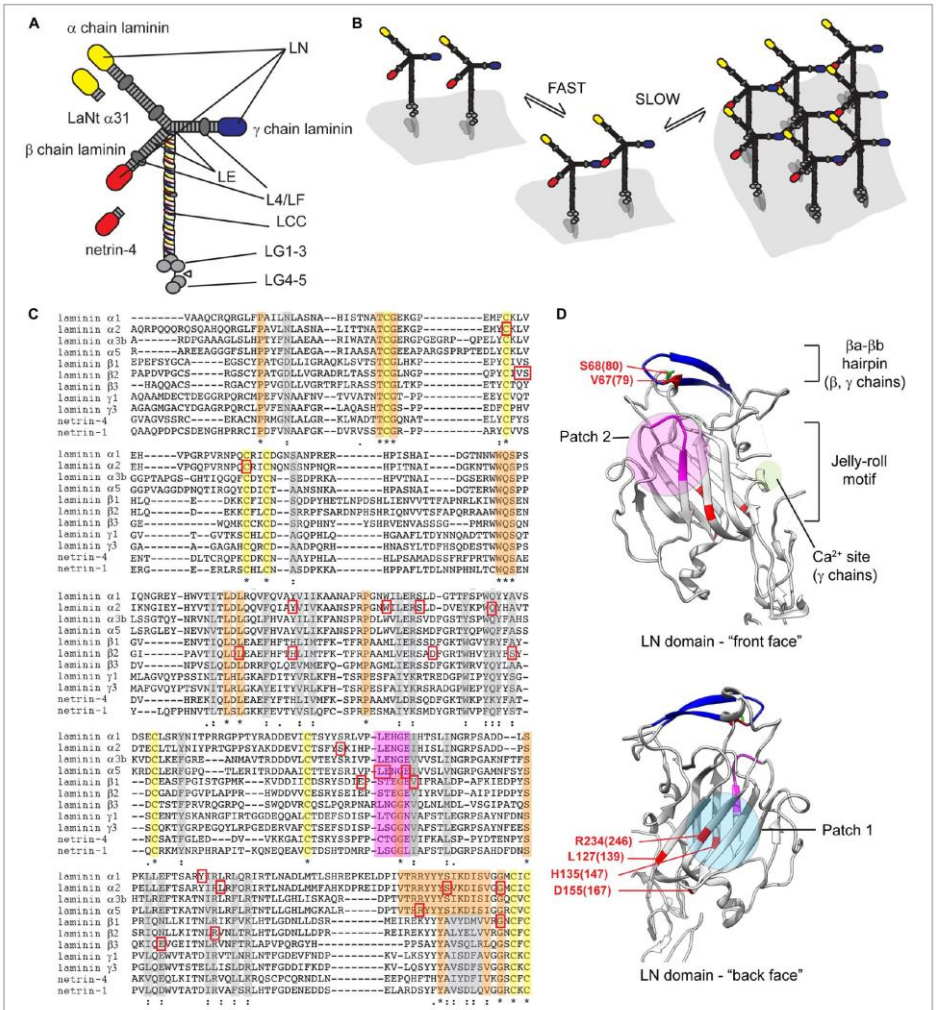

FIGURE 1 | (A) Diagrammatic representation of archetypal LM structure. Yellow ovals αLN domains, red = βLN domains and blue = γLN domains. LE, laminin-type EGF-like repeat; LCC, laminin coiled coil domain; LG, laminin globular domains. **(B)** Two-step laminin network assembly. Secreted LMs associated with cell surface receptors, predominantly *via* their LG domain regions, β – γ LN domain interactions are then facilitated in a reaction with rapid on/off kinetics, then in the propagation step β – γ interactions are stabilized *via* incorporation of an α-chain leading to a stable cell-associated network. **(C)** Sequence alignments of LN domains from human laminin chains, netrin-1 and netrin-4. Yellow, orange, and gray highlights indicated conserved cysteines, fully conserved residues, or partially conserved residues. Magenta highlight identifies LENGE region. Red squares indicate pathogenic missense mutations. **(D)** Crystal structures of LN domains. View of the front and back face of the β1 chain is shown with features of conserved patches involved in LN-interaction (patch 2) and required for domain folding (patch 1). Amino acids associated Pierson syndrome mutations are indicated numbered based on LMβ1 with LMβ2 equivalent in parenthesis. Crystal structures derived from Hussain et al. (2011) and Carafoli et al. (2012) rendered using UCSF chimera (Pettersen et al., 2004). * = conserved residue, : = conservation of residues with strongly similar properties, . = conservation of residues with weakly similar properties.

LG domain interactions and likely are involved in localization to allow polymerization rather than signal propagation.

Laminin LN Domains and Human Genetic Disease

The importance of LN domains to tissue function becomes apparent when the variety of LN domains mutations which lead to human disease are considered. Each affected LM results in a distinct set of syndromic disorders reflecting isoform-specific distribution and functions (**Table 1**).

LAMB2 Mutations (Pierson Syndrome)

Pierson syndrome first described in 1963, is a severe congenital nephrotic syndrome with eye abnormalities (Pierson et al., 1963), caused by mutations in LAMB2 (LMβ2). LMβ2 is highly expressed in the glomerular basement membrane, multiple ocular structures (lens, retina, and cornea), and neuromuscular synapses (Hunter et al., 1989; Noakes et al., 1995; Libby et al., 2000; Bystrom et al., 2006). In addition to the defining features of congenital nephrotic syndrome that rapidly progresses to end-stage renal failure, and microcoria, many patients develop complications of motor delay, speech difficulties, intellectual disability, and seizures (Bowen et al., 1964). Indeed, the spectrum of LAMB2-related phenotypes is vast. The severest forms of the disease are associated with knockout mutations, whereas the majority of missense and indel mutations cluster to the LN domain and result in milder forms of the disease (**Table 1**).

One of the earliest studied LMβ2 LN mutations, R246W, is characterized by severe end-stage renal disease and microcoria (McKee et al., 2018). Similarly, R246Q, resulted in severe glomerular abnormalities and impaired secretion (Chen et al., 2011). Conservation of this arginine led to predictions that mutations impair LM polymerization, and *in vitro* this mutant polymerize substantially less effectively than the wild type protein (Zenker et al., 2004). However, R246W also reduced abundance of LM in BMs, likely due to disturbed protein processing (Matejas et al., 2010). Together these data indicate that this arginine has a role in protein folding. A second highly studied missense mutation, S80R, affects the highly conserved βa-βb and directly prevents LN–LN domain interactions with polymerization disrupted *in vitro* (Matejas et al., 2010; Carafoli et al., 2012; Purvis and Hohenester, 2012). Again, the importance of this region was further highlighted by an adjacent V79del patient (Matejas et al., 2006), presenting with milder symptoms of atypical diffuse mesangial sclerosis, retinal detachment, and myopia.

Other β2LN mutations with variable phenotypes include H147R (Mohney et al., 2011), L139P (Matejas et al., 2010), D167Y (Kagan et al., 2008), and S179F (Choi et al., 2008). Similar to R26Q, H147R caused a partial reduction in polymerization ability *in vitro*. L139P and D167Y mutations are near each other and are predicted to affect LN domain folding, and together suggest this region to be particularly sensitive to changes. L139P interferes with the hydrophobic core, is associated with a particularly severe phenotype. In contrast, the D167, and H147 result in milder phenotypes.

LAMA2 Mutations – (Merosin-Deficient Congenital Muscular Dystrophy Type 1A)

Mutations affecting α LN domains affect the stabilization step of ternary node assembly. The best example is merosin-deficient congenital muscular dystrophy type 1A (MDC1A), caused by mutations to LAMA2 (LMα2) (Helbling-Leclerc et al., 1995). This affects LM211 and LM221, the most abundant LMs in skeletal muscles (Ehrig et al., 1990), peripheral nerves, astrocytes and pericytes in the brain (Voit et al., 1995).

In LMα2 knockout conditions, MDC1A presents with disabilities of the proximal and distal limb muscles, with patients unable to walk more than a few steps unaided (Philpot et al., 1995; Jones et al., 2001). Weakness in facial muscles result in reduced sucking and swallowing capabilities, life-threatening problems can arise from failure of the respiratory muscles (Mendell et al., 2006), and cases with intellectual disability and epilepsy have been reported (Philpot et al., 1995; Muntoni and Voit, 2004; Mendell et al., 2006). In knockout situations, LM411 replaces LM211 in muscle basement membranes (Ringelmann et al., 1999). LMα4 lacks an LN domain and is unable to polymerize, resulting in a weakened BM. LMα4 and LMα2 also differ in their receptor binding interaction repertoire and affinities (Talts et al., 2000), for example, LMα2 binds integrin α7β1 whereas LMα4 cannot, and LMα4 has weaker affinity for α-dystroglycan (Nishiuchi et al., 2006). Comparison between missense mutations and knockout mutations allows differentiation between polymerization and receptor-mediated effects, although these inferences are complicated by not every affected tissue expressing LM411.

Many mutations have been reported throughout LAMA2's 65 exons in MDC1A and are cataloged in LAMA2 gene variant database[1] (Oliveira et al., 2018). Again, the LN domain contains a cluster of missense and in frame deletions (Patton et al., 2008; Oliveira et al., 2018). For example, a point mutation in the highly conserved CxxC motif, C79R, led to a milder form of MDC1A, which affects the myelination of Schwann cells in spinal roots and the stability of the skeletal muscles (Patton et al., 2008). This amyelination was not attributed to a change in abundance or mislocalization, and *in vitro* assays confirmed a dramatic effect on LM polymerization (McKee et al., 2018). Other pathogenic missense variants include Q167P, Y138H, G284R on the surface of α2 LN domain and C86Y, W152G, S157F, S277L, S204F, L243P in the interior (Yurchenco et al., 2018; **Table 1**). The S204F mutation lies at one extreme of the phenotypic spectrum, whereby the patient was misdiagnosed with a peripheral neuropathy, presenting with mild proximal weakness. Muscle biopsy revealed depletion of LMα2 in intramuscular nerve, subtly depleted LMα2 expression in muscle BMs and diffusely upregulated LMα5 expression (Chan et al., 2014). To the other extreme, Q167P maps to near the polymerization face, and consistent with this, causes a 60% drop in *in vitro* polymerization capability. This leads to ambulatory muscular dystrophy (McKee et al., 2018). More severe still, G284R causes proximal weakness, with a loss of functional gait with age accompanied by frequent falls, and epilepsy. The

[1] https://www.lovd.nl/LAMA2

TABLE 1 | Pathogenic LN domain mutations.

Protein	Mutation	Effect	Phenotype	References
LMα1	Y265C	LN interaction	[mouse] Retinal vasculopathy	Edwards et al., 2010
LMα2	C79R	LM poly/fold[C]	[mouse] mild muscular dystrophy	Patton et al., 2008
	C86Y	fold[P]	MDC1A	Oliveira et al., 2018
	Y138H	LM poly[P]	MDC1A	Oliveira et al., 2008
	W152G	fold[P]	Limb-girdle–type dystrophy	Gavassini et al., 2011
	S157F	fold[P]	MDC1A	Geranmayeh et al., 2010
	Q167P	LM poly[C]	Limb-girdle–type dystrophy	Di Blasi et al., 2005
	S204F	fold[P]	Mild muscular dystrophy, mild proximal weakness	Chan et al., 2014
	L243P	fold[P]	Mild MDC1A	Gavassini et al., 2011
	S277L	fold[P]	MDC1A	Beytia Mde et al., 2014
	G284R	LM poly[P]	limb-girdle–type dystrophy	Gavassini et al., 2011
LMα5	R286L	LM poly[C]	Focal segmental glomerulosclerosis, hearing loss, craniofacial dysmorphism, limb development	Jones et al., 2020
LMβ1	E215K	LM poly[C]	[fly] heart development defects	Hollfelder et al., 2014
	V226E		[fly] heart development defects	Hollfelder et al., 2014
	G286R		[fly] heart development defects	Hollfelder et al., 2014
LMβ2	R246W R246Q	LM Secretion/Fold	End-stage renal disease, nephrotic proteinuria, diffuse mesangial sclerosis, focal and segmental glomerulosclerosis, microcoria, lens abnormalities, nystagmus hypotonia, cognitive defects, muscle delay	Zenker et al., 2004; Hasselbacher et al., 2006; Bredrup et al., 2008; Matejas et al., 2010
	V79del	LM poly[P]	Retinal detachment, cataracts, progressive vision loss, diffuse mesangial sclerosis, end-stage renal disease	Matejas et al., 2006
	S80R	LM poly[C]	Nephrotic proteinuria, atypical diffuse mesangial sclerosis, myopia, retinal detachment. [mouse S83R] Detrimental on Alport syndrome background	Matejas et al., 2010; Funk et al., 2018
	H147R	LM fold[P]	Nephrotic proteinuria, diffuse mesangial sclerosis, proliferative glomerulonephritis, hypertension, heart failure, microcoria, retinal detachment, lens abnormalities	Mohney et al., 2011
	D167Y	LM Secretion[P]	End-stage renal disease, myopia, retinal detachment, severe visual impairment	Kagan et al., 2008
	L139P	LM fold[P]	Diffuse mesangial sclerosis, lens abnormalities, severe visual impairment, hypotonia, muscle delay, cognitive deficits	Matejas et al., 2010
	S179F	LM fold[P]	End-stage renal disease, focal and segmented glomerulosclerosis, retinal detachment, severe visual impairments	Choi et al., 2008
LMβ3	E210K	Splicing[C] + fold[P]	Skin fragility, nail dystrophy, alopecia	Mellerio et al., 1998

[P]predicted [C]confirmed in vitro assays.

mutation effect is yet to be confirmed but predicted to inhibit LM polymerization (Gavassini et al., 2011).

LAMA5 Mutations (Kidney, Craniofacial, and Limb Development Syndrome)

LMα5 is almost ubiquitous to all adult BMs. Unsurprisingly, knockout mice die before birth with a failure in neural tube closure, and no human knockouts have been reported (Miner et al., 1998). However, a patient with R286L in LMα5 LN has been identified. They presented with a complex syndromic disease characterized by defects in kidney, craniofacial and limb development (Jones et al., 2020). The affected residue lies adjacent to the conserved PLENGE sequence required for LM polymerization (Hussain et al., 2011), and R286L abrogated *in vitro* polymerization potential (Jones et al., 2020). We cannot compare the LN mutation against knockout; however, a patient with V3140M, in the LG3 domain has been reported (Sampaolo et al., 2017). Both the LG3 mutation and R286L lead to complex syndromic disorders with similarity in tissues affected but with notable differences. Specifically, in the skin V3140M caused alopecia, lack of eyebrows and body hair, features not present in the R286L patient. V3140M patients also had retinal rod degeneration whereas the R286L had hearing loss but no sight abnormalities. Kidney defects were common to both with R286L presenting with atypical focal segmental glomerulosclerosis progressing to end stage kidney disease compared with floating kidney syndrome in V3140M. Finally, R286L presented with numerous dysmorphic issues include craniofacial dysmorphism, syndactyly, and pyloric web.

LAMB3 Mutation (Junctional Epidermolysis Bullosa)

LMβ3 is expressed in most epithelial tissues where it forms part of LM3a32 and LM3b32 (Matsui et al., 1995; Ferrigno et al., 1997). The resulting heterotrimers have either one or two LN domains and are unable to polymerize independently (Yurchenco and Cheng, 1994; Cheng et al., 1997). One would assume that LN domain mutations are tolerated for this LM chain. However, patients were identified where the pathogenic mutation caused E210K, which gives rise to a phenotype of trauma-induced blisters, nail dystrophy and alopecia (mild junctional

epidermolysis bullosa) (McGrath et al., 1995; Mellerio et al., 1998; Posteraro et al., 2004). In comparison, homozygous knockout of LMβ3 leads to much more extensive skin blistering complications and early lethality (Pulkkinen et al., 1994; Kuster et al., 1997; Ryan et al., 1999; Meng et al., 2003).

Interpretation of the E210K mutation is complicated; the affected base pair is at a splice junction and in a knock-in mouse model led to skipping of the out-of-frame, and no detectable LMβ3 in the skin. However, in humans, miss-splicing has been reported for some, but not all patients, which can be rescued by second-site mutations (Pasmooij et al., 2007). Numerous alternative splice products are produced, including some full-length transcripts. Modeling of the E210K mutation indicates it is unlikely to be required for laminin polymerization but also is not predicted to affect protein folding or secretion (Mittwollen et al., 2020). The most common in-frame deletion is predicted to remove several of the central β-strands and disrupt the fold. Overall, the evidence from these patients does not point toward a LM polymerization effect but does suggest a role for the LMβ3 LN domain in protein function. Direct evidence for the importance of the LMβ3 LN domain has been obtained from keratinocytes expressing either full-length or LN domain-deleted LMβ3 and grafted as skin equivalents onto immunodeficient mice (Sakai et al., 2010). Here, the LN deleted versions displayed subepidermal blistering, erosions, and prominent granulation tissue, not associated with reduced LM332 deposition pointing LN domain roles beyond polymerization.

Non-human LN Domain Mutations

LMα1 is extremely important for developmental processes, with knockout mice embryonic lethal. However, Y256C mice are viable with retinal defects of vitreal fibroplasia, vascular tortuosity and hypervascularization, and abnormalities to the retinal inner limiting membrane (Edwards et al., 2010). No reduction in LMα1 was noted, and a two-hybrid screen identified the mutation affects LN–LN interaction. Random mutagenesis in Drosophila has identified three LN domain mutations in LMβ1 that led to heart developmental defects, E215K, V226E, and G286R (Hollfelder et al., 2014). Of these, E215K was tested in *in vitro* assays and reduced polymerization (McKee et al., 2018).

LM Network Regulators: Netrin-4 and LaNt α31

The netrins family of proteins are structurally and ancestrally related to LMs (Tessier-Lavigne and Goodman, 1996; Fahey and Degnan, 2012). Each netrin comprises a LN domain and stretch of LE repeats followed by a unique C-terminal region (Kappler et al., 2000; Yurchenco and Wadsworth, 2004). The LN domains of most netrins have diverged that they do not influence LM network assembly. However, for netrin-4 the situation is dramatically different where the β-type LN domain of netrin-4 can potently disrupt LM networks (Schneiders et al., 2007; Reuten et al., 2016, 2021). The physiological implications of this ability are beginning to be appreciated; recent work has demonstrated that netrin-4 levels are a key determinant of basement membrane stiffness with knock-on effects to cell behavior and tumor metastasis (Reuten et al., 2016, 2021).

Whereas netrins have evolved as independent genes, alternative splicing from LM genes or proteolytic processing of LM proteins leads to generation of LN domain containing fragments (Kariya et al., 2004; Hamill et al., 2009; Horejs et al., 2014). These fragments contain "perfect" LN domains that are likely to compete for binding sites (with reduced potency compared with netrin-4). One LAMA3-derived alternative splice isoform, Laminin N terminus α31 (LaNt α31) has widespread expression in human tissues (Troughton et al., 2020b), is upregulated during wounding and corneal limbal stem cell activation (Barrera et al., 2018) and emerging data indicate that it can modulate LM organization *in vitro* (Troughton et al., 2020a). *In vivo* overexpression is embryonic lethal during development with tissue defects that resemble LM network disruption phenotypes (Sugden et al., 2020).

From an evolutionary perspective, netrin-4, LaNt α31 and proteolytically released LN fragments represent multiple mechanisms to fine-tune LM network assembly. Although human diseases directly associated with loss-of-function mutations have not been identified, a SNP in the netrin-4 gene (causing Y205H) has been associated with late onset Alzheimer's disease (Saad et al., 2015), and dysregulation of expression appear to contribute to tumor pathogenesis and point toward an additional important aspect of BM biology (Schneiders et al., 2007; Reuten et al., 2016, 2021; Troughton et al., 2020c).

Rescuing LN Domain Defects

Although the standard gene and protein therapy toolbox are available to treat LN domain disorders, the large size of LM genes and associated challenges of producing and delivering recombinant therapy-grade LM protein presents challenges. However, promising results have been obtained recently from delivering the 800 kDa LM521 to the blood stream of LAMB2-null mice which rescues some aspects of Pierson syndrome. The delivered LM521 accumulated in the glomerular basement membrane in the correct orientation and led to reduced expression of the podocyte injury markers, and delayed the onset of proteinuria. However, the exogenous LM521 did not migrate to the podocytes nor fully restore the glomerular filtration barrier. Smaller, or hybrid proteins, may be a solution to overcome these challenges (Lin et al., 2018). For some LM disorders, upregulating expression of a compensatory LM may be a viable option. While there are differences, LMα1 and LMα2 are very similar both structurally and functionally, therefore in LMα2-deficient MDC1A, increasing LMα1 could compensate for the lack of functional LMα2. LMα1 expression is usually downregulated following development; however, encouraging progress has been made here using guide RNA to target the LMα1 promoter with inactive Cas9 coupled to VP160 transcription activation domain. In mouse models, electroporation of the gRNA-containing plasmids into the tibialis anterior of 4-week old animals led to increased expression of LM111 with appropriate localization 2-weeks post-electroporation (Perrin et al., 2017). This data provides an encouraging base for development that may be exploitable for other conditions using a similar approach.

A particularly innovative solution exploiting the knowledge gained from studying LM polymerization and counteracting the inherent LM size problems is using protein chimeras to act as linkers (McKee et al., 2009, 2017; Reinhard et al., 2017). Three such "Frankenstein" chimeric proteins have been created, a fusion of a functional LN domain to the LM binding region of nidogen, a miniature form of agrin (mini-agrin) containing only the LM-binding regions and α-dystroglycan binding regions, and a fusion between LM-binding domains of agrin and the dystroglycan binding domain of perlecan. As LM411 is upregulated in MDC1A but cannot compensate for LM211 dysfunction, the nidogen/LN domain chimeric protein can be used to bind the γ1 chain of LM411 *via* the nidogen region and provide the missing αLN domain needed to allow LM411 polymerization (Reinhard et al., 2017). The mini-agrin/perlecan chimeras can be used in concert with the nidogen chimera to compensate for α-dystroglycan binding (Talts et al., 2000; Moll et al., 2001). Where patients harbor LN mutations, only the nidogen fusion would be required, whereas for knockout both the LN/nidogen and mini-agrin would be necessary. Promising results have been observed with these chimeras in mouse models. Moreover, switching the LN domain from an αLN to βLN, this approach is likely to also be effective for Pierson syndrome patients.

DISCUSSION AND PERSPECTIVES

Comparison between knockout and missense mutation associated phenotypes in LM genes has provided valuable information to identify which LMs are essential for individual tissues, but also which domains are involved. Rather than a binary outcome caused by ability or inability to polymerize, we see system-wide differences highlighting the multifaceted roles of LN domains. The variety of pathologies arising from mutations within a stretch of ∼250 amino acids illustrate the importance of LN domains to tissue function.

AUTHOR CONTRIBUTIONS

LS, CS, and KH wrote and edited the manuscript. All authors read and approved the final version of the manuscript for publication.

FUNDING

This work was supported by the Biotechnology and Biological Sciences Research Council (Grant No. BB/P025773/1) and The University of Liverpool Crossley Barnes Bequest fund.

REFERENCES

Aumailley, M. (2013). The laminin family. *Cell Adh. Migr.* 7, 48–55. doi: 10.4161/cam.22826

Aumailley, M., Bruckner-Tuderman, L., Carter, W. G., Deutzmann, R., Edgar, D., Ekblom, P., et al. (2005). A simplified laminin nomenclature. *Matrix Biol.* 24, 326–332. doi: 10.1016/j.matbio.2005.05.006

Barrera, V., Troughton, L. D., Iorio, V., Liu, S., Oyewole, O., Sheridan, C. M., et al. (2018). Differential distribution of Laminin N-Terminus alpha31 across the ocular surface: implications for corneal wound repair. *Invest. Ophthalmol. Vis. Sci.* 59, 4082–4093. doi: 10.1167/iovs.18-24037

Beytia Mde, L., Dekomien, G., Hoffjan, S., Haug, V., Anastasopoulos, C., and Kirschner, J. (2014). High creatine kinase levels and white matter changes: clinical and genetic spectrum of congenital muscular dystrophies with laminin alpha-2 deficiency. *Mol. Cell Probes* 28, 118–122. doi: 10.1016/j.mcp.2013.11.002

Bowen, P., Lee, C. S., Zellweger, H., and Lindenberg, R. (1964). A familial syndrome of multiple congenital defects. *Bull. Johns Hopkins Hosp.* 114, 402–414.

Bredrup, C., Matejas, V., Barrow, M., Blahova, K., Bockenhauer, D., Fowler, D. J., et al. (2008). Ophthalmological aspects of Pierson syndrome. *Am. J. Ophthalmol.* 146, 602–611.

Bystrom, B., Virtanen, I., Rousselle, P., Gullberg, D., and Pedrosa-Domellof, F. (2006). Distribution of laminins in the developing human eye. *Invest. Ophthalmol. Vis. Sci.* 47, 777–785. doi: 10.1167/iovs.05-0367

Carafoli, F., Hussain, S. A., and Hohenester, E. (2012). Crystal structures of the network-forming short-arm tips of the laminin beta1 and gamma1 chains. *PLoS One* 7:e42473. doi: 10.1371/journal.pone.0042473

Champliaud, M. F., Lunstrum, G. P., Rousselle, P., Nishiyama, T., Keene, D. R., and Burgeson, R. E. (1996). Human amnion contains a novel laminin variant, laminin 7, which like laminin 6, covalently associates with laminin 5 to promote stable epithelial-stromal attachment. *J. Cell Biol.* 132, 1189–1198. doi: 10.1083/jcb.132.6.1189

Chan, S. H., Foley, A. R., Phadke, R., Mathew, A. A., Pitt, M., Sewry, C., et al. (2014). Limb girdle muscular dystrophy due to LAMA2 mutations: diagnostic difficulties due to associated peripheral neuropathy. *Neuromuscul. Disord.* 24, 677–683. doi: 10.1016/j.nmd.2014.05.008

Chen, M., Marinkovich, M. P., Veis, A., Cai, X., Rao, C. N., O'Toole, E. A., et al. (1997). Interactions of the amino-terminal noncollagenous (NC1) domain of type VII collagen with extracellular matrix components. A potential role in epidermal-dermal adherence in human skin. *J. Biol. Chem.* 272, 14516–14522. doi: 10.1074/jbc.272.23.14516

Chen, Y. M., Kikkawa, Y., and Miner, J. H. (2011). A missense LAMB2 mutation causes congenital nephrotic syndrome by impairing laminin secretion. *J. Am. Soc. Nephrol.* 22, 849–858. doi: 10.1681/asn.2010060632

Cheng, Y. S., Champliaud, M. F., Burgeson, R. E., Marinkovich, M. P., and Yurchenco, P. D. (1997). Self-assembly of laminin isoforms. *J. Biol. Chem.* 272, 31525–31532. doi: 10.1074/jbc.272.50.31525

Choi, H. J., Lee, B. H., Kang, J. H., Jeong, H. J., Moon, K. C., Ha, I. S., et al. (2008). Variable phenotype of Pierson syndrome. *Pediatr. Nephrol.* 23, 995–1000. doi: 10.1007/s00467-008-0748-7

Colognato, H., MacCarrick, M., O'Rear, J. J., and Yurchenco, P. D. (1997). The laminin alpha2-chain short arm mediates cell adhesion through both the alpha1beta1 and alpha2beta1 integrins. *J. Biol. Chem.* 272, 29330–29336. doi: 10.1074/jbc.272.46.29330

Di Blasi, C., Piga, D., Brioschi, P., Moroni, I., Pini, A., Ruggieri, A., et al. (2005). LAMA2 gene analysis in congenital muscular dystrophy: new mutations, prenatal diagnosis, and founder effect. *Arch. Neurol.* 62, 1582–1586.

Domogatskaya, A., Rodin, S., and Tryggvason, K. (2012). Functional diversity of laminins. *Annu. Rev. Cell Dev. Biol.* 28, 523–553. doi: 10.1146/annurev-cellbio-101011-155750

Edwards, M. M., Mammadova-Bach, E., Alpy, F., Klein, A., Hicks, W. L., Roux, M., et al. (2010). Mutations in Lama1 disrupt retinal vascular development and inner limiting membrane formation. *J. Biol. Chem.* 285, 7697–7711. doi: 10.1074/jbc.m109.069575

Ehrig, K., Leivo, I., Argraves, W. S., Ruoslahti, E., and Engvall, E. (1990). Merosin, a tissue-specific basement membrane protein, is a laminin-like protein. *Proc. Natl. Acad. Sci. U.S.A.* 87, 3264–3268. doi: 10.1073/pnas.87.9.3264

Engel, J., Hunter, I., Schulthess, T., Beck, K., Dixon, T. W., and Parry, D. A. (1991). Assembly of laminin isoforms by triple- and double-stranded coiled-coil structures. *Biochem. Soc. Trans.* 19, 839–843. doi: 10.1042/bst0190839

Ettner, N., Gohring, W., Sasaki, T., Mann, K., and Timpl, R. (1998). The N-terminal globular domain of the laminin alpha1 chain binds to

alpha1beta1 and alpha2beta1 integrins and to the heparan sulfate-containing domains of perlecan. *FEBS Lett.* 430, 217–221. doi: 10.1016/s0014-5793(98)00601-2

Fahey, B., and Degnan, B. M. (2012). Origin and evolution of laminin gene family diversity. *Mol. Bio.l Evol.* 29, 1823–1836. doi: 10.1093/molbev/mss060

Ferrigno, O., Virolle, T., Galliano, M. F., Chauvin, N., Ortonne, J. P., Meneguzzi, G., et al. (1997). Murine laminin alpha3A and alpha3B isoform chains are generated by usage of two promoters and alternative splicing. *J. Biol. Chem.* 272, 20502–20507. doi: 10.1074/jbc.272.33.20502

Funk, S. D., Bayer, R. H., Malone, A. F., McKee, K. K., Yurchenco, P. D., and Miner, J. H. (2018). Pathogenicity of a human laminin beta2 mutation revealed in models of alport syndrome. *J. Am. Soc. Nephrol.* 29, 949–960. doi: 10.1681/asn.2017090997

Garbe, J. H., Gohring, W., Mann, K., Timpl, R., and Sasaki, T. (2002). Complete sequence, recombinant analysis and binding to laminins and sulphated ligands of the N-terminal domains of laminin alpha3B and alpha5 chains. *Biochem. J.* 362(Pt 1), 213–221. doi: 10.1042/bj3620213

Gavassini, B. F., Carboni, N., Nielsen, J. E., Danielsen, E. R., Thomsen, C., Svenstrup, K., et al. (2011). Clinical and molecular characterization of limb-girdle muscular dystrophy due to LAMA2 mutations. *Muscle Nerve* 44, 703–709. doi: 10.1002/mus.22132

Geranmayeh, F., Clement, E., Feng, L. H., Sewry, C., Pagan, J., Mein, R., et al. (2010). Genotype-phenotype correlation in a large population of muscular dystrophy patients with LAMA2 mutations. *Neuromuscul. Disord.* 20, 241–250. doi: 10.1016/j.nmd.2010.02.001

Hamill, K. J., Langbein, L., Jones, J. C., and McLean, W. H. (2009). Identification of a novel family of laminin N-terminal alternate splice isoforms: structural and functional characterization. *J. Biol. Chem.* 284, 35588–35596. doi: 10.1074/jbc.m109.052811

Hasselbacher, K., Wiggins, R. C., Matejas, V., Hinkes, B. G., Mucha, B., Hoskins, B. E., et al. (2006). Recessive missense mutations in LAMB2 expand the clinical spectrum of LAMB2-associated disorders. *Kidney Int.* 70, 1008–1012. doi: 10.1038/sj.ki.5001679

Helbling-Leclerc, A., Zhang, X., Topaloglu, H., Cruaud, C., Tesson, F., Weissenbach, J., et al. (1995). Mutations in the laminin alpha 2-chain gene (LAMA2) cause merosin-deficient congenital muscular dystrophy. *Nat. Genet.* 11, 216–218. doi: 10.1038/ng1095-216

Hohenester, E., and Yurchenco, P. D. (2013). Laminins in basement membrane assembly. *Cell Adh. Migr.* 7, 56–63. doi: 10.4161/cam.21831

Hollfelder, D., Frasch, M., and Reim, I. (2014). Distinct functions of the laminin beta LN domain and collagen IV during cardiac extracellular matrix formation and stabilization of alary muscle attachments revealed by EMS mutagenesis in *Drosophila*. *BMC Dev. Biol.* 14:26. doi: 10.1186/1471-213X-14-26

Horejs, C. M., Serio, A., Purvis, A., Gormley, A. J., Bertazzo, S., Poliniewicz, A., et al. (2014). Biologically-active laminin-111 fragment that modulates the epithelial-to-mesenchymal transition in embryonic stem cells. *Proc. Natl. Acad. Sci. U.S.A.* 111, 5908–5913. doi: 10.1073/pnas.1403139111

Hozumi, K., Ishikawa, M., Hayashi, T., Yamada, Y., Katagiri, F., Kikkawa, Y., et al. (2012). Identification of cell adhesive sequences in the N-terminal region of the laminin alpha2 chain. *J. Biol. Chem.* 287, 25111–25122. doi: 10.1074/jbc.m112.348151

Hunter, D. D., Shah, V., Merlie, J. P., and Sanes, J. R. (1989). A laminin-like adhesive protein concentrated in the synaptic cleft of the neuromuscular junction. *Nature* 338, 229–234. doi: 10.1038/338229a0

Hussain, S. A., Carafoli, F., and Hohenester, E. (2011). Determinants of laminin polymerization revealed by the structure of the alpha5 chain amino-terminal region. *EMBO Rep.* 12, 276–282. doi: 10.1038/embor.2011.3

Jones, K. J., Morgan, G., Johnston, H., Tobias, V., Ouvrier, R. A., Wilkinson, I., et al. (2001). The expanding phenotype of laminin alpha2 chain (merosin) abnormalities: case series and review. *J. Med. Genet.* 38, 649–657. doi: 10.1136/jmg.38.10.649

Jones, L. K., Lam, R., McKee, K. K., Aleksandrova, M., Dowling, J., Alexander, S. I., et al. (2020). A mutation affecting laminin alpha 5 polymerisation gives rise to a syndromic developmental disorder. *Development* 147:dev189183.

Kagan, M., Cohen, A. H., Matejas, V., Vlangos, C., and Zenker, M. (2008). A milder variant of Pierson syndrome. *Pediatr. Nephrol.* 23, 323–327. doi: 10.1007/s00467-007-0624-x

Kalb, E., and Engel, J. (1991). Binding and calcium-induced aggregation of laminin onto lipid bilayers. *J. Biol. Chem.* 266, 19047–19052. doi: 10.1016/s0021-9258(18)55170-x

Kappler, J., Franken, S., Junghans, U., Hoffmann, R., Linke, T., Muller, H. W., et al. (2000). Glycosaminoglycan-binding properties and secondary structure of the C-terminus of netrin-1. *Biochem. Biophys. Res. Commun.* 271, 287–291. doi: 10.1006/bbrc.2000.2583

Kariya, Y., Yasuda, C., Nakashima, Y., Ishida, K., Tsubota, Y., and Miyazaki, K. (2004). Characterization of laminin 5B and NH2-terminal proteolytic fragment of its alpha3B chain: promotion of cellular adhesion, migration, and proliferation. *J. Biol. Chem.* 279, 24774–24784. doi: 10.1074/jbc.m400670200

Kunneken, K., Pohlentz, G., Schmidt-Hederich, A., Odenthal, U., Smyth, N., Peter-Katalinic, J., et al. (2004). Recombinant human laminin-5 domains. Effects of heterotrimerization, proteolytic processing, and N-glycosylation on alpha3beta1 integrin binding. *J. Biol. Chem.* 279, 5184–5193.

Kuster, J. E., Guarnieri, M. H., Ault, J. G., Flaherty, L., and Swiatek, P. J. (1997). IAP insertion in the murine LamB3 gene results in junctional epidermolysis bullosa. *Mamm. Genome* 8, 673–681. doi: 10.1007/s003359900535

Li, S., Harrison, D., Carbonetto, S., Fassler, R., Smyth, N., Edgar, D., et al. (2002). Matrix assembly, regulation, and survival functions of laminin and its receptors in embryonic stem cell differentiation. *J. Cell Biol.* 157, 1279–1290. doi: 10.1083/jcb.200203073

Li, S., Liquari, P., McKee, K. K., Harrison, D., Patel, R., Lee, S., et al. (2005). Laminin-sulfatide binding initiates basement membrane assembly and enables receptor signaling in Schwann cells and fibroblasts. *J. Cell Biol.* 169, 179–189. doi: 10.1083/jcb.200501098

Libby, R. T., Champliaud, M. F., Claudepierre, T., Xu, Y., Gibbons, E. P., Koch, M., et al. (2000). Laminin expression in adult and developing retinae: evidence of two novel CNS laminins. *J. Neurosci.* 20, 6517–6528. doi: 10.1523/jneurosci.20-17-06517.2000

Lin, M. H., Miller, J. B., Kikkawa, Y., Suleiman, H. Y., Tryggvason, K., Hodges, B. L., et al. (2018). Laminin-521 protein therapy for glomerular basement membrane and podocyte abnormalities in a model of pierson syndrome. *J. Am. Soc. Nephrol.* 29, 1426–1436. doi: 10.1681/asn.2017060690

Matejas, V., Al-Gazali, L., Amirlak, I., and Zenker, M. (2006). A syndrome comprising childhood-onset glomerular kidney disease and ocular abnormalities with progressive loss of vision is caused by mutated LAMB2. *Nephrol. Dial. Transplant* 21, 3283–3286. doi: 10.1093/ndt/gfl463

Matejas, V., Hinkes, B., Alkandari, F., Al-Gazali, L., Annexstad, E., Aytac, M. B., et al. (2010). Mutations in the human laminin beta2 (LAMB2) gene and the associated phenotypic spectrum. *Hum. Mutat.* 31, 992–1002. doi: 10.1002/humu.21304

Matsui, C., Wang, C. K., Nelson, C. F., Bauer, E. A., and Hoeffler, W. K. (1995). The assembly of laminin-5 subunits. *J. Biol. Chem.* 270, 23496–23503. doi: 10.1074/jbc.270.40.23496

McGrath, J. A., Pulkkinen, L., Christiano, A. M., Leigh, I. M., Eady, R. A., and Uitto, J. (1995). Altered laminin 5 expression due to mutations in the gene encoding the beta 3 chain (LAMB3) in generalized atrophic benign epidermolysis bullosa. *J. Invest. Dermatol.* 104, 467–474. doi: 10.1111/1523-1747.ep12605904

McKee, K. K., Aleksandrova, M., and Yurchenco, P. D. (2018). Chimeric protein identification of dystrophic, Pierson and other laminin polymerization residues. *Matrix Biol.* 67, 32–46. doi: 10.1016/j.matbio.2018.01.012

McKee, K. K., Capizzi, S., and Yurchenco, P. D. (2009). Scaffold-forming and adhesive contributions of synthetic laminin-binding proteins to basement membrane assembly. *J. Biol. Chem.* 284, 8984–8994. doi: 10.1074/jbc.m809719200

McKee, K. K., Crosson, S. C., Meinen, S., Reinhard, J. R., Ruegg, M. A., and Yurchenco, P. D. (2017). Chimeric protein repair of laminin polymerization ameliorates muscular dystrophy phenotype. *J. Clin. Invest.* 127, 1075–1089. doi: 10.1172/jci90854

McKee, K. K., Harrison, D., Capizzi, S., and Yurchenco, P. D. (2007). Role of laminin terminal globular domains in basement membrane assembly. *J. Biol. Chem.* 282, 21437–21447. doi: 10.1074/jbc.m702963200

Mellerio, J. E., Eady, R. A., Atherton, D. J., Lake, B. D., and McGrath, J. A. (1998). E210K mutation in the gene encoding the beta3 chain of laminin-5 (LAMB3) is predictive of a phenotype of generalized atrophic benign epidermolysis bullosa. *Br. J. Dermatol.* 139, 325–331. doi: 10.1046/j.1365-2133.1998.02377.x

Mendell, J. R., Boue, D. R., and Martin, P. T. (2006). The congenital muscular dystrophies: recent advances and molecular insights. *Pediatr. Dev. Pathol.* 9, 427–443. doi: 10.2350/06-07-0127.1

Meng, X., Klement, J. F., Leperi, D. A., Birk, D. E., Sasaki, T., Timpl, R., et al. (2003). Targeted inactivation of murine laminin gamma2-chain gene recapitulates human junctional epidermolysis bullosa. *J. Invest. Dermatol.* 121, 720–731. doi: 10.1046/j.1523-1747.2003.12515.x

Miner, J. H., Cunningham, J., and Sanes, J. R. (1998). Roles for laminin in embryogenesis: exencephaly, syndactyly, and placentopathy in mice lacking the laminin alpha5 chain. *J. Cell Biol.* 143, 1713–1723. doi: 10.1083/jcb.143.6.1713

Mittwollen, R., Wohlfart, S., Park, J., Grosch, E., Has, C., Hohenester, E., et al. (2020). Aberrant splicing as potential modifier of the phenotype of junctional epidermolysis bullosa. *J. Eur. Acad. Dermatol Venereol.* 34, 2127–2134. doi: 10.1111/jdv.16332

Mohney, B. G., Pulido, J. S., Lindor, N. M., Hogan, M. C., Consugar, M. B., Peters, J., et al. (2011). A novel mutation of LAMB2 in a multigenerational mennonite family reveals a new phenotypic variant of Pierson syndrome. *Ophthalmology* 118, 1137–1144. doi: 10.1016/j.ophtha.2010.10.009

Moll, J., Barzaghi, P., Lin, S., Bezakova, G., Lochmuller, H., Engvall, E., et al. (2001). An agrin minigene rescues dystrophic symptoms in a mouse model for congenital muscular dystrophy. *Nature* 413, 302–307. doi: 10.1038/35095054

Muntoni, F., and Voit, T. (2004). The congenital muscular dystrophies in 2004: a century of exciting progress. *Neuromuscul. Disord.* 14, 635–649. doi: 10.1016/j.nmd.2004.06.009

Nielsen, P. K., and Yamada, Y. (2001). Identification of cell-binding sites on the Laminin alpha 5 N-terminal domain by site-directed mutagenesis. *J. Biol. Chem.* 276, 10906–10912. doi: 10.1074/jbc.m008743200

Nishiuchi, R., Takagi, J., Hayashi, M., Ido, H., Yagi, Y., Sanzen, N., et al. (2006). Ligand-binding specificities of laminin-binding integrins: a comprehensive survey of laminin-integrin interactions using recombinant alpha3beta1, alpha6beta1, alpha7beta1 and alpha6beta4 integrins. *Matrix Biol.* 25, 189–197. doi: 10.1016/j.matbio.2005.12.001

Nissinen, M., Vuolteenaho, R., Boot-Handford, R., Kallunki, P., and Tryggvason, K. (1991). Primary structure of the human laminin A chain. Limited expression in human tissues. *Biochem. J.* 276(Pt 2), 369–379. doi: 10.1042/bj2760369

Noakes, P. G., Gautam, M., Mudd, J., Sanes, J. R., and Merlie, J. P. (1995). Aberrant differentiation of neuromuscular junctions in mice lacking s-laminin/laminin beta 2. *Nature* 374, 258–262. doi: 10.1038/374258a0

Nomizu, M., Yokoyama, F., Suzuki, N., Okazaki, I., Nishi, N., Ponce, M. L., et al. (2001). Identification of homologous biologically active sites on the N-terminal domain of laminin alpha chains. *Biochemistry* 40, 15310–15317. doi: 10.1021/bi011552c

Oliveira, J., Gruber, A., Cardoso, M., Taipa, R., Fineza, I., Goncalves, A., et al. (2018). LAMA2 gene mutation update: toward a more comprehensive picture of the laminin-alpha2 variome and its related phenotypes. *Hum. Mutat.* 39, 1314–1337. doi: 10.1002/humu.23599

Oliveira, J., Santos, R., Soares-Silva, I., Jorge, P., Vieira, E., Oliveira, M. E., et al. (2008). LAMA2 gene analysis in a cohort of 26 congenital muscular dystrophy patients. *Clin. Genet.* 74, 502–512. doi: 10.1111/j.1399-0004.2008.01068.x

Pasmooij, A. M., Pas, H. H., Bolling, M. C., and Jonkman, M. F. (2007). Revertant mosaicism in junctional epidermolysis bullosa due to multiple correcting second-site mutations in LAMB3. *J. Clin. Invest.* 117, 1240–1248. doi: 10.1172/jci30465

Patton, B. L., Wang, B., Tarumi, Y. S., Seburn, K. L., and Burgess, R. W. (2008). A single point mutation in the LN domain of LAMA2 causes muscular dystrophy and peripheral amyelination. *J. Cell Sci.* 121(Pt 10), 1593–1604. doi: 10.1242/jcs.015354

Paulsson, M. (1992). Basement membrane proteins: structure, assembly, and cellular interactions. *Crit. Rev. Biochem. Mol. Biol.* 27, 93–127.

Paulsson, M., Deutzmann, R., Timpl, R., Dalzoppo, D., Odermatt, E., and Engel, J. (1985). Evidence for coiled-coil alpha-helical regions in the long arm of laminin. *EMBO J.* 4, 309–316. doi: 10.1002/j.1460-2075.1985.tb03630.x

Perrin, A., Rousseau, J., and Tremblay, J. P. (2017). Increased Expression of Laminin Subunit Alpha 1 Chain by dCas9-VP160. *Mol. Ther. Nucleic Acids* 6, 68–79. doi: 10.1016/j.omtn.2016.11.004

Pettersen, E. F., Goddard, T. D., Huang, C. C., Couch, G. S., Greenblatt, D. M., Meng, E. C., et al. (2004). UCSF Chimera–a visualization system for exploratory research and analysis. *J. Comput. Chem.* 25, 1605–1612. doi: 10.1002/jcc.20084

Pfaff, M., Gohring, W., Brown, J. C., and Timpl, R. (1994). Binding of purified collagen receptors (alpha 1 beta 1, alpha 2 beta 1) and RGD-dependent integrins to laminins and laminin fragments. *Eur. J. Biochem.* 225, 975–984. doi: 10.1111/j.1432-1033.1994.0975b.x

Philpot, J., Sewry, C., Pennock, J., and Dubowitz, V. (1995). Clinical phenotype in congenital muscular dystrophy: correlation with expression of merosin in skeletal muscle. *Neuromuscul. Disord.* 5, 301–305. doi: 10.1016/0960-8966(94)00069-1

Pierson, M., Cordier, J., Hervouuet, F., and Rauber, G. (1963). [an unusual congenital and familial congenital malformative combination involving the eye and kidney]. *J. Genet. Hum.* 12, 184–213.

Posteraro, P., De Luca, N., Meneguzzi, G., El Hachem, M., Angelo, C., Gobello, T., et al. (2004). Laminin-5 mutational analysis in an Italian cohort of patients with junctional epidermolysis bullosa. *J. Invest. Dermatol.* 123, 639–648. doi: 10.1111/j.0022-202x.2004.23302.x

Pulkkinen, L., Christiano, A. M., Airenne, T., Haakana, H., Tryggvason, K., and Uitto, J. (1994). Mutations in the gamma 2 chain gene (LAMC2) of kalinin/laminin 5 in the junctional forms of epidermolysis bullosa. *Nat. Genet.* 6, 293–297. doi: 10.1038/ng0394-293

Purvis, A., and Hohenester, E. (2012). Laminin network formation studied by reconstitution of ternary nodes in solution. *J. Biol. Chem.* 287, 44270–44277. doi: 10.1074/jbc.m112.418426

Reinhard, J. R., Lin, S., McKee, K. K., Meinen, S., Crosson, S. C., Sury, M., et al. (2017). Linker proteins restore basement membrane and correct LAMA2-related muscular dystrophy in mice. *Sci. Transl. Med.* 9:eaal4649. doi: 10.1126/scitranslmed.aal4649

Reuten, R., Patel, T. R., McDougall, M., Rama, N., Nikodemus, D., Gibert, B., et al. (2016). Structural decoding of netrin-4 reveals a regulatory function towards mature basement membranes. *Nat. Commun.* 7:13515.

Reuten, R., Zendehroud, S., Nicolau, M., Fleischhauer, L., Laitala, A., Kiderlen, S., et al. (2021). Basement membrane stiffness determines metastases formation. *Nat. Mater.* 20, 892–903. doi: 10.1038/s41563-020-00894-0

Ringelmann, B., Roder, C., Hallmann, R., Maley, M., Davies, M., Grounds, M., et al. (1999). Expression of laminin alpha1, alpha2, alpha4, and alpha5 chains, fibronectin, and tenascin-C in skeletal muscle of dystrophic 129ReJ dy/dy mice. *Exp. Cell Res.* 246, 165–182. doi: 10.1006/excr.1998.4244

Rousselle, P., and Beck, K. (2013). Laminin 332 processing impacts cellular behavior. *Cell Adh. Migr.* 7, 122–134. doi: 10.4161/cam.23132

Rousselle, P., Keene, D. R., Ruggiero, F., Champliaud, M. F., Rest, M., and Burgeson, R. E. (1997). Laminin 5 binds the NC-1 domain of type VII collagen. *J. Cell Biol.* 138, 719–728. doi: 10.1083/jcb.138.3.719

Ryan, M. C., Lee, K., Miyashita, Y., and Carter, W. G. (1999). Targeted disruption of the LAMA3 gene in mice reveals abnormalities in survival and late stage differentiation of epithelial cells. *J. Cell Biol.* 145, 1309–1323. doi: 10.1083/jcb.145.6.1309

Ryan, M. C., Tizard, R., VanDevanter, D. R., and Carter, W. G. (1994). Cloning of the LamA3 gene encoding the alpha 3 chain of the adhesive ligand epiligrin. Expression in wound repair. *J. Biol. Chem.* 269, 22779–22787. doi: 10.1016/s0021-9258(17)31713-1

Saad, M., Brkanac, Z., and Wijsman, E. M. (2015). Family-based genome scan for age at onset of late-onset Alzheimer's disease in whole exome sequencing data. *Genes Brain Behav.* 14, 607–617. doi: 10.1111/gbb.12250

Sakai, N., Waterman, E. A., Nguyen, N. T., Keene, D. R., and Marinkovich, M. P. (2010). Observations of skin grafts derived from keratinocytes expressing selectively engineered mutant laminin-332 molecules. *J. Invest. Dermatol.* 130, 2147–2150. doi: 10.1038/jid.2010.85

Sampaolo, S., Napolitano, F., Tirozzi, A., Reccia, M. G., Lombardi, L., Farina, O., et al. (2017). Identification of the first dominant mutation of LAMA5 gene causing a complex multisystem syndrome due to dysfunction of the extracellular matrix. *J. Med. Genet.* 54, 710–720. doi: 10.1136/jmedgenet-2017-104555

Schneiders, F. I., Maertens, B., Bose, K., Li, Y., Brunken, W. J., Paulsson, M., et al. (2007). Binding of netrin-4 to laminin short arms regulates basement membrane assembly. *J. Biol. Chem.* 282, 23750–23758. doi: 10.1074/jbc.m703137200

Smyth, N., Vatansever, H. S., Meyer, M., Frie, C., Paulsson, M., and Edgar, D. (1998). The targeted deletion of the LAMC1 gene. *Ann. N. Y. Acad. Sci.* 857, 283–286. doi: 10.1111/j.1749-6632.1998.tb10133.x

Sugden, C. J., Iorio, V., Troughton, L. D., Liu, K., Bou-Gharios, G., and Hamill, K. J. (2020). Laminin N-terminus α31 expression during development is lethal and causes widespread tissue-specific defects in a transgenic mouse model. *bioRxiv* [Preprint]. doi: 10.1101/2020.07.26.221663

Talts, J. F., Sasaki, T., Miosge, N., Gohring, W., Mann, K., Mayne, R., et al. (2000). Structural and functional analysis of the recombinant G domain of the laminin alpha4 chain and its proteolytic processing in tissues. *J. Biol. Chem.* 275, 35192–35199. doi: 10.1074/jbc.m003261200

Tessier-Lavigne, M., and Goodman, C. S. (1996). The molecular biology of axon guidance. *Science* 274, 1123–1133. doi: 10.1126/science.274.5290.1123

Timpl, R., Tisi, D., Talts, J. F., Andac, Z., Sasaki, T., and Hohenester, E. (2000). Structure and function of laminin LG modules. *Matrix Biol.* 19, 309–317. doi: 10.1016/s0945-053x(00)00072-x

Troughton, L. D., Iorio, V., Shaw, L., Sugden, C. J., Yamamoto, K., and Hamill, K. J. (2020a). Laminin N-terminus α31 regulates keratinocyte adhesion and migration through modifying the organisation and proteolytic processing of laminin 332. *bioRxiv* [Preprint]. doi: 10.1101/617597

Troughton, L. D., Reuten, R., Sugden, C. J., and Hamill, K. J. (2020b). Laminin N-terminus alpha31 protein distribution in adult human tissues. *PLoS One* 15:e0239889. doi: 10.1371/journal.pone.0239889

Troughton, L. D., Zech, T., and Hamill, K. J. (2020c). Laminin N-terminus α31 is upregulated in invasive ductal breast cancer and changes the mode of tumour invasion. *bioRxiv* [Preprint]. doi: 10.1101/2020.05.28.120964

Utani, A., Nomizu, M., Timpl, R., Roller, P. P., and Yamada, Y. (1994). Laminin chain assembly. Specific sequences at the C terminus of the long arm are required for the formation of specific double- and triple-stranded coiled-coil structures. *J. Biol. Chem.* 269, 19167–19175. doi: 10.1016/s0021-9258(17)32290-1

Voit, T., Sewry, C. A., Meyer, K., Hermann, R., Straub, V., Muntoni, F., et al. (1995). Preserved merosin M-chain (or laminin-alpha 2) expression in skeletal muscle distinguishes Walker-Warburg syndrome from Fukuyama muscular dystrophy and merosin-deficient congenital muscular dystrophy. *Neuropediatrics* 26, 148–155. doi: 10.1055/s-2007-979745

Yurchenco, P. D., and Cheng, Y. S. (1994). Laminin self-assembly: a three-arm interaction hypothesis for the formation of a network in basement membranes. *Contrib. Nephrol.* 107, 47–56. doi: 10.1159/000422960

Yurchenco, P. D., McKee, K. K., Reinhard, J. R., and Ruegg, M. A. (2018). Laminin-deficient muscular dystrophy: molecular pathogenesis and structural repair strategies. *Matrix Biol.* 7, 174–187. doi: 10.1016/j.matbio.2017.11.009

Yurchenco, P. D., and Wadsworth, W. G. (2004). Assembly and tissue functions of early embryonic laminins and netrins. *Curr. Opin. Cell Biol.* 16, 572–579. doi: 10.1016/j.ceb.2004.07.013

Zenker, M., Aigner, T., Wendler, O., Tralau, T., Muntefering, H., Fenski, R., et al. (2004). Human laminin beta2 deficiency causes congenital nephrosis with mesangial sclerosis and distinct eye abnormalities. *Hum. Mol. Genet.* 13, 2625–2632. doi: 10.1093/hmg/ddh284

Zimmerman, T., and Blanco, F. J. (2007). The coiled-coil structure potential of the laminin LCC domain is very fragmented and does not differentiate between natural and non-detected isoforms. *J. Biomol. Struct. Dyn.* 24, 413–420. doi: 10.1080/07391102.2007.10507129

Conflict of Interest: The authors declare that the research was conducted in the absence of any commercial or financial relationships that could be construed as a potential conflict of interest.

Publisher's Note: All claims expressed in this article are solely those of the authors and do not necessarily represent those of their affiliated organizations, or those of the publisher, the editors and the reviewers. Any product that may be evaluated in this article, or claim that may be made by its manufacturer, is not guaranteed or endorsed by the publisher.

Received: 2 December 2020 | Revised: 28 March 2022 | Accepted: 5 April 2022

DOI: 10.1096/fj.202002588RRR

THE FASEB JOURNAL

RESEARCH ARTICLE

Laminin N-terminus α31 expression during development is lethal and causes widespread tissue-specific defects in a transgenic mouse model

Conor J. Sugden[1] | Valentina Iorio[1] | Lee D. Troughton[2] | Ke Liu[1] | Mychel R. P. T. Morais[3] | Rachel Lennon[3] | George Bou-Gharios[1] | Kevin J. Hamill[1]

[1]Institute of Life Course and Medical Sciences, University of Liverpool, Liverpool, UK

[2]Department of Cell and Molecular Physiology, Stritch School of Medicine, Loyola University Chicago, Maywood, Illinois, USA

[3]Wellcome Centre for Cell-Matrix Research, Division of Cell-Matrix Biology and Regenerative Medicine, The University of Manchester, Manchester, UK

Correspondence
Kevin J. Hamill, University of Liverpool, William Henry Duncan Building, 6 West Derby Street, Liverpool L7 8TX, UK.
Email: khamill@liverpool.ac.uk

Funding information
This work was supported by the Biotechnology and Biological Sciences Research Council [grant number BB/L020513/1] and the University of Liverpool Crossley Barnes Bequest fund.

Abstract

Laminins (LMs) are essential components of all basement membranes where they regulate an extensive array of tissue functions. Alternative splicing from the laminin α3 gene produces a non-laminin but netrin-like protein, Laminin N terminus α31 (LaNt α31). LaNt α31 is widely expressed in intact tissue and is upregulated in epithelial cancers and during wound healing. In vitro functional studies have shown that LaNt α31 can influence numerous aspects of epithelial cell behavior *via* modifying matrix organization, suggesting a new model of laminin auto-regulation. However, the function of this protein has not been established in vivo. Here, a mouse transgenic line was generated using the ubiquitin C promoter to drive inducible expression of LaNt α31. When expression was induced at embryonic day 15.5, LaNt α31 transgenic animals were not viable at birth, exhibiting localized regions of erythema. Histologically, the most striking defect was widespread evidence of extravascular bleeding across multiple tissues. Additionally, LaNt α31 transgene expressing animals exhibited kidney epithelial detachment, tubular dilation, disruption of the epidermal basal cell layer and of the hair follicle outer root sheath, and ~50% reduction of cell numbers in the liver, associated with depletion of hematopoietic erythrocytic foci. These findings provide the first in vivo evidence that LaNt α31 can influence tissue morphogenesis.

KEYWORDS

basement membrane, development, laminin, netrin

Abbreviations: BM, basement membrane; DMEM, Dulbecco's Modified Eagle Medium; ECM, extracellular matrix; hK14, human keratin 14; IP, intraperitoneal injection; LaNt α31, laminin N-terminus α31; LE, laminin-type epidermal growth factor-like domain; LM, laminin; LN, laminin N-terminal; mEFs, mouse embryonic fibroblasts; SDS-PAGE, sodium dodecyl sulfate polyacrylamide gel electrophoresis.

George Bou-Gharios and Kevin J. Hamill are joint senior authors.

1 | INTRODUCTION

Basement membranes (BMs) are specialized extracellular matrix (ECM) structures with essential and diverse roles in regulating cell and tissue behavior; including differentiation, cell adhesion, and migration.[1,2] BMs not only provide the mechanical attachment points that support sheets of cells to resist stresses but also influence signaling cascades via direct binding to cell surface receptors or indirectly through the sequestration and controlled release of growth factors, or mechanically by providing biomechanical cues, as reviewed in.[3,4] BMs are also dynamic structures that are remodeled in terms of composition and structure throughout life, with the most extensive changes occurring during development.[5,6] At the core of every BM are two networks of structural proteins; type IV collagens and laminins (LMs).[7]

Each LM is an obligate αβγ heterotrimer formed from one of five α chains (*LAMA1-5*), one of three β chains (*LAMB1-3*) and one of three γ chains (*LAMC1-3*), with each chain displaying spatio-temporal distribution patterns, as reviewed in.[8–11] Assembly of LM structural networks involves LM-LM interactions *via* their laminin N-terminal (LN) domains forming a ternary node comprised of one LN domain from each of the α, β and a γ chains.[12,13] These αβγ LN ternary nodes assemble in a two-step process involving an initial rapid formation of unstable βγ LN intermediate which is then stabilized through the incorporation of an α LN domain.[14–17] The biological importance of these LN-LN interactions is exemplified by a group of human disorders where missense mutations affecting the LN domains of the *LAMA2*, *LAMB2* or *LAMA5* genes give rise to syndromic disorders; muscular dystrophy in merosin-deficient muscular dystrophy for LAMA2, kidney and ocular developmental defects in Pierson syndrome for LAMB2, or defects in kidney, craniofacial and limb development for LAMA5.[18–23] Although these disorders demonstrate that LM network assembly is essential for homeostasis of numerous tissues, not all LM chains contain an LN domain. Specifically, LMα4, which is expressed at high levels in the vasculature, and the LMα3a and LMγ2 chains, which are abundant in surface epithelium including the skin, have shortened amino termini which lack this domain but yet still form functional BMs.[9,24–27] This raises questions of whether LN domains are important in all tissue contexts or whether additional proteins compensate for the intrinsic inability of these LMs to form networks.

Alongside their main LM transcripts, the *LAMA3* and *LAMA5* genes produce short transcripts encoding proteins that are unable to trimerize to form LM heterotrimers, but which contain LN domains as their characteristic feature.[24] At least one of these "laminin N terminus" (LaNt) proteins encodes a functional protein, LaNt α31, comprised of the LMα3 LN domain followed by a short stretch of laminin-type epidermal growth factor-like (LE) domains and a unique C-terminal region with no conserved domain architecture. In addition to the LaNt proteins, the laminin-superfamily includes the netrin genes which also encode proteins with either a β or γ laminin-like LN domain, stretches of LE repeats and unique C-terminal regions (as reviewed in Ref. [28]). Furthermore, proteolytic processing of LMs has also been identified as releasing similar LN domain containing fragments from LMα1,[29] LMβ1,[30] and LMα3b.[31] Some of the LN domain-containing netrin proteins and cryptic fragments have cell surface receptor binding capabilities and can act as signaling molecules (reviewed in Ref. [32]). However, netrin-4 also has LM-network disrupting capabilities due to its unusually high affinity for the LMγ1 LN domain[33,34] and when netrin-4 is overexpressed in vivo, it causes increased lymphatic permeability.[35] The netrin-4 LN domain has greatest homology with LM β LN domains whereas LaNt α31 contains an exact version of the LMα3b LN domain, which has lower affinity for LN domains; therefore, although LaNt α31 could act similarly to these proteins, it likely plays a different role depending on the LM context.

LaNt α31 is expressed in the basal layer of epithelia in the skin,[24] cornea[36] and digestive tract, the ECM around terminal duct lobular units of the breast and alveolar air sacs in the lung, and is widely expressed by endothelial cells.[37] Increased expression is associated with breast ductal carcinoma and in vitro overexpression leads to a change in the mode of breast cancer cell invasion through LM-rich matrices.[38] LaNt α31 is also transiently upregulated during re-epithelialization of ex vivo corneal burn wounds and in limbal stem cell activation assays.[36] In epidermal and corneal keratinocytes, knockdown or overexpression experiments revealed that modulating LaNt α31 levels leads to reduced migration rates and changes to cell-to-matrix adhesion.[24,39] Increased expression LaNt α31 also caused changes to LM332, including formation of tight clusters beneath cells and increasing the proteolytic processing of LMα3 by matrix metalloproteinases.[39]

Although the previous in vitro findings all support LaNt α31 as being a mediator of cell behavior, the in vivo impact is as yet unknown, in particular the role it plays in matrixes that are actively being remodeled. Here, we present the first in vivo study of LaNt α31 overexpression in newly developed mouse transgenic models. Analysis revealed that induction of LaNt α31 expression during embryogenesis leads to widespread extravascular red blood cell accumulation associated with capillary BM disruption.

2 | MATERIALS AND METHODS

2.1 | Ethics

All procedures were licensed by the UK Home Office under the Animal (Specific Procedures) Act 1986, project license numbers (PPL) 70/9047 and 70/7288. All mice were housed and maintained within the University of Liverpool Biological Services Unit in specific pathogen-free conditions in accordance with UK Home Office guidelines. Food and water were available ad libitum.

2.2 | Antibodies

Rabbit monoclonal antibodies against the influenza hemagglutinin epitope (HA) (C29F4, Cell Signalling Technology) were used for immunoblotting at 67 ng/ml. Goat polyclonal antibodies against DDDDK (equivalent to Flag sequence, ab1257, Abcam), rabbit polyclonal antibodies against 6X-His (ab137839, Abcam), and rabbit polyclonal antibodies against lamin A/C (4C11, Cell Signalling Technology) were used at 1 μg/ml for immunoblotting. Mouse monoclonal antibodies against LaNt α31[36] were used at 0.225 μg/ml for immunoblotting. Rabbit polyclonal antibodies against mCherry (ab183628, Abcam) were used at 2.5 μg/ml for immunofluorescence. Antibodies against laminin α4-subunit (clone 377b) and laminin α5-subunit (clone 504) were kindly provided by Prof. L. Sorokin (Institute of Physiological Chemistry and Pathobiochemistry; Münster University).[40] J18 polyclonal antiserum was raised in a rabbit using rat LM 332 purified from ECM preparations of 804G cells, as previously described.[41] Alexa fluor 647 conjugated goat anti-rabbit IgG recombinant secondary antibodies were obtained from Thermo Fisher Scientific and used at 2 μg/ml for indirect immunofluorescence microscopy.

2.3 | pUbC-LoxP-LaNtα31-T2A-tdTomato

A gBlock was synthesized (Integrated DNA Technologies) containing *Nde*I and *Nhe*I restriction enzyme sites, T7 promoter binding site,[42] Kozak consensus sequence,[43] Igκ secretion signal (METDTLLLWVLLLWVPGSTGD),[44] LaNt α31-encoding cDNA (amino acids 38–488),[24] Flag (DYKDDDDK)[45] and HA (YPYDVPDYA)[46] tag sequences, T2A sequence (EGRGSLLTCGDVEENPGP),[47] and *BamH*I. The gBlock DNA was inserted into pCSCMV:tdTomato (a gift from Gerhart Ryffel, Addgene plasmid #30530; http://n2t.net/addgene:30530; RRID:Addgene_30530) using *Nde*I and *BamH*I (New England Biolabs), to produce pCS-LaNtα31-T2A-tdTomato. LaNtα31-T2A-tdTomato was then removed from this backbone using *Nhe*I and *EcoR*I, and inserted into a vector containing the Ubiquitin C (UbC) promoter and a floxed stop cassette, all flanked by cHS4 insulator elements, producing pUbC-LoxP-LaNtα31-T2A-tdTomato.

2.4 | Cloning procedures

Restriction digests were set up with 1 μg of plasmid DNA, 1 μg of PCR product, or 100 ng of gBlock DNA, 20 U of each enzyme and CutSmart buffer (50 mM potassium acetate, 20 mM Tris-acetate, 10 mM magnesium acetate, 100 μg/ml BSA (New England Biolabs) and incubated at 37°C for 1 h. Enzymatic activity was inactivated by 20 min incubation at 65°C. PCR or cloning products were separated using 1% (w/v) agarose gels (Thermo Fisher Scientific) dissolved in 1 × TAE electrophoresis buffer (40 mM Tris pH 7.6, 20 mM acetic acid, 1 mM EDTA) containing ethidium bromide (Sigma Aldrich), and visualized using a UV transilluminator ChemiDoc MP System (BioRad). DNA bands were excised from the gel and purified using the GenElute™ Gel Extraction Kit, following manufacturer's protocol (Sigma Aldrich). Purified inserts were ligated into vectors at 3:1 molar ratios, either using Instant Sticky-end Ligase Master Mix (New England Biolabs) following manufacturers protocol, or using 400 U of T4 DNA ligase and 1× reaction buffer (50 mM Tris-HCl, 10 mM $MgCl_2$ 1 mM ATP, 10 mM DTT, New England Biolabs) at 16°C overnight, followed by enzymatic inactivation at 65°C for 10 min. Ligated DNA was heat-shock transformed into One-Shot TOP10 chemically competent E. coli cells (Thermo Fisher Scientific) following manufacturer's protocol, then plated onto LB plates containing the appropriate antibiotic (100 μg/ml ampicillin, 50 μg/ml kanamycin or 25 μg/ml chloramphenicol, Sigma Aldrich). Plasmid DNA was extracted from bacteria using the GenElute™ Plasmid Miniprep Kit (Sigma Aldrich), following the manufacturer's protocol. Plasmids were sequenced by DNASeq (University of Dundee).

2.5 | Cell culture

KERA-308 murine epidermal keratinocyte cells,[48] were purchased from CLS (Cell Lines Service GmbH) and maintained in high glucose (4.5 g/L) Dulbecco's Modified Eagle Medium (DMEM, Sigma Aldrich) supplemented with 10% fetal calf serum (FCS, LabTech) and 2 mM L-glutamine (Sigma Aldrich). HEK293A cells were maintained in DMEM supplemented with 10% FCS and 4 mM L-glutamine.

2.6 | Cell transfections

1×10^6 KERA-308 or 4×10^5 HEK293A cells were seeded in 6-well plates (Greiner-BioOne) 24 h prior to transfection. For KERA-308 cells, 2 μg of hK14-LaNtα31-T2A-mCherry or LaNt-α31-pSec-Tag and 2 μl Lipofectamine 2000 (Thermo Fisher Scientific) were used. For HEK293A cells, either 1 μg pCAG-Cre:GFP and 2 μl Lipofectamine 2000, 2 μg of pUbC-LoxP-LaNtα31-T2A-tdTomato and 5 μl Lipofectamine 2000, or 2 μg of pUbC-LoxP-LaNtα31-T2A-tdTomato, 1 μg of pCAG-Cre:GFP and 7 μl Lipofectamine 2000 (Thermo Fisher Scientific), were mixed with 2 ml of Gibco™ Opti-MEM™ Reduced Serum Medium (Thermo Fisher Scientific) and incubated for 10 min at room temperature. The DNA-lipofectamine complex was added to the wells, and the media was replaced with DMEM high glucose after 6 h.

2.7 | Explant culture method

Hair was removed from mouse skin tissue using Veet hair removal cream (Reckitt Benckiser) and the skin washed in Dulbecco's phosphate buffered saline (DPBS) containing 200 U/ml penicillin, 200 U/ml streptomycin, and 5 U/ml amphotericin B1 (all Sigma Aldrich). The skin was then dissected into 2–3 mm^2 pieces using a surgical scalpel and 3 or 4 pieces placed per well of a 6-well dish (Greiner Bio-One, Kremsmünster, Austria) with the dermis in contact with the dish. 300 μl of DMEM supplemented with 20% FCS, 2 mM L-glutamine, 200 μg/ml penicillin, 200 μg/ml streptomycin, and 5 μg/ml fungizone (all Sigma Aldrich) was added to the wells. After 24 h, each well was topped up with 1 ml of media, and the media was replenished every 48 h thereafter.

2.8 | Transgenic line establishment

Generation of transgenic mice were carried out based on the protocol described in Ref. [49] C57Bl6CBAF1 females (Charles River Laboratories) between 6 and 8 weeks were superovulated by intraperitoneal (IP) injections of 5 IU pregnant mare's serum gonadotrophin (PMSG; in 100 μl H_2O) (Sigma Aldrich), followed 46 h later by 5 IU of human chorionic gonadotropin (hCG, Sigma Aldrich). Treated females were mated with C57Bl6CBAF1 males overnight. Mated females were identified from the presence of copulation plugs, anaesthetized, and oviducts removed and dissected in M2 media (Millipore). Day-1 oocytes (C57BL/6Jx CBA F1) were transferred into clean media by mouth pipetting. Cumulus cells were removed by hyaluronidase (300 μg/ml, Merck) treatment in M2 media (Millipore, Speciality Media, EmbryoMax) with gentle shaking until detached from the egg surface. Oocytes were then rinsed and transferred to M16 media (Millipore, Speciality Media, EmbryoMax) ready for injection.

DNA was diluted to a final concentration of 2 ng/μl in embryo water (Sigma Aldrich) and filter-purified using Durapore-PVDF 0.22 μM centrifuge filters (Merck). Injection pipettes were used to pierce the outer layers of the oocyte and to inject DNA. DNA was injected into the pronuclei of the oocyte. Undamaged eggs were transferred to clean M16 media and incubated at 37°C until transferred into pseudopregnant CD1 females on the same day. Meanwhile, pseudopregnant females were obtained by mating vasectomized CD1 males overnight. Copulation plugs were checked and females were used 1 d post-coitum. Females were anaesthetized by inhalation of isoflurane (Sigma Aldrich). Thirty injected oocytes were transferred to plugged pseudopregnant female oviducts through the infundibulum.

In generating the pUbC-LoxP-LaNtα31-T2A-tdTomato line, 460 mouse zygotes were injected over four sessions. 87% of these zygotes survived and were transferred into 11 recipient CD1 mothers. From these mothers, 42 pups were born. Of the 10 F0 mice that gave a positive genotype result, four passed on the transgene to the F1 generation. Mice that did not pass on the transgene to the F1 generation were culled, the four F0 mice were mated and one line was continued for investigation.

R26CreERT2 (Jax Lab 008463)[50] mice were purchased from The Jackson Laboratory.

2.9 | In vivo transgene induction

Tamoxifen (Sigma Aldrich) was dissolved in corn oil (Sigma Aldrich) and administered IP at 25 or 75 mg/kg. Progesterone (Sigma Aldrich) was dissolved in corn oil (Sigma Aldrich) and was co-administered alongside tamoxifen at half of the corresponding tamoxifen dose (12.5 or 25 mg/kg).

2.10 | DNA extraction

Four weeks after birth, ear notches were collected from mouse pups and digested in 100 μl lysis buffer (50 mM Tris-HCl pH 8.0, 0.1 M NaCl, 1% SDS, 20 mM EDTA) and 10 μl of proteinase K (10 mg/ml, all Sigma Aldrich) overnight at 55°C. The following day, samples were cooled, spun at 13 000 rpm for 3 min and the supernatant transferred to clean 1.5 ml tubes (Eppendorf). An equal volume of isopropanol (Sigma Aldrich) was added, gently inverted and spun at 13 214 g, and supernatant

discarded. Pellets were washed with 500 µl of 70% EtOH (Sigma Aldrich), then air-dried for 10 min, and resuspended in 50 µl ddH_2O.

2.11 | PCR

50 ng of genomic DNA was mixed with 12.5 µl of REDtaq ReadyMix PCR Reaction Mix (20 mM Tris-HCl pH 8.3, 100 mM KCl, 3 mM $MgCl_2$, 0.002% gelatin, 0.4 mM dNTP mix, 0.06 unit/ml of Taq DNA Polymerase, Sigma Aldrich) and 0.5 µM of each primer; ddH_2O was added to make the reaction mixture up to 25 µl. Primer pairs for genotyping were as follows: LaNt α31 to tdTomato Forward 5′-ATCTATGCTGGTGGAGGGGT-3′, Reverse 5′-TCTTTGATGACCTCCTCGCC-3′; Cre Forward 5′-GCATTACCGGTCGATGCAACGAGTGATGAG-3′, Reverse 5′-GAGTGAACGAACCTGGTCGAAATCAGTGCG-3′; Recombination Forward 5′-TCCGCTAAATTCTGGCCGTT-3′, Reverse 5′-GTGCTTTCCTGGGGTCTTCA-3′ (all from Integrated DNA Technologies). Cycle conditions were as follows: Genotyping – 1 cycle of 95°C for 5 min, 35 cycles of 95°C for 15 s; 56°C for 30 s; 72°C for 40 s, followed by a final cycle of 72°C for 5 min. For assessing recombination: 1 cycle of 95°C for 5 min, 35 cycles of 95°C for 15 s; 60°C for 30 s; 72°C for 90 s, followed by a final cycle of 72°C for 7 min. PCR products were separated by gel electrophoresis and imaged using a BioRad Gel Doc XR+ System.

2.12 | Sodium dodecyl sulfate polyacrylamide gel electrophoresis (SDS-PAGE) and western immunoblotting

Cells were homogenized by scraping into 90 µl Urea/SDS buffer (10 mM Tris-HCl pH 6.8, 6.7 M urea, 1% w/v SDS, 10% v/v glycerol and 7.4 µM bromophenol blue, containing 50 µM phenylmethysulfonyl fluoride and 50 µM N-methylmaleimide, all Sigma Aldrich). Lysates were sonicated and 10% v/v β-mercaptoethanol (Sigma Aldrich) added. Proteins were separated by SDS-PAGE using 10% polyacrylamide gels; 1.5 M Tris, 0.4% w/v SDS, 10% acrylamide/bis-acrylamide (all Sigma Aldrich), electrophoresis buffer; 25 mM tris-HCl, 190 mM glycine, 0.1% w/v SDS, pH 8.5 (all Sigma Aldrich). Proteins were transferred to a nitrocellulose membrane using the TurboBlot™ system (BioRad) and blocked at room temperature in Odyssey® TBS-Blocking Buffer (Li-Cor BioSciences) for 1 h. The membranes were probed overnight at 4°C diluted in blocking buffer, washed 3 × 5 min in PBS with 0.1% Tween (both Sigma Aldrich) and probed for 1 h at room temperature in the dark with IRDye® conjugated secondary Abs against goat IgG (800 CW) and rabbit IgG (680 CW), raised in goat or donkey (LiCor BioSciences), diluted in Odyssey® TBS-Blocking Buffer at 0.05 µg/ml. Membranes were then washed for 3 × 5 min in PBS with 0.1% Tween, rinsed with ddH_2O and imaged using the Odyssey® CLX 9120 infrared imaging system (LiCor BioSciences). Image Studio Light v.5.2 was used to process scanned membranes.

2.13 | Tissue processing

For cryosections, P0 pups were culled by cervical dislocation, and fixed in 4% paraformaldehyde (Merck) for 2 h at 4°C. Samples were cryoprotected in 30% sucrose/PBS solutions then in 30% sucrose/PBS:O.C.T (1:1) solutions (Tissue-Tek, Sakura Finetek Europe), each overnight at 4°C. Samples were embedded in OCT compound (Tissue-Tek) and transferred on dry ice. Embedded samples were sectioned at 10 µm using a Leica CM1850 cryostat (Leica). For paraffin sections, Tissues were fixed in 10% neutral buffered formalin (Leica,) for 24 h, then processed through graded ethanol and xylene before being embedded in paraffin wax. 5 µm sections were cut using a rotary microtome RM2235 (Leica), adhered to microscope slides, then dried overnight at 37°C. Sections were dewaxed and rehydrated with xylene followed by a series of decreasing ethanol concentrations.

2.14 | Hematoxylin and eosin (H&E) staining

Sections were dewaxed and rehydrated with xylene followed by a series of decreasing ethanol concentrations. Sections were then stained in Harris hematoxylin solution (Leica) for 5 min, H_2O for 1 min, acid alcohol (Leica) for 5 s, H_2O for 5 min, aqueous eosin (Leica) for 3 min, H_2O for 15 s, followed by dehydration through graded ethanol and xylene. Slides were coverslipped with DPX mounting media (Sigma Aldrich).

2.15 | Immunohistochemistry

Slides were incubated in ice-cold acetone for 10 min, PBS for 10 min, then blocked in PBS containing 10% normal goat serum (NGS) at room temperature for 1 h. Samples were probed with the primary antibodies diluted in PBS-Tween (0.05%) with 5% NGS at 4°C overnight, washed for 3 × 5 min in PBS-Tween (0.05%), then probed with secondary antibodies diluted in PBS-Tween (0.05%) with 5% NGS at room temperature for 1 h. Samples were washed for 3 × 5 min in PBS-Tween (0.05%), then mounted with

VECTASHIELD® Antifade Mounting Medium with DAPI (VECTASHIELD®).

2.16 | Image acquisition

H&E images were acquired using a Zeiss Axio Scan. Z1 equipped with an Axiocam colour CCD camera using the ZEN Blue software (all from Zeiss). Live cell images were acquired using a Nikon Eclipse Ti-E microscope (Nikon). Immunofluorescence images of tissues were acquired using a Zeiss LSM 800 confocal microscope (Zeiss).

2.17 | Transmission electron microscopy

Kidneys and backskin were dissected from the p0 mice and placed immediately into 4% (w/v) paraformaldehyde, 2.5% (w/v) glutaraldehyde in cacodylate pH7.4 for 30 min at room temperature. The samples were then dissected into 3 mm^3 pieces and placed into fresh fixative and rotated overnight at room temperature. Samples were washed 4 × 5 min with 0.1 M cacodylate buffer, before staining with reduced osmium (final concentration 1% (w/v) OsO_4, 1.5% (w/v) potassium ferrocyanide, 0.1 M cacodylate buffer) in a Pelco Biowave® Pro (Ted Pella Inc.). Following this, samples were washed 5 × 5 min in ddH_2O, and incubated overnight in aqueous 1% uranyl acetate at 4°C. After further ddH_2O washes Samples were dehydrated through increasing concentrations of acetone (30%, 50%, 70%, 90% for 15 min each then 3 × 100%) Samples were infiltrated in 1:1 acetone TAAB 812 medium resin for 2 days followed by 4 × 100% resin for 1 h each, before final embedding and curing at 60°C for 48 h. Tissue was sectioned at 70–75 nm on a ultramicrotome (Leica) and the viewed in a FEI 120 Kv Tecnai Spirtit BioTwin TEM (FEI Company), fitted with a Gatan RIO16 digital camera (Gatan).

2.18 | Image analysis

Images were processed using either Zen 2.6 (blue edition) (Zeiss) or Fiji/ImageJ (National Institutes of Health).[51] Stardist plugin[52] was used for segmentation of nuclei from H&E images. Images were thresholded manually to remove areas containing no tissue in the images. Hemidesmosome number per µm in transmission electron micrographs was determined using the freehand selection tool on Fiji/ImageJ to measure BM length per image and manually counting hemidesmosomes. Hemidesmosome size was determined using the freehand selection tool to measure the length of electron dense plaques at the plasma membrane.

3 | RESULTS

3.1 | Inducible LaNt α31 construct validation

To investigate the consequences of LaNt α31 overexpression in vivo, an inducible system for conditional LaNt α31 transgene expression was generated (Figure 1A). An expression construct was created containing the ubiquitin C promoter driving expression of the human LaNt α31 cDNA. To focus our studies on extracellular role of LaNt a31, the native secretion signal was replaced by mouse immunoglobulin κ leader sequence.[44] This signal sequence has been used to increase protein secretion efficiency in mammalian cells.[53–55] Flag and HA epitope tags were added to the C-terminus of the LaNt α31 coding region. A T2A element was included to enable expression of td-Tomato from the same transgene but not directly fused to LaNt α31.[47] A floxed stop-cassette was inserted between the promoter and the start of the construct to prevent transgene expression until Cre-mediated removal of this cassette. The entire construct was flanked with the cHS4 β-globin insulator to protect against chromatin-mediated gene silencing[56] (Figure 1A). Restriction enzyme digests and plasmid sequencing confirmed the assembled pUbC-LoxP-LaNtα31-T2A-tdTomato plasmid.

To confirm the construct expressed only following exposure to Cre recombinase, the pUbC-LoxP-LaNtα31-T2A-tdTomato was co-transfected alongside pCAG-Cre:GFP, encoding GFP-tagged Cre recombinase, into HEK293A cells. tdTomato signal was observed only in cells transfected with both plasmids (Figure 1B). PCR using primers flanking the STOP cassette also confirmed that the cassette was removed only in cells transfected with both plasmids (Figure 1C). Western blotting using polyclonal anti-Flag antibodies confirmed expression of the predicted ~57 kDa band in co-transfected cell lysates (Figure 1D), this also confirmed that the T2A element was cleaved in the final product releasing the tdTomato tag. Together, these results demonstrated that the pUbC-LoxP-LaNtα31-T2A-tdTomato plasmid allows for the Cre-inducible expression of LaNt α31 and tdTomato.

3.2 | Generation and validation of a LaNt α31 transgenic mouse line

The pUbC-LoxP-LaNtα31-T2A-tdTomato construct was linearized, and transgenic F0 mice generated by pronuclear microinjection into oocytes. To confirm transgene expression, F0 mice were mated with WT (C57BL/6J) mice, embryos were collected at E11.5, and mouse embryonic fibroblasts (mEFs) were isolated from the

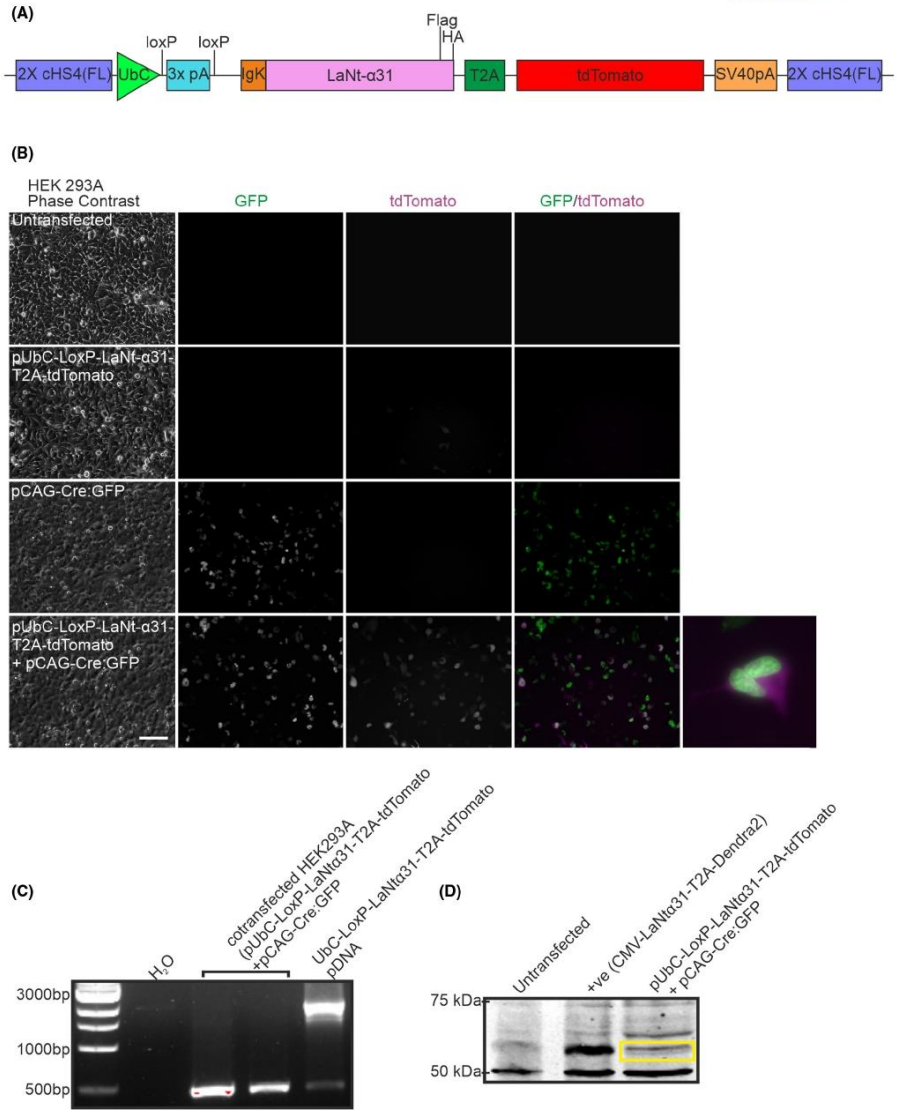

FIGURE 1 Validation of UbCLaNt Cre-inducible construct in vitro. (A) Diagram of the pUbC-LoxP-LaNt-α31-T2A-tdTomato construct. (B) HEK 293A cells were transfected with pUbC-LoxP-LaNt-α31-T2A-tdTomato, pCAG-Cre:GFP, or pUbC-LoxP-LaNt-α31-T2A-tdTomato and pCAG-Cre:GFP and imaged 48 h after transfection. Scale bar 100 μm. (C) PCR products using primers flanking the stop cassette on DNA extracted from HEK293A cells co-transfected with pUbC-LoxP-LaNt-α31-T2A-tdTomato and pCAG-Cre:GFP. (D) Western blot of lysates from HEK293 cells either untransfected or transfected with CMV- LaNt-α31-T2A-Dendra2 (positive control), or pUbC-LoxP-LaNt-α31-T2A-tdTomato and pCAG-Cre:GFP then probed with anti-Flag antibodies

embryos. Presence of the UbC-LoxP-LaNtα31-T2A-tdTomato transgene (hereafter UbCLaNt) was confirmed by PCR (Figure S1A). mEFs were transduced with an adenovirus encoding codon-optimized Cre recombinase (ad-CMV-iCre). Analysis by immunoblotting with anti-HA-antibodies (Figure S1B) revealed a ~57 KDa band and fluorescence microscopy confirmed tdTomato expression in samples containing both the UbC-LaNt transgene and the ad-CMV-iCre only (Figure S1C).

Male UbCLaNt mice were mated with females from the tamoxifen-inducible ubiquitous Cre line R26CreERT2. Transgene expression was induced by IP injection of tamoxifen at E13.5, and embryos collected at E19.5. PCR confirmed that Cre/LoxP mediated recombination only occurred in the embryos with both the UbCLaNt and the R26CreERT2 transgenes (Figure 2A). Explants were generated from the skin of these embryos, and only the explants grown from double transgenic embryos exhibited tdTomato expression by fluorescence microscopy (Figure 2B) and HA-tagged LaNt α31 expression by western immunoblotting (Figure 2C). Together, these data confirmed the generation of tamoxifen-inducible LaNt α31 mouse line, without detectable leakiness (UbCLaNt::R26CreERT2).

3.3 | UbCLaNt::R26CreERT2 expression in utero causes death and localized regions of erythema at birth

To determine the impact of LaNt α31 during development, tamoxifen was administered to pregnant UbCLaNt::R26CreERT2 mice at E15.5 via gavage and pregnancies allowed to continue to term. Across three litters from three different mothers, two from six pups, three from five pups, and one from five pups respectively were intact but not viable at birth, while the remaining littermates were healthy. The non-viable pups displayed localized regions of erythema with varying severity between the mice, but were otherwise fully developed and the same size as littermates (Figure 3A). Endpoint PCR genotyping using primers amplifying the LaNt α31 transgene and Cre recombinase transgene confirmed mice possessed both transgenes (Figure S2A). To confirm that the lack of viability was associated with transgene expression, OCT-embedded skin sections of UbCLaNt::R26CreERT2 were imaged using confocal microscopy, revealing tdTomato fluorescence only in the non-viable animals (Figure 3B) and skin explants were established and tdTomato fluorescence in explants from non-viable pups was confirmed by microscopy (Figure 3C). Western immunoblot analysis of total protein extracts from the explanted cells and from whole embryo lysates also revealed transgene expression in non-viable pups, although expression levels varied between the mice (Figure 3D). Together these data confirmed that only non-viable mice expressed the LaNt α31 transgene. Hereafter, UbCLaNt::R26CreERT2 animals are therefore labeled as either "LaNt α31 TG-expressing" or, for non-expressing, "littermate controls".

To identify LaNt α31 effects at the tissue level, the pups were formalin-fixed and paraffin-embedded then processed for H&E staining and immunohistochemistry. All organs were present in the mice and appeared intact at the macroscopic level. A consistent feature in every transgenic animal was extensive evidence of bleeding within tissues. Indeed, although there was mouse-to-mouse variability in extent of this bleeding, every major organ in all animals were affected to some extent.

We focused our attention on kidney, skin and lung as examples of tissues where the BMs with distinct differences in LM composition and where LaNt α31 could elicit context-specific effects. Each of these three tissues also express LaNt α31 in adult human tissue, and are, therefore, tissues where dysregulation of expression regulation could be physiologically relevant.[37] Specifically, the predominant LMs in the kidney contain three LN domains, and mutations affecting LM polymerization lead to Pierson syndrome,[19,57–60] whereas the major LM in the skin contains one LN domain, LM332, and loss of function leads to skin fragility, reviewed in,[61] and granulation tissue disorders.[62,63] In the lung, LM311, a two LN domain LM, is enriched[64,65] and absence of LM α3 is associated with pulmonary fibrosis.[66]

3.4 | LaNt α31 overexpression leads to epithelial detachment, tubular dilation and interstitial bleeding in the kidney and disruption of capillary BM integrity

Dissected kidneys from the transgene-expressing animals were markedly darker than non-expressing animals (Figure 4A). Histological examination confirmed that this difference reflected differences in the vessels of the kidney, with extensive bleeding into the interstitial and sub tubular surroundings (Figure 4B, yellow arrows). Detachment of the lining epithelia in collecting ducts and uteric bud segments was also apparent (Figure 4B, black arrows). Indirect IF processing of tissue using pan-LM antibodies revealed LM localization to be largely unchanged (Figure 4C). However, ultrastructural examination by transmission electron microscopy identified that the

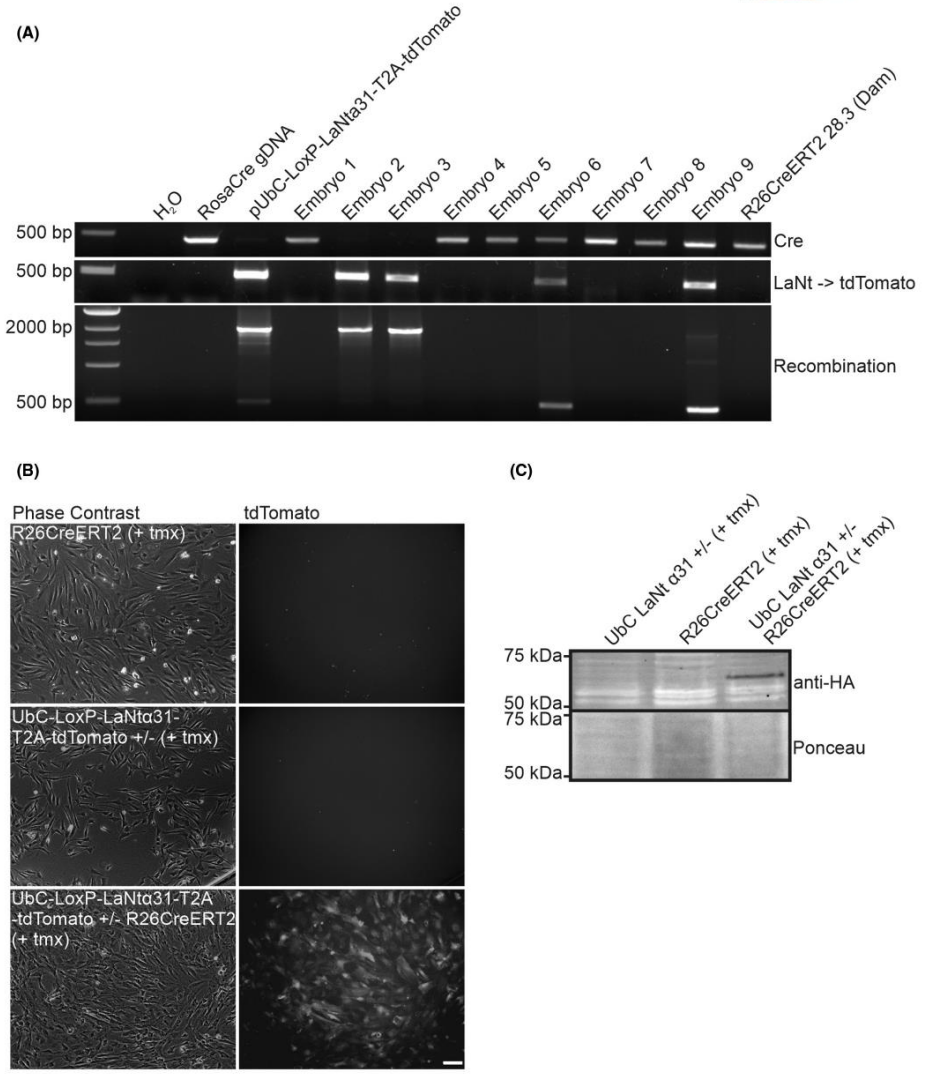

FIGURE 2 UbCLaNtα31 x R26CreERT2 ER transgenic mice express the UbC-LaNtα31 transgene following exposure to tamoxifen. (A) PCR products on DNA extracted from transgenic mouse from UbCLaNtα31 x R26CreERT2 mating embryos using primers flanking the stop cassette. (B) Phase contrast and fluorescence microscopy images of explanted cells from UbCLaNtα31::R26CreERT2 embryos. Scale bar =100 μm. (C) Western blot of lysates from UbCLaNtα31::R26CreERT2 embryo explants processed with anti-HA antibodies

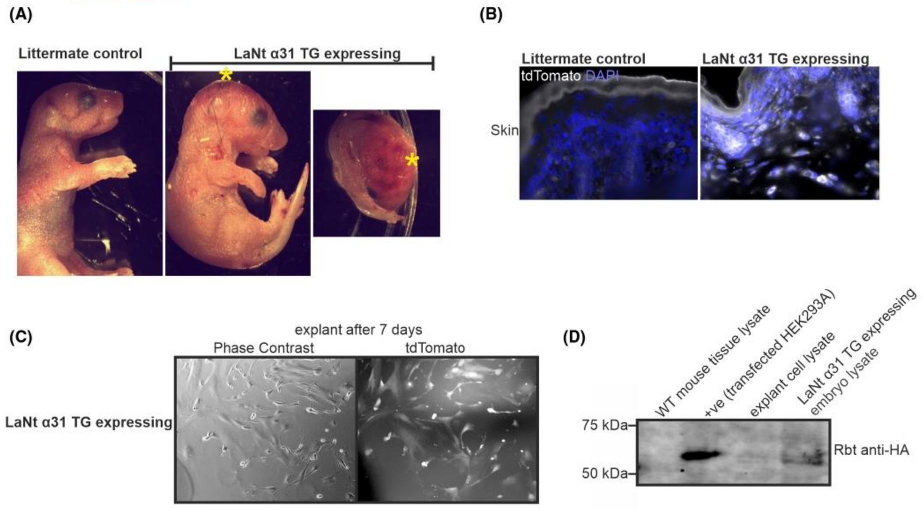

FIGURE 3 Transgenic mice overexpressing LaNtα31 display localized regions of erythema. (A) Representative images of UbCLaNtα31::R26CreERT2 embryos. Animals subsequently confirmed as expressing the LaNt α31 transgene are labeled as LaNt α31 TG expressing. *Indicates regions of visible erythema. (B) Representative fluorescence microscopy UbCLaNtα31::R26CreERT2 OCT sections tdTomato fluorescence. Scale bar =100 μm. (C) Fluorescence microscopy images of explanted cells from LaNt α31 TG expressing. Scale bar =100 μm. (D) Western blot of tissue lysates from WT, UbCLaNtα31::R26CreERT2 embryos or explanted cells processed with anti-HA antibodies. HEK293A cells cotransfected with the LaNt α31 transgene expression construct and Cre-GFP expression construct are included as a positive control

majority of extravascular red blood cells present in the tissue were outside of capillary structures (Figure 4D).

3.5 | LaNt α31 overexpression disrupts epidermal basal cell layer organization

Histological examination of the dorsal skin of the LaNt α31 TG expressing mice revealed localized disruption of the epidermal basal cell layer, with a loss of the tight cuboidal structure of the stratum basale (Figure 5A). Basal layer disruption was also observed in the outer root sheath of the hair follicles (Figure 5A). There was no evidence of blistering at the dermal-epidermal junction. However, extravascular erythrocytes were observed through the skin (Figure 5A, yellow chevron). Indirect IF processing revealed that the localization of LMα5, LM 332, and type IV collagen was unchanged in LaNt α31 TG expressing animals, although increased immunoreactivity of LM α5 was observed (Figure 5B, Figure S3). This increase in immunoreactivity was also observed in samples processed with a pan-LM antibody (Figure 5B). The immunoreactivity of LMα4 appeared unchanged in vessels; but this laminin chain was also detected at the dermal-epidermal junction in LaNt α31 TG expressing animals (Figure 5B). Ultrastructural analyses of the dermal-epidermal junction revealed no major disruption to the BM. However, in the LaNt α31 TG specimens, hemidesmosomes were larger (Figure 5C, chevrons, Figure 5D, littermate median 0.11 95% CI 0.09–0.12 μm, LaNt α31 TG median 0.26 95% CI 0.24–0.28 μm, $p < .001$ Mann-Whitney test).

3.6 | Mice expressing the LaNt α31 transgene display structural differences in the lung and a reduction of hematopoietic colonies in the liver

Erythrocytes were present throughout the lung tissue and liver tissue of transgene expressing animals (Figure 6A,B). Structural differences were also apparent in the lungs, although it should be noted that the lungs of P0 mice were not inflated prior to fixation. Mice expressing LaNt α31 also displayed fewer, and less densely-packed alveolar epithelial cells. The livers of mice expressing the

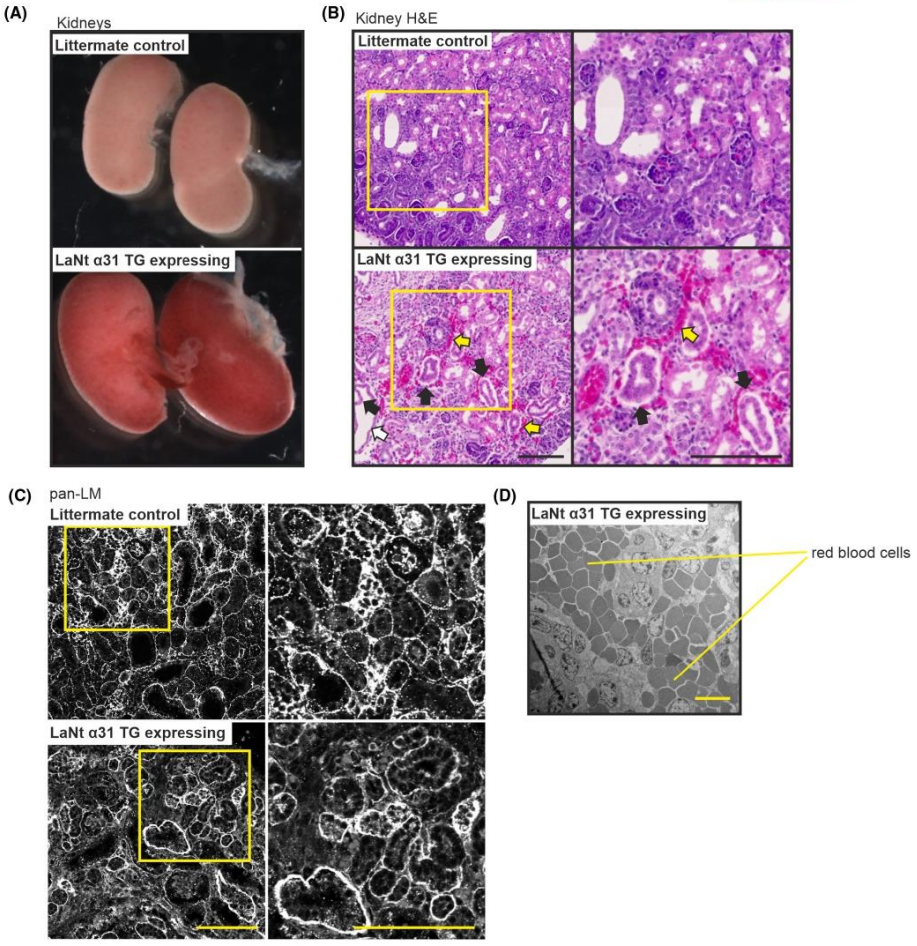

FIGURE 4 LaNt α31 overexpression leads to epithelial detachment, tubular dilation and interstitial bleeding in the kidney and disruption of capillary basement membrane integrity. (A) Representative images of whole kidneys of newborn UbCLaNtα31::R26CreERT2 mouse kidneys from non-expressing littermate controls (top) or LaNt α31 TG expressing animals (bottom). (B) Representative images of H&E stained FFPE sections (5 μm) of newborn littermate controls of LaNt α31 TG expressing mouse kidneys. Right column shows areas of increased magnification. Black arrows point to areas of epithelial detachment. White arrows point to tubular dilation. Yellow arrows point to areas of interstitial bleeding. (C) FFPE sections (5 μm) from littermate controls or LaNt α31 TG expressing animals processed for immunohistochemistry with pan-laminin polyclonal antibodies. Right column shows areas of increased magnification. Scale bars =100 μm

LaNt α31 transgene exhibited a reduction in hematopoietic foci (Figure 6B,C). This reduction corresponded to a >33% reduction of total cell number (mean ± SD nuclei/mm^2 littermate controls =11.0 ± 0.52, LaNt α31 expressing =5.8 ± 0.50, p =<.0001 determined by unpaired t test; Figure 6D,E). The bile ducts, sinusoid endothelium and hepatocyte morphology were histologically unchanged.

3.7 | Keratin 14-driven constitutive LaNt α31 induces a low offspring number

We generated an additional construct using the human keratin 14 (K14) promoter to drive expression of human LaNt α31, followed by a T2A element and a mCherry reporter (Figure S4A). The K14 promoter is expressed in the skin and the epithelia of tongue, mouth, forestomach, trachea, thymus and respiratory and urinary tracts,[67–69] and has been described in the oocyte.[70] The new construct was validated by transfecting into KERA 308 mouse epidermal keratinocytes and visualizing the mCherry fluorescence (Figure S4B) and immunoblotting for the LaNt α31 protein (Figure S4C). K14-LaNtα31 transgenic mice were generated by pronuclear microinjection. However, unusually small litters were obtained from recipient CD1 mothers and mice containing the transgene DNA (Figure S4D) did not express the transgene at the protein level (Figure S4F,G). The unusually low offspring sizes, combined with the lack of protein expression in genotype-positive mice suggests that expression of LaNt α31 under the control of the K14 promoter is lethal during development.

4 | DISCUSSION

This study has demonstrated that LaNt α31 overexpression ubiquitously during development is lethal, causing widespread blood exudate throughout most tissues as well as changes to the tubules of the kidney and the basal layer of the epidermis, depletion of hematopoietic colonies in the liver, and evidence of capillary BM disruption. These findings build upon previous in vitro and ex vivo work that have implicated LaNt α31 in the regulation of cell adhesion, migration, and LM deposition.[24,36,39] Importantly, they provide the first in vivo evidence that this little-studied *LAMA3*-derived splice isoform and newest member of the laminin superfamily has biological importance in BM and tissue formation during development and provide a valuable platform for onward investigation.

There are several plausible overlapping reasons that can explain the phenotype. As LM network assembly requires binding of an α, β, and γ LN domain,[14–17,71] the presence of an αLN domain within LaNt α31 could influence LM-LM interactions and therefore BM assembly or integrity. Indeed, LaNt α31, contains a perfect match to the LMα3b LN domain and biochemical assays have shown that the LMα3b LN domain is the most potent of the LM LN domains at disrupting LM111 polymerization in vitro.[72] In vivo, the LaNt α31 protein would occupy βγ nodes but be unable to complete the polymer as a sheet-like structure and, especially at locally high concentrations, would disrupt the laminin network. Consistent with this network disruption model, much of the LaNt α31 TG phenotype resemble those from mice where LM networks cannot form due to LN domain mutations. Specifically, whereas LMα5 knockout animals die at E17, LMα5 LN domain mutants were born at term with some animals surviving for weeks or months after birth. The LN domain mutant mice exhibited defective lung development and vascular abnormalities in the kidneys.[73] Mice with LM β2 LN domain mutations or deletion of the LM β2 LN domain both exhibit renal defects, and although viable at birth, become progressively weaker and die between postnatal day 15 and 30.[74–79] In comparison with the LN-domain specific mutant lines, the LaNt α31 TG expressing animals BM-associated defects are somewhat similar although the overall effect is more severe and affects more tissues than each individual LN mutant line as anticipated by the more widespread expression of the transgene driven by UBC and R26 promoter activities.

Within the model of LaNt α31 inhibiting LM network assembly, there remains the question of how LaNt α31 influences tissues where the expressed LMs do not contain an α LN domain, and therefore are not able to polymerize.[16] For example, The LM composition present within vessel BMs during development and lymph vessels is rich in the non-polymerizing LM411.[80–82] Here it should be noted that transgenic mice expressing the potent LM network disrupting protein netrin-4 under the control of the K14 promoter were born smaller, redder, and with

FIGURE 5 LaNt α31 overexpression disrupts epidermal-dermal cell organization. (A) H&E staining of FFPE sections (5 μm) of newborn UbCLaNtα31::R26CreERT2 transgenic mice dorsal skin. Upper panel non-expressing littermate controls, lower panels LaNt α31TG expressing animals. Yellow chevrons indicate areas of extravascular erythrocytes. Middle and right columns show increased magnification of the epithelium or hair follicles respectively. Yellow arrows indicate basal layer of epithelial cells. Scale bar =100 μm. (B) Littermate controls (left) or LaNt α31 TG expressing OCT sections (10 μm) processed for immunohistochemistry with anti-laminin 111 (pan-LM), anti-laminin α4 (LM α4), anti-laminin α5 (LM α5), anti-laminin 332 (LM 332) and anti-Type IV collagen (Col IV). Scale bar =50 μm. (C) Transmission electron micrographs of littermate control or LaNt α31 TG expressing skin sections imaged at the dermal-epidermal junctions. Chevrons indicate hemidesmosomes. Scale bar =0.5 μm. (D) Box and whisker graphs of quantification of hemidesmosome number per μm of basement membrane ($n = 12$ and 17 images), and of size of the hemidesmome measured as the length of the electron dense plaque at the cell membrane ($n = 67$ and 81 hemidesmosomes). Boxes represent 25th–75th percentile with line at median, whiskers 5th and 95th percentile. Dots represent outliers

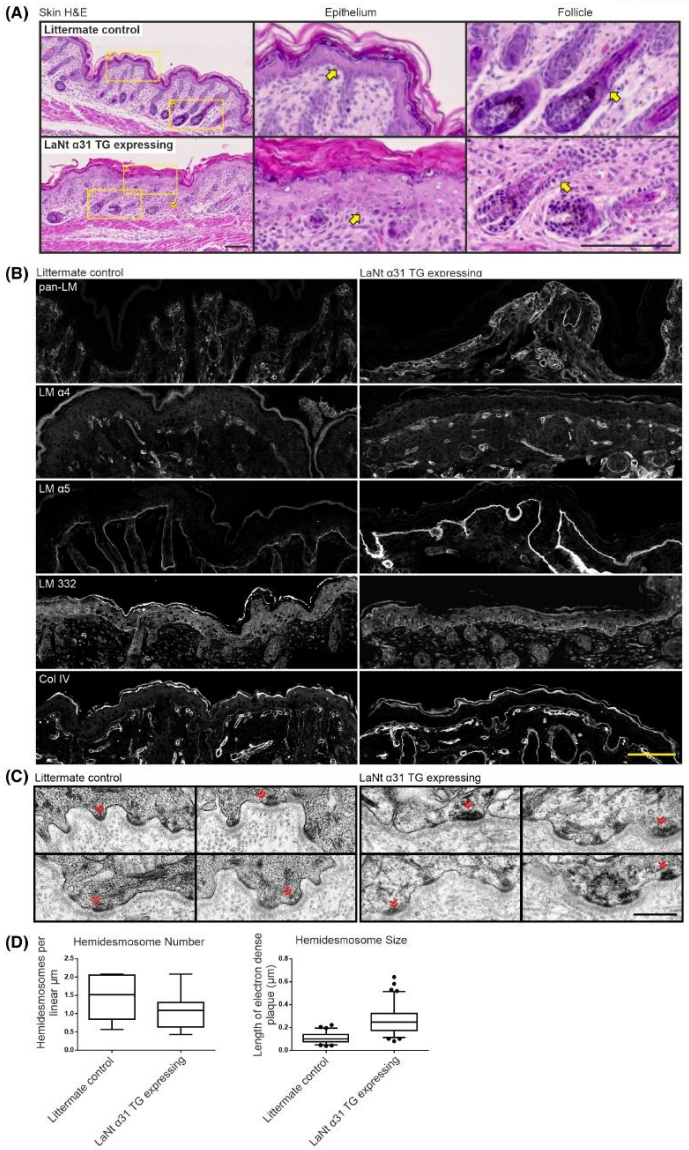

increased lymphatic permeability.[35] In contrast, one might have anticipated that the LaNt α31 LN domain could compensate for the "missing" α LN domain in the vasculature and stabilize the weak, transient βγ LN dimers made by the LMβ1 and γ1 LN domains.[15,17,71] However, the observed phenotype of blood exudate throughout the mouse tissues instead indicates that the LaNt α31 has a disruptive rather than stabilizing role.

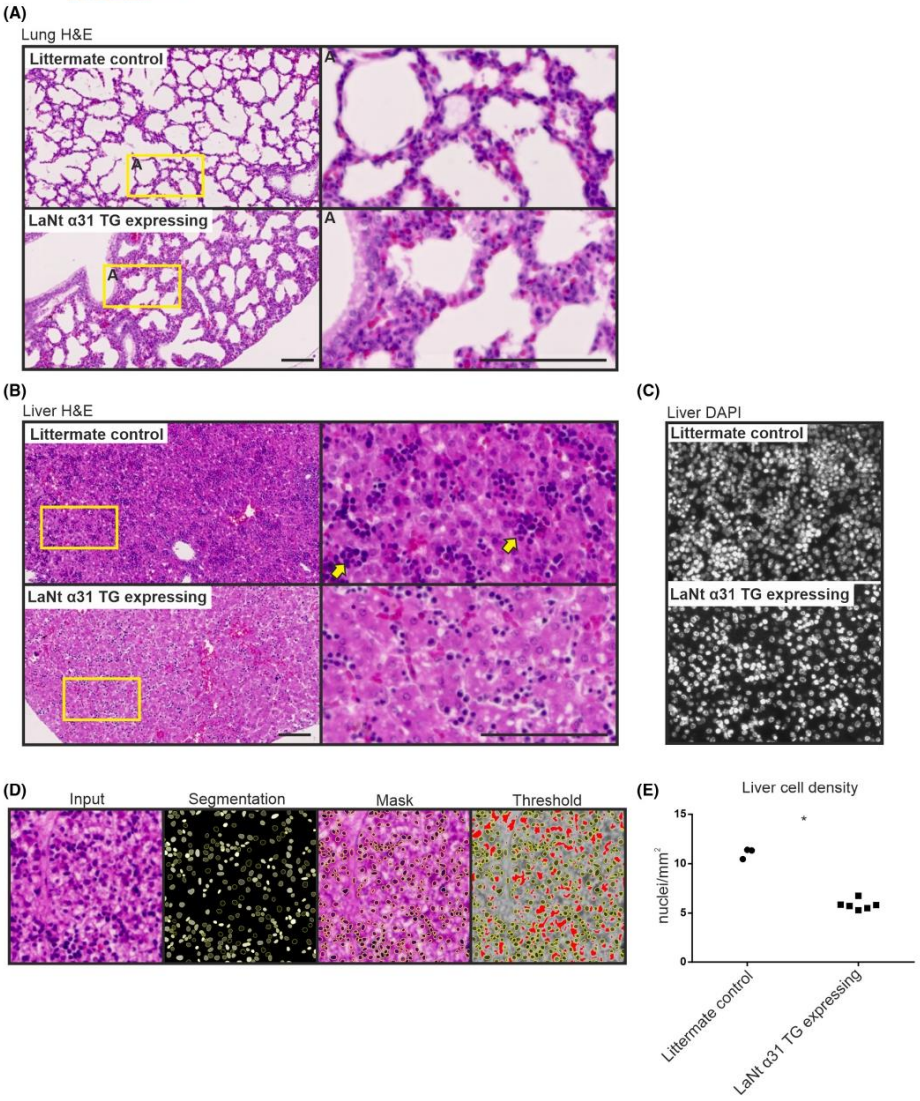

FIGURE 6 Mice expressing the LaNtα31 transgene display structural differences in the lung and a reduction of hematopoietic colonies in the liver. (A) H&E staining of FFPE sections (5 μm) of newborn UbCLaNtα31::R26CreERT2 transgenic mice lungs (A) and liver (B). Upper panel non-expressing littermate controls, lower panels LaNt α31TG expressing animals. Right columns show increased magnification. Yellow arrowheads highlight areas of increased cell density. Scale bars =100 μm. (C) DAPI staining of littermate controls or LaNt α31 TG expressing mouse livers. (D) Representative image analysis method of determining nuclei count. (E) Quantification of nuclei. Each point represents the mean of the quantification of nuclei/mm^2 from 2 separate microscope slides at different sectioning depths per mouse

It is also possible that the LaNt α31 transgene effects represent a signaling rather than structural role. Integrin-mediated signaling from LaNt α31-like proteolytically released LN-domain containing fragments from LM α3b, α1, and β1 chains have been reported[29–31] and some aspects of the UbCLaNt::R26CreERT2 phenotype are consistent with LaNt α31 acting in this way. For example one of the most striking phenotypes observed in the LaNt α31 transgenic mice was depletion of hematopoietic colonies in the liver, an essential stem cell niche during development.[83–85] Integrins α6 and β1 are highly expressed in hematopoietic stem cells, and are central to the process of migration both in and out of the fetal liver.[86–88] A netrin-4/laminin γ1 complex has been shown to signal through the integrin α6β1 receptor to ERK1/2 and regulate neural stem cell proliferation and migration.[89] LaNt α31 is also enriched in human and porcine limbal stem cell niche of adult corneas, with expression further upregulated upon ex vivo stem cell activation and wound repair.[36] While these combined data suggest that direct signaling effects are possible with LaNt α31 binding to cell surface receptors, indirect effects are also probable. Altering LM network structural organization changes matrix stiffness, as has been demonstrated for netrin-4,[90] and also could influence outside-in signaling through changing presentation of ligands or by modifying growth factor sequestration and release rates.[91] Indeed, LM networks are also known to be critical for maintaining progenitor cell "stemness".[92–95] Dissecting the direct versus indirect roles of LaNt α31 in intact tissue contexts is now a priority and the new transgenic mouse line provides a valuable resource to facilitate those onward investigations.

Moving forward, the role of LaNt α31 can now be determined in a tissue and context specific manner. Considering the widespread expression of LaNt α31,[37] and the dramatic effects observed in this study, it is now important to determine effects in adult animals in normal conditions and following intervention and under lineage specific control. These studies should include tissues where no overt LaNt α31-induced phenotype was observed. For example, although no muscle defects were observed in the animals in this study, LM network integrity is critical to muscle function, with the effects of LM α2 LN domain mutations or deletions developing muscular dystrophy and peripheral neuropathy with time[96–98]; therefore, longer-term studies may reveal further phenotypes once tissues are placed under stress. Importantly, the biological function of LaNt α31 may be different at lower compared to higher concentration. At low concentrations, LaNt α31 may exploit the existing β-γ LN domains to enable BM attachment in order to deliver a new receptor ligand to the BM. Therefore, a knockout model would also be valuable as well as further in vitro and biochemical analyses to dissect function.

Inherited disorders driven by variants to α LN domain have robustly established that LN domains are important for tissue function.[19,22,73,99,100] The findings here add a new layer to this regulation. LaNt α31 is a naturally occurring protein generated from a laminin-encoding gene via alternative splicing. These new results show that LaNt α31 is functional within a biological context. This is important as it raises the possibility of active regulation of LaNt α31 production via control of the splicing event as a mechanism to influence BM assembly/disassembly or matrix-signaling by titrating LaNt α31 levels.[24] Alternative splicing rates often change in normal situations during development and tissue remodeling, or in response to damage such as in wound repair, and are frequently dysregulated in pathological situations including frequently in cancer.[101–103] Considered in this way, the finding the LaNt α31 is biologically active in vivo has exciting and far-reaching implications for our understanding of BM biology.

ACKNOWLEDGEMENTS

We are grateful to the staff at the University of Liverpool Biomedical Services Unit. The authors would like to thank Alison Beckett and Lucy Isherwood at the Biomedical EM Unit for support and advice. We would like to thank Prof Peter Yurchenco, Dr Karen McKee, Prof Jonathan Jones and Dr. Takao Sakai, for helpful discussions during the writing of this manuscript. We thank Prof. Lydia Sorokin for kindly providing antibodies raised against laminin α4 and laminin α5 subunits.

DISCLOSURES

The authors declare that there are no conflicts of interests.

AUTHOR CONTRIBUTIONS

Conor J. Sugden: methodology, validation, formal analysis, investigation, data curation, writing – original draft, writing – review & editing, visualization. **Valentina Iorio:** methodology, investigation, data curation, writing – review & editing. **Lee D. Troughton:** methodology, writing – original draft, writing – review & editing. **Ke Liu:** methodology, writing – review & editing. **Mychel R. P. T. Morais**: methodology, formal analysis, writing – review & editing. **Rachel Lennon:** methodology, formal analysis, writing – review & editing. **George Bou-Gharios:** conceptualization, methodology, writing – review & editing, supervision. **Kevin Hamill:** conceptualization, methodology, writing – original draft, writing – review & editing, supervision, funding acquisition.

DATA AVAILABILITY STATEMENT

The data that support the findings of this study are available in the methods and/or supplementary material of this article. The transgenic mouse strains and plasmids are available on request from the corresponding author.

ORCID

Conor J. Sugden https://orcid.org/0000-0002-9543-1676
Lee D. Troughton https://orcid.org/0000-0003-3836-7249
Mychel R. P. T. Morais https://orcid.org/0000-0001-5237-9524
Rachel Lennon https://orcid.org/0000-0001-6400-0227
George Bou-Gharios https://orcid.org/0000-0002-9563-9418
Kevin J. Hamill https://orcid.org/0000-0002-7852-1944

REFERENCES

1. Yamada KM, Collins JW, Cruz Walma DA, et al. Extracellular matrix dynamics in cell migration, invasion and tissue morphogenesis. *Int J Exp Pathol*. 2019;100:144-152.
2. Sekiguchi R, Yamada KM. Basement membranes in development and disease. *Curr Top Dev Biol*. 2018;130:143-191.
3. Yurchenco PD. Basement membranes: cell scaffoldings and signaling platforms. *Cold Spring Harb Perspect Biol*. 2011;3(2):a004911.
4. Pozzi A, Yurchenco PD, Iozzo RV. The nature and biology of basement membranes. *Matrix Biol*. 2017;57-58:1-11.
5. Walma DAC, Yamada KM. The extracellular matrix in development. *Development*. 2020;147. 10.1242/dev.175596
6. Morrissey MA, Sherwood DR. An active role for basement membrane assembly and modification in tissue sculpting. *J Cell Sci*. 2015;128:1661-1668.
7. Theocharis AD, Skandalis SS, Gialeli C, Karamanos NK. Extracellular matrix structure. *Adv Drug Deliv Rev*. 2016;97:4-27.
8. Hamill KJ, Paller AS, Jones JC. Adhesion and migration, the diverse functions of the laminin alpha3 subunit. *Dermatol Clin*. 2010;28:79-87.
9. Hohenester E, Yurchenco PD. Laminins in basement membrane assembly. *Cell Adh Migr*. 2013;7:56-63.
10. Aumailley M. The laminin family. *Cell Adh Migr*. 2013;7:48-55.
11. Aumailley M, Bruckner-tuderman L, Carter W, et al. A simplified laminin nomenclature. *Matrix Biol*. 2005;24:326-332.
12. Cheng YS, Champliaud MF, Burgeson RE, Marinkovich MP, Yurchenco PD. Self-assembly of laminin isoforms. *J Biol Chem*. 1997;272:31525-31532.
13. Odenthal U, Haehn S, Tunggal P, et al. Molecular analysis of laminin N-terminal domains mediating self-interactions. *J Biol Chem*. 2004;279:44504-44512.
14. Schittny JC, Yurchenco PD. Terminal short arm domains of basement membrane laminin are critical for its self-assembly. *J Cell Biol*. 1990;110:825-832.
15. Yurchenco PD, Cheng YS. Laminin self-assembly: a three-arm interaction hypothesis for the formation of a network in basement membranes. *Contrib Nephrol*. 1994;107:47-56.
16. Purvis A, Hohenester E. Laminin network formation studied by reconstitution of ternary nodes in solution. *J Biol Chem*. 2012;287:44270-44277.
17. Carafoli F, Hussain SA, Hohenester E. Crystal structures of the network-forming short-arm tips of the laminin beta1 and gamma1 chains. *PLoS One*. 2012;7:e42473.
18. McKee KK, Aleksandrova M, Yurchenco PD. Chimeric protein identification of dystrophic, Pierson and other laminin polymerization residues. *Matrix Biol*. 2018;67:32-46.
19. Matejas V, Hinkes B, Alkandari F, et al. Mutations in the human laminin beta2 (LAMB2) gene and the associated phenotypic spectrum. *Hum Mutat*. 2010;31:992-1002.
20. Funk SD, Lin MH, Miner JH. Alport syndrome and Pierson syndrome: diseases of the glomerular basement membrane. *Matrix Biol*. 2018;71-72:250-261.
21. Gawlik KI, Durbeej M. Skeletal muscle laminin and MDC1A: pathogenesis and treatment strategies. *Skelet Muscle*. 2011;1:9.
22. Funk SD, Bayer RH, Malone AF, et al. Pathogenicity of a human laminin beta2 mutation revealed in models of Alport syndrome. *J Am Soc Nephrol*. 2018;29:949-960.
23. Shaw L, Sugden CJ, Hamill KJ. Laminin polymerization and inherited disease: lessons from genetics. *Front Genet*. 2021;12. 10.3389/fgene.2021.707087
24. Hamill KJ, Langbein L, Jones JC, McLean WH. Identification of a novel family of laminin N-terminal alternate splice isoforms: structural and functional characterization. *J Biol Chem*. 2009;284:35588-35596.
25. Hohenester E. Structural biology of laminins. *Essays Biochem*. 2019;63:285-295.
26. Yousif LF, Di Russo J, Sorokin L. Laminin isoforms in endothelial and perivascular basement membranes. *Cell Adh Migr*. 2013;7:101-110.
27. Hamill KJ, Kligys K, Hopkinson SB, Jones JC. Laminin deposition in the extracellular matrix: a complex picture emerges. *J Cell Sci*. 2009;122:4409-4417.
28. Rajasekharan S, Kennedy TE. The netrin protein family. *Genome Biol*. 2009;10:239.
29. Ettner N, Gohring W, Sasaki T, Mann K, Timpl R. The N-terminal globular domain of the laminin alpha1 chain binds to alpha-1beta1 and alpha2beta1 integrins and to the heparan sulfate-containing domains of perlecan. *FEBS Lett*. 1998;430:217-221.
30. Horejs C-M, Serio A, Purvis A, et al. Biologically-active laminin-111 fragment that modulates the epithelial-to-mesenchymal transition in embryonic stem cells. *Proc Natl Acad Sci USA*. 2014;111:5908-5913.
31. Kariya Y, Yasuda C, Nakashima Y, et al. Characterization of laminin 5B and NH2-terminal proteolytic fragment of its alpha3B chain: promotion of cellular adhesion, migration, and proliferation. *J Biol Chem*. 2004;279:24774-24784.
32. Sun KLW, Correia JP, Kennedy TE. Netrins: versatile extracellular cues with diverse functions. *Development*. 2011;138(11):2153-2169.
33. Reuten R, Patel TR, McDougall M, et al. Structural decoding of netrin-4 reveals a regulatory function towards mature basement membranes. *Nat Commun*. 2016;7:13515.
34. Schneiders FI, Maertens B, Boöse K, et al. Binding of netrin-4 to laminin short arms regulates basement membrane assembly. *J Biol Chem*. 2007;282:23750-23758.
35. Larrieu-Lahargue F, Welm AL, Thomas KR, Li DY. Netrin-4 induces lymphangiogenesis in vivo. *Blood*. 2010;115:5418-5426.
36. Barrera V, Troughton LD, Iorio V, et al. Differential distribution of laminin N-terminus alpha31 across the ocular surface:

implications for corneal wound repair. *Invest Ophthalmol Vis Sci*. 2018;59:4082-4093.
37. Troughton LD, Reuten R, Sugden CJ, Hamill KJ. Laminin N-terminus alpha31 protein distribution in adult human tissues. *PLoS One*. 2020;15:e0239889.
38. Troughton LD, O'Loughlin DA, Zech T, Hamill KJ. Laminin N-terminus α31 is upregulated in invasive ductal breast cancer and changes the mode of tumour invasion. *PLoS One*. 2022;17:e0264430.
39. Iorio V, Troughton LD, Barrera V, Hamill KJ. LaNt α31 modulates LM332 organisation during matrix deposition leading to cell-matrix adhesion and migration defects. *bioRxiv*, 2019;617597. 10.1101/617597
40. Di Russo J, Luik A-L, Yousif L, et al. Endothelial basement membrane laminin 511 is essential for shear stress response. *EMBO J*. 2017;36:1464.
41. Langhofer M, Hopkinson SB, Jones JC. The matrix secreted by 804G cells contains laminin-related components that participate in hemidesmosome assembly in vitro. *J Cell Sci*. 1993;105(Pt 3):753-764.
42. Pribnow D. Nucleotide sequence of an RNA polymerase binding site at an early T7 promoter. *Proc Natl Acad Sci USA*. 1975;72:784-788.
43. Kozak M. An analysis of 5'-noncoding sequences from 699 vertebrate messenger RNAs. *Nucleic Acids Res*. 1987;15:8125-8148.
44. Coloma MJ, Hastings A, Wims LA, Morrison SL. Novel vectors for the expression of antibody molecules using variable regions generated by polymerase chain reaction. *J Immunol Methods*. 1992;152:89-104.
45. Brizzard BL, Chubet RG, Vizard DL. Immunoaffinity purification of FLAG epitope-tagged bacterial alkaline phosphatase using a novel monoclonal antibody and peptide elution. *Biotechniques*. 1994;16:730-735.
46. Field J, Nikawa J, Broek D, et al. Purification of a RAS-responsive adenylyl cyclase complex from Saccharomyces cerevisiae by use of an epitope addition method. *Mol Cell Biol*. 1988;8:2159-2165.
47. Kim JH, Lee S-R, Li L-H, et al. High cleavage efficiency of a 2A peptide derived from porcine teschovirus-1 in human cell lines, zebrafish and mice. *PLoS One*. 2011;6:e18556.
48. Yuspa SH, Harris CC. Altered differentiation of mouse epidermal cells treated with retinyl acetate in vitro. *Exp Cell Res*. 1974;86:95-105.
49. Ittner LM, Gotz J. Pronuclear injection for the production of transgenic mice. *Nat Protoc*. 2007;2:1206-1215.
50. Ventura A, Kirsch DG, McLaughlin ME, et al. Restoration of p53 function leads to tumour regression in vivo. *Nature*. 2007;445:661-665.
51. Schneider CA, Rasband WS, Eliceiri KW. NIH Image to ImageJ: 25 years of image analysis. *Nat Methods*. 2012;9:671-675.
52. Schmidt U, Weigert M, Broaddus C, Myers G. Cell detection with star-convex polygons. In: Frangi A, Schnabel J, Davatzikos C, Alberola-López C, Fichtinger G, eds. *Medical Image Computing and Computer Assisted Intervention – MICCAI 2018. MICCAI 2018. Lecture Notes in Computer Science*. vol 11071. Springer; 2018.
53. Cheng K-W, Wang F, Lopez GA, et al. Evaluation of artificial signal peptides for secretion of two lysosomal enzymes in CHO cells. *Biochem J*. 2021;478:2309-2319.
54. Güler-Gane G, Kidd S, Sridharan S, et al. Overcoming the refractory expression of secreted recombinant proteins in mammalian cells through modification of the signal peptide and adjacent amino acids. *PLoS One*. 2016;11:e0155340.
55. Ido H, Ito S, Taniguchi Y, et al. Laminin isoforms containing the gamma3 chain are unable to bind to integrins due to the absence of the glutamic acid residue conserved in the C-terminal regions of the gamma1 and gamma2 chains. *J Biol Chem*. 2008;283:28149-28157.
56. Ochiai H, Harashima H, Kamiya H. Effects of insulator cHS4 on transgene expression from plasmid DNA in a positive feedback system. *J Biosci Bioeng*. 2011;112:432-434.
57. Zenker M, Aigner T, Wendler O, et al. Human laminin beta2 deficiency causes congenital nephrosis with mesangial sclerosis and distinct eye abnormalities. *Hum Mol Genet*. 2004;13:2625-2632.
58. Zenker M, Pierson M, Jonveaux P, Reis A. Demonstration of two novel LAMB2 mutations in the original Pierson syndrome family reported 42 years ago. *Am J Med Genet A*. 2005;138:73-74.
59. Hinkes BG, Mucha B, Vlangos CN, et al. Nephrotic syndrome in the first year of life: two thirds of cases are caused by mutations in 4 genes (NPHS1, NPHS2, WT1, and LAMB2). *Pediatrics*. 2007;119:e907-e919.
60. Chen YM, Kikkawa Y, Miner JH. A missense LAMB2 mutation causes congenital nephrotic syndrome by impairing laminin secretion. *J Am Soc Nephrol*. 2011;22:849-858.
61. Kiritsi D, Has C, Bruckner-Tuderman L. Laminin 332 in junctional epidermolysis bullosa. *Cell Adh Migr*. 2013;7:135-141.
62. McLean WH, Irvine AD, Hamill KJ, et al. An unusual N-terminal deletion of the laminin alpha3a isoform leads to the chronic granulation tissue disorder laryngo-onycho-cutaneous syndrome. *Hum Mol Genet*. 2003;12:2395-2409.
63. Barzegar M, Mozafari N, Kariminejad A, Asadikani Z, Ozoemena L, McGrath JA. A new homozygous nonsense mutation in LAMA3A underlying laryngo-onycho-cutaneous syndrome. *Br J Dermatol*. 2013;169:1353-1356.
64. Pierce RA, Griffin GL, Susan Mudd M, et al. Expression of laminin alpha3, alpha4, and alpha5 chains by alveolar epithelial cells and fibroblasts. *Am J Respir Cell Mol Biol*. 1998;19:237-244.
65. DeBiase PJ, Lane K, Budinger S, et al. Laminin-311 (Laminin-6) fiber assembly by type I-like alveolar cells. *J Histochem Cytochem*. 2006;54:665-672.
66. Morales-Nebreda LI, Rogel MR, Eisenberg JL, et al. Lung-specific loss of alpha3 laminin worsens bleomycin-induced pulmonary fibrosis. *Am J Respir Cell Mol Biol*. 2015;52:503-512.
67. Coulombe PA, Kopan R, Fuchs E. Expression of keratin K14 in the epidermis and hair follicle: insights into complex programs of differentiation. *J Cell Biol*. 1989;109:2295-2312.
68. Vasioukhin V, Degenstein L, Wise B, Fuchs E. The magical touch: genome targeting in epidermal stem cells induced by tamoxifen application to mouse skin. *Proc Natl Acad Sci USA*. 1999;96:8551-8556.
69. Wang X, Zinkel S, Polonsky K, Fuchs E. Transgenic studies with a keratin promoter-driven growth hormone transgene: prospects for gene therapy. *Proc Natl Acad Sci USA*. 1997;94:219-226.
70. Hafner M, Wenk J, Nenci A, et al. Keratin 14 Cre transgenic mice authenticate keratin 14 as an oocyte-expressed protein. *Genesis*. 2004;38:176-181.
71. Hussain SA, Carafoli F, Hohenester E. Determinants of laminin polymerization revealed by the structure of the alpha5 chain amino-terminal region. *EMBO Rep*. 2011;12:276-282.

72. Garbe JH, Gohring W, Mann K, Timpl R, Sasaki T. Complete sequence, recombinant analysis and binding to laminins and sulphated ligands of the N-terminal domains of laminin alpha3B and alpha5 chains. *Biochem J*. 2002;362:213-221.
73. Jones LK, Lam R, McKee KK, et al. A mutation affecting laminin alpha 5 polymerisation gives rise to a syndromic developmental disorder. *Development*. 2020. 10.1242/dev.189183
74. Noakes PG, Gautam M, Mudd J, Sanes JR, Merlie JP. Aberrant differentiation of neuromuscular junctions in mice lacking s-laminin/laminin beta 2. *Nature*. 1995;374:258-262.
75. Noakes PG, Miner JH, Gautam M, Cunningham JM, Sanes JR, Merlie JP. The renal glomerulus of mice lacking s-laminin/laminin beta 2: nephrosis despite molecular compensation by laminin beta 1. *Nat Genet*. 1995;10:400-406.
76. Miner JH, Go G, Cunningham J, Patton BL, Jarad G. Transgenic isolation of skeletal muscle and kidney defects in laminin beta2 mutant mice: implications for Pierson syndrome. *Development*. 2006;133:967-975.
77. Jarad G, Cunningham J, Shaw AS, Miner JH. Proteinuria precedes podocyte abnormalities inLamb2-/- mice, implicating the glomerular basement membrane as an albumin barrier. *J Clin Invest*. 2006;116:2272-2279.
78. Libby RT, Lavallee CR, Balkema GW, Brunken WJ, Hunter DD. Disruption of laminin beta2 chain production causes alterations in morphology and function in the CNS. *J Neurosci*. 1999;19:9399-9411.
79. Dénes V, Witkovsky P, Koch M, et al. Laminin deficits induce alterations in the development of dopaminergic neurons in the mouse retina. *Vis Neurosci*. 2007;24:549-562.
80. Hallmann R, Horn N, Selg M, et al. Expression and function of laminins in the embryonic and mature vasculature. *Physiol Rev*. 2005;85:979-1000.
81. Petajaniemi N, Korhonen M, Kortesmaa J, et al. Localization of laminin alpha4-chain in developing and adult human tissues. *J Histochem Cytochem*. 2002;50:1113-1130.
82. Vainionpää N, Bützow R, Hukkanen M, et al. Basement membrane protein distribution in LYVE-1-immunoreactive lymphatic vessels of normal tissues and ovarian carcinomas. *Cell Tissue Res*. 2007;328:317-328.
83. Moore MA, Metcalf D. Ontogeny of the haemopoietic system: yolk sac origin of in vivo and in vitro colony forming cells in the developing mouse embryo. *Br J Haematol*. 1970;18:279-296.
84. Sanchez MJ, Holmes A, Miles C, Dzierzak E. Characterization of the first definitive hematopoietic stem cells in the AGM and liver of the mouse embryo. *Immunity*. 1996;5:513-525.
85. Dzierzak E, Speck NA. Of lineage and legacy: the development of mammalian hematopoietic stem cells. *Nat Immunol*. 2008;9:129-136.
86. Qian H, Georges-Labouesse E, Nyström A, et al. Distinct roles of integrins alpha6 and alpha4 in homing of fetal liver hematopoietic stem and progenitor cells. *Blood*. 2007;110:2399-2407.
87. Potocnik AJ, Brakebusch C, Fassler R. Fetal and adult hematopoietic stem cells require beta1 integrin function for colonizing fetal liver, spleen, and bone marrow. *Immunity*. 2000;12:653-663.
88. Hirsch E, Iglesias A, Potocnik AJ, Hartmann U, Fassler R. Impaired migration but not differentiation of haematopoietic stem cells in the absence of beta1 integrins. *Nature*. 1996;380:171-175.
89. Staquicini FI, Dias-Neto E, Li J, et al. Discovery of a functional protein complex of netrin-4, laminin gamma1 chain, and integrin alpha6beta1 in mouse neural stem cells. *Proc Natl Acad Sci USA*. 2009;106:2903-2908.
90. Reuten R, Zendehroud S, Nicolau M, et al. Basement membrane stiffness determines metastases formation. *Nat Mater*. 2021;20(6):892-903.
91. Sher I, Zisman-Rozen S, Eliahu L, et al. Targeting perlecan in human keratinocytes reveals novel roles for perlecan in epidermal formation. *J Biol Chem*. 2006;281:5178-5187.
92. Penton CM, Badarinarayana V, Prisco J, et al. Laminin 521 maintains differentiation potential of mouse and human satellite cell-derived myoblasts during long-term culture expansion. *Skelet Muscle*. 2016;6:44.
93. Kiyozumi D, Nakano I, Sato-Nishiuchi R, Tanaka S, Sekiguchi K. Laminin is the ECM niche for trophoblast stem cells. *Life Sci Alliance*. 2020;3:e201900515.
94. Rodin S, Domogatskaya A, Ström S, et al. Long-term self-renewal of human pluripotent stem cells on human recombinant laminin-511. *Nat Biotechnol*. 2010;28:611-615.
95. Polisetti N, Sorokin L, Okumura N, et al. Laminin-511 and -521-based matrices for efficient ex vivo-expansion of human limbal epithelial progenitor cells. *Sci Rep*. 2017;7:5152.
96. Sunada Y, Edgar TS, Lotz BP, Rust RS, Campbell KP. Merosin-negative congenital muscular dystrophy associated with extensive brain abnormalities. *Neurology*. 1995;45:2084-2089.
97. Xu H, Wu XR, Wewer UM, Engvall E. Murine muscular dystrophy caused by a mutation in the laminin alpha 2 (Lama2) gene. *Nat Genet*. 1994;8:297-302.
98. Payne S, De Val S, Neal A. Endothelial-specific Cre mouse models. *Arterioscler Thromb Vasc Biol*. 2018;38:2550-2561.
99. Patton BL, Wang B, Tarumi YS, Seburn KL, Burgess RW. A single point mutation in the LN domain of LAMA2 causes muscular dystrophy and peripheral amyelination. *J Cell Sci*. 2008;121:1593-1604.
100. Yurchenco PD, McKee KK, Reinhard JR, Ruegg MA. Laminin-deficient muscular dystrophy: molecular pathogenesis and structural repair strategies. *Matrix Biol*. 2018;71-72:174-187.
101. Poulos MG, Batra R, Charizanis K, Swanson MS. Developments in RNA splicing and disease. *Cold Spring Harb Perspect Biol*. 2011;3:a000778.
102. Baralle FE, Giudice J. Alternative splicing as a regulator of development and tissue identity. *Nat Rev Mol Cell Biol*. 2017;18:437-451.
103. Ffrench-Constant C, Van de Water L, Dvorak HF, Hynes RO. Reappearance of an embryonic pattern of fibronectin splicing during wound healing in the adult rat. *J Cell Biol*. 1989;109:903-914.

SUPPORTING INFORMATION

Additional supporting information may be found in the online version of the article at the publisher's website.

How to cite this article: Sugden CJ, Iorio V, Troughton LD, et al. Laminin N-terminus α31 expression during development is lethal and causes widespread tissue-specific defects in a transgenic mouse model. *FASEB J*. 2022;36:e22318. doi:10.1096/fj.202002588RRR

Appendix VII: Cryopreservation records of LaNt α31 transgenic mouse lines.

Liverpool Cryopreservation Record

Date: 24/01/19
Name of User: Conor/GBG

Strain Name: Ubc-LaNt (Line 7.5)
Age of Male:
Age of Female: 8-10 wks
Time of PMS/hCG: 12:30pm/1pm
No. of Male/Female: 4/6
No. of females plugged: 3
No. of embryos collected/frozen: 56/90 2-cells (1st medium)

Storage Bank:
Can: 10
Cane: 43
Vial: 43-1, 43-2
Contents: 28, 28
Date removed:

Method:
Simple Vitrification of Mouse Embryos
http://card.medic.kumamoto-u.ac.jp/card/english/sigen/manual/ebvitri.htm

Liverpool Cryopreservation Record

Date: 28/02/19
Name of User: Conor/GBG

Strain Name: Ubc-LaNt (Line 3.1)
Age of Male:
Age of Female: 8-10 wks
Time of PMS/hCG: 12:30pm/1pm
No. of Male/Female: 8/8
No. of females plugged: 5
No. of embryos collected/frozen: 120/120 1-cell (1st) The embryos looked like fertilised 44-1-3
100/100 1 cell (1st) The embryos looked like fertilised 45-1

Storage Bank:
Can: 6
Cane: 44
Vial: 44-1, 44-2, 44-3, 45-1

Contents: 40, 40, 40, 100
Date removed:

Method:
Simple Vitrification of Mouse Embryos
http://card.medic.kumamoto-u.ac.jp/card/english/sigen/manual/ebvitri.htm

Liverpool Cryopreservation Record

Date: 05/09/19
Name of User: Conor/GBG

Strain Name: UBCLaNTRoseCre (Line 9.3)
Age of Male:
Age of Female: 7 wks
Time of PMS/hCG: 12:30pm/1pm
No. of Male/Female:9/9
No. of females plugged: 6
No. of embryos collected/frozen: 200/140 1-cell (1st)
Storage Bank: 2
Can: 6
Cane: 54 & 55
Vial: 54-1, 54-2, 55-1, 55-2
Contents: 35, 35, 35, 35
Date removed:

Method:
Simple Vitrification of Mouse Embryos
http://card.medic.kumamoto-u.ac.jp/card/english/sigen/manual/ebvitri.htm

Reference list

1 Yamada, K. M. *et al.* Extracellular matrix dynamics in cell migration, invasion and tissue morphogenesis. *Int J Exp Pathol* **100**, 144-152, doi:10.1111/iep.12329 (2019).

2 Sekiguchi, R. & Yamada, K. M. Basement Membranes in Development and Disease. *Curr Top Dev Biol* **130**, 143-191, doi:10.1016/bs.ctdb.2018.02.005 (2018).

3 Yurchenco, P. D. Basement membranes: cell scaffoldings and signaling platforms. *Cold Spring Harb Perspect Biol* **3**, doi:10.1101/cshperspect.a004911 (2011).

4 Pozzi, A., Yurchenco, P. D. & Iozzo, R. V. The nature and biology of basement membranes. *Matrix Biol* **57-58**, 1-11, doi:10.1016/j.matbio.2016.12.009 (2017).

5 Walma, D. A. C. & Yamada, K. M. The extracellular matrix in development. *Development* **147**, doi:10.1242/dev.175596 (2020).

6 Morrissey, M. A. & Sherwood, D. R. An active role for basement membrane assembly and modification in tissue sculpting. *J Cell Sci* **128**, 1661-1668, doi:10.1242/jcs.168021 (2015).

7 Theocharis, A. D., Skandalis, S. S., Gialeli, C. & Karamanos, N. K. Extracellular matrix structure. *Adv Drug Deliv Rev* **97**, 4-27, doi:10.1016/j.addr.2015.11.001 (2016).

8 Yurchenco, P. D., Tsilibary, E. C., Charonis, A. S. & Furthmayr, H. Laminin polymerization in vitro. Evidence for a two-step assembly with domain specificity. *J Biol Chem* **260**, 7636-7644 (1985).

9 Purvis, A. & Hohenester, E. Laminin network formation studied by reconstitution of ternary nodes in solution. *J Biol Chem* **287**, 44270-44277, doi:10.1074/jbc.M112.418426 (2012).

10 Paulsson, M. Basement membrane proteins: structure, assembly, and cellular interactions. *Crit Rev Biochem Mol Biol* **27**, 93-127, doi:10.3109/10409239209082560 (1992).

11 Khalilgharibi, N. & Mao, Y. To form and function: on the role of basement membrane mechanics in tissue development, homeostasis and disease. *Open Biol* **11**, 200360, doi:10.1098/rsob.200360 (2021).

12 McCarthy, K. J. The Basement Membrane Proteoglycans Perlecan and Agrin: Something Old, Something New. *Curr Top Membr* **76**, 255-303, doi:10.1016/bs.ctm.2015.09.001 (2015).

13 Mayer, U., Kohfeldt, E. & Timpl, R. Structural and genetic analysis of laminin-nidogen interaction. *Ann N Y Acad Sci* **857**, 130-142, doi:10.1111/j.1749-6632.1998.tb10113.x (1998).

14 Dziadek, M. Role of laminin-nidogen complexes in basement membrane formation during embryonic development. *Experientia* **51**, 901-913, doi:10.1007/BF01921740 (1995).

15 Farach-Carson, M. C. & Carson, D. D. Perlecan--a multifunctional extracellular proteoglycan scaffold. *Glycobiology* **17**, 897-905, doi:10.1093/glycob/cwm043 (2007).
16 Noonan, D. M. *et al.* The complete sequence of perlecan, a basement membrane heparan sulfate proteoglycan, reveals extensive similarity with laminin A chain, low density lipoprotein-receptor, and the neural cell adhesion molecule. *J Biol Chem* **266**, 22939-22947 (1991).
17 Henry, M. D. *et al.* Distinct roles for dystroglycan, beta1 integrin and perlecan in cell surface laminin organization. *J Cell Sci* **114**, 1137-1144, doi:10.1242/jcs.114.6.1137 (2001).
18 Khoshnoodi, J., Pedchenko, V. & Hudson, B. G. Mammalian collagen IV. *Microsc Res Tech* **71**, 357-370, doi:10.1002/jemt.20564 (2008).
19 Timpl, R., Wiedemann, H., van Delden, V., Furthmayr, H. & Kuhn, K. A network model for the organization of type IV collagen molecules in basement membranes. *Eur J Biochem* **120**, 203-211, doi:10.1111/j.1432-1033.1981.tb05690.x (1981).
20 Johansson, C., Butkowski, R. & Wieslander, J. The structural organization of type IV collagen. Identification of three NC1 populations in the glomerular basement membrane. *J Biol Chem* **267**, 24533-24537 (1992).
21 Vandenberg, P. *et al.* Characterization of a type IV collagen major cell binding site with affinity to the alpha 1 beta 1 and the alpha 2 beta 1 integrins. *J Cell Biol* **113**, 1475-1483, doi:10.1083/jcb.113.6.1475 (1991).
22 Yurchenco, P. D. & Furthmayr, H. Self-assembly of basement membrane collagen. *Biochemistry* **23**, 1839-1850, doi:10.1021/bi00303a040 (1984).
23 Miner, J. H. & Yurchenco, P. D. Laminin functions in tissue morphogenesis. *Annu Rev Cell Dev Biol* **20**, 255-284, doi:10.1146/annurev.cellbio.20.010403.094555 (2004).
24 Tryggvason, K. The laminin family. *Curr Opin Cell Biol* **5**, 877-882, doi:10.1016/0955-0674(93)90038-r (1993).
25 Aumailley, M. The laminin family. *Cell Adh Migr* **7**, 48-55, doi:10.4161/cam.22826 (2013).
26 Yurchenco, P. D. & Cheng, Y. S. Self-assembly and calcium-binding sites in laminin. A three-arm interaction model. *J Biol Chem* **268**, 17286-17299 (1993).
27 Colognato, H., MacCarrick, M., O'Rear, J. J. & Yurchenco, P. D. The laminin alpha2-chain short arm mediates cell adhesion through both the alpha1beta1 and alpha2beta1 integrins. *J Biol Chem* **272**, 29330-29336, doi:10.1074/jbc.272.46.29330 (1997).
28 Scheele, S. *et al.* Laminin isoforms in development and disease. *J Mol Med (Berl)* **85**, 825-836, doi:10.1007/s00109-007-0182-5 (2007).
29 Tzu, J. & Marinkovich, M. P. Bridging structure with function: structural, regulatory, and developmental role of laminins. *Int J Biochem Cell Biol* **40**, 199-214, doi:10.1016/j.biocel.2007.07.015 (2008).
30 Wiradjaja, F., DiTommaso, T. & Smyth, I. Basement membranes in development and disease. *Birth Defects Res C Embryo Today* **90**, 8-31, doi:10.1002/bdrc.20172 (2010).

31 Hohenester, E. Structural biology of laminins. *Essays Biochem* **63**, 285-295, doi:10.1042/EBC20180075 (2019).
32 Beck, K., Hunter, I. & Engel, J. Structure and function of laminin: anatomy of a multidomain glycoprotein. *FASEB J* **4**, 148-160, doi:10.1096/fasebj.4.2.2404817 (1990).
33 Timpl, R. *et al.* Structure and function of laminin LG modules. *Matrix Biol* **19**, 309-317, doi:10.1016/s0945-053x(00)00072-x (2000).
34 Dempsey, C. E., Bigotti, M. G., Adams, J. C. & Brancaccio, A. Analysis of alpha-Dystroglycan/LG Domain Binding Modes: Investigating Protein Motifs That Regulate the Affinity of Isolated LG Domains. *Front Mol Biosci* **6**, 18, doi:10.3389/fmolb.2019.00018 (2019).
35 Armony, G. *et al.* Cross-linking reveals laminin coiled-coil architecture. *Proc Natl Acad Sci U S A* **113**, 13384-13389, doi:10.1073/pnas.1608424113 (2016).
36 Nomizu, M. *et al.* Mechanism of laminin chain assembly into a triple-stranded coiled-coil structure. *Biochemistry* **35**, 2885-2893, doi:10.1021/bi951555n (1996).
37 Macdonald, P. R., Lustig, A., Steinmetz, M. O. & Kammerer, R. A. Laminin chain assembly is regulated by specific coiled-coil interactions. *J Struct Biol* **170**, 398-405, doi:10.1016/j.jsb.2010.02.004 (2010).
38 Yurchenco, P. D. *et al.* The alpha chain of laminin-1 is independently secreted and drives secretion of its beta- and gamma-chain partners. *Proc Natl Acad Sci U S A* **94**, 10189-10194, doi:10.1073/pnas.94.19.10189 (1997).
39 Peters, B. P. *et al.* The biosynthesis, processing, and secretion of laminin by human choriocarcinoma cells. *J Biol Chem* **260**, 14732-14742 (1985).
40 Tsubota, Y., Ogawa, T., Oyanagi, J., Nagashima, Y. & Miyazaki, K. Expression of laminin gamma2 chain monomer enhances invasive growth of human carcinoma cells in vivo. *Int J Cancer* **127**, 2031-2041, doi:10.1002/ijc.25231 (2010).
41 Moran, T., Gat, Y. & Fass, D. Laminin L4 domain structure resembles adhesion modules in ephrin receptor and other transmembrane glycoproteins. *FEBS J* **282**, 2746-2757, doi:10.1111/febs.13319 (2015).
42 Engvall, E. & Wewer, U. M. Domains of laminin. *J Cell Biochem* **61**, 493-501, doi:10.1002/(SICI)1097-4644(19960616)61:4%3C493::AID-JCB2%3E3.0.CO;2-J (1996).
43 Rajasekharan, S. & Kennedy, T. E. The netrin protein family. *Genome Biol* **10**, 239, doi:10.1186/gb-2009-10-9-239 (2009).
44 Panayotou, G., End, P., Aumailley, M., Timpl, R. & Engel, J. Domains of laminin with growth-factor activity. *Cell* **56**, 93-101, doi:10.1016/0092-8674(89)90987-2 (1989).
45 Schenk, S. *et al.* Binding to EGF receptor of a laminin-5 EGF-like fragment liberated during MMP-dependent mammary gland involution. *J Cell Biol* **161**, 197-209, doi:10.1083/jcb.200208145 (2003).
46 Garbe, J. H., Gohring, W., Mann, K., Timpl, R. & Sasaki, T. Complete sequence, recombinant analysis and binding to laminins and sulphated ligands of the N-terminal domains of laminin alpha3B and alpha5 chains. *Biochem J* **362**, 213-221, doi:10.1042/0264-6021:3620213 (2002).

47 Yurchenco, P. D. & Cheng, Y. S. Laminin self-assembly: a three-arm interaction hypothesis for the formation of a network in basement membranes. *Contrib Nephrol* **107**, 47-56, doi:10.1159/000422960 (1994).
48 Hohenester, E. & Yurchenco, P. D. Laminins in basement membrane assembly. *Cell Adh Migr* **7**, 56-63, doi:10.4161/cam.21831 (2013).
49 McKee, K. K., Harrison, D., Capizzi, S. & Yurchenco, P. D. Role of laminin terminal globular domains in basement membrane assembly. *J Biol Chem* **282**, 21437-21447, doi:10.1074/jbc.M702963200 (2007).
50 Hussain, S. A., Carafoli, F. & Hohenester, E. Determinants of laminin polymerization revealed by the structure of the alpha5 chain amino-terminal region. *EMBO Rep* **12**, 276-282, doi:10.1038/embor.2011.3 (2011).
51 Hamill, K. J., Langbein, L., Jones, J. C. & McLean, W. H. Identification of a novel family of laminin N-terminal alternate splice isoforms: structural and functional characterization. *J Biol Chem* **284**, 35588-35596, doi:10.1074/jbc.M109.052811 (2009).
52 Troughton, L. D., Reuten, R., Sugden, C. J. & Hamill, K. J. Laminin N-terminus alpha31 protein distribution in adult human tissues. *PLoS One* **15**, e0239889, doi:10.1371/journal.pone.0239889 (2020).
53 Barrera, V. *et al.* Differential Distribution of Laminin N-Terminus alpha31 Across the Ocular Surface: Implications for Corneal Wound Repair. *Invest Ophthalmol Vis Sci* **59**, 4082-4093, doi:10.1167/iovs.18-24037 (2018).
54 Troughton, L. D. *et al.* Laminin N-terminus α31 regulates keratinocyte adhesion and migration through modifying the organization and proteolytic processing of laminin 332. *bioRxiv*, 617597, doi:10.1101/617597 (2020).
55 Troughton, L. D., O'Loughlin, D. A., Zech, T. & Hamill, K. J. Laminin N-terminus α31 is upregulated in invasive ductal breast cancer and changes the mode of tumour invasion. *PLOS ONE* **17**, e0264430, doi:10.1371/journal.pone.0264430 (2022).
56 Carafoli, F., Hussain, S. A. & Hohenester, E. Crystal structures of the network-forming short-arm tips of the laminin beta1 and gamma1 chains. *PLoS One* **7**, e42473, doi:10.1371/journal.pone.0042473 (2012).
57 McKee, K. K., Hohenester, E., Aleksandrova, M. & Yurchenco, P. D. Organization of the laminin polymer node. *Matrix Biol* **98**, 49-63, doi:10.1016/j.matbio.2021.05.004 (2021).
58 Reuten, R. *et al.* Structural decoding of netrin-4 reveals a regulatory function towards mature basement membranes. *Nat Commun* **7**, 13515, doi:10.1038/ncomms13515 (2016).
59 Hamill, K. J., Kligys, K., Hopkinson, S. B. & Jones, J. C. Laminin deposition in the extracellular matrix: a complex picture emerges. *J Cell Sci* **122**, 4409-4417, doi:10.1242/jcs.041095 (2009).
60 Yousif, L. F., Di Russo, J. & Sorokin, L. Laminin isoforms in endothelial and perivascular basement membranes. *Cell Adh Migr* **7**, 101-110, doi:10.4161/cam.22680 (2013).
61 Champliaud, M. F. *et al.* Human amnion contains a novel laminin variant, laminin 7, which like laminin 6, covalently associates with laminin 5 to promote stable epithelial-stromal attachment. *J Cell Biol* **132**, 1189-1198, doi:10.1083/jcb.132.6.1189 (1996).

62 Brittingham, R., Uitto, J. & Fertala, A. High-affinity binding of the NC1 domain of collagen VII to laminin 5 and collagen IV. *Biochem Biophys Res Commun* **343**, 692-699, doi:10.1016/j.bbrc.2006.03.034 (2006).
63 Nishie, W., Kiritsi, D., Nystrom, A., Hofmann, S. C. & Bruckner-Tuderman, L. Dynamic interactions of epidermal collagen XVII with the extracellular matrix: laminin 332 as a major binding partner. *Am J Pathol* **179**, 829-837, doi:10.1016/j.ajpath.2011.04.019 (2011).
64 Utani, A., Nomizu, M. & Yamada, Y. Fibulin-2 binds to the short arms of laminin-5 and laminin-1 via conserved amino acid sequences. *J Biol Chem* **272**, 2814-2820, doi:10.1074/jbc.272.5.2814 (1997).
65 Rousselle, P. & Beck, K. Laminin 332 processing impacts cellular behavior. *Cell Adh Migr* **7**, 122-134, doi:10.4161/cam.23132 (2013).
66 Nishiuchi, R. *et al.* Ligand-binding specificities of laminin-binding integrins: a comprehensive survey of laminin-integrin interactions using recombinant alpha3beta1, alpha6beta1, alpha7beta1 and alpha6beta4 integrins. *Matrix Biol* **25**, 189-197, doi:10.1016/j.matbio.2005.12.001 (2006).
67 Humphries, M. J. Insights into integrin-ligand binding and activation from the first crystal structure. *Arthritis Res* **4 Suppl 3**, S69-78, doi:10.1186/ar563 (2002).
68 Schiro, J. A. *et al.* Integrin alpha 2 beta 1 (VLA-2) mediates reorganization and contraction of collagen matrices by human cells. *Cell* **67**, 403-410, doi:10.1016/0092-8674(91)90191-z (1991).
69 Elices, M. J. & Hemler, M. E. The human integrin VLA-2 is a collagen receptor on some cells and a collagen/laminin receptor on others. *Proc Natl Acad Sci U S A* **86**, 9906-9910, doi:10.1073/pnas.86.24.9906 (1989).
70 Belkin, A. M. & Stepp, M. A. Integrins as receptors for laminins. *Microsc Res Tech* **51**, 280-301, doi:10.1002/1097-0029(20001101)51:3<280::AID-JEMT7>3.0.CO;2-O (2000).
71 von der Mark, H. *et al.* Alternative splice variants of alpha 7 beta 1 integrin selectively recognize different laminin isoforms. *J Biol Chem* **277**, 6012-6016, doi:10.1074/jbc.M102188200 (2002).
72 von der Mark, H. *et al.* Distinct acidic clusters and hydrophobic residues in the alternative splice domains X1 and X2 of alpha7 integrins define specificity for laminin isoforms. *J Mol Biol* **371**, 1188-1203, doi:10.1016/j.jmb.2007.05.074 (2007).
73 Wu, C., Chung, A. E. & McDonald, J. A. A novel role for alpha 3 beta 1 integrins in extracellular matrix assembly. *J Cell Sci* **108 (Pt 6)**, 2511-2523, doi:10.1242/jcs.108.6.2511 (1995).
74 Jones, J. C., Kurpakus, M. A., Cooper, H. M. & Quaranta, V. A function for the integrin alpha 6 beta 4 in the hemidesmosome. *Cell Regul* **2**, 427-438, doi:10.1091/mbc.2.6.427 (1991).
75 Hall, D. E. *et al.* The alpha 1/beta 1 and alpha 6/beta 1 integrin heterodimers mediate cell attachment to distinct sites on laminin. *J Cell Biol* **110**, 2175-2184, doi:10.1083/jcb.110.6.2175 (1990).
76 Chang, A. C. *et al.* Alpha 3 beta 1 and alpha 6 beta 1 integrins mediate laminin/merosin binding and function as costimulatory molecules for human thymocyte proliferation. *J Immunol* **154**, 500-510 (1995).

77 Ettner, N., Gohring, W., Sasaki, T., Mann, K. & Timpl, R. The N-terminal globular domain of the laminin alpha1 chain binds to alpha1beta1 and alpha2beta1 integrins and to the heparan sulfate-containing domains of perlecan. *FEBS Lett* **430**, 217-221, doi:10.1016/s0014-5793(98)00601-2 (1998).
78 Horejs, C. M. *et al.* Biologically-active laminin-111 fragment that modulates the epithelial-to-mesenchymal transition in embryonic stem cells. *Proc Natl Acad Sci U S A* **111**, 5908-5913, doi:10.1073/pnas.1403139111 (2014).
79 Kariya, Y. *et al.* Characterization of laminin 5B and NH2-terminal proteolytic fragment of its alpha3B chain: promotion of cellular adhesion, migration, and proliferation. *J Biol Chem* **279**, 24774-24784, doi:10.1074/jbc.M400670200 (2004).
80 Staquicini, F. I. *et al.* Discovery of a functional protein complex of netrin-4, laminin gamma1 chain, and integrin alpha6beta1 in mouse neural stem cells. *Proc Natl Acad Sci U S A* **106**, 2903-2908, doi:10.1073/pnas.0813286106 (2009).
81 Georges-Labouesse, E. *et al.* Absence of integrin alpha 6 leads to epidermolysis bullosa and neonatal death in mice. *Nat Genet* **13**, 370-373, doi:10.1038/ng0796-370 (1996).
82 Guo, C. *et al.* Absence of alpha 7 integrin in dystrophin-deficient mice causes a myopathy similar to Duchenne muscular dystrophy. *Hum Mol Genet* **15**, 989-998, doi:10.1093/hmg/ddl018 (2006).
83 Fassler, R. & Meyer, M. Consequences of lack of beta 1 integrin gene expression in mice. *Genes Dev* **9**, 1896-1908, doi:10.1101/gad.9.15.1896 (1995).
84 Pulkkinen, L. & Uitto, J. Mutation analysis and molecular genetics of epidermolysis bullosa. *Matrix Biol* **18**, 29-42, doi:10.1016/s0945-053x(98)00005-5 (1999).
85 Cloutier, G., Sallenbach-Morrissette, A. & Beaulieu, J. F. Non-integrin laminin receptors in epithelia. *Tissue Cell* **56**, 71-78, doi:10.1016/j.tice.2018.12.005 (2019).
86 Barresi, R. & Campbell, K. P. Dystroglycan: from biosynthesis to pathogenesis of human disease. *J Cell Sci* **119**, 199-207, doi:10.1242/jcs.02814 (2006).
87 Godfrey, C., Foley, A. R., Clement, E. & Muntoni, F. Dystroglycanopathies: coming into focus. *Curr Opin Genet Dev* **21**, 278-285, doi:10.1016/j.gde.2011.02.001 (2011).
88 Carulli, S. *et al.* Cell surface proteoglycans syndecan-1 and -4 bind overlapping but distinct sites in laminin alpha3 LG45 protein domain. *J Biol Chem* **287**, 12204-12216, doi:10.1074/jbc.M111.300061 (2012).
89 Saunders, S., Jalkanen, M., O'Farrell, S. & Bernfield, M. Molecular cloning of syndecan, an integral membrane proteoglycan. *J Cell Biol* **108**, 1547-1556, doi:10.1083/jcb.108.4.1547 (1989).
90 Marynen, P., Zhang, J., Cassiman, J. J., Van den Berghe, H. & David, G. Partial primary structure of the 48- and 90-kilodalton core proteins of cell surface-associated heparan sulfate proteoglycans of lung fibroblasts. Prediction of an integral membrane domain and evidence for multiple distinct core

proteins at the cell surface of human lung fibroblasts. *J Biol Chem* **264**, 7017-7024 (1989).
91 Bernfield, M. *et al.* Biology of the syndecans: a family of transmembrane heparan sulfate proteoglycans. *Annu Rev Cell Biol* **8**, 365-393, doi:10.1146/annurev.cb.08.110192.002053 (1992).
92 Gould, S. E., Upholt, W. B. & Kosher, R. A. Syndecan 3: a member of the syndecan family of membrane-intercalated proteoglycans that is expressed in high amounts at the onset of chicken limb cartilage differentiation. *Proc Natl Acad Sci U S A* **89**, 3271-3275, doi:10.1073/pnas.89.8.3271 (1992).
93 Kojima, T. *et al.* Plasma levels of syndecan-4 (ryudocan) are elevated in patients with acute myocardial infarction. *Thromb Haemost* **85**, 793-799 (2001).
94 Spring, J. *et al.* Mapping of the syndecan genes in the mouse: linkage with members of the myc gene family. *Genomics* **21**, 597-601, doi:10.1006/geno.1994.1319 (1994).
95 Spring, J., Paine-Saunders, S. E., Hynes, R. O. & Bernfield, M. Drosophila syndecan: conservation of a cell-surface heparan sulfate proteoglycan. *Proc Natl Acad Sci U S A* **91**, 3334-3338, doi:10.1073/pnas.91.8.3334 (1994).
96 Bass, M. D., Morgan, M. R. & Humphries, M. J. Integrins and syndecan-4 make distinct, but critical, contributions to adhesion contact formation. *Soft Matter* **3**, 372-376, doi:10.1039/b614610d (2007).
97 Wang, X. *et al.* Shed Syndecan-1 is involved in chemotherapy resistance via the EGFR pathway in colorectal cancer. *Br J Cancer* **111**, 1965-1976, doi:10.1038/bjc.2014.493 (2014).
98 Hozumi, K., Suzuki, N., Nielsen, P. K., Nomizu, M. & Yamada, Y. Laminin alpha1 chain LG4 module promotes cell attachment through syndecans and cell spreading through integrin alpha2beta1. *J Biol Chem* **281**, 32929-32940, doi:10.1074/jbc.M605708200 (2006).
99 Ogawa, T., Tsubota, Y., Hashimoto, J., Kariya, Y. & Miyazaki, K. The short arm of laminin gamma2 chain of laminin-5 (laminin-332) binds syndecan-1 and regulates cellular adhesion and migration by suppressing phosphorylation of integrin beta4 chain. *Mol Biol Cell* **18**, 1621-1633, doi:10.1091/mbc.e06-09-0806 (2007).
100 Okamoto, O. *et al.* Normal human keratinocytes bind to the alpha3LG4/5 domain of unprocessed laminin-5 through the receptor syndecan-1. *J Biol Chem* **278**, 44168-44177, doi:10.1074/jbc.M300726200 (2003).
101 Couchman, J. R. & Woods, A. Syndecan-4 and integrins: combinatorial signaling in cell adhesion. *J Cell Sci* **112 (Pt 20)**, 3415-3420, doi:10.1242/jcs.112.20.3415 (1999).
102 Araki, E. *et al.* Clustering of syndecan-4 and integrin beta1 by laminin alpha 3 chain-derived peptide promotes keratinocyte migration. *Mol Biol Cell* **20**, 3012-3024, doi:10.1091/mbc.E08-09-0977 (2009).
103 Echtermeyer, F. *et al.* Delayed wound repair and impaired angiogenesis in mice lacking syndecan-4. *J Clin Invest* **107**, R9-R14, doi:10.1172/JCI10559 (2001).
104 Elenius, V., Gotte, M., Reizes, O., Elenius, K. & Bernfield, M. Inhibition by the soluble syndecan-1 ectodomains delays wound repair in mice

overexpressing syndecan-1. *J Biol Chem* **279**, 41928-41935, doi:10.1074/jbc.M404506200 (2004).
105 Vanhoutte, D. *et al.* Increased expression of syndecan-1 protects against cardiac dilatation and dysfunction after myocardial infarction. *Circulation* **115**, 475-482, doi:10.1161/CIRCULATIONAHA.106.644609 (2007).
106 Nelson, J. *et al.* The 67 kDa laminin receptor: structure, function and role in disease. *Biosci Rep* **28**, 33-48, doi:10.1042/BSR20070004 (2008).
107 Rao, C. N. *et al.* Evidence for a precursor of the high-affinity metastasis-associated murine laminin receptor. *Biochemistry* **28**, 7476-7486, doi:10.1021/bi00444a047 (1989).
108 Romanov, V. I., Wrathall, L. S., Simmons, T. D., Pinto da Silva, P. & Sobel, M. E. Protein synthesis is required for laminin-induced expression of the 67-kDa laminin receptor and its 37-kDa precursor. *Biochem Biophys Res Commun* **208**, 637-643, doi:10.1006/bbrc.1995.1386 (1995).
109 Menard, S., Castronovo, V., Tagliabue, E. & Sobel, M. E. New insights into the metastasis-associated 67 kD laminin receptor. *J Cell Biochem* **67**, 155-165 (1997).
110 Mafune, K. & Ravikumar, T. S. Anti-sense RNA of 32-kDa laminin-binding protein inhibits attachment and invasion of a human colon carcinoma cell line. *J Surg Res* **52**, 340-346, doi:10.1016/0022-4804(92)90113-e (1992).
111 Canfield, S. M. & Khakoo, A. Y. The nonintegrin laminin binding protein (p67 LBP) is expressed on a subset of activated human T lymphocytes and, together with the integrin very late activation antigen-6, mediates avid cellular adherence to laminin. *J Immunol* **163**, 3430-3440 (1999).
112 Satoh, K. *et al.* Diminution of 37-kDa laminin binding protein expression reduces tumour formation of murine lung cancer cells. *Br J Cancer* **80**, 1115-1122, doi:10.1038/sj.bjc.6690474 (1999).
113 Tanaka, M. *et al.* Expression of the 37-kDa laminin binding protein in murine lung tumor cell correlates with tumor angiogenesis. *Cancer Lett* **153**, 161-168, doi:10.1016/s0304-3835(00)00365-7 (2000).
114 Yap, L., Tay, H. G., Nguyen, M. T. X., Tjin, M. S. & Tryggvason, K. Laminins in Cellular Differentiation. *Trends Cell Biol* **29**, 987-1000, doi:10.1016/j.tcb.2019.10.001 (2019).
115 Fidler, A. L., Boudko, S. P., Rokas, A. & Hudson, B. G. The triple helix of collagens - an ancient protein structure that enabled animal multicellularity and tissue evolution. *J Cell Sci* **131**, doi:10.1242/jcs.203950 (2018).
116 Pook, M. *et al.* Changes in Laminin Expression Pattern during Early Differentiation of Human Embryonic Stem Cells. *PLoS One* **10**, e0138346, doi:10.1371/journal.pone.0138346 (2015).
117 Noakes, P. G., Gautam, M., Mudd, J., Sanes, J. R. & Merlie, J. P. Aberrant differentiation of neuromuscular junctions in mice lacking s-laminin/laminin beta 2. *Nature* **374**, 258-262, doi:10.1038/374258a0 (1995).
118 Patton, B. L., Miner, J. H., Chiu, A. Y. & Sanes, J. R. Distribution and function of laminins in the neuromuscular system of developing, adult, and mutant mice. *J Cell Biol* **139**, 1507-1521, doi:10.1083/jcb.139.6.1507 (1997).

119 Noakes, P. G. *et al.* The renal glomerulus of mice lacking s-laminin/laminin beta 2: nephrosis despite molecular compensation by laminin beta 1. *Nat Genet* **10**, 400-406, doi:10.1038/ng0895-400 (1995).
120 Aumailley, M. & Rousselle, P. Laminins of the dermo-epidermal junction. *Matrix Biol* **18**, 19-28, doi:10.1016/s0945-053x(98)00004-3 (1999).
121 Miner, J. H. *et al.* The laminin alpha chains: expression, developmental transitions, and chromosomal locations of alpha1-5, identification of heterotrimeric laminins 8-11, and cloning of a novel alpha3 isoform. *J Cell Biol* **137**, 685-701, doi:10.1083/jcb.137.3.685 (1997).
122 Hallmann, R. *et al.* Expression and function of laminins in the embryonic and mature vasculature. *Physiol Rev* **85**, 979-1000, doi:10.1152/physrev.00014.2004 (2005).
123 Nystrom, A., Holmblad, J., Pedrosa-Domellof, F., Sasaki, T. & Durbeej, M. Extraocular muscle is spared upon complete laminin alpha2 chain deficiency: comparative expression of laminin and integrin isoforms. *Matrix Biol* **25**, 382-385, doi:10.1016/j.matbio.2006.05.001 (2006).
124 Pouliot, N., Nice, E. C. & Burgess, A. W. Laminin-10 mediates basal and EGF-stimulated motility of human colon carcinoma cells via alpha(3)beta(1) and alpha(6)beta(4) integrins. *Exp Cell Res* **266**, 1-10, doi:10.1006/excr.2001.5197 (2001).
125 Pouliot, N. & Kusuma, N. Laminin-511: a multi-functional adhesion protein regulating cell migration, tumor invasion and metastasis. *Cell Adh Migr* **7**, 142-149, doi:10.4161/cam.22125 (2013).
126 Aberdam, D. *et al.* Developmental expression of nicein adhesion protein (laminin-5) subunits suggests multiple morphogenic roles. *Cell Adhes Commun* **2**, 115-129, doi:10.3109/15419069409004431 (1994).
127 Ryan, M. C., Lee, K., Miyashita, Y. & Carter, W. G. Targeted disruption of the LAMA3 gene in mice reveals abnormalities in survival and late stage differentiation of epithelial cells. *J Cell Biol* **145**, 1309-1323, doi:10.1083/jcb.145.6.1309 (1999).
128 Kuster, J. E., Guarnieri, M. H., Ault, J. G., Flaherty, L. & Swiatek, P. J. IAP insertion in the murine LamB3 gene results in junctional epidermolysis bullosa. *Mamm Genome* **8**, 673-681, doi:10.1007/s003359900535 (1997).
129 Lako, M. *et al.* Hair follicle dermal cells repopulate the mouse haematopoietic system. *J Cell Sci* **115**, 3967-3974, doi:10.1242/jcs.00060 (2002).
130 Richardson, G. D. *et al.* Cultured cells from the adult human hair follicle dermis can be directed toward adipogenic and osteogenic differentiation. *J Invest Dermatol* **124**, 1090-1091, doi:10.1111/j.0022-202X.2005.23734.x (2005).
131 Cotsarelis, G. Gene expression profiling gets to the root of human hair follicle stem cells. *J Clin Invest* **116**, 19-22, doi:10.1172/JCI27490 (2006).
132 Cotsarelis, G., Sun, T. T. & Lavker, R. M. Label-retaining cells reside in the bulge area of pilosebaceous unit: implications for follicular stem cells, hair cycle, and skin carcinogenesis. *Cell* **61**, 1329-1337, doi:10.1016/0092-8674(90)90696-c (1990).

133 Taylor, G., Lehrer, M. S., Jensen, P. J., Sun, T. T. & Lavker, R. M. Involvement of follicular stem cells in forming not only the follicle but also the epidermis. *Cell* **102**, 451-461, doi:10.1016/s0092-8674(00)00050-7 (2000).
134 Kiritsi, D., Has, C. & Bruckner-Tuderman, L. Laminin 332 in junctional epidermolysis bullosa. *Cell Adh Migr* **7**, 135-141, doi:10.4161/cam.22418 (2013).
135 Marinkovich, M. P., Lunstrum, G. P., Keene, D. R. & Burgeson, R. E. The dermal-epidermal junction of human skin contains a novel laminin variant. *J Cell Biol* **119**, 695-703, doi:10.1083/jcb.119.3.695 (1992).
136 Marinkovich, M. P., Lunstrum, G. P. & Burgeson, R. E. The anchoring filament protein kalinin is synthesized and secreted as a high molecular weight precursor. *J Biol Chem* **267**, 17900-17906 (1992).
137 Setty, S. *et al.* Differential expression of laminin isoforms in diabetic nephropathy and other renal diseases. *Mod Pathol* **25**, 859-868, doi:10.1038/modpathol.2011.216 (2012).
138 Miner, J. H. & Patton, B. L. Laminin-11. *Int J Biochem Cell Biol* **31**, 811-816, doi:10.1016/s1357-2725(99)00030-8 (1999).
139 Miner, J. H. & Li, C. Defective glomerulogenesis in the absence of laminin alpha5 demonstrates a developmental role for the kidney glomerular basement membrane. *Dev Biol* **217**, 278-289, doi:10.1006/dbio.1999.9546 (2000).
140 Kikkawa, Y. *et al.* Laminin beta2 variants associated with isolated nephropathy that impact matrix regulation. *JCI Insight* **6**, doi:10.1172/jci.insight.145908 (2021).
141 Chen, Y. M., Kikkawa, Y. & Miner, J. H. A missense LAMB2 mutation causes congenital nephrotic syndrome by impairing laminin secretion. *J Am Soc Nephrol* **22**, 849-858, doi:10.1681/ASN.2010060632 (2011).
142 Funk, S. D. *et al.* Pathogenicity of a Human Laminin beta2 Mutation Revealed in Models of Alport Syndrome. *J Am Soc Nephrol* **29**, 949-960, doi:10.1681/ASN.2017090997 (2018).
143 Chen, Y. M. *et al.* Laminin beta2 gene missense mutation produces endoplasmic reticulum stress in podocytes. *J Am Soc Nephrol* **24**, 1223-1233, doi:10.1681/ASN.2012121149 (2013).
144 Nguyen, N. M. & Senior, R. M. Laminin isoforms and lung development: all isoforms are not equal. *Dev Biol* **294**, 271-279, doi:10.1016/j.ydbio.2006.03.032 (2006).
145 Pierce, R. A., Griffin, G. L., Miner, J. H. & Senior, R. M. Expression patterns of laminin alpha1 and alpha5 in human lung during development. *Am J Respir Cell Mol Biol* **23**, 742-747, doi:10.1165/ajrcmb.23.6.4202 (2000).
146 Nguyen, N. M. *et al.* Epithelial laminin alpha5 is necessary for distal epithelial cell maturation, VEGF production, and alveolization in the developing murine lung. *Dev Biol* **282**, 111-125, doi:10.1016/j.ydbio.2005.02.031 (2005).
147 Pierce, R. A. *et al.* Expression of laminin alpha3, alpha4, and alpha5 chains by alveolar epithelial cells and fibroblasts. *Am J Respir Cell Mol Biol* **19**, 237-244, doi:10.1165/ajrcmb.19.2.3087 (1998).

148 Jones, J. C. *et al.* Laminin-6 assembles into multimolecular fibrillar complexes with perlecan and participates in mechanical-signal transduction via a dystroglycan-dependent, integrin-independent mechanism. *J Cell Sci* **118**, 2557-2566, doi:10.1242/jcs.02395 (2005).
149 Urich, D. *et al.* Lung-specific loss of the laminin alpha3 subunit confers resistance to mechanical injury. *J Cell Sci* **124**, 2927-2937, doi:10.1242/jcs.080911 (2011).
150 DeBiase, P. J. *et al.* Laminin-311 (Laminin-6) fiber assembly by type I-like alveolar cells. *J Histochem Cytochem* **54**, 665-672, doi:10.1369/jhc.5A6889.2006 (2006).
151 Morales-Nebreda, L. I. *et al.* Lung-specific loss of alpha3 laminin worsens bleomycin-induced pulmonary fibrosis. *Am J Respir Cell Mol Biol* **52**, 503-512, doi:10.1165/rcmb.2014-0057OC (2015).
152 Wagner, J. U. G. *et al.* Switch in Laminin beta2 to Laminin beta1 Isoforms During Aging Controls Endothelial Cell Functions-Brief Report. *Arterioscler Thromb Vasc Biol* **38**, 1170-1177, doi:10.1161/ATVBAHA.117.310685 (2018).
153 Hallmann, R. *et al.* The role of basement membrane laminins in vascular function. *Int J Biochem Cell Biol* **127**, 105823, doi:10.1016/j.biocel.2020.105823 (2020).
154 Kariya, Y. *et al.* Localization of laminin alpha3B chain in vascular and epithelial basement membranes of normal human tissues and its down-regulation in skin cancers. *J Mol Histol* **39**, 435-446, doi:10.1007/s10735-008-9183-0 (2008).
155 Wang, S. *et al.* Venular basement membranes contain specific matrix protein low expression regions that act as exit points for emigrating neutrophils. *J Exp Med* **203**, 1519-1532, doi:10.1084/jem.20051210 (2006).
156 Song, J. *et al.* Endothelial Basement Membrane Laminin 511 Contributes to Endothelial Junctional Tightness and Thereby Inhibits Leukocyte Transmigration. *Cell Rep* **18**, 1256-1269, doi:10.1016/j.celrep.2016.12.092 (2017).
157 Vainionpaa, N. *et al.* Basement membrane protein distribution in LYVE-1-immunoreactive lymphatic vessels of normal tissues and ovarian carcinomas. *Cell Tissue Res* **328**, 317-328, doi:10.1007/s00441-006-0366-2 (2007).
158 DeHahn, K. C. *et al.* The alpha4 laminin subunit regulates endothelial cell survival. *Exp Cell Res* **294**, 281-289, doi:10.1016/j.yexcr.2003.11.006 (2004).
159 Doi, M. *et al.* Recombinant human laminin-10 (alpha5beta1gamma1). Production, purification, and migration-promoting activity on vascular endothelial cells. *J Biol Chem* **277**, 12741-12748, doi:10.1074/jbc.M111228200 (2002).
160 Geberhiwot, T. *et al.* Laminin-8 (alpha4beta1gamma1) is synthesized by lymphoid cells, promotes lymphocyte migration and costimulates T cell proliferation. *J Cell Sci* **114**, 423-433, doi:10.1242/jcs.114.2.423 (2001).
161 Sixt, M. *et al.* Endothelial cell laminin isoforms, laminins 8 and 10, play decisive roles in T cell recruitment across the blood-brain barrier in experimental autoimmune encephalomyelitis. *J Cell Biol* **153**, 933-946, doi:10.1083/jcb.153.5.933 (2001).

162 Vainionpaa, N., Lehto, V. P., Tryggvason, K. & Virtanen, I. Alpha4 chain laminins are widely expressed in renal cell carcinomas and have a de-adhesive function. *Lab Invest* **87**, 780-791, doi:10.1038/labinvest.3700592 (2007).
163 Smyth, N. *et al.* Absence of basement membranes after targeting the LAMC1 gene results in embryonic lethality due to failure of endoderm differentiation. *J Cell Biol* **144**, 151-160, doi:10.1083/jcb.144.1.151 (1999).
164 Sasaki, T. *et al.* Laminin-121--recombinant expression and interactions with integrins. *Matrix Biol* **29**, 484-493, doi:10.1016/j.matbio.2010.05.004 (2010).
165 Velling, T. *et al.* Distinct alpha 7A beta 1 and alpha 7B beta 1 integrin expression patterns during mouse development: alpha 7A is restricted to skeletal muscle but alpha 7B is expressed in striated muscle, vasculature, and nervous system. *Dev Dyn* **207**, 355-371, doi:10.1002/(SICI)1097-0177(199612)207:4<355::AID-AJA1>3.0.CO;2-G (1996).
166 Nguyen, M. T. X. *et al.* Differentiation of Human Embryonic Stem Cells to Endothelial Progenitor Cells on Laminins in Defined and Xeno-free Systems. *Stem Cell Reports* **7**, 802-816, doi:10.1016/j.stemcr.2016.08.017 (2016).
167 Rodin, S. *et al.* Long-term self-renewal of human pluripotent stem cells on human recombinant laminin-511. *Nat Biotechnol* **28**, 611-615, doi:10.1038/nbt.1620 (2010).
168 Rodin, S. *et al.* Clonal culturing of human embryonic stem cells on laminin-521/E-cadherin matrix in defined and xeno-free environment. *Nat Commun* **5**, 3195, doi:10.1038/ncomms4195 (2014).
169 Tjin, M. S. *et al.* Biologically relevant laminin as chemically defined and fully human platform for human epidermal keratinocyte culture. *Nat Commun* **9**, 4432, doi:10.1038/s41467-018-06934-3 (2018).
170 Pinzon-Duarte, G., Daly, G., Li, Y. N., Koch, M. & Brunken, W. J. Defective formation of the inner limiting membrane in laminin beta2- and gamma3-null mice produces retinal dysplasia. *Invest Ophthalmol Vis Sci* **51**, 1773-1782, doi:10.1167/iovs.09-4645 (2010).
171 Glentis, A., Gurchenkov, V. & Matic Vignjevic, D. Assembly, heterogeneity, and breaching of the basement membranes. *Cell Adh Migr* **8**, 236-245, doi:10.4161/cam.28733 (2014).
172 Chang, T. T., Thakar, D. & Weaver, V. M. Force-dependent breaching of the basement membrane. *Matrix Biol* **57-58**, 178-189, doi:10.1016/j.matbio.2016.12.005 (2017).
173 van den Berg, M. C. W. *et al.* Proteolytic and Opportunistic Breaching of the Basement Membrane Zone by Immune Cells during Tumor Initiation. *Cell Rep* **27**, 2837-2846 e2834, doi:10.1016/j.celrep.2019.05.029 (2019).
174 Kelley, L. C., Lohmer, L. L., Hagedorn, E. J. & Sherwood, D. R. Traversing the basement membrane in vivo: a diversity of strategies. *J Cell Biol* **204**, 291-302, doi:10.1083/jcb.201311112 (2014).
175 Caceres, R. *et al.* Forces drive basement membrane invasion in Caenorhabditis elegans. *Proc Natl Acad Sci U S A* **115**, 11537-11542, doi:10.1073/pnas.1808760115 (2018).

176 Glentis, A. *et al.* Author Correction: Cancer-associated fibroblasts induce metalloprotease-independent cancer cell invasion of the basement membrane. *Nat Commun* **9**, 1036, doi:10.1038/s41467-018-03304-x (2018).
177 Wu, L. *et al.* Laminin degradation by matrix metalloproteinase 9 promotes ketamine-induced neuronal apoptosis in the early developing rat retina. *CNS Neurosci Ther* **26**, 1058-1068, doi:10.1111/cns.13428 (2020).
178 Quintero-Fabian, S. *et al.* Role of Matrix Metalloproteinases in Angiogenesis and Cancer. *Front Oncol* **9**, 1370, doi:10.3389/fonc.2019.01370 (2019).
179 Jablonska-Trypuc, A., Matejczyk, M. & Rosochacki, S. Matrix metalloproteinases (MMPs), the main extracellular matrix (ECM) enzymes in collagen degradation, as a target for anticancer drugs. *J Enzyme Inhib Med Chem* **31**, 177-183, doi:10.3109/14756366.2016.1161620 (2016).
180 Edwards, M. M. *et al.* Mutations in Lama1 disrupt retinal vascular development and inner limiting membrane formation. *J Biol Chem* **285**, 7697-7711, doi:10.1074/jbc.M109.069575 (2010).
181 Patton, B. L., Wang, B., Tarumi, Y. S., Seburn, K. L. & Burgess, R. W. A single point mutation in the LN domain of LAMA2 causes muscular dystrophy and peripheral amyelination. *J Cell Sci* **121**, 1593-1604, doi:10.1242/jcs.015354 (2008).
182 Oliveira, J. *et al.* LAMA2 gene mutation update: Toward a more comprehensive picture of the laminin-alpha2 variome and its related phenotypes. *Hum Mutat* **39**, 1314-1337, doi:10.1002/humu.23599 (2018).
183 Oliveira, J. *et al.* LAMA2 gene analysis in a cohort of 26 congenital muscular dystrophy patients. *Clin Genet* **74**, 502-512, doi:10.1111/j.1399-0004.2008.01068.x (2008).
184 Gavassini, B. F. *et al.* Clinical and molecular characterization of limb-girdle muscular dystrophy due to LAMA2 mutations. *Muscle Nerve* **44**, 703-709, doi:10.1002/mus.22132 (2011).
185 Geranmayeh, F. *et al.* Genotype-phenotype correlation in a large population of muscular dystrophy patients with LAMA2 mutations. *Neuromuscul Disord* **20**, 241-250, doi:10.1016/j.nmd.2010.02.001 (2010).
186 Di Blasi, C. *et al.* LAMA2 gene analysis in congenital muscular dystrophy: new mutations, prenatal diagnosis, and founder effect. *Arch Neurol* **62**, 1582-1586, doi:10.1001/archneur.62.10.1582 (2005).
187 Chan, S. H. *et al.* Limb girdle muscular dystrophy due to LAMA2 mutations: diagnostic difficulties due to associated peripheral neuropathy. *Neuromuscul Disord* **24**, 677-683, doi:10.1016/j.nmd.2014.05.008 (2014).
188 Beytia Mde, L. *et al.* High creatine kinase levels and white matter changes: clinical and genetic spectrum of congenital muscular dystrophies with laminin alpha-2 deficiency. *Mol Cell Probes* **28**, 118-122, doi:10.1016/j.mcp.2013.11.002 (2014).
189 Jones, L. K. *et al.* A mutation affecting laminin alpha 5 polymerization gives rise to a syndromic developmental disorder. *Development* **147**, doi:10.1242/dev.189183 (2020).
190 Hollfelder, D., Frasch, M. & Reim, I. Distinct functions of the laminin beta LN domain and collagen IV during cardiac extracellular matrix formation and

stabilization of alary muscle attachments revealed by EMS mutagenesis in Drosophila. *BMC Dev Biol* **14**, 26, doi:10.1186/1471-213X-14-26 (2014).
191 Hasselbacher, K. *et al.* Recessive missense mutations in LAMB2 expand the clinical spectrum of LAMB2-associated disorders. *Kidney Int* **70**, 1008-1012, doi:10.1038/sj.ki.5001679 (2006).
192 Zenker, M. *et al.* Human laminin beta2 deficiency causes congenital nephrosis with mesangial sclerosis and distinct eye abnormalities. *Hum Mol Genet* **13**, 2625-2632, doi:10.1093/hmg/ddh284 (2004).
193 Matejas, V. *et al.* Mutations in the human laminin beta2 (LAMB2) gene and the associated phenotypic spectrum. *Hum Mutat* **31**, 992-1002, doi:10.1002/humu.21304 (2010).
194 Bredrup, C. *et al.* Ophthalmological aspects of Pierson syndrome. *Am J Ophthalmol* **146**, 602-611, doi:10.1016/j.ajo.2008.05.039 (2008).
195 Matejas, V., Al-Gazali, L., Amirlak, I. & Zenker, M. A syndrome comprising childhood-onset glomerular kidney disease and ocular abnormalities with progressive loss of vision is caused by mutated LAMB2. *Nephrol Dial Transplant* **21**, 3283-3286, doi:10.1093/ndt/gfl463 (2006).
196 Mohney, B. G. *et al.* A novel mutation of LAMB2 in a multigenerational mennonite family reveals a new phenotypic variant of Pierson syndrome. *Ophthalmology* **118**, 1137-1144, doi:10.1016/j.ophtha.2010.10.009 (2011).
197 Kagan, M., Cohen, A. H., Matejas, V., Vlangos, C. & Zenker, M. A milder variant of Pierson syndrome. *Pediatr Nephrol* **23**, 323-327, doi:10.1007/s00467-007-0624-x (2008).
198 Choi, H. J. *et al.* Variable phenotype of Pierson syndrome. *Pediatr Nephrol* **23**, 995-1000, doi:10.1007/s00467-008-0748-7 (2008).
199 Mellerio, J. E., Eady, R. A., Atherton, D. J., Lake, B. D. & McGrath, J. A. E210K mutation in the gene encoding the beta3 chain of laminin-5 (LAMB3) is predictive of a phenotype of generalized atrophic benign epidermolysis bullosa. *Br J Dermatol* **139**, 325-331, doi:10.1046/j.1365-2133.1998.02377.x (1998).
200 Pierson, M., Cordier, J., Hervouuet, F. & Rauber, G. [an Unusual Congenital and Familial Congenital Malformative Combination Involving the Eye and Kidney]. *J Genet Hum* **12**, 184-213 (1963).
201 Libby, R. T. *et al.* Laminin expression in adult and developing retinae: evidence of two novel CNS laminins. *J Neurosci* **20**, 6517-6528 (2000).
202 Bystrom, B., Virtanen, I., Rousselle, P., Gullberg, D. & Pedrosa-Domellof, F. Distribution of laminins in the developing human eye. *Invest Ophthalmol Vis Sci* **47**, 777-785, doi:10.1167/iovs.05-0367 (2006).
203 Hunter, D. D., Shah, V., Merlie, J. P. & Sanes, J. R. A laminin-like adhesive protein concentrated in the synaptic cleft of the neuromuscular junction. *Nature* **338**, 229-234, doi:10.1038/338229a0 (1989).
204 Bowen, P., Lee, C. S., Zellweger, H. & Lindenberg, R. A Familial Syndrome of Multiple Congenital Defects. *Bull Johns Hopkins Hosp* **114**, 402-414 (1964).
205 Zenker, M. *et al.* Congenital nephrosis, mesangial sclerosis, and distinct eye abnormalities with microcoria: an autosomal recessive syndrome. *Am J Med Genet A* **130A**, 138-145, doi:10.1002/ajmg.a.30310 (2004).

206 VanDeVoorde, R., Witte, D., Kogan, J. & Goebel, J. Pierson syndrome: a novel cause of congenital nephrotic syndrome. *Pediatrics* **118**, e501-505, doi:10.1542/peds.2005-3154 (2006).
207 McKee, K. K., Aleksandrova, M. & Yurchenco, P. D. Chimeric protein identification of dystrophic, Pierson and other laminin polymerization residues. *Matrix Biol* **67**, 32-46, doi:10.1016/j.matbio.2018.01.012 (2018).
208 Philpot, J., Sewry, C., Pennock, J. & Dubowitz, V. Clinical phenotype in congenital muscular dystrophy: correlation with expression of merosin in skeletal muscle. *Neuromuscul Disord* **5**, 301-305, doi:10.1016/0960-8966(94)00069-l (1995).
209 Jones, K. J. *et al.* The expanding phenotype of laminin alpha2 chain (merosin) abnormalities: case series and review. *J Med Genet* **38**, 649-657, doi:10.1136/jmg.38.10.649 (2001).
210 Muntoni, F. & Voit, T. The congenital muscular dystrophies in 2004: a century of exciting progress. *Neuromuscul Disord* **14**, 635-649, doi:10.1016/j.nmd.2004.06.009 (2004).
211 Mendell, J. R., Boue, D. R. & Martin, P. T. The congenital muscular dystrophies: recent advances and molecular insights. *Pediatr Dev Pathol* **9**, 427-443, doi:10.2350/06-07-0127.1 (2006).
212 Yurchenco, P. D., McKee, K. K., Reinhard, J. R. & Ruegg, M. A. Laminin-deficient muscular dystrophy: Molecular pathogenesis and structural repair strategies. *Matrix Biol* **71-72**, 174-187, doi:10.1016/j.matbio.2017.11.009 (2018).
213 Matsui, C., Wang, C. K., Nelson, C. F., Bauer, E. A. & Hoeffler, W. K. The assembly of laminin-5 subunits. *J Biol Chem* **270**, 23496-23503, doi:10.1074/jbc.270.40.23496 (1995).
214 Ferrigno, O. *et al.* Murine laminin alpha3A and alpha3B isoform chains are generated by usage of two promoters and alternative splicing. *J Biol Chem* **272**, 20502-20507, doi:10.1074/jbc.272.33.20502 (1997).
215 Cheng, Y. S., Champliaud, M. F., Burgeson, R. E., Marinkovich, M. P. & Yurchenco, P. D. Self-assembly of laminin isoforms. *J Biol Chem* **272**, 31525-31532, doi:10.1074/jbc.272.50.31525 (1997).
216 McGrath, J. A. *et al.* Altered laminin 5 expression due to mutations in the gene encoding the beta 3 chain (LAMB3) in generalized atrophic benign epidermolysis bullosa. *J Invest Dermatol* **104**, 467-474, doi:10.1111/1523-1747.ep12605904 (1995).
217 Posteraro, P. *et al.* Laminin-5 mutational analysis in an Italian cohort of patients with junctional epidermolysis bullosa. *J Invest Dermatol* **123**, 639-648, doi:10.1111/j.0022-202X.2004.23302.x (2004).
218 Pulkkinen, L. *et al.* Mutations in the gamma 2 chain gene (LAMC2) of kalinin/laminin 5 in the junctional forms of epidermolysis bullosa. *Nat Genet* **6**, 293-297, doi:10.1038/ng0394-293 (1994).
219 Meng, X. *et al.* Targeted inactivation of murine laminin gamma2-chain gene recapitulates human junctional epidermolysis bullosa. *J Invest Dermatol* **121**, 720-731, doi:10.1046/j.1523-1747.2003.12515.x (2003).
220 Pasmooij, A. M., Pas, H. H., Bolling, M. C. & Jonkman, M. F. Revertant mosaicism in junctional epidermolysis bullosa due to multiple correcting

second-site mutations in LAMB3. *J Clin Invest* **117**, 1240-1248, doi:10.1172/JCI30465 (2007).
221 Mittwollen, R. *et al.* Aberrant splicing as potential modifier of the phenotype of junctional epidermolysis bullosa. *J Eur Acad Dermatol Venereol* **34**, 2127-2134, doi:10.1111/jdv.16332 (2020).
222 Sakai, N., Waterman, E. A., Nguyen, N. T., Keene, D. R. & Marinkovich, M. P. Observations of skin grafts derived from keratinocytes expressing selectively engineered mutant laminin-332 molecules. *J Invest Dermatol* **130**, 2147-2150, doi:10.1038/jid.2010.85 (2010).
223 Waterman, E. A. *et al.* A laminin-collagen complex drives human epidermal carcinogenesis through phosphoinositol-3-kinase activation. *Cancer Res* **67**, 4264-4270, doi:10.1158/0008-5472.CAN-06-4141 (2007).
224 Miner, J. H., Go, G., Cunningham, J., Patton, B. L. & Jarad, G. Transgenic isolation of skeletal muscle and kidney defects in laminin beta2 mutant mice: implications for Pierson syndrome. *Development* **133**, 967-975, doi:10.1242/dev.02270 (2006).
225 Jarad, G., Cunningham, J., Shaw, A. S. & Miner, J. H. Proteinuria precedes podocyte abnormalities inLamb2-/- mice, implicating the glomerular basement membrane as an albumin barrier. *J Clin Invest* **116**, 2272-2279, doi:10.1172/JCI28414 (2006).
226 Libby, R. T., Lavallee, C. R., Balkema, G. W., Brunken, W. J. & Hunter, D. D. Disruption of laminin beta2 chain production causes alterations in morphology and function in the CNS. *J Neurosci* **19**, 9399-9411 (1999).
227 Denes, V. *et al.* Laminin deficits induce alterations in the development of dopaminergic neurons in the mouse retina. *Vis Neurosci* **24**, 549-562, doi:10.1017/S0952523807070514 (2007).
228 Miner, J. H., Cunningham, J. & Sanes, J. R. Roles for laminin in embryogenesis: exencephaly, syndactyly, and placentopathy in mice lacking the laminin alpha5 chain. *J Cell Biol* **143**, 1713-1723, doi:10.1083/jcb.143.6.1713 (1998).
229 Lin, M. H. *et al.* Laminin-521 Protein Therapy for Glomerular Basement Membrane and Podocyte Abnormalities in a Model of Pierson Syndrome. *J Am Soc Nephrol* **29**, 1426-1436, doi:10.1681/ASN.2017060690 (2018).
230 Perrin, A., Rousseau, J. & Tremblay, J. P. Increased Expression of Laminin Subunit Alpha 1 Chain by dCas9-VP160. *Mol Ther Nucleic Acids* **6**, 68-79, doi:10.1016/j.omtn.2016.11.004 (2017).
231 McKee, K. K. *et al.* Chimeric protein repair of laminin polymerization ameliorates muscular dystrophy phenotype. *J Clin Invest* **127**, 1075-1089, doi:10.1172/JCI90854 (2017).
232 Reinhard, J. R. *et al.* Linker proteins restore basement membrane and correct LAMA2-related muscular dystrophy in mice. *Sci Transl Med* **9**, doi:10.1126/scitranslmed.aal4649 (2017).
233 McKee, K. K., Capizzi, S. & Yurchenco, P. D. Scaffold-forming and Adhesive Contributions of Synthetic Laminin-binding Proteins to Basement Membrane Assembly. *J Biol Chem* **284**, 8984-8994, doi:10.1074/jbc.M809719200 (2009).

234 Talts, J. F. *et al.* Structural and functional analysis of the recombinant G domain of the laminin alpha4 chain and its proteolytic processing in tissues. *J Biol Chem* **275**, 35192-35199, doi:10.1074/jbc.M003261200 (2000).
235 Moll, J. *et al.* An agrin minigene rescues dystrophic symptoms in a mouse model for congenital muscular dystrophy. *Nature* **413**, 302-307, doi:10.1038/35095054 (2001).
236 Fahey, B. & Degnan, B. M. Origin and evolution of laminin gene family diversity. *Mol Biol Evol* **29**, 1823-1836, doi:10.1093/molbev/mss060 (2012).
237 Tessier-Lavigne, M. & Goodman, C. S. The molecular biology of axon guidance. *Science* **274**, 1123-1133, doi:10.1126/science.274.5290.1123 (1996).
238 Barallobre, M. J., Pascual, M., Del Rio, J. A. & Soriano, E. The Netrin family of guidance factors: emphasis on Netrin-1 signalling. *Brain Res Brain Res Rev* **49**, 22-47, doi:10.1016/j.brainresrev.2004.11.003 (2005).
239 Kappler, J. *et al.* Glycosaminoglycan-binding properties and secondary structure of the C-terminus of netrin-1. *Biochem Biophys Res Commun* **271**, 287-291, doi:10.1006/bbrc.2000.2583 (2000).
240 Yurchenco, P. D. & Wadsworth, W. G. Assembly and tissue functions of early embryonic laminins and netrins. *Curr Opin Cell Biol* **16**, 572-579, doi:10.1016/j.ceb.2004.07.013 (2004).
241 Keino-Masu, K. *et al.* Deleted in Colorectal Cancer (DCC) encodes a netrin receptor. *Cell* **87**, 175-185, doi:10.1016/s0092-8674(00)81336-7 (1996).
242 Yebra, M. *et al.* Recognition of the neural chemoattractant Netrin-1 by integrins alpha6beta4 and alpha3beta1 regulates epithelial cell adhesion and migration. *Dev Cell* **5**, 695-707, doi:10.1016/s1534-5807(03)00330-7 (2003).
243 Nikolopoulos, S. N. & Giancotti, F. G. Netrin-integrin signaling in epithelial morphogenesis, axon guidance and vascular patterning. *Cell Cycle* **4**, e131-135 (2005).
244 Schneiders, F. I. *et al.* Binding of netrin-4 to laminin short arms regulates basement membrane assembly. *J Biol Chem* **282**, 23750-23758, doi:10.1074/jbc.M703137200 (2007).
245 Reuten, R. *et al.* Basement membrane stiffness determines metastases formation. *Nat Mater*, doi:10.1038/s41563-020-00894-0 (2021).
246 Reuten, R. *et al.* Basement membrane stiffness determines metastases formation. *Nat Mater* **20**, 892-903, doi:10.1038/s41563-020-00894-0 (2021).
247 Larrieu-Lahargue, F., Welm, A. L., Thomas, K. R. & Li, D. Y. Netrin-4 induces lymphangiogenesis in vivo. *Blood* **115**, 5418-5426, doi:10.1182/blood-2009-11-252338 (2010).
248 Nacht, M. *et al.* Netrin-4 regulates angiogenic responses and tumor cell growth. *Exp Cell Res* **315**, 784-794, doi:10.1016/j.yexcr.2008.11.018 (2009).
249 Troughton, L. D., Reuten, R., Sugden, C. J. & Hamill, K. J. Laminin N-terminus α31 protein distribution in adult human tissues. *bioRxiv*, 2020.2005.2021.108134, doi:10.1101/2020.05.21.108134 (2020).
250 Troughton, L. D., Zech, T. & Hamill, K. J. Laminin N-terminus α31 is upregulated in invasive ductal breast cancer and changes the mode of

tumour invasion. *bioRxiv*, 2020.2005.2028.120964, doi:10.1101/2020.05.28.120964 (2020).
251 Iorio, V., Troughton, L. D., Barrera, V. & Hamill, K. J. LaNt α31 modulates LM332 organization during matrix deposition leading to cell-matrix adhesion and migration defects. *bioRxiv*, 617597, doi:10.1101/617597 (2019).
252 Langhofer, M., Hopkinson, S. B. & Jones, J. C. The matrix secreted by 804G cells contains laminin-related components that participate in hemidesmosome assembly in vitro. *J Cell Sci* **105 (Pt 3)**, 753-764, doi:10.1242/jcs.105.3.753 (1993).
253 Di Russo, J. *et al.* Endothelial basement membrane laminin 511 is essential for shear stress response. *EMBO J* **36**, 183-201, doi:10.15252/embj.201694756 (2017).
254 Robertson, D. M. *et al.* Characterization of growth and differentiation in a telomerase-immortalized human corneal epithelial cell line. *Invest Ophthalmol Vis Sci* **46**, 470-478, doi:10.1167/iovs.04-0528 (2005).
255 Yuspa, S. H. & Harris, C. C. Altered differentiation of mouse epidermal cells treated with retinyl acetate in vitro. *Exp Cell Res* **86**, 95-105, doi:10.1016/0014-4827(74)90653-3 (1974).
256 Schneider, C. A., Rasband, W. S. & Eliceiri, K. W. NIH Image to ImageJ: 25 years of image analysis. *Nat Methods* **9**, 671-675, doi:10.1038/nmeth.2089 (2012).
257 Pribnow, D. Nucleotide sequence of an RNA polymerase binding site at an early T7 promoter. *Proc Natl Acad Sci U S A* **72**, 784-788, doi:10.1073/pnas.72.3.784 (1975).
258 Kozak, M. An analysis of 5'-noncoding sequences from 699 vertebrate messenger RNAs. *Nucleic Acids Res* **15**, 8125-8148, doi:10.1093/nar/15.20.8125 (1987).
259 Cheng, K. W. *et al.* Evaluation of artificial signal peptides for secretion of two lysosomal enzymes in CHO cells. *Biochem J* **478**, 2309-2319, doi:10.1042/BCJ20210015 (2021).
260 Brizzard, B. L., Chubet, R. G. & Vizard, D. L. Immunoaffinity purification of FLAG epitope-tagged bacterial alkaline phosphatase using a novel monoclonal antibody and peptide elution. *Biotechniques* **16**, 730-735 (1994).
261 Field, J. *et al.* Purification of a RAS-responsive adenylyl cyclase complex from Saccharomyces cerevisiae by use of an epitope addition method. *Mol Cell Biol* **8**, 2159-2165, doi:10.1128/mcb.8.5.2159 (1988).
262 Trichas, G., Begbie, J. & Srinivas, S. Use of the viral 2A peptide for bicistronic expression in transgenic mice. *BMC Biol* **6**, 40, doi:10.1186/1741-7007-6-40 (2008).
263 Ittner, L. M. & Gotz, J. Pronuclear injection for the production of transgenic mice. *Nat Protoc* **2**, 1206-1215, doi:10.1038/nprot.2007.145 (2007).
264 Ventura, A. *et al.* Restoration of p53 function leads to tumour regression in vivo. *Nature* **445**, 661-665, doi:10.1038/nature05541 (2007).
265 Vidal, F. *et al.* Cloning of the laminin alpha 3 chain gene (LAMA3) and identification of a homozygous deletion in a patient with Herlitz junctional epidermolysis bullosa. *Genomics* **30**, 273-280, doi:10.1006/geno.1995.9877 (1995).

266 Johnson, M. *et al.* NCBI BLAST: a better web interface. *Nucleic Acids Res* **36**, W5-9, doi:10.1093/nar/gkn201 (2008).
267 Miettinen, M., Lindenmayer, A. E. & Chaubal, A. Endothelial cell markers CD31, CD34, and BNH9 antibody to H- and Y-antigens--evaluation of their specificity and sensitivity in the diagnosis of vascular tumors and comparison with von Willebrand factor. *Mod Pathol* **7**, 82-90 (1994).
268 Pusztaszeri, M. P., Seelentag, W. & Bosman, F. T. Immunohistochemical expression of endothelial markers CD31, CD34, von Willebrand factor, and Fli-1 in normal human tissues. *J Histochem Cytochem* **54**, 385-395, doi:10.1369/jhc.4A6514.2005 (2006).
269 Pisacane, A. M., Picciotto, F. & Risio, M. CD31 and CD34 expression as immunohistochemical markers of endothelial transdifferentiation in human cutaneous melanoma. *Cell Oncol* **29**, 59-66, doi:10.1155/2007/486579 (2007).
270 Petajaniemi, N. *et al.* Localization of laminin alpha4-chain in developing and adult human tissues. *J Histochem Cytochem* **50**, 1113-1130, doi:10.1177/002215540205000813 (2002).
271 Di Russo, J. *et al.* Vascular laminins in physiology and pathology. *Matrix Biol* **57-58**, 140-148, doi:10.1016/j.matbio.2016.06.008 (2017).
272 Di Russo, J. *et al.* Endothelial basement membrane laminin 511 is essential for shear stress response. *EMBO J* **36**, 1464, doi:10.15252/embj.201797000 (2017).
273 Miner, J. H. The glomerular basement membrane. *Exp Cell Res* **318**, 973-978, doi:10.1016/j.yexcr.2012.02.031 (2012).
274 Miner, J. H. Developmental biology of glomerular basement membrane components. *Curr Opin Nephrol Hypertens* **7**, 13-19, doi:10.1097/00041552-199801000-00003 (1998).
275 Miner, J. H. & Sanes, J. R. Collagen IV alpha 3, alpha 4, and alpha 5 chains in rodent basal laminae: sequence, distribution, association with laminins, and developmental switches. *J Cell Biol* **127**, 879-891, doi:10.1083/jcb.127.3.879 (1994).
276 Bordeaux, J. *et al.* Antibody validation. *Biotechniques* **48**, 197-209, doi:10.2144/000113382 (2010).
277 Manic, G. *et al.* 3' self-inactivating long terminal repeat inserts for the modulation of transgene expression from lentiviral vectors. *Hum Gene Ther Methods* **23**, 84-97, doi:10.1089/hgtb.2011.154 (2012).
278 Page, S. M. & Brownlee, G. G. Differentiation-specific enhancer activity in transduced keratinocytes: a model for epidermal gene therapy. *Gene Ther* **5**, 394-402, doi:10.1038/sj.gt.3300591 (1998).
279 Qin, J. Y. *et al.* Systematic comparison of constitutive promoters and the doxycycline-inducible promoter. *PLoS One* **5**, e10611, doi:10.1371/journal.pone.0010611 (2010).
280 Mehta, A. K., Majumdar, S. S., Alam, P., Gulati, N. & Brahmachari, V. Epigenetic regulation of cytomegalovirus major immediate-early promoter activity in transgenic mice. *Gene* **428**, 20-24, doi:10.1016/j.gene.2008.09.033 (2009).

281 Norrman, K. *et al.* Quantitative comparison of constitutive promoters in human ES cells. *PLoS One* **5**, e12413, doi:10.1371/journal.pone.0012413 (2010).
282 Coloma, M. J., Hastings, A., Wims, L. A. & Morrison, S. L. Novel vectors for the expression of antibody molecules using variable regions generated by polymerase chain reaction. *J Immunol Methods* **152**, 89-104, doi:10.1016/0022-1759(92)90092-8 (1992).
283 Lukyanov, K. A., Chudakov, D. M., Lukyanov, S. & Verkhusha, V. V. Innovation: Photoactivatable fluorescent proteins. *Nat Rev Mol Cell Biol* **6**, 885-891, doi:10.1038/nrm1741 (2005).
284 Lippincott-Schwartz, J. & Patterson, G. H. Photoactivatable fluorescent proteins for diffraction-limited and super-resolution imaging. *Trends Cell Biol* **19**, 555-565, doi:10.1016/j.tcb.2009.09.003 (2009).
285 Subach, F. V. *et al.* Photoactivatable mCherry for high-resolution two-color fluorescence microscopy. *Nat Methods* **6**, 153-159, doi:10.1038/nmeth.1298 (2009).
286 Betzig, E. *et al.* Imaging intracellular fluorescent proteins at nanometer resolution. *Science* **313**, 1642-1645, doi:10.1126/science.1127344 (2006).
287 Hess, S. T., Girirajan, T. P. & Mason, M. D. Ultra-high resolution imaging by fluorescence photoactivation localization microscopy. *Biophys J* **91**, 4258-4272, doi:10.1529/biophysj.106.091116 (2006).
288 Rust, M. J., Bates, M. & Zhuang, X. Sub-diffraction-limit imaging by stochastic optical reconstruction microscopy (STORM). *Nat Methods* **3**, 793-795, doi:10.1038/nmeth929 (2006).
289 Ahier, A. & Jarriault, S. Simultaneous expression of multiple proteins under a single promoter in Caenorhabditis elegans via a versatile 2A-based toolkit. *Genetics* **196**, 605-613, doi:10.1534/genetics.113.160846 (2014).
290 Daniels, R. W., Rossano, A. J., Macleod, G. T. & Ganetzky, B. Expression of multiple transgenes from a single construct using viral 2A peptides in Drosophila. *PLoS One* **9**, e100637, doi:10.1371/journal.pone.0100637 (2014).
291 Liu, Z. *et al.* Systematic comparison of 2A peptides for cloning multi-genes in a polycistronic vector. *Sci Rep* **7**, 2193, doi:10.1038/s41598-017-02460-2 (2017).
292 Donnelly, M. L. L. *et al.* The 'cleavage' activities of foot-and-mouth disease virus 2A site-directed mutants and naturally occurring '2A-like' sequences. *J Gen Virol* **82**, 1027-1041, doi:10.1099/0022-1317-82-5-1027 (2001).
293 Donnelly, M. L. L. *et al.* Analysis of the aphthovirus 2A/2B polyprotein 'cleavage' mechanism indicates not a proteolytic reaction, but a novel translational effect: a putative ribosomal 'skip'. *J Gen Virol* **82**, 1013-1025, doi:10.1099/0022-1317-82-5-1013 (2001).
294 Zufferey, R., Donello, J. E., Trono, D. & Hope, T. J. Woodchuck hepatitis virus posttranscriptional regulatory element enhances expression of transgenes delivered by retroviral vectors. *J Virol* **73**, 2886-2892, doi:10.1128/JVI.73.4.2886-2892.1999 (1999).
295 Akasaka, E., Kleiser, S., Sengle, G., Bruckner-Tuderman, L. & Nystrom, A. Diversity of Mechanisms Underlying Latent TGF-beta Activation in Recessive

Dystrophic Epidermolysis Bullosa. *J Invest Dermatol* **141**, 1450-1460 e1459, doi:10.1016/j.jid.2020.10.024 (2021).
296 Sprenger, A. *et al.* Comparative quantitation of proteome alterations induced by aging or immortalization in primary human fibroblasts and keratinocytes for clinical applications. *Mol Biosyst* **6**, 1579-1582, doi:10.1039/c003962d (2010).
297 Garlick, J. A. & Taichman, L. B. Effect of TGF-beta 1 on re-epithelialization of human keratinocytes in vitro: an organotypic model. *J Invest Dermatol* **103**, 554-559, doi:10.1111/1523-1747.ep12396847 (1994).
298 Troughton, L. D. *A "splicing Switch" Provides Dual Layers of Regulation of Laminin Alpha 3: Implications for Wound Healing and Squamous Cell Carcinoma*. (University of Liverpool, 2019).
299 Kariya, Y., Sato, H., Katou, N., Kariya, Y. & Miyazaki, K. Polymerized laminin-332 matrix supports rapid and tight adhesion of keratinocytes, suppressing cell migration. *PLoS One* **7**, e35546, doi:10.1371/journal.pone.0035546 (2012).
300 Qin, P. & Kurpakus, M. A. The role of laminin-5 in TGF alpha/EGF-mediated corneal epithelial cell motility. *Exp Eye Res* **66**, 569-579, doi:10.1006/exer.1997.0455 (1998).
301 Hasenson, S. *et al.* The immortalized human corneal epithelial cells adhere to laminin-10 by using Lutheran glycoproteins and integrin alpha3beta1. *Exp Eye Res* **81**, 415-421, doi:10.1016/j.exer.2005.02.015 (2005).
302 Lu, W., Ebihara, N., Miyazaki, K. & Murakami, A. Reduced expression of laminin-5 in corneal epithelial cells under high glucose condition. *Cornea* **25**, 61-67, doi:10.1097/01.ico.0000179932.21104.3c (2006).
303 Glick, B. R. & Patten, C. L. *Molecular biotechnology: principles and applications of recombinant DNA*. Vol. 34 (John Wiley & Sons, 2017).
304 Torricelli, A. A., Singh, V., Agrawal, V., Santhiago, M. R. & Wilson, S. E. Transmission electron microscopy analysis of epithelial basement membrane repair in rabbit corneas with haze. *Invest Ophthalmol Vis Sci* **54**, 4026-4033, doi:10.1167/iovs.13-12106 (2013).
305 Dlugosz, A. A. & Yuspa, S. H. Coordinate changes in gene expression which mark the spinous to granular cell transition in epidermis are regulated by protein kinase C. *J Cell Biol* **120**, 217-225, doi:10.1083/jcb.120.1.217 (1993).
306 Sanz-Gomez, N., Freije, A. & Gandarillas, A. Keratinocyte Differentiation by Flow Cytometry. *Methods Mol Biol* **2109**, 83-92, doi:10.1007/7651_2019_237 (2020).
307 Lavker, R. M. & Sun, T. T. Epidermal stem cells: properties, markers, and location. *Proc Natl Acad Sci U S A* **97**, 13473-13475, doi:10.1073/pnas.250380097 (2000).
308 Rasmussen, C., Thomas-Virnig, C. & Allen-Hoffmann, B. L. Classical human epidermal keratinocyte cell culture. *Methods Mol Biol* **945**, 161-175, doi:10.1007/978-1-62703-125-7_11 (2013).
309 Pummi, K. *et al.* Epidermal tight junctions: ZO-1 and occludin are expressed in mature, developing, and affected skin and in vitro differentiating keratinocytes. *J Invest Dermatol* **117**, 1050-1058, doi:10.1046/j.0022-202x.2001.01493.x (2001).

310 Egles, C., Garlick, J. A. & Shamis, Y. Three-dimensional human tissue models of wounded skin. *Methods Mol Biol* **585**, 345-359, doi:10.1007/978-1-60761-380-0_24 (2010).
311 Iorio, V. D.
312 Hershko, A. & Ciechanover, A. The ubiquitin system. *Annu Rev Biochem* **67**, 425-479, doi:10.1146/annurev.biochem.67.1.425 (1998).
313 Schorpp, M. *et al.* The human ubiquitin C promoter directs high ubiquitous expression of transgenes in mice. *Nucleic Acids Res* **24**, 1787-1788, doi:10.1093/nar/24.9.1787 (1996).
314 Schmidt, E. V., Christoph, G., Zeller, R. & Leder, P. The cytomegalovirus enhancer: a pan-active control element in transgenic mice. *Mol Cell Biol* **10**, 4406-4411, doi:10.1128/mcb.10.8.4406 (1990).
315 Furth, P. A., Hennighausen, L., Baker, C., Beatty, B. & Woychick, R. The variability in activity of the universally expressed human cytomegalovirus immediate early gene 1 enhancer/promoter in transgenic mice. *Nucleic Acids Res* **19**, 6205-6208, doi:10.1093/nar/19.22.6205 (1991).
316 Sands, A. T. *et al.* Cytoplasmic beta-actin promoter produces germ cell and preimplantation embryonic transgene expression. *Mol Reprod Dev* **34**, 117-126, doi:10.1002/mrd.1080340202 (1993).
317 Kim, H., Kim, M., Im, S. K. & Fang, S. Mouse Cre-LoxP system: general principles to determine tissue-specific roles of target genes. *Lab Anim Res* **34**, 147-159, doi:10.5625/lar.2018.34.4.147 (2018).
318 Feil, S., Valtcheva, N. & Feil, R. Inducible Cre mice. *Methods Mol Biol* **530**, 343-363, doi:10.1007/978-1-59745-471-1_18 (2009).
319 Shaner, N. C. *et al.* Improved monomeric red, orange and yellow fluorescent proteins derived from Discosoma sp. red fluorescent protein. *Nat Biotechnol* **22**, 1567-1572, doi:10.1038/nbt1037 (2004).
320 Winnard, P. T., Jr., Kluth, J. B. & Raman, V. Noninvasive optical tracking of red fluorescent protein-expressing cancer cells in a model of metastatic breast cancer. *Neoplasia* **8**, 796-806, doi:10.1593/neo.06304 (2006).
321 Sachs, A. The role of poly(A) in the translation and stability of mRNA. *Curr Opin Cell Biol* **2**, 1092-1098, doi:10.1016/0955-0674(90)90161-7 (1990).
322 Schek, N., Cooke, C. & Alwine, J. C. Definition of the upstream efficiency element of the simian virus 40 late polyadenylation signal by using in vitro analyzes. *Mol Cell Biol* **12**, 5386-5393, doi:10.1128/mcb.12.12.5386 (1992).
323 Gil, A. & Proudfoot, N. J. Position-dependent sequence elements downstream of AAUAAA are required for efficient rabbit beta-globin mRNA 3' end formation. *Cell* **49**, 399-406, doi:10.1016/0092-8674(87)90292-3 (1987).
324 Mutskov, V. J., Farrell, C. M., Wade, P. A., Wolffe, A. P. & Felsenfeld, G. The barrier function of an insulator couples high histone acetylation levels with specific protection of promoter DNA from methylation. *Genes Dev* **16**, 1540-1554, doi:10.1101/gad.988502 (2002).
325 Sharma, N. *et al.* The impact of cHS4 insulators on DNA transposon vector mobilization and silencing in retinal pigment epithelium cells. *PLoS One* **7**, e48421, doi:10.1371/journal.pone.0048421 (2012).

326 Matsuda, T. & Cepko, C. L. Controlled expression of transgenes introduced by in vivo electroporation. *Proc Natl Acad Sci U S A* **104**, 1027-1032, doi:10.1073/pnas.0610155104 (2007).
327 Zenker, M., Pierson, M., Jonveaux, P. & Reis, A. Demonstration of two novel LAMB2 mutations in the original Pierson syndrome family reported 42 years ago. *Am J Med Genet A* **138**, 73-74, doi:10.1002/ajmg.a.30894 (2005).
328 Hinkes, B. G. *et al.* Nephrotic syndrome in the first year of life: two thirds of cases are caused by mutations in 4 genes (NPHS1, NPHS2, WT1, and LAMB2). *Pediatrics* **119**, e907-919, doi:10.1542/peds.2006-2164 (2007).
329 McLean, W. H. *et al.* An unusual N-terminal deletion of the laminin alpha3a isoform leads to the chronic granulation tissue disorder laryngo-onycho-cutaneous syndrome. *Hum Mol Genet* **12**, 2395-2409, doi:10.1093/hmg/ddg234 (2003).
330 Barzegar, M. *et al.* A new homozygous nonsense mutation in LAMA3A underlying laryngo-onycho-cutaneous syndrome. *Br J Dermatol* **169**, 1353-1356, doi:10.1111/bjd.12522 (2013).
331 Schittny, J. C. & Yurchenco, P. D. Terminal short arm domains of basement membrane laminin are critical for its self-assembly. *J Cell Biol* **110**, 825-832, doi:10.1083/jcb.110.3.825 (1990).
332 Jones, L. K. *et al.* A mutation affecting laminin alpha 5 polymerization gives rise to a syndromic developmental disorder. *Development*, doi:10.1242/dev.189183 (2020).
333 Sato, H. *et al.* Amino-terminal fragments of laminin gamma2 chain retract vascular endothelial cells and increase vascular permeability. *Cancer Sci* **105**, 168-175, doi:10.1111/cas.12323 (2014).
334 Wu, C. *et al.* Endothelial basement membrane laminin alpha5 selectively inhibits T lymphocyte extravasation into the brain. *Nat Med* **15**, 519-527, doi:10.1038/nm.1957 (2009).
335 Thyboll, J. *et al.* Deletion of the laminin alpha4 chain leads to impaired microvessel maturation. *Mol Cell Biol* **22**, 1194-1202, doi:10.1128/MCB.22.4.1194-1202.2002 (2002).
336 Moore, M. A. & Metcalf, D. Ontogeny of the haemopoietic system: yolk sac origin of in vivo and in vitro colony forming cells in the developing mouse embryo. *Br J Haematol* **18**, 279-296, doi:10.1111/j.1365-2141.1970.tb01443.x (1970).
337 Sanchez, M. J., Holmes, A., Miles, C. & Dzierzak, E. Characterization of the first definitive hematopoietic stem cells in the AGM and liver of the mouse embryo. *Immunity* **5**, 513-525, doi:10.1016/s1074-7613(00)80267-8 (1996).
338 Dzierzak, E. & Speck, N. A. Of lineage and legacy: the development of mammalian hematopoietic stem cells. *Nat Immunol* **9**, 129-136, doi:10.1038/ni1560 (2008).
339 Qian, H. *et al.* Distinct roles of integrins alpha6 and alpha4 in homing of fetal liver hematopoietic stem and progenitor cells. *Blood* **110**, 2399-2407, doi:10.1182/blood-2006-10-051276 (2007).
340 Potocnik, A. J., Brakebusch, C. & Fassler, R. Fetal and adult hematopoietic stem cells require beta1 integrin function for colonizing fetal liver, spleen,

and bone marrow. *Immunity* **12**, 653-663, doi:10.1016/s1074-7613(00)80216-2 (2000).
341 Hirsch, E., Iglesias, A., Potocnik, A. J., Hartmann, U. & Fassler, R. Impaired migration but not differentiation of haematopoietic stem cells in the absence of beta1 integrins. *Nature* **380**, 171-175, doi:10.1038/380171a0 (1996).
342 Sher, I. *et al.* Targeting perlecan in human keratinocytes reveals novel roles for perlecan in epidermal formation. *J Biol Chem* **281**, 5178-5187, doi:10.1074/jbc.M509500200 (2006).
343 Hynes, R. O. The extracellular matrix: not just pretty fibrils. *Science* **326**, 1216-1219, doi:10.1126/science.1176009 (2009).
344 Vlodavsky, I. *et al.* Sequestration and release of basic fibroblast growth factor. *Ann N Y Acad Sci* **638**, 207-220, doi:10.1111/j.1749-6632.1991.tb49032.x (1991).
345 Lu, P., Takai, K., Weaver, V. M. & Werb, Z. Extracellular matrix degradation and remodeling in development and disease. *Cold Spring Harb Perspect Biol* **3**, doi:10.1101/cshperspect.a005058 (2011).
346 Bonnans, C., Chou, J. & Werb, Z. Remodelling the extracellular matrix in development and disease. *Nat Rev Mol Cell Biol* **15**, 786-801, doi:10.1038/nrm3904 (2014).
347 Penton, C. M. *et al.* Laminin 521 maintains differentiation potential of mouse and human satellite cell-derived myoblasts during long-term culture expansion. *Skelet Muscle* **6**, 44, doi:10.1186/s13395-016-0116-4 (2016).
348 Kiyozumi, D., Nakano, I., Sato-Nishiuchi, R., Tanaka, S. & Sekiguchi, K. Laminin is the ECM niche for trophoblast stem cells. *Life Sci Alliance* **3**, doi:10.26508/lsa.201900515 (2020).
349 Polisetti, N. *et al.* Laminin-511 and -521-based matrices for efficient ex vivo-expansion of human limbal epithelial progenitor cells. *Sci Rep* **7**, 5152, doi:10.1038/s41598-017-04916-x (2017).
350 Schaff, M. *et al.* Integrin alpha6beta1 is the main receptor for vascular laminins and plays a role in platelet adhesion, activation, and arterial thrombosis. *Circulation* **128**, 541-552, doi:10.1161/CIRCULATIONAHA.112.000799 (2013).
351 Sunada, Y., Edgar, T. S., Lotz, B. P., Rust, R. S. & Campbell, K. P. Merosin-negative congenital muscular dystrophy associated with extensive brain abnormalities. *Neurology* **45**, 2084-2089, doi:10.1212/wnl.45.11.2084 (1995).
352 Xu, H., Wu, X. R., Wewer, U. M. & Engvall, E. Murine muscular dystrophy caused by a mutation in the laminin alpha 2 (Lama2) gene. *Nat Genet* **8**, 297-302, doi:10.1038/ng1194-297 (1994).
353 Payne, S., De Val, S. & Neal, A. Endothelial-Specific Cre Mouse Models. *Arterioscler Thromb Vasc Biol* **38**, 2550-2561, doi:10.1161/ATVBAHA.118.309669 (2018).
354 Poulos, M. G., Batra, R., Charizanis, K. & Swanson, M. S. Developments in RNA splicing and disease. *Cold Spring Harb Perspect Biol* **3**, a000778, doi:10.1101/cshperspect.a000778 (2011).

355 Baralle, F. E. & Giudice, J. Alternative splicing as a regulator of development and tissue identity. *Nat Rev Mol Cell Biol* **18**, 437-451, doi:10.1038/nrm.2017.27 (2017).
356 Ffrench-Constant, C., Van de Water, L., Dvorak, H. F. & Hynes, R. O. Reappearance of an embryonic pattern of fibronectin splicing during wound healing in the adult rat. *J Cell Biol* **109**, 903-914, doi:10.1083/jcb.109.2.903 (1989).
357 Pickup, M. W., Mouw, J. K. & Weaver, V. M. The extracellular matrix modulates the hallmarks of cancer. *EMBO Rep* **15**, 1243-1253, doi:10.15252/embr.201439246 (2014).